

**MINGLING OF MULTIPLE CRYSTALS MUSHES IN THE FOGO
BATHOLITH**

By

© Benjamin Graham B.Sc. (Hons)

A Thesis submitted to the School of Graduate Studies in partial fulfillment of
the requirements for the degree of

Master of Science

Department of Earth Science

Memorial University of Newfoundland

October 2017

Abstract

This field, petrographic, and geochemical study examines mingling of compositionally similar rocks at multiple scales. Evidence of complex magma mingling in a multi-component crystal mush reservoir is preserved at Wild Cove East, located along the northeast shoreline of Fogo Island, Newfoundland. The irregular contacts and lack of chilled margins between units, the back-intrusion of younger units by older units, the similar composition of units, and an overlap in U/Pb zircon ages suggest all units interacted as viscous crystal mushes at similar temperatures in the shallow crust. Abundant rounded to ellipsoidal magmatic enclaves, of which there are at least three different populations based on composition and crystallinity, appear to represent separate magmas that were entrained either as earlier mush material or crystal-poor intrusions that experienced break-up at depth. Evidence of exchange of liquid at deeper levels is preserved both in the field and at the mineral-scale, where it is highlighted by abrupt compositional spikes in traverses across early forming minerals such as plagioclase and pyroxene. Heterogeneity in textures and composition of both major minerals (plagioclase and pyroxene) and an accessory mineral (zircon) suggest processes such as crystal exchange and capture affected mush host rocks, enclaves, and other intrusions in the study area earlier in their histories at deeper levels.

Acknowledgements

First, I would like to first thank my supervisors Alison Leitch and Greg Dunning for offering me the opportunity to study at Memorial University and to do field work on beautiful Fogo Island. I greatly appreciate all the support and feedback both of you have given me over the last couple years. I would also like to thank Hibernia for providing the funding for this project through the Hibernia Geophysics Fund.

I would like to extend my gratitude to faculty and staff at Memorial University who have helped me along the way including Pam King, Wanda Alyward, and Roberta Hicks. I would also like to thank Emily Gorner who was my field assistant in 2015 and was great company during those two months.

Finally, I thank my friends and family for their encouragement and support.

Table of Contents

Abstract.....	ii
Acknowledgments.....	iii
List of Figures.....	viii
List of Tables.....	xii
List of Appendices.....	xiii
Chapter 1: Introduction and Background.....	1
1.1 Tectonic Setting.....	2
1.2 Fogo Island Geology.....	7
1.2.1 Previous Work.....	7
1.2.2 Geological Units.....	8
1.3 Magma Chamber Processes.....	11
1.3.1 Crystal-Rich Magmas “Crystal Mushes”.....	11
1.3.2 Magmatic Processes in Crystal Mushes.....	13
1.3.3 Models of Emplacement of Mafic Magmatic Enclaves (MMEs).....	15
1.3.4 Mixing and Mingling of Magmas.....	17
Chapter 2: Field Area and Relationships.....	27
2.1 Methods.....	27
2.2 Map Units.....	29
2.2.1 Biotite Granite.....	30
2.2.2 Enclave-Poor Tonalite.....	31
2.2.3 Enclave-Rich Tonalite.....	32
2.3 Dykes and Sills.....	33
2.3.1 Minor Intrusions.....	33
2.3.2 Dislocated Tonalite Dyke.....	35
2.3.3 Quartz Diorite Dyke.....	36
2.3.4 Diorite Sill.....	36

2.3.5	Mafic Layered Intrusion.....	37
2.4	Field Evidence for Mingling and Movement of Crystal Mushes...37	
2.4.1	Irregular Boundaries Between Units.....	38
2.4.2	Enclaves.....	39
2.4.3	Magmatic Pipes and Tubes/Ladder Structures.....	40
2.4.4	Schlieren.....	40
2.5	Discussion.....	41
Chapter 3:	Petrography.....	66
3.1	Estimating Emplacement Crystallinity.....	66
3.2	Host Rock Petrography.....	67
3.2.1	Biotite Granite.....	68
3.2.2	Enclave-Poor Tonalite.....	68
3.2.3	Enclave-Rich Tonalite	69
3.3	Enclave Petrography.....	71
3.3.1	Group 1 Enclaves.....	71
3.3.2	Group 2 Enclaves.....	74
3.3.3	Group 3 Enclaves.....	76
3.4	Dyke and Sill Petrography.....	77
3.4.1	Dislocated Tonalite Dyke.....	78
3.4.2	Quartz Diorite Dykes.....	78
3.4.3	Diorite Sill.....	80
3.4.4	Layered Mafic Intrusion.....	80
3.5	Unit Contact Petrography.....	81
3.6	Discussion.....	83
Chapter 4:	Geochemistry.....	107
4.1	ICP-MS Major and Trace Element Results.....	107
4.1.1	Methods.....	107

4.1.2	Major and Trace Element Geochemistry.....	108
4.2	Analysis of Main Rock Forming Minerals.....	111
4.2.1	Methods and Sample Selection.....	111
4.2.2	Plagioclase Compositions.....	113
4.2.3	Pyroxene Compositions.....	114
4.2.4	Biotite and Hornblende Compositions.....	116
4.2.5	Plagioclase Feldspar Chemistry.....	116
4.2.6	Zoned Clinopyroxene Chemistry.....	119
4.2.7	Evidence of Magma Mixing and Transport.....	120
4.2.8	Comparison of Phenocryst Rims to Groundmass Plagioclase in Enclaves.....	122
4.2.9	Comparison of Enclave and Host Rock Plagioclase.....	122
4.3	Discussion.....	124
Chapter 5: Physical Properties of Crystal Mushes		152
5.1	Temperature and Heat Transfer in Magma Bodies.....	152
5.1.1	Liquidus and Solidus Temperatures.....	152
5.1.2	Heat Transfer and Magma Reservoirs.....	154
5.2	Rheological Properties of Magmas.....	157
5.2.1	Viscosity.....	157
5.2.2	Density.....	158
5.2.3	Estimated Viscosities and Densities using KWare MAGMA.....	159
5.2.4	Cooling Rate Modelling using KWare HEAT....	162
5.3	Discussion.....	164

Chapter 6: U-Pb Zircon Geochronology.....	174
6.1 Methods.....	174
6.2 Results.....	177
6.2.1 Biotite Granite.....	178
6.2.2 Enclave-Poor Tonalite.....	178
6.2.3 Diorite Sill.....	179
6.2.4 Chilled Diorite Dyke.....	179
6.3 Discussion.....	180
 Chapter 7: Summary and Conclusions.....	 185
7.1 Tectonic Setting.....	185
7.2 Mingling of Compositionally Similar Crystal Mushes.....	186
7.3 Injection of New Magmas into a Crystal Mush Reservoir.....	188
7.3.1 Proposed formation of Group 1 enclaves.....	189
7.3.2 Proposed formation of Group 2 and 3 enclaves...190	
7.3.3 Mineral evidence for changing chemical environments.....	190
7.4 Mixing of Crystals in a Crystal Mush Reservoir.....	191
7.5 Movement and Cooling of Enclaves in a Crystal Mush.....	193
7.6 Emplacement of Wild Cove East Units.....	194
7.7 Conclusion.....	196
 References.....	 201

List of Figures

Figure 1.1. Interpretation of the Iapetus Ocean with respect to lithotectonic elements of the Appalachians in Canada.....	19
Figure 1.2. Geological map displaying different tectonic zones of Newfoundland: Humber Zone, Dunnage Zone, Gander Zone, and Avalon Zone.....	20
Figure 1.3. Tectonic setting of Iapetus Ocean in Middle Ordovician – Early Devonian (van Stall and Barr, 2012).....	21
Figure 1.4. Location of major Silurian-Devonian plutons in northern Newfoundland: 507± 3 Ma Twillingate pluton, 408 ± 2 Ma Loon Bay batholith, 440 Ma Long Island batholith, and 422±2 composite dykes.....	22
Figure 1.5. Fogo Island and Change Islands geological map modified by Kerr (2013) after Baird (1958) and Currie (2003).....	23
Figure 1.6. Model for formation of a crystallization front in a magma chamber.....	24
Figure 1.7. Examples of magmatic structures from the Tuolumne Batholith, Sierra Nevada, California (Paterson et al, 2009).....	26
Figure 2.1. Map displaying location of study area.....	45
Figure 2.2. Geological map of Wild Cove East produced in ArcMap.....	46
Figure 2.3. Photos of detailed map area.....	48
Figure 2.4. Geological map of detailed map area produced in ArcMap.....	49
Figure 2.5. Field photographs of boundaries along biotite granite.....	51
Figure 2.6. Field photographs of enclave-poor tonalite unit.....	52
Figure 2.7. Field photographs of enclaves.....	53
Figure 2.8. Field photographs of enclave-free inclusions within enclave rich host.....	54
Figure 2.9. Examples of minor dykes located throughout study area.....	56
Figure 2.10. Field photographs of tonalite dyke in the detailed map area.....	57
Figure 2.11. Field photographs of quartz diorite dyke.....	58
Figure 2.12. Photographs of structures suggesting pulsed intrusion of diorite sill.....	59
Figure 2.13. Field photographs of mafic layered intrusion.....	60
Figure 2.14. Field photographs of visible contact between the enclave-poor tonalite	

And enclave-rich tonalite units.....	61
Figure 2.15. Field photographs of magmatic structures suggesting movement of crystal mush in diorite sill.....	62
Figure 2.16. Field photograph of schlieren in enclave-rich tonalite unit.....	63
Figure 2.17. Field photograph of schlieren “tail” behind enclave.....	64
Figure 2.18. Field photograph of schlieren in enclave-poor tonalite unit.....	65
Figure 3.1. Estimated emplacement crystallinity of enclave-poor tonalite unit.....	88
Figure 3.2. Estimated emplacement crystallinity of enclave-rich tonalite unit.....	89
Figure 3.3. Estimated emplacement crystallinity of Group-1 enclave.....	90
Figure 3.4. Estimated emplacement crystallinity of Group-2 enclave.....	91
Figure 3.5. Photomicrographs of textures in biotite granite unit.....	92
Figure 3.6. Photomicrographs of textures in enclave-poor tonalite unit.....	93
Figure 3.7. Photomicrographs of textures in enclave-rich tonalite unit.....	95
Figure 3.8. Photomicrographs of textures in Group 1 enclaves.....	96
Figure 3.9. Photomicrographs of textures in Group 2 enclaves.....	98
Figure 3.10. Photomicrographs of textures in Group-3 enclaves.....	100
Figure 3.11. Photomicrographs of textures in broken-up tonalite dyke of Figure 2.11.....	102
Figure 3.12. Photomicrographs of textures in quartz diorite dyke of Figure 2.12.....	103
Figure 3.13. Photomicrographs of mafic layered intrusion.....	104
Figure 3.14. Photomicrographs of mingled contacts between units.....	105
Figure 4.1. Major element Harker diagrams for enclaves and host rocks displaying mingling relationships in the study area.....	127
Figure 4.2. AFM diagram for host rocks, enclaves, and dykes/sills that display mingling relationships in the study area.....	128
Figure 4.3. Th-Hf-Ta plot of Wood (1980) for selected host rocks, enclaves, and dykes/sills.....	129

Figure 4.4. TAS (total alkalis vs. silica) plot following Lebas <i>et al.</i> (1986) for mingled host rocks, enclaves (numbered by group), and dykes/sills in the study area.....	130
Figure 4.5. Trace element Harker diagrams for enclaves, host rocks, and dykes in the study area.....	131
Figure 4.6. Plot of Ba/Sr vs SiO ₂ for selected host rocks, enclave and dyke/sills.....	132
Figure 4.7. Plots displaying negative correlation of P ₂ O ₂ with SiO ₂ and a positive correlation of P ₂ O ₅ with Nb.....	133
Figure 4.8. Chondrite-normalized REE patterns for selected host rocks, enclaves, dykes, and sills in study area.....	134
Figure 4.9. MORB-normalized REE plots for host rocks, enclaves, dykes, and sills that display mingling relationships in the study area.....	135
Figure 4.10. EMORB-normalized multielement plot for host rocks, enclaves, dykes, and sill that display mingling relationships in the study area.....	136
Figure 4.11. Plot of incompatible elements normalized to upper continental crust for selected host rocks, enclave, and dykes/sills.....	137
Figure 4.12. Feldspar ternary plots of selected host rocks, enclaves, and dykes/sill in the study area.....	138
Figure 4.13. Pyroxene quadrilateral plots for selected host rocks, enclaves, and dykes in the study area.....	140
Figure 4.14. EPMA traverse across a resorbed plagioclase phenocryst contained in Group 1 tonalite enclave.....	142
Figure 4.15. EPMA traverse across two resorbed plagioclase phenocrysts contained within a Group 2 biotite tonalite enclave.....	144
Figure 4.16. EPMA traverse across two resorbed plagioclase phenocrysts contained within a quartz diorite dyke that located at the northernmost end of the study area.....	146

Figure 4.17. EPMA traverse across zoned clinopyroxene contained within a Group 1 enclave.....	148
Figure 4.18. EPMA traverse across zoned clinopyroxene within quartz diorite dyke located at the northernmost end of the study area.....	149
Figure 4.19. Summary of compositional range for pyroxene and plagioclase in major units.....	150
Figure 5.1. Change in melt silica content and melt viscosity with increasing crystallinity as calculated for a magma of tholeiitic composition by MELTS.....	167
Figure 5.2. Temperature (°C) vs. viscosity (Pa/s) assuming constant pressure and crystallinity (KWare MAGMA).....	168
Figure 5.3. Temperature (°C) vs. density (kg/m ³) assuming constant pressure and crystallinity (KWare MAGMA).....	169
Figure 5.4. Crystallinity (vol %) vs. viscosity (Pa/s) assuming constant temperature, pressure, and crystal size (KWare MAGMA).....	170
Figure 5.5. Crystallinity (vol %) vs. density (kg/m ³) assuming constant temperature, pressure, and crystal size (KWare MAGMA).....	171
Figure 5.6. Temperature (°C) vs viscosity (Pa/s) assuming temperature dependence of crystallinity (KWare MAGMA).....	172
Figure 5.7. Initial conditions for 3DHeat modelling of a 3-D cooling of intermediate enclave in an intermediate host	173
Figure 6.1. Concordia diagrams of U/Pb results of zircon from Wild Cove East.....	183
Figure 6.2. Cathodoluminescence of zircon crystals representative of the type analyzed from each sample.....	184
Figure 7.1. Simulation of mixing in a crystal mush due to hot injection from below.....	198
Figure 7.2. Illustration for formation of Group 1 and 2 enclaves.....	199
Figure 7.3. Illustration for formation of Group 2 and 3 enclaves.....	200

List of Tables

Table 3.1. Petrographic properties of key units in the study area.....86

Table 6.1. U/Pb zircon data from rocks of Wild Cove East.....182

List of Appendices

Appendix A. Sample numbers and locations.....	212
Appendix B. Petrographic characteristics of units.....	216
Appendix C. Results of geochemical analyses.....	220
Appendix D. Rheological properties of units.....	243

Chapter 1 – Introduction and Background

Fogo Island, located off the northern coast of Newfoundland, is underlain by a Silurian-Devonian magmatic body called the Fogo batholith along with several volcano-sedimentary sequences (Baird, 1958; Currie, 2003; Kerr, 2013). The Fogo batholith is comprised of plutonic rocks ranging from gabbro-diorite to granite and is interpreted to represent an amalgamation of multiple plutonic bodies as suggested by limited geochronological data including a 411 +/- 13 Ma Rb-Sr isotopic age on northern granites (Sandeman and Malpas, 1995), a 420 +/- 2 Ma U-Pb age from a monzogranite of the Sandy-Wild Cove Suite (Aydin, 1994) and a 408 +/- 2 Ma U-Pb age from a quartz diorite Sandy-Wild Cove Suite (Aydin, 1994). These ages are consistent with multiple Appalachian orogenic events that affected much of Newfoundland during the end Silurian to early Devonian.

The goal of this chapter is to provide the reader with the necessary information regarding the previous work done on both Fogo Island geology along with modern ideas concerning magma chamber processes that are relevant to this study. The chapter will begin by briefly discussing the tectonic setting of the Fogo batholith relative to the Newfoundland Appalachians. Following this, previous work done on Fogo Island will be described including a detailed description of the geological units and a discussion of the proposed models of emplacement for the batholith. The final section of this chapter will

discuss modern ideas regarding magmatic processes that occur in shallow crustal magma chambers.

1.1. Tectonic Setting

The North American Appalachians represent a complex orogenic cycle that involved the opening and subsequent closure of the Iapetus and Rheic oceans during the Early to Late Paleozoic. One popular tectonic model suggests the Appalachians comprised six separate and successive events (Penobscotian, Taconic, Salinic, Acadian, Neo-Acadian, and Alleghanian orogenies), each of which involved the orthogonal closure of marginal seaways within the Iapetus and Rheic Oceans (Williams *et al*, 1988; van Staal and Barr, 2012; Figure 1.1). A different model by Murphy *et al* (2010) suggests the Appalachians represent a three-plate orogenic event involving the collision of Laurentia, Baltica, and Gondwana. Both models agree that, over the course of the Paleozoic, the tectonic style of the Appalachians changed from an accretionary orogeny to an oblique strike-slip collisional orogeny after the terminal closure of the Iapetus and Rheic Oceans.

The tectonic history of the Newfoundland Appalachians is dominantly represented by the opening and closure of the Iapetus Ocean, whereas the effects of the Rheic Ocean closure are limited compared to other parts of eastern North America (Murphy *et al*, 2010). In the model by van Staal and Barr (2012), it is suggested Newfoundland rocks experienced multiple orogenic events during the closure of Iapetus due to the collision of multiple arcs and microcontinents with the eastward expanding Laurentian margin. These

events include the Late Cambrian to Late Ordovician (500-460 Ma) Taconic orogeny, the Early Silurian (440-423 Ma) Salinic orogeny, and the Late Silurian to Early Devonian (421-400 Ma) Acadian orogeny. A different tectonic model by Murphy *et al* (2010) suggests that Iapetus closure similarly involved arc-back-arc accretionary events but complete closure was achieved by the Mid Silurian due to the collision of Laurentia and Baltica to form Laurussia. In this model, the collision of Gondwana and Laurussia in the Carboniferous resulted in the closure of the Rheic Ocean.

The effects of both the Early Silurian Salinic and the Late Silurian-Early Devonian Acadian orogenies are pronounced in the rocks of Central Newfoundland and are interpreted to have been particularly important with respect to the emplacement of the Fogo batholith. The tectonic model by van Staal and Barr (2012) suggests the Salinic orogeny (440-423 Ma) and Acadian orogeny (421-400 Ma) represent the collision of the peri-Gondwanan Ganderia and Avalonia microcontinents, respectively, with the Laurentian margin. Their model suggests that immediately prior to the main phase of Salinic orogenesis, the Popelogan-Victoria Arc, representing the leading edge of the Ganderia microcontinent, collided with the eastern margin of Laurentia (Figure 1.3). The Popelogan-Victoria Arc was separated from the rest of Ganderia by the Tetagouche-Exploits back-arc basin and its closure is represented by a major strike-slip fault in Central Newfoundland called the Dog Bay Line, along which the Fogo batholith currently lies (Williams *et al*, 1993; Pollock *et al*, 2007; Figure 1.2). In a different model by Murphy *et al* (2010), Ganderia and Avalonia were part of a single large composite terrane that had

separated from Gondwana in the Late Cambrian to form the Rheic Ocean and accreted to Baltica by the Early Silurian, and to Laurussia by the Middle Silurian. In this model, the Salinic orogeny is interpreted to have taken place during the collision between Laurussia and the Ganderia/Avalonia composite terrane in the Mid-Silurian.

During the Silurian-Devonian the Appalachians experienced another tectonic event, called the Acadian orogeny. Due to the heterogeneity of Silurian-Devonian tectonics, magmatism, and sedimentation, a variety of interpretations have been made regarding regional-scale Acadian kinematics. Popular models relate Acadian tectonism primarily to Late Silurian – Early Devonian convergent motion between Laurentia and Avalonia resulting in the closure of the Acadian Seaway (Bradley, 1983; van Staal, 2005; Valverde-Vaquero *et al*, 2006; 3rd panel of Figure 1.3). Other workers have suggested Acadian tectonism involved a considerable component of transcurrent motion between Laurentia and Avalonia (Williams and Hatcher, 1982; Ferrill and Thomas, 1988; van der Pluijm and van Staal, 1988). A separate model by Murphy *et al* (2010) characterizes the Acadian orogeny as a tectonothermal event reflecting the northward shallow subduction of Rheic oceanic lithosphere beneath amalgamated Avalonia-Laurussia during the Late Silurian – Late Devonian.

Much of the Acadian record has been erased, particularly in the central and southern Appalachians, due to modification by post-Devonian deformation and erosion (ver Straeten, 2010). Except for parts of Nova Scotia, the Acadian Orogeny affected much of Newfoundland and the timing best constrained by the inversions of the Mascarene and

La Poile basins at 421 Ma (O'Brien *et al*, 1991; Fyffe *et al*, 1999). Dextral shear overprinting sinistral shear has been documented along the Dover Fault of eastern Newfoundland and indicates a significant rotation of shortening axes to a more E-W direction (Holdsworth, 1991; Hibbard, 1994). Similarly found along the Cape Ray Fault, located in southwest Newfoundland, is overprinting of early oblique sinistral structures of amphibole grade metamorphism by later dextral motion and greenschist mineral assemblages interpreted to represent Salinic and Acadian deformation, respectively (Dube *et al*, 1992).

Acadian deformation affected rocks in each of the four tectonic zones of Newfoundland: Humber, Dunnage, Gander, and Avalon zones (Williams, 1993; Figure 1.2). The westernmost Humber Zone is interpreted to represent the east margin of Laurentia in the Early Paleozoic and is characterized by west-directed allochthons that were thrust over carbonate-dominant shelf succession during the Middle Ordovician Taconic orogeny (Williams and Hiscott, 1987; Waldron and Milne, 1991; van Staal and Barr, 2012). In central Newfoundland, accreted Ordovician oceanic and arc material of the Dunnage Zone represent vestiges of the Iapetus Ocean, which existed between Laurentia and Gondwana from the Neoproterozoic to the Mid-Paleozoic (Williams *et al*, 1988). The Dunnage Zone is divided by the Red Indian Line into the Notre Dame and Exploits Subzones representing peri-Laurentian and peri-Gondwanan affinities, respectively (Williams *et al*, 1988). The Gander Zone and Avalon Zones are interpreted to represent remnants of the Gondwana-derived Ganderia and Avalonia microcontinents, respectively (Williams, 1979; van Staal). Acadian-related deformation and metamorphism was most influential in the Gander Zone

and generally decreases towards the Avalon Zone and west of the Red Indian Line (Van Staal *et al*, 2014).

It is suggested that Acadian plutonism affected much of Newfoundland, with Silurian-Devonian ages having been obtained for approximately thirty percent of exposed plutons on the island (Williams, 1993). Large granitic and bimodal plutons of Late Silurian-Devonian age occur in all parts of both the Dunnage and Gander zones, the eastern Humber zone, and the westernmost Avalon zone. These rocks are usually marked by a pre-tectonic or syn-tectonic fabric (Williams, 1993). Examples of early Acadian intrusions in central Newfoundland include the 408 \pm 2 Ma Loon Bay intrusive suite, a 424 \pm 2 Ma gabbro phase of the Mount Peyton Batholith, and 422 \pm 2 Ma granitic to diabasic composite dykes that intrude the Llandoveryian Botwood Group on the Port Albert Peninsula (Elliot *et al*, 1991; McNicoll *et al*, 2006; Figure 1.4). The bimodal nature of these intrusions is interpreted to represent crustal weakening and magma underplating beneath the Ganderian continental crust (Van Staal *et al*, 2014; Figure 1.3). Based on U/Pb ages of 420 \pm 2 Ma and 408 \pm 2 Ma and its proximity to the Dog Bay Line, it is interpreted that the Fogo batholith was emplaced during dextral-slip reactivation of the Dog Bay Line due to Acadian related orogenesis in the Late Silurian – Early Devonian (van Staal and Barr, 2012; Kerr, 2013).

1.2 Fogo Island Geology

1.2.1 Previous Work

Relatively little geological research has been done on Fogo Island apart from thorough work by a handful of individuals from both the Geological Survey of Newfoundland and Memorial University of Newfoundland. The first geological maps of Fogo Island were produced by Baird (1958) and are still considered to be the most accurate maps of the region. Another major mapping project was carried out by Currie (1997) of the Geological Survey of Canada and offered some different interpretations of the geology than those of Baird (1958).

Both authors interpreted the geology of Fogo Island to represent a section through a bimodal magma chamber, called the Fogo batholith, based on the position of gabbroic rocks in the south-east and granitic rocks in the north-central parts of the island (Currie, 2003). The major gabbroic and granitic units were originally defined by Baird (1958) as the Seldom Gabbro and Shoal Bay Granite, respectively. Both Baird (1958) and Currie (1997) acknowledged the presence of hybridized intermediate rocks located between the granite and gabbro units. However, Currie (1997) defined them as a separate mixed unit whereas Baird (1958) did not. This is summarized in the modified geological map of the island by Kerr (2003) in Figure 1.5.

Two volcanoclastic sequences appear on the northwest part of the island and were named by Baird (1958) as the Fogo Harbour and Brimstone Head Formations. The Fogo

Harbour Formation is composed of a mixture of sandstone and siltstone interlayered with felsic tuff units whereas the Brimstone Head Formation is made of felsic volcanic and pyroclastic material (Kerr, 2003). The sedimentary Fogo Harbour Formation is interpreted as the country rock into which plutons of the Fogo Batholith were intruded. A U-Pb zircon age of 421 +/- 0.6 Ma from a basal rhyolite of Brimstone Head Formation suggests it may, at least partially, represent an extrusive component to the Fogo Island intrusion (Hamilton and Kerr, 2016).

The configuration of gabbroic rocks overlain by granitic rock has led researchers to model the island as a section through a bimodal magma chamber where dense mafic magma once underlay buoyant felsic magma. Currie (2003) suggested crustal anatexis above mantle-derived underplated mafic magma produced the granitic rocks which make up the upper part of the batholith followed by the emplacement of intermediate magmas along fractures related to dextral strike-slip movement along the Dog Bay Line.

1.2.2 Geological Units

The Seldom Gabbro unit, found in southern Fogo Island, is characterized by plutonic rocks of gabbro-diorite composition that are composed of Ca-rich plagioclase and clinopyroxene along with minor hornblende and sodic plagioclase (Baird, 1958; Kerr, 2013). Igneous textures such as subtle cumulate layering and magmatic fabric have been observed in many outcrops (Kerr, 2013). Close to the southern town of Seldom, swarms

of bimodal diabase-rhyolite dykes are found that intrude the Seldom Gabbro. These dykes are interpreted to represent conduits that transported magma to higher stratigraphic levels within the magma chamber (Kerr, 2013). A contact between the Seldom Gabbro and the underlying sedimentary Fogo Harbour Formation, interpreted to be the country rock through which the Seldom Gabbro intruded, is seen on the south side of the island. The boundary between the Seldom Gabbro and the overlying Shoal Bay Granite is a complicated region of hybridized rocks that has been called both an intrusion breccia by Baird (1958) and a separate diorite unit by Currie (1997).

Most of the granitic rocks of northern Fogo Island are included in the Shoal Bay Granite unit, which is defined as homogeneous, medium- to coarse-grained white-pink monzogranite to granite (Baird, 1958; Kerr, 2013). There are small magmatic enclaves scattered throughout this unit, with most being found along to the coastline (Baird, 1958; Currie, 2003; Kerr, 2013). The enclaves exist in a variety of different axial styles and are interpreted to have formed due to mingling between separate mafic and felsic magmas that occurred at various stratigraphic levels within the Fogo batholith. Hornfelsed metasedimentary xenoliths, interpreted to have been derived from the Fogo Harbour Formation, are found within localized “intrusion breccia zones” of the Shoal Bay Granite which are located primarily along the coast (Baird, 1958; Kerr, 2013). Two minor granitoid units were also defined by Baird (1958) include: 1) the Hare Bay Granite: an orange-red K-feldspar-rich granite containing miarolitic cavities that outcrops just south of Fogo town,

and 2) the Rogers Cove Granite: a fine-grained granitoid rock that outcrops near the town of Rogers Cove in southwest Fogo Island.

The northwestern part of the island, proximal to the town of Fogo, is characterized by grey siltstone/sandstone belonging to the Fogo Harbour Formation, along with massive ignimbrites and pyroclastic breccia of the Brimstone Head Formation (Baird, 1958). Features such as soft-sediment deformation in thin beds, sand dykes, current ripples, and intraformational breccias are present in the Fogo Harbour Formation (Kerr, 2013). The conformable transition from the Fogo Harbour Formation to the Brimstone Head Formation is recognized by matrix-supported conglomerates and is located near the town of Fogo (Kerr, 2013). Rocks suggested to be equivalents of both the Fogo Harbour and Brimstone Head Formations have been mapped by Currie (1997) on the Change Islands, located 5km west of Fogo Island.

A small ultramafic layered intrusion, called the Tilting Layered Suite (TLS), occurs near the town of Tilting, located in eastern Fogo Island. A study by Aydin (1994) focused on characterizing the TLS, but little is known about how it relates to surrounding plutonic rocks (Kerr, 2013). Aydin (1994) identified two main crystallization sequences within the TLS: one characterized by early crystallization of cumulus orthopyroxene and the other by late crystallization of cumulus orthopyroxene. The variation in crystallization order has been explained by the presence of multiple different primitive liquids, magma recharge, varying degrees of fractionation and wall-rock assimilation, or the presence of a significant chemical and thermal gradient within the magma chamber (Aydin, 1994).

The TLS is surrounded by two high-level granitoid units defined by Aydin (1994) as: 1) the Fogo Suite (FS) composed of monzogranite and minor granodiorite, and 2) the Wild-Sandy Cove Suite (W-SCS) comprising diorite to quartz diorite. The FS is generally free of inclusions compared to the W-SCS which contains numerous country rock xenoliths and magmatic enclaves (Aydin, 1994). The W-SCS is further subdivided into three zones of distinct lithology: the Pigeon Island Unit, Sandy Unit, and Wild Unit. This study will focus on the Wild Unit, where the highest concentrations of magmatic enclaves are located, and build on previous observations made by Aydin (1994).

1.3. Magma Chamber Processes

1.3.1 *Crystal-rich magmas (“Crystal Mushes”)*

There has been a push in recent years to differentiate the term “crystal mush” from “magma” because the rheological properties of magma change significantly as they cool below liquidus temperatures. It has been suggested that even at low crystallinities in magmas, a strong framework is formed between crystals and the relative motion between liquid and crystals becomes inhibited, forming a “mush-like” fluid that is commonly regarded as a “crystal-mush” (Irvine *et al*, 1998). Mush zones form in the shallow crust and behave as sponge-like rigid crystal networks with roughly 40-60 % crystallinity along with interstitial melt (Ruprecht *et al*, 2012). Combined geochemical and geophysical

observations suggest shallow magma reservoirs exist as crystal mushes for large portions of their existence (Bergantz *et al*, 2015).

The viscosity of a magma increases drastically during crystallization and the biggest change occurs when the proportion of crystals to melt becomes nearly equal (Marsh, 2002). Above this rheological “lock-in” point, crystals form an interlocking network with enough rigidity to prevent the relative movement of crystals and interstitial liquid. Plagioclase-rich melts tend to form strong crystal networks at crystallinities as low as 25% (Philpotts and Carol, 1996; Marsh, 2002). During reheating events, such as mafic recharge or underplating, crystals in a mush can become “unlocked” and are once again free to move independently within the melt (Burgisser and Bergantz, 2011). At very low crystallinities (10-15%), crystals are weakly suspended in the melt and can be removed from the magma entirely due to processes such as forceful injection of new magma or by strong thermal convection in the chamber (Marsh, 2002; Figure 1.6).

Field relationships and textures that indicate crystal mushes include: (1) high concentration in schlieren of magmatic minerals that would have existed in the magma flow before deposition; (2) gradation of some layers into the host magma; (3) back-intrusion of host magma into intruding structures, suggesting both components were above solidus temperatures; and (4) partial overprinting of structures by late magmatic fabric (Paterson *et al*, 2009).

1.3.2 *Magmatic Processes in Crystal Mushes*

Recent ideas concerning silicic magma production suggest that magma chambers are assembled incrementally in batches fed by conduits or dykes and can generate eruptible magma over short timescales (e.g. Clemens and Mawer, 1992; Petford *et al*, 2000; Paterson *et al*, 2011). This is evidenced in volcanic and plutonic rocks that display a mixture of crystals with different chemistry, zoning patterns, or ages (Storm *et al*, 2011; Bergantz *et al*, 2015). For example, the wide range in zircon ages from rhyolites in the Tarawera Volcano, New Zealand are interpreted to represent remobilization and remelting of near-solidus crystal-rich magma due to periodic intrusion of mafic dykes (Storm *et al*, 2011).

Numerous studies of magma chamber processes have suggested that the intermittent injection of mafic magmas at the base of shallow magma chambers may supply heat and energy to extend the thermal lifetime of crystal mushes (Smith, 1979; Wiebe ,1994) It is interpreted that in bimodal magma chambers mafic magma is preferentially injected along the crystal-rich floor below a more liquid-rich felsic component (Vogel, 1982; Wiebe, 1994). Evidence of this process can be seen by flame and load structures on the base on some mafic sheets along with the presence of mafic magmatic enclaves (MMEs) above an otherwise unchilled upper margin (Wiebe and Collins, 1998). The underlying felsic rocks generally show evidence of compaction, with leucocratic veins intruding the mafic material due to filter pressing of the interstitial liquid in the underlying mush. There is usually evidence of mechanical mixing between the

unchilled top of the mafic sheets and the overlying granite, such as an increased abundance of leucocratic minerals towards the top of the sheet (Wiebe, 1994).

It is suggested that a strong rheological transition occurs in lower portions of mafic-silicic intrusions where mafic sheets pond and flow across a granitic crystal mush and beneath crystal-poor silicic magma (Wiebe *et al*, 2007). These rheological transition zones preserve structures that are interpreted to be the physical record of magmatic processes (eg. mafic schlieren and magmatic tubes/ladder dikes; Wiebe, 2017). Such structures are well preserved in parts of the Tuolumne batholith in the Sierra Nevada, California, although their origin is still debated. Paterson *et al* (2009) described two types of steeply-dipping structures in the Tuolumne batholith, magmatic tubes and magmatic pipes, which are interpreted to have been vertically-oriented when they formed. Tubes are defined as cylindrical, schlieren-bounded structures that contain layering that is compositionally distinct compared to the host rock and that occur in two general types: migrating tubes in which the tube axis moves laterally with time, and stationary tubes that lack migration (Paterson, 2009; Figure 1.7). Pipes consist of a homogeneous mineralogy in contrast to the repeated layering seen in tube structures. Other researchers argue that these structures are shallow-dipping and therefore reflect downward flow of an intrusion due to erosion of structural weaknesses in the underlying granitic crystal mush (Glazner *et al*, 2012; Wiebe, 2017).

1.3.3 Models of Emplacement of Mafic Magmatic Enclaves (MMEs)

The term “enclave” was originally proposed by Lacroix (1890) to describe fragments of rock that are enclosed in a homogenous igneous host. However, there has been debate over the correct terminology for describing rounded to ellipsoidal mafic inclusions contained within a granitoid host. The term “mafic microgranitoid enclave” was proposed by Vernon (1984) to describe the granitoid composition of inclusions. Barbarin (1988) suggested that although enclaves are always finer-grained than their hosts, they can contain minerals that have grain sizes of up to 2 or 3 mm, and thus preferred the term “mafic magmatic enclave (MME)” to describe them. Since the terms are used interchangeably in the literature, for the remainder of this thesis I will use the term “enclave” to describe rounded to ellipsoidal igneous bodies that are more mafic and finer-grained than their enclosing igneous hosts.

There are multiple proposed mechanisms by which enclaves can form. It is suggested that crystal-poor mafic dykes, upon intrusion into a more viscous felsic magma, will experience break-up and form enclaves due to the difference in rheological properties between the two magmas (Frost and Mahood, 1987; Wiebe *et al*, 1997). Recurrent dyke injections can result in compositionally distinct enclave populations that can be randomly distributed throughout a magma chamber by processes such as thermal convection. It is suggested that enclaves can also form due to the disruption of intermediate layers in compositionally stratified magma chambers. The compositions of these intermediate layers would be dependent on the relative volumes of mafic and silicic magma in the

chamber, the rate of recharge by mafic injections, and fractional crystallization (Wiebe *et al*, 1997). Thus, the hybridization of enclaves formed in this manner will be related to processes that occurred at depth, rather than due to chemical exchange between the enclave and enclosing granite host (Wiebe *et al*, 1997). Another proposed mechanism for enclave formation involves the break-up of cumulate material near the margin of a pluton (Wiebe *et al*, 1997).

While enclaves can be irregularly distributed throughout a pluton, localized accumulations are common and are referred to as “enclave swarms” (Pabst, 1928; Didier, 1973; Fernandez and Barbarin, 1991; Tobisch *et al*, 1997). The most common sites for enclaves to accumulate are along pluton margins, within fractures, or near the pluton roof (Pabst, 1928; Tobisch *et al*, 1997). Processes that would encourage the formation of enclave swarms include: 1) velocity-gradient flow sorting, 2) gravitational sorting, and 3) break-up of heterogeneous dykes (Tobisch *et al*, 1997). The likelihood of enclave deposition can increase due to either an increase or decrease in flow velocity. In a divergent flow regime, where flow velocity decreases systematically in the flow direction, enclave accumulation can occur when the velocity of the host magma reaches a critical minimum. Accumulation of enclaves can also occur in a convergent flow regime when an increase in magma flow velocity through a small volume, causes enclaves to be trapped due to “log-jamming” (Tobisch *et al*, 1997). Any vertically-oriented irregularities along chamber walls may also serve as traps for enclave accumulation (Tobisch *et al*, 1997).

Fernandez and Barbarin (1991) studied enclaves in granitic hosts. Due to enclaves being more mafic and therefore denser than their hosts, they argued that a high yield strength must be present in the granites to prevent enclaves from sinking during ascent. They estimated that a granite crystal mush of around 30% crystallinity is necessary to prevent the sinking of diorite-composition enclaves. However, this percentage can be less if the compositions and density of the two magmas are similar. In addition to composition and density, the rheological properties of magmas also vary with crystallization, as the viscosity of a magma will increase steadily as it moves towards its solidus temperature. Viscosity in both enclave and host magmas is highly dependent on the sizes, shapes, and distribution of crystals (Fernandez and Barbarin, 1991).

1.3.4 Mixing and Mingling of Magmas

There are three different styles of interaction that can take place between coeval felsic and mafic magmas: mixing, mingling, and chemical exchange (Fernandez and Barbarin, 1991). Magma mixing typically results in a homogeneous “hybrid” magma whereas mingling refers to magma interaction that has resulted in physically distinct magmas with heterogeneous compositions (Johnson and Barnes, 2006). The type of interaction is dependent on multiple variables including initial temperatures of the magmas, their relative viscosities, the degree of crystallization, and their compositions. Ultimately, the difference in rheology between two coexisting magmas is responsible for whether mixing or mingling will take place: low rheological contrasts favor mixing and

higher contrasts prevent mixing and only mingling occurs (Huppert et al, 1984; Fernandez and Barbarin, 1991). In general, mixing takes place at depth where magmas have lower viscosities whereas mingling takes place at shallower levels.

Mafic magma can be introduced into felsic magma at various times over the duration of pluton construction. The rheological properties of both the injecting and ambient magmas will change over the plutons evolution and, similarly, the rheological gradient between host and intruding magmas will also change. This will result in different types of interactions depending of the crystallinity and rheology of both magmas at the time of injection (Fernandez and Barbarin, 1991). At low crystallinities in the felsic host, the injection of mafic magma can result in the hybridization of the two magmas and early crystals will either be dissolved or incorporated as xenocrysts in the new mixed magma (Fernandez and Barbarin, 1991). As crystallization increases in the felsic host, mafic injections will begin to break up into enclaves due to the rheological difference between the two magmas. If mafic magma is injected into a nearly solid felsic host, only localized interaction will take place and lead to the formation of fragmented synplutonic dykes (Fernandez and Barbarin, 1991).

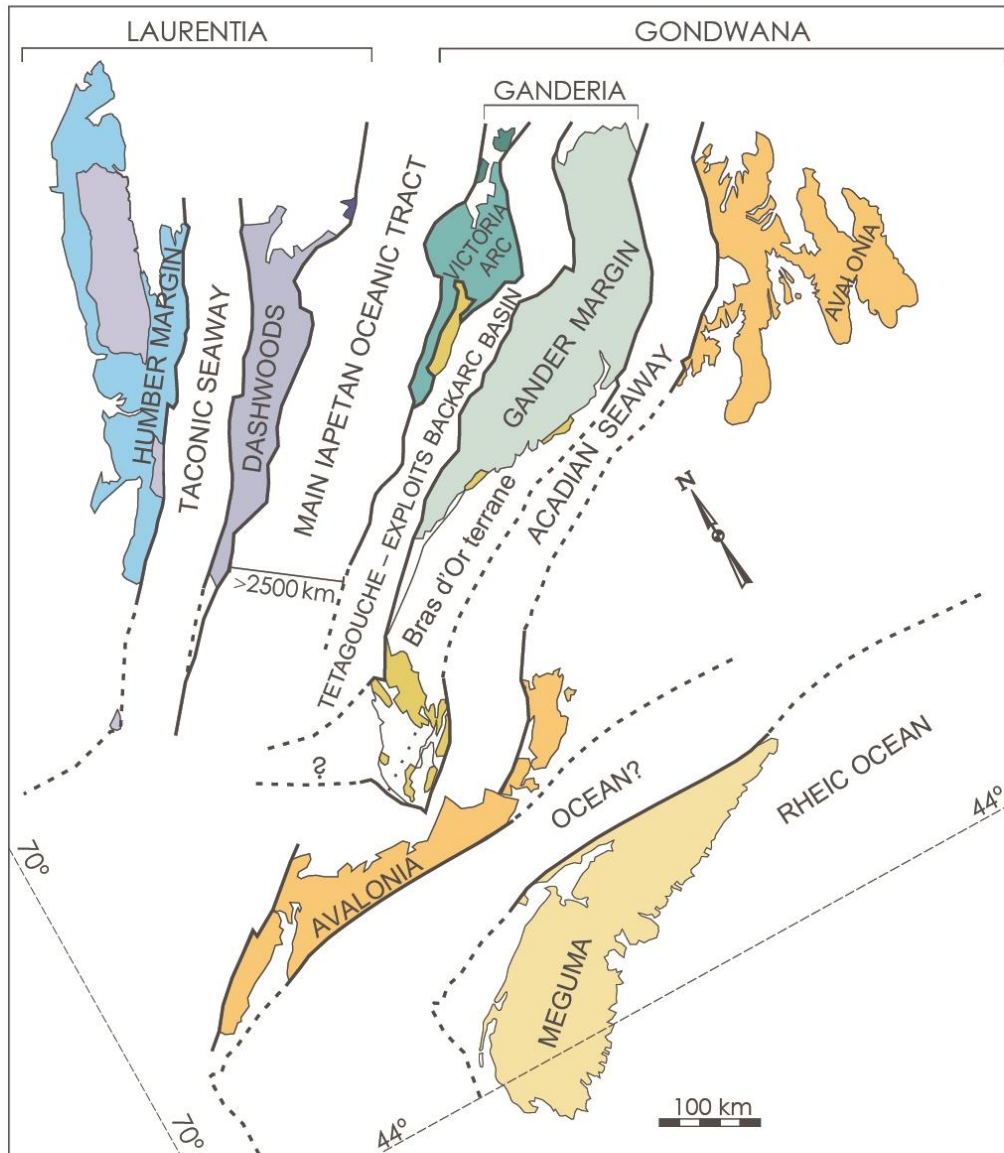


Fig 1.1. Interpretation of the Iapetus Ocean with respect to lithotectonic elements of the Appalachians in Canada. The closure of Acadian Seaway between Avalonia and the Laurentian margin in the Mid Devonian is interpreted by van Staal and Barr, 2012 to represent the onset of Acadian orogenesis.

GENERALIZED INTERPRETIVE MAP- NEWFOUNDLAND APPALACHIANS

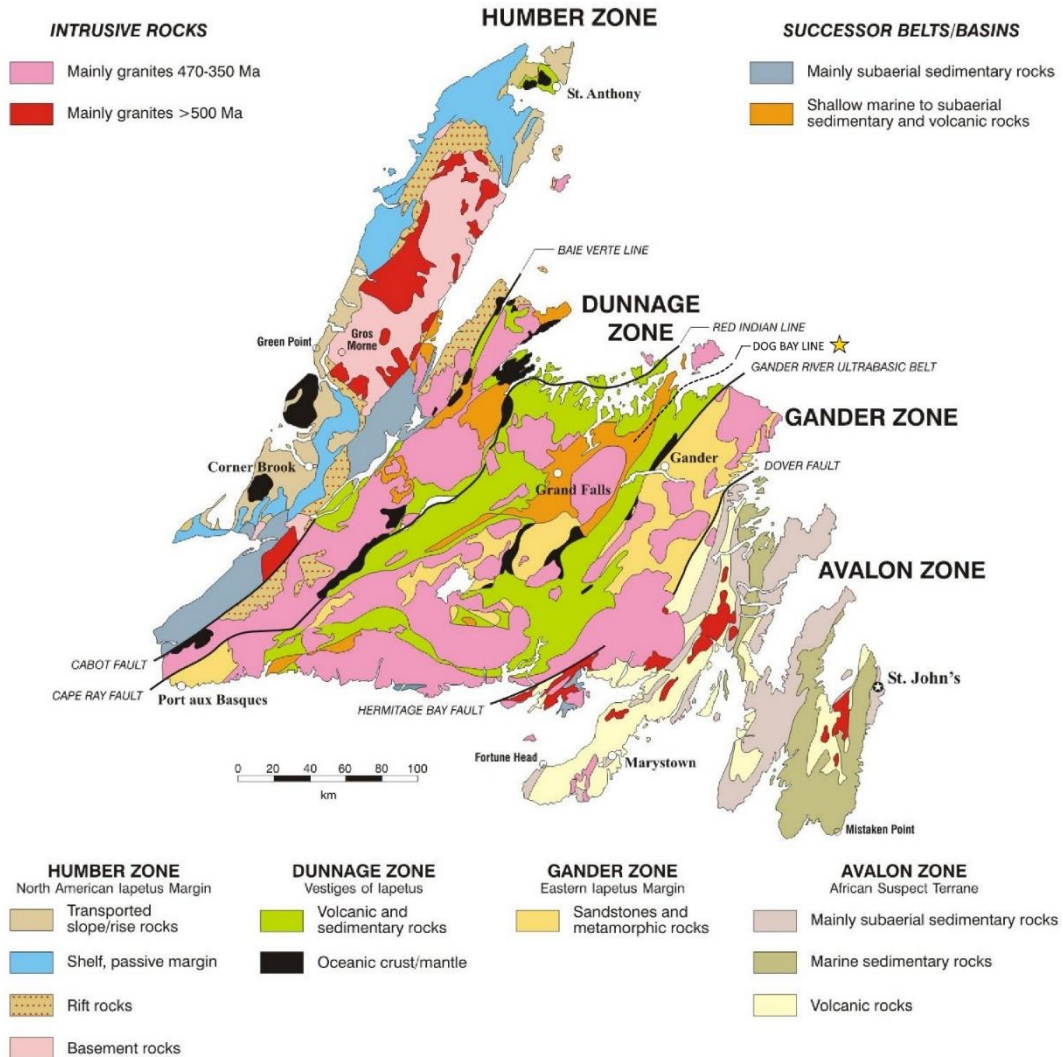


Figure 1.2. Geological map displaying different tectonic zones of Newfoundland: Humber Zone, Dunnage Zone, Gander Zone, and Avalon Zone. Major Sutures include the Baie Verte Line, Red Indian Line, Gander River, Dover Fault, and Dog Bay Line. Map Compiled by Hayes (1987) and modified by Williams (2004).

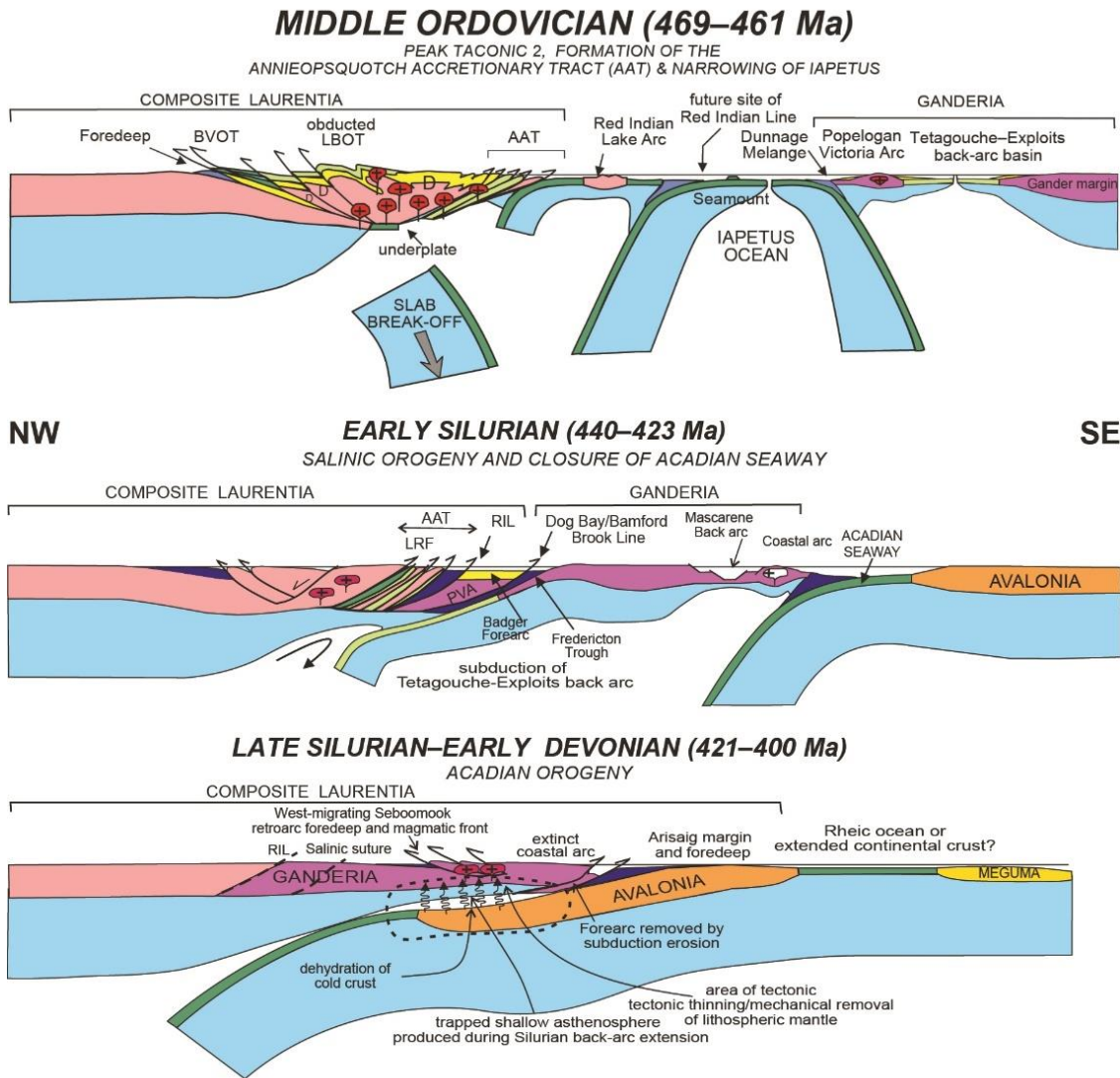


Figure 1.3. Interpretation of the tectonic setting of Iapetus Ocean in the Middle Ordovician – Early Devonian by van Staal and Barr, 2012.

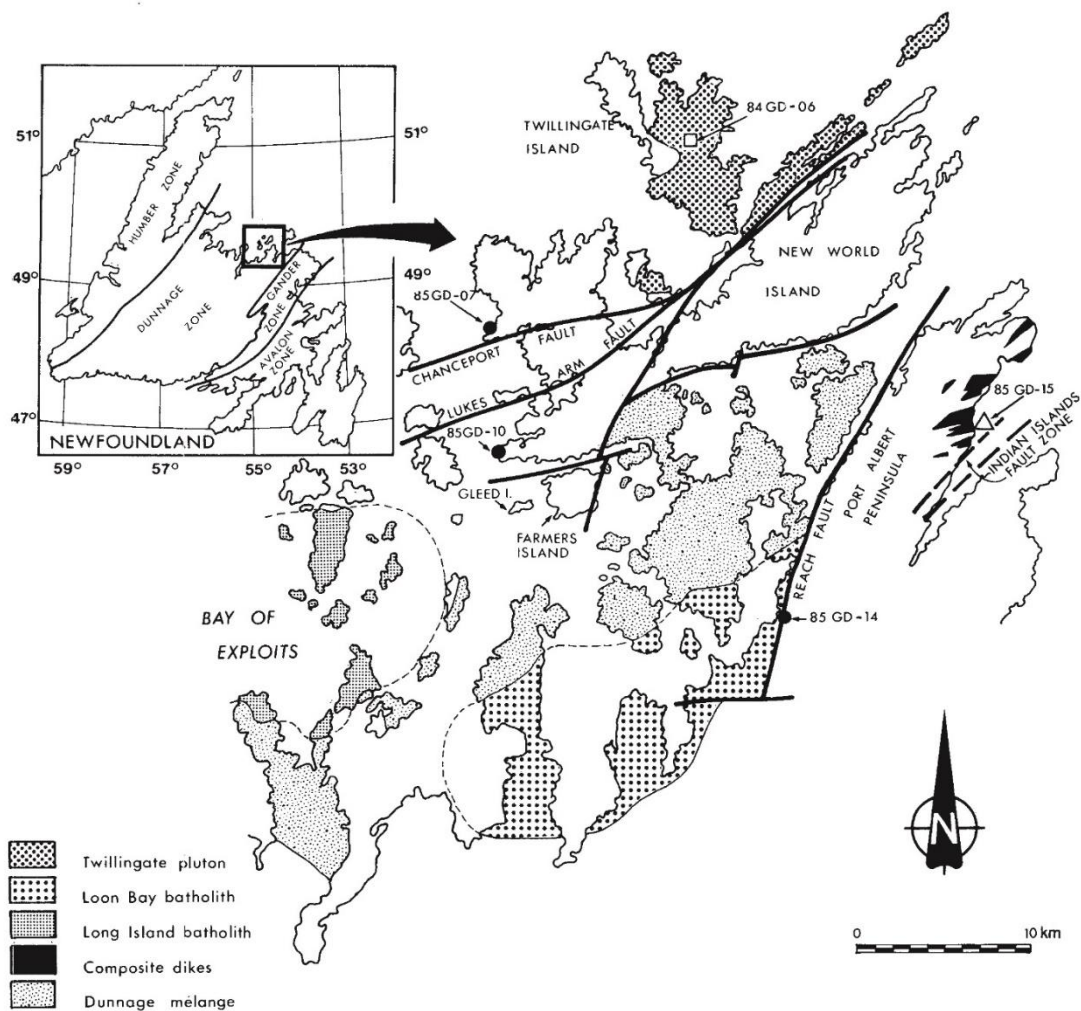


Figure 1.4. Location of several Silurian-Devonian plutons in northern Newfoundland: 507 \pm 3 Ma Twillingate pluton, 408 \pm 2 Ma Loon Bay batholith, 440 Ma Long Island batholith, and 422 \pm 2 composite dykes (Elliot et al, 1991).

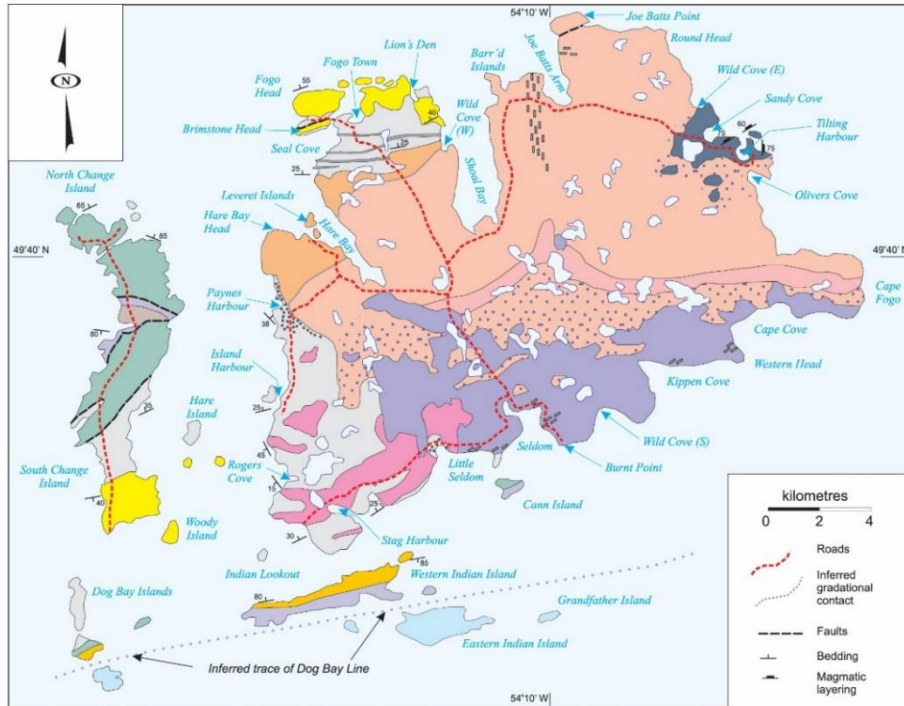
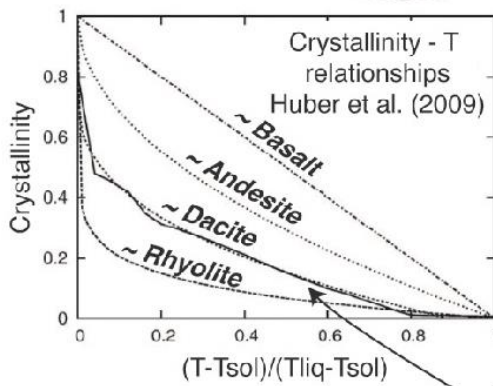
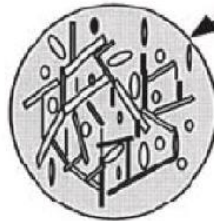
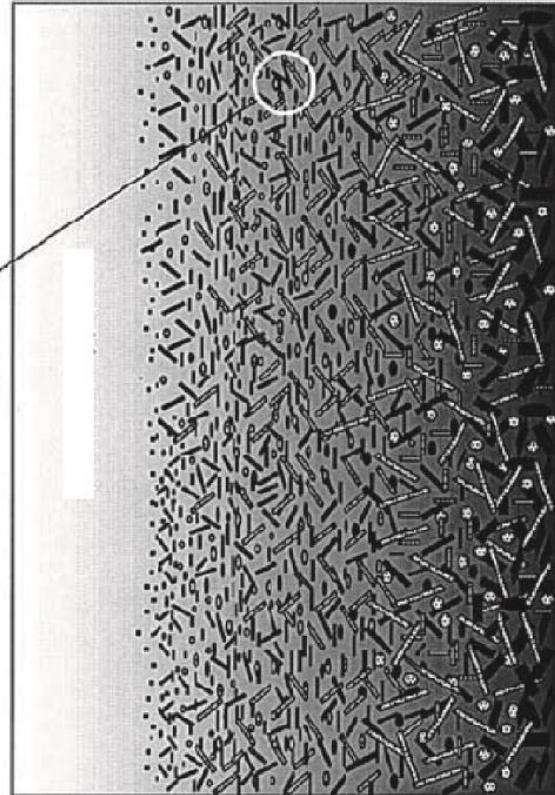


Fig 1.5. Modified geological map of Fogo Island and Change Islands by Kerr (2013) after Baird (1958) and Currie (2003).

Total amount of Joules per kg of magma between liquidus and solidus
 ~ 300000 Joules/kg for the sensible heat +
 ~ 270000 Joules/kg for Latent heat
 (see heat capacity and latent heat values compiled in Bachmann and Bergantz, 2006)

T liquidus ΔT ~200-250 °C T solidus



Suspension Mush Rigid crust

Solid line = calculated from MELTS software using a dacitic initial composition (Pagosa Peak Dacite, Bachmann et al., 2002)

Figure 1.6. Model of the formation of a crystallization stability front in a magma chamber. At crystallinities as low as 50%, a rigid crystal network is formed and the relative movement of crystals and melt is strongly inhibited. Crystals are held until a crystallinity falls below a critical point (~30%), below which crystals are suspended in the melt and can be displaced from the stability front by processes like convection or forceful injection of new magma (Marsh, 2002). Crystallization rate, except in basaltic magmas, does not increase linearly with decreasing temperature (Bachmann and Huber, 2016).

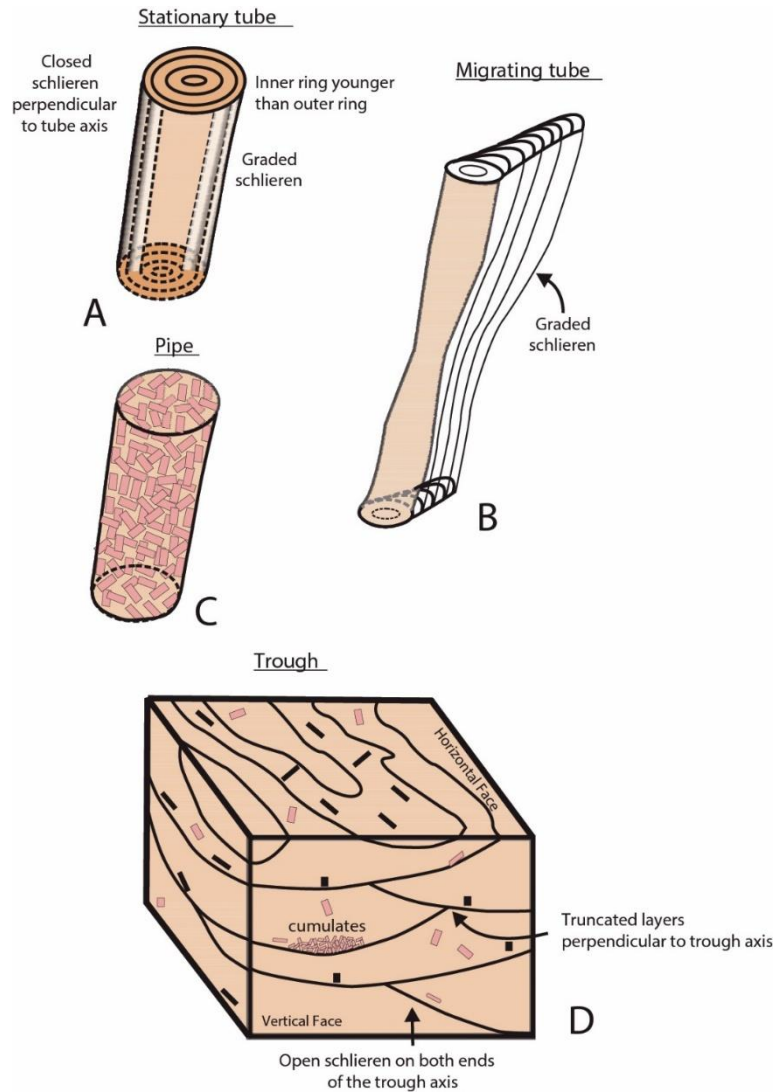


Figure 1.7. Magmatic structures observed in the Tuolumne Batholith, Sierra Nevada, California: A) Stationary tube, B) Migrating tube, C) Pipe, D) Trough (Paterson et al, 2009).

Chapter 2 - Field Area and Relationships

The study area is located along the north-eastern shore of Fogo Island, at Wild Cove East, and makes up part of the Wild Unit defined by Aydin (1994). A map showing the location of the field area relative to Fogo Island and eastern Newfoundland is shown in Figure 2.1. Accessing the field area can be done by following the Turpin's Trail hiking path located outside the town of Tilting until the coastline is reached. The rock units of Wild Cove East contain structures and relationships that suggest mingling of compositionally similar magmas took place at shallow level in the crust. A list of sample locations is provided in Table A.1 of Appendix A. This chapter will describe the field work that was done for this project including a report of the mapping techniques and a detailed description of the map units. The evidence for magma mingling in the study area will then be presented followed by a discussion of the associated implications for magma chamber processes.

2.1 Methods

Due to the small scale of this study, existing air photos had inadequate resolution and remote imaging specialists CloudBreaker™ were hired to produce a basemap of the field area. Over the course of one day, 735 high-resolution ortho-rectified images were taken at both 25 meter and 50 meter altitudes using a drone helicopter. These photos

were subsequently stitched together into a photo mosaic basemap by Cloudbreaker™ personnel using digital imaging software.

Mapping was conducted with the aid of the basemap in addition to thorough examination, discussion, and interpretation of the rocks. The mapping team included myself, Greg Dunning, and Alison Leitch along with assistance from Emily Gorner and Roberta Hicks from the Earth Science Department at Memorial University of Newfoundland. Due to surface weathering, staining, shadows, and the overall similarity of the rock types, “boots-on-the-ground” mapping was required for accurate interpretation of the units. After careful discussion, the major map units were drawn on a sheet of mylar placed over the basemap. The map was later digitized by myself into ArcMap, as shown in Figure 2.2.

A significant amount of time was spent mapping in detail a small location found in the central part of the study area (yellow box in Figure 2.2) which displayed some of the most complicated mingling relationships (Figure 2.3). Hand-drawn maps were produced of this area by setting up a 10x20 meter grid divided into 200 1x1 meter units, which is referred to as “Grid 1” in Appendices A and B. These maps were later digitized into ArcMap, as illustrated in Figure 2.4.

2.2 Map Units

Apart from a biotite granite unit, all host rocks in the study area are intermediate and have a narrow compositional range from quartz diorite to tonalite. The intermediate rocks are divided into two main groups based on the abundance of enclaves, with 20-30% of the surface area of one unit being represented by enclaves whereas they are absent to highly scarce in the second unit. Three major host rock units are thus defined in the map represented by Figure 2.2: enclave-poor tonalite, enclave-rich tonalite, and biotite granite. Although the name tonalite is used for both intermediate units and is the most common composition in each, they both span a narrow compositional range from quartz diorite to tonalite. In the field study, however, these slight variations in rock type could not be differentiated. The boundaries between all three units are consistently irregular and chilled margins are absent.

The intrusive history of the units can be inferred based on the relationships observed in the detailed map area of Figure 2.4. Since blocks of the granite unit appear in both the enclave-poor tonalite and enclave-rich tonalite units, it is inferred that the granite is the oldest unit in this area. The enclave-poor tonalite unit later intruded the granite in this area and caused it to be displaced in an approximately north-south direction. The enclave-rich tonalite unit is interpreted to be the youngest unit based on the termination of a broken-up dyke against it, which is otherwise seen cutting the granite and enclave-poor tonalite. Both the enclave-poor tonalite and granite were displaced in an east-west direction due to the intrusion of the enclave-rich tonalite in this area.

Inclusions of both the granite and enclave-poor tonalite are found within the enclave-rich tonalite. In the following section, a detailed description of each map unit from oldest to youngest will be provided.

2.2.1 Biotite Granite

The most silicic unit is a biotite granite that outcrops in the form of irregular bodies and, based on the relationship with other units, appears to represent the oldest rocks in the study area. The unit is composed of medium-grained potassium feldspar, quartz, plagioclase, and biotite. It is a homogenous, medium- to coarse-grained biotite granite that displays compositional similarity to monzogranite of the Fogo Suite defined by Aydin (1994), located several hundred meters inland from the Figure 2.2. The unit is fully enclosed in both intermediate host units and commonly shares an irregular boundary with each. The blocky shape of the unit suggests it was solid and brittle when the younger intermediate units intruded. The biotite granite in the map area represented by Figure 2.4 displays a shallow dipping contact with the overlying enclave-poor tonalite unit (318/21 NE).

Fine-grained sedimentary xenoliths are common in the biotite granite unit. The angular inclusions range in size from several centimeters to 3 meters in size and presumably represent material that was stoped from the country rock during the emplacement of the granite (Fig 2.5B). While observed locally in the western part of the

study area, the highest accumulation of metasedimentary xenoliths is contained within a 10-meter-wide granite in the central part of the field area (21N, 709807m E, 5511578m N; *a* in Figure 2.2).

2.2.2. Enclave-poor tonalite

The enclave-poor tonalite unit is composed of medium-grained biotite quartz diorite to biotite tonalite and contains scarce enclaves. Despite having an orange appearance due to surface weathering, the rocks are dominantly composed of medium-grained plagioclase, quartz, biotite, minor pyroxene and hornblende, along with magnetite, ilmenite, apatite, and zircon (Fig 2.6A). The unit commonly shares an irregular boundary with both the enclave-rich tonalite and biotite granite units. Enclaves range in composition from diorite to tonalite and are generally small (5-30 cm), making up less than 5% of the surface area of this unit. Rounded to ellipsoidal enclaves are most abundant in the north and easternmost parts of the unit whereas large parts in the southwest lack enclaves entirely. Scarce metasedimentary xenoliths are contained within the enclave-poor tonalite unit in the northern part of the study area.

A faint flow foliation, defined by the preferred alignment of elongate plagioclase, is seen in all parts of the unit, but does not display a clear trend, suggesting there are variable flow directions in the mush. Evidence of crystal mush movement in the enclave-poor tonalite is also suggested by schlieren, which are formed by the alignment of mafic

minerals (biotite and hornblende) due to the deformation of crystal-rich material during pluton construction (Wiebe *et al*, 2007). Mirolitic cavities, defined by small (5-10 cm-wide) pockets of coarse potassium feldspar and quartz, are also common in this unit (Fig 2.6B).

2.2.3. Enclave-Rich Tonalite

The enclave-rich tonalite unit is characterized by a surface area that ubiquitously contains around 20-30% enclaves of diorite to tonalite composition (Figure 2.7A). Apart from the higher abundance of enclaves, the unit looks identical to the enclave-poor tonalite unit and is quartz-diorite to tonalite in composition. A wide range is observed in the size of the enclaves, with the smallest being only a few centimeters wide and the largest being nearly a full meter in length. Enclaves are rounded to ellipsoidal and generally display a greater degree of stretching compared to the enclave-poor tonalite unit (Figure 2.7B). Rounded to angular inclusions of enclave-poor tonalite are found within the unit suggesting the enclave-rich tonalite is the youngest unit in the study area (Figure 2.8). The unit shares an irregular boundary with adjacent units and commonly outcrops along the coastline except for in the northwest where, at areas of recessed outcrop elevation, it is found beneath the enclave-poor tonalite. A faint magmatic foliation, defined by the alignment of elongate plagioclase, is observed in all areas and is always parallel to the elongation direction of the enclaves. Schlieren are usually curved and are

commonly associated with the enclaves themselves. Mirolitic cavities, like those observed in the enclave-poor tonalite, are observed in this unit.

2.3. Dykes and Sills

A wide variety of dyke-like structures that range in both size and composition are observed throughout the study area. In general, dykes displaying the sharpest margins are those that are the most compositionally distinct from their immediate hosts and represent late intrusions through highly crystalline rock. These late dykes are found in all parts of the study area and generally strike to the north and dip steeply to the east. Dykes that display compositional similarity to their intermediate hosts, however, often have irregular margins suggesting intrusion occurred earlier when the host was less crystalline and more mobile. Some of these intermediate dykes contain enclaves and intrude enclave-poor tonalite host, suggesting they acted as a conduit for enclave transport (Fig. 2.9A).

The following section will begin by describing minor intrusions located within the study area and then will describe several of the most prominent intrusions including: a dislocated tonalite dyke in the detailed map area Grid 1 (tonalite dyke in Figure 2.4), a pair of quartz diorite dykes displaying evidence of enclave formation (A in Figure 2.2), a 30-meter wide diorite sill (B in Figure 2.2), and a mafic layered intrusion bordering the eastern end of the study area (C in Figure 2.2).

2.3.1. Minor Intrusions

Thin (5-20 cm wide) mafic and felsic dykes are abundant throughout all parts of the study area and display a variety of different styles. Some of these structures have straight margins with slight brittle offset and appear to be related to minor mafic or felsic injections into nearly solid intermediate host (Figure 2.9B). Others have curved margins and were likely intruded into a mobile mush (Figure 2.9C). In a few cases, these boundaries are associated with late oblique vertical fault movement as evidenced by the displacement of enclaves and blocks along it. Thin felsic intrusions in the west are composed of fine-grained aplite in the centre and pegmatite along the margins (plagioclase, quartz, and K-feldspar) (Figure 2.9D). A small ~20-meter-wide chilled diorite dyke is found in the eastern part of the study area, adjacent to the mafic layered intrusion (dark blue unit in Figure 2.2). This dyke is the only unit to display a straight chilled margin and is thus interpreted to be among the youngest units in the study area.

Several meters away to the north from the diorite sill is a large (5 meter-wide) angular inclusion that is compositionally similar in mineralogy/grain size to the sill (Figure 2.8B). However, no chilled margin is observed on the inclusion therefore ruling out its association with the sill. Proximal to this inclusion are a relatively high abundance of sedimentary xenoliths and miarolitic cavities. Multiple orders of magnitude of inclusion sizes occur close to the diorite sill and may reflect varying degrees of disaggregation of both the country rock and the tonalite crystal mush.

2.3.2. Dislocated Tonalite Dyke

Evidence of movement within the crystal mush units is provided by the displacement of a 20-cm wide tonalite dyke that cuts across both the enclave-poor tonalite and granite units in Figure 2.4. Despite being broken-up, the original path of the intrusion can be easily inferred. Pieces of the dyke can be identified in the host tonalite units due to being darker, finer-grained, and more angular than nearby enclaves (Figure 2.10A). The existence of this dyke suggests that the both host units must have been sufficiently crystalline to sustain brittle deformation at the time of dyke intrusion. After the dyke cooled, however, movement in the still-mobile hosts caused the dyke to be pulled-apart, displaced, and back-intruded by host material. This re-intrusion often involved only the more felsic phenocryst-free component of the host, particularly in the granite, but in other cases phenocryst-bearing material is seen re-intruding the dyke (Figure 2.10B). The dyke displacement is noticeably higher in the quartz diorite unit compared to the granite suggesting that the granite was more coherent at the time of intrusion. Based on the above field evidence, it seems likely that these units co-existed as crystal-rich magmas when dykes were intruded and subsequently displaced due to movement within the mush units. Another possibility, based on the appearance of rounded pieces within the granite host (Figure 2.10B), is that this section represents a later intrusion of a deeper part of the dyke where it had mingled with tonalite and broken up.

2.3.3. Quartz Diorite Dykes

The most prominent feature in the westernmost part of the cove is a pair of dykes that, while appearing dark on the weathered surface, are quartz diorite in composition (Figure 2.11A; A in Figure 2.2). Locally, the dykes are seen pillowing into rounded globules due to interaction with host material, representing a potential mechanism by which enclaves were formed (Wiebe *et al*, 1997; Figure 2.11B). Progressively more globules are seen within the margins of the dyke moving along strike towards the shoreline. The globules are contained within the boundaries of the dyke suggesting that parts of the dyke began breaking-up due to rheological instability between the injecting and ambient magmas (Wiebe *et al*, 1997).

2.3.4. Diorite Sill

A 30-meter-wide diorite sill of unknown thickness (B in Figure 2.2) displays distinct magmatic structures that are not observed elsewhere in the field area. The sill shares an irregular margin with the surrounding enclave-poor tonalite unit. The composition grades from diorite at the margins towards quartz diorite in the middle of the intrusion. The nearly horizontal bottom of the sill can be observed in the limited vertical relief of the outcrop and a vertical way-up direction is determined by the occurrence of steeply dipping magmatic pipe structures within the intrusion (Paterson *et al*, 2009). Small mm-

sized rounded felsic segregations or pipes are collected along faint internal contacts within the sill (Figure 2.12).

2.3.5. Mafic Layered Intrusion

Bordering the eastern end of the study area is a compositionally layered intrusion (location C, green unit in Figure 2.2.) that grades from enstatite hornblende troctolite at the bottom to biotite hornblende quartz diorite at the top (Figure 2.13A). The intrusion is roughly 300 meters across and shares an irregular chilled boundary with the adjacent enclave-rich tonalite at its western end. In the east, the intrusion grades towards a composition that is nearly identical to the enclave-poor tonalite and a clear boundary between them is not visible. However, the intrusion can be distinguished from surrounding rocks, at both the top and bottom, by the presence of coarse hornblende oikocrysts. A hornblende pegmatite differentiate is located towards the center of the intrusion (Figure 2.13B).

2.4 Field Evidence for Mingling and Movement of Crystal Mushes

Evidence for both magma mingling and movement of crystal mushes in the study area include: 1) the irregular nature of boundaries between units, 2) absence of chilled margins between units, 3) high abundance of elongate enclaves, and 4) schlieren occurring both in regions where enclaves are present and in areas where they are absent.

The following section will describe each of these elements and discuss their implications for magmatic processes.

2.4.1 Irregular Boundaries Between Units

The boundaries between all units in the study area are consistently irregular and lack chilled margins, suggesting the units coexisted at similar temperatures between their respective liquidus and solidus. The contact between the enclave-rich tonalite and enclave-poor tonalite is clearly visible in many parts of the field area, but must be inferred in some areas based on the relative change in enclave abundance. An example of a visible contact region is presented in Figure 2.14A, where enclaves are terminated against a steeply-dipping boundary and are noticeably more abundant on one side than the other. Defining this boundary is a thin (5-10 cm thick) anastomosing dark contact that is primarily composed of clinopyroxene. A smooth margin is seen on the enclave-poor tonalite side whereas a more irregular or cusped boundary is seen on the enclave-rich tonalite side, suggesting a strong rheological gradient across these units (Figure 2.14B). A possible explanation for these structures is that they are related to the settling and deposition of early forming crystals preferably along the boundary between the two tonalite units.

2.4.2 Enclaves

The high abundance of enclaves represents the most immediately striking evidence of magma mingling in the study area. Both the enclaves and the rocks that enclose them are medium to fine grained and are ubiquitously intermediate in composition. The enclaves were divided into three main types based on hand sample-scale textures: 1. Fine-grained dark enclaves containing feldspar phenocrysts, 2. Fine-grained dark enclaves that lack phenocrysts, 3. Medium-grained equigranular intermediate enclaves.

In many parts of the study area, particularly in the central and eastern regions of the enclave-rich tonalite, enclaves of different mineralogy are observed close to and, in some cases, are impinged against each other. This suggests the enclaves reflect multiple injections that occurred at deeper levels in the magma chamber that were later stirred and transported together to the current interpreted shallow level, possibly by thermal convection (Wiebe *et al*, 1997). However, it is possible that some of the enclave-forming injections occurred close to the current erosional depth based enclaves occurring as elongated “trains” in certain parts of the study area. The largest of these regions occurs in the enclave-rich tonalite on the eastern side of the study area, where enclaves are elongated in an approximately east-west direction (average strike = 263) (21N, 709980m E, 5511555m N; *b* in Figure 2.2). This region also hosts the largest enclaves in the entire study area, with several exceeding lengths of three meters.

2.4.3 Magmatic Pipes and Tubes/Ladder Structures

Magmatic pipes, defined as steeply-dipping cylindrical shaped leucocratic structures that are mineralogically distinct from surrounding rock, occur within the diorite sill (B in Figure 2.2). Examples of these structures were observed both in cross-sectional view (Figure 2.15A) and as rounded leucocratic “tops” on the surface of the sill. Immediately outside the sill margin exist magmatic tube-like structures that are seen protruding through the host tonalite material. A single magmatic tube is also found within the sill, which is of similar composition to the host material but is distinguished by trail of rounded schlieren (Paterson *et al*, 2009; Figure 2.15B). Due to limited vertical relief of the outcrop, the dip of the tube structures could not be measured. Thus, it is unknown whether they best fit the steeply-dipping “tube” model or the shallow-dipping “ladder dyke” model of Glazner *et al* (2012).

2.4.4 Schlieren

Schlieren are defined as fine-grained mafic bands that record the presence of deformable crystal-rich material during pluton construction (Wiebe *et al*, 2007). Different styles of schlieren are observed in the enclave-rich tonalite compared to the enclave-poor tonalite unit. Schlieren in the enclave-rich tonalite are curved and commonly related to the enclaves themselves. In several cases, schlieren were observed “tailing-behind” individual enclaves suggesting they formed due to the differential movement between

the enclave and host mush (Wiebe *et al*, 2007; Figure 2.16). In another example, the chilled outer margin of an enclave appeared to be “peeled off” as it moved against the host mush, which subsequently filled in the void space left behind by the enclave (Figure 2.17). Although these associations between schlieren and enclaves suggest differential movement between the separate magmas, field observations alone cannot determine whether the schlieren represent sinking, rising, or lateral migration of the enclaves within their host.

Schlieren in the enclave-poor tonalite occur as straight planar sets up to one meter wide and consist of thin layers of biotite and hornblende. The structures appear to have formed due to shear induced in the mush during movement. In localized parts of the unit, variably dipping schlieren structures are observed suggesting magmatic flow and current deposition (Figure 2.18). The shape of the schlieren suggests a more consistent flow direction within the enclave-poor tonalite compared to its enclave-rich counterpart and their orientation is approximately north-south ([176/80 W] and [172/80 W]).

2.5 Discussion

Despite its small areal extent, Wild Cove East presents ample evidence for mingling of compositionally similar magmas. The occurrence of enclaves with different compositions suggest mingling not only took place at the current interpreted shallow level but also at deeper levels in the crust. Structures such as metasedimentary xenoliths and

miarolitic cavities are abundant, the latter of which develop in granitic melts at lithostatic pressures lower than 2-1.5 kbar, and together imply reservoir storage occurred close to the walls or roof of a pluton at depths not much greater than 1-km (Burnham and Ohmoto, 1980; Peretyazhko, 2010).

Apart from the biotite granite unit and the mafic layered intrusion bordering the eastern end of the study area, all units are diorite to tonalite in composition. The compositional similarity most of the intermediate units in the study area (host rocks, enclaves, and dykes), along with the lack of chilled margins, suggest they first interacted at similar temperatures. The irregular margins shared between the quartz diorite-tonalite host rocks and dykes suggest these units were contemporaneously intruded either as crystal-free liquids or as crystal mushes. An exception is the biotite granite which, based on its blocky shape, appears to have been solid but was partially molten at its boundaries during the intrusion of the younger intermediate units. The large temperature interval between liquidus and solidus for intermediate rocks, along with a continuous heat supply by the injection of new magmas at depth, likely kept the intermediate units in a mushy state for a prolonged period.

A broken-up tonalite dyke in the detailed map area suggest a smaller rheological gradient between injected and ambient magmas. The sequence of dyke intrusion, quenching, dislocation, displacement, and then back-intrusion from the host suggests the dyke was intruded during periods of mobility in the enclave-poor tonalite and biotite

granite hosts. In addition, the occurrence of thin (5-15 cm wide) mafic and felsic dykes that display sharp chilled contacts suggest injections also occurred after complete solidification of the host rock. Based on the different styles of intrusions in the study area, it appears injection occurred throughout the crystallization history of the reservoir as ambient magmas evolved towards a crystal mush and eventually solid rock.

Features such as schlieren, stretching of enclaves, and magmatic pipes/tubes suggest significant movement of crystals and melt occurred within the units. Schlieren appear to be related to both flow in the mush (planar schlieren in enclave-poor tonalite) and differential motion between enclaves and hosts (curved schlieren in enclave-rich tonalite). Evidence of independent movement of melt within a diorite sill are preserved via magmatic tubes and pipes. The tube structures are interpreted to have formed by buoyant rise and lateral migration of crystals and melt within the underlying crystal mush due to processes such as filter pressing or compaction (Paterson *et al*, 2009). Magmatic pipes found in the diorite sill similarly suggest the underlying host was a crystal mush at the time of intrusion and, being more felsic, buoyantly rose through the denser sill (Paterson *et al*, 2009).

Wild Cove East preserves evidence of complex interactions between partially crystallized magmas and intrusions including dykes, sills, and enclaves. Unlike previous studies where mingling occurred between compositionally distinct magmas like the granite and basalts of the Cadillac Mountain Granite (Wiebe and Collins, 1998), interactions at Wild Cove East are primarily between units of intermediate composition.

The details of these interactions will be further investigated in Chapter 3 (petrography) and Chapter 4 (geochemistry).

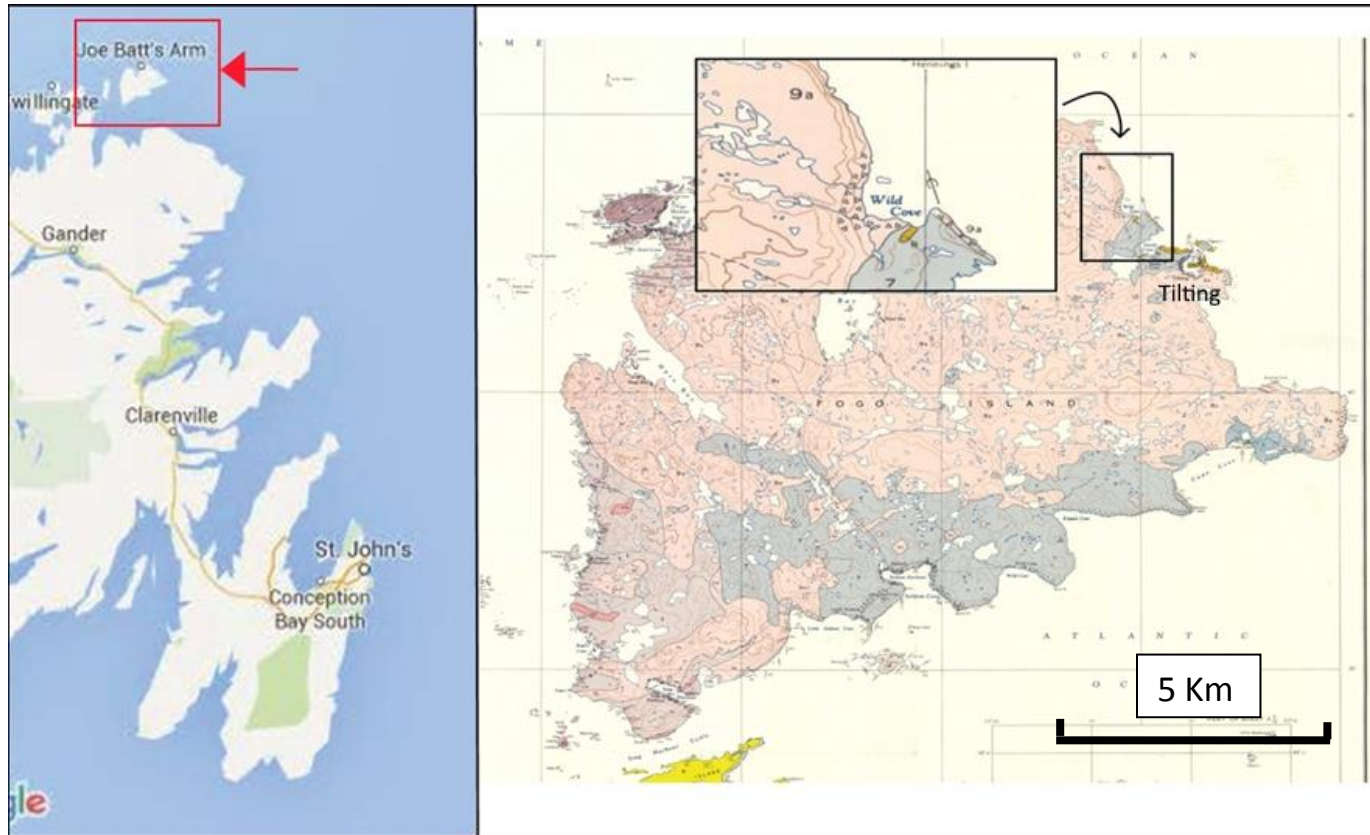


Figure 2.1. Map displaying location of study area. Left) Location of Fogo Island relative to the Avalon Peninsula and St. John's (red box), Newfoundland. Right) Location of study area (Wild Cove East) with relation to Fogo Island geological map (Baird, 1958; pink = Shoal Bay Granite, blue = Seldom Gabbro, grey = Hare Bay Granite, light purple = Fogo Harbour Formation, dark purple = Brimstone Head Formation).

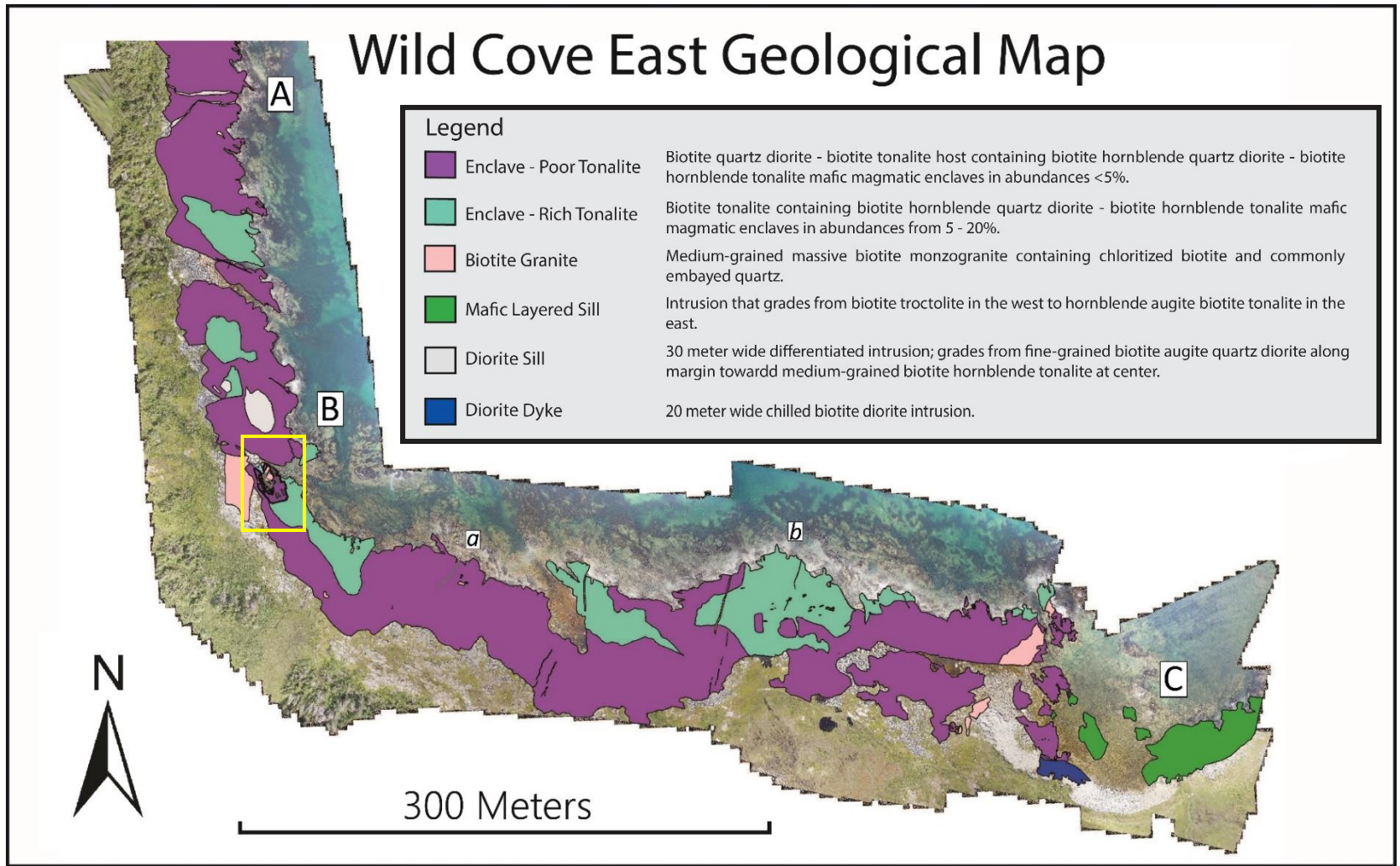


Figure 2.2. Geological map of Wild Cove East produced in ArcMap. Digital basemap produced by Cloudbreaker™ drone imagery. Yellow box denotes the location of the detailed map area described in Figure 2.3. The locations of three prominent intrusions are represented by: A (quartz diorite dykes; Figure 2.12), B (broken-up tonalite dyke; Figure 2.11), and C (mafic layered intrusion; Figure 2.14). The location with the highest abundance of metasedimentary xenoliths is represented by (a) and the location with the largest enclaves is represented by (b).

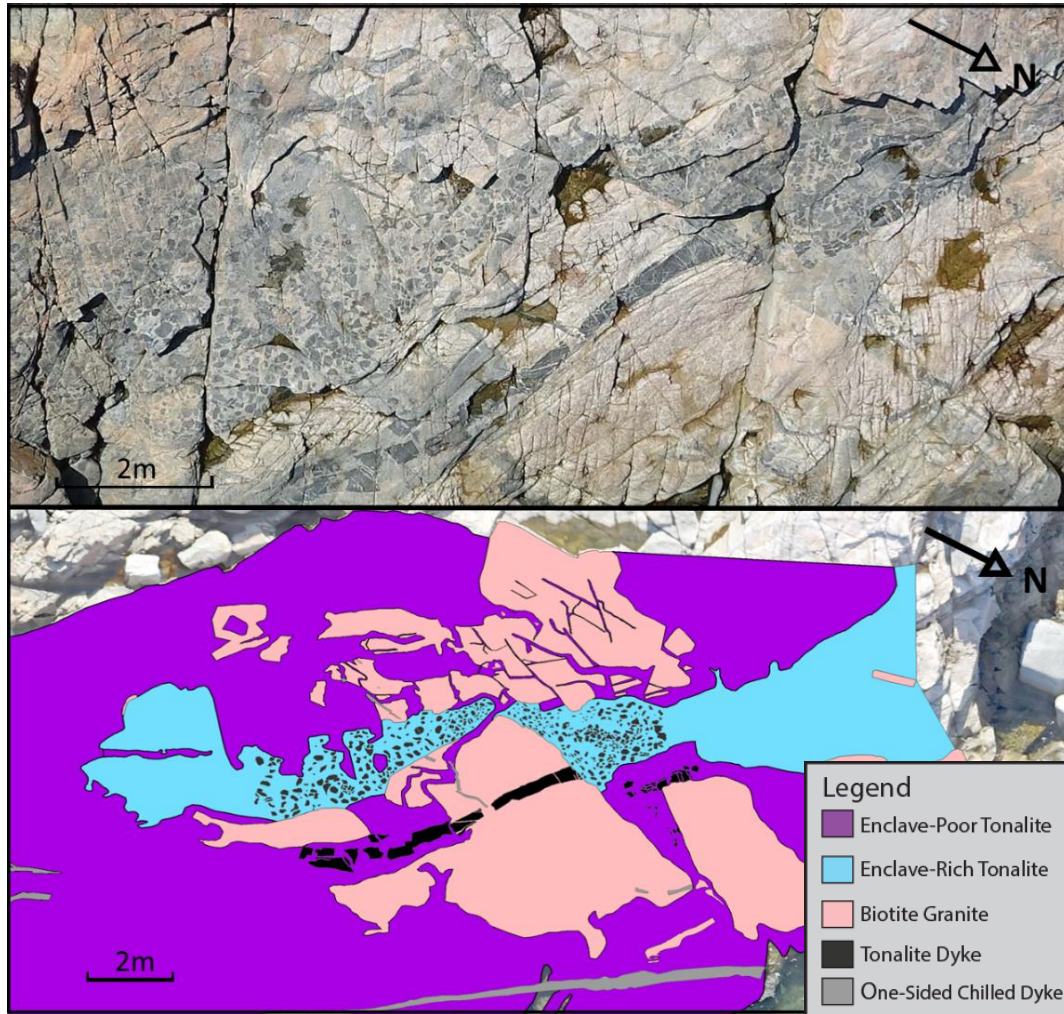


Figure 2.3. Photos of detailed map area. Above) Drone aerial photo (25-meter elevation) of detailed map area. Below) Digital map of area produced in ArcMap. In addition to hand-drawn grid based maps, the drone aerial photo (above) was used as an aid during digitization of data into ArcMap.

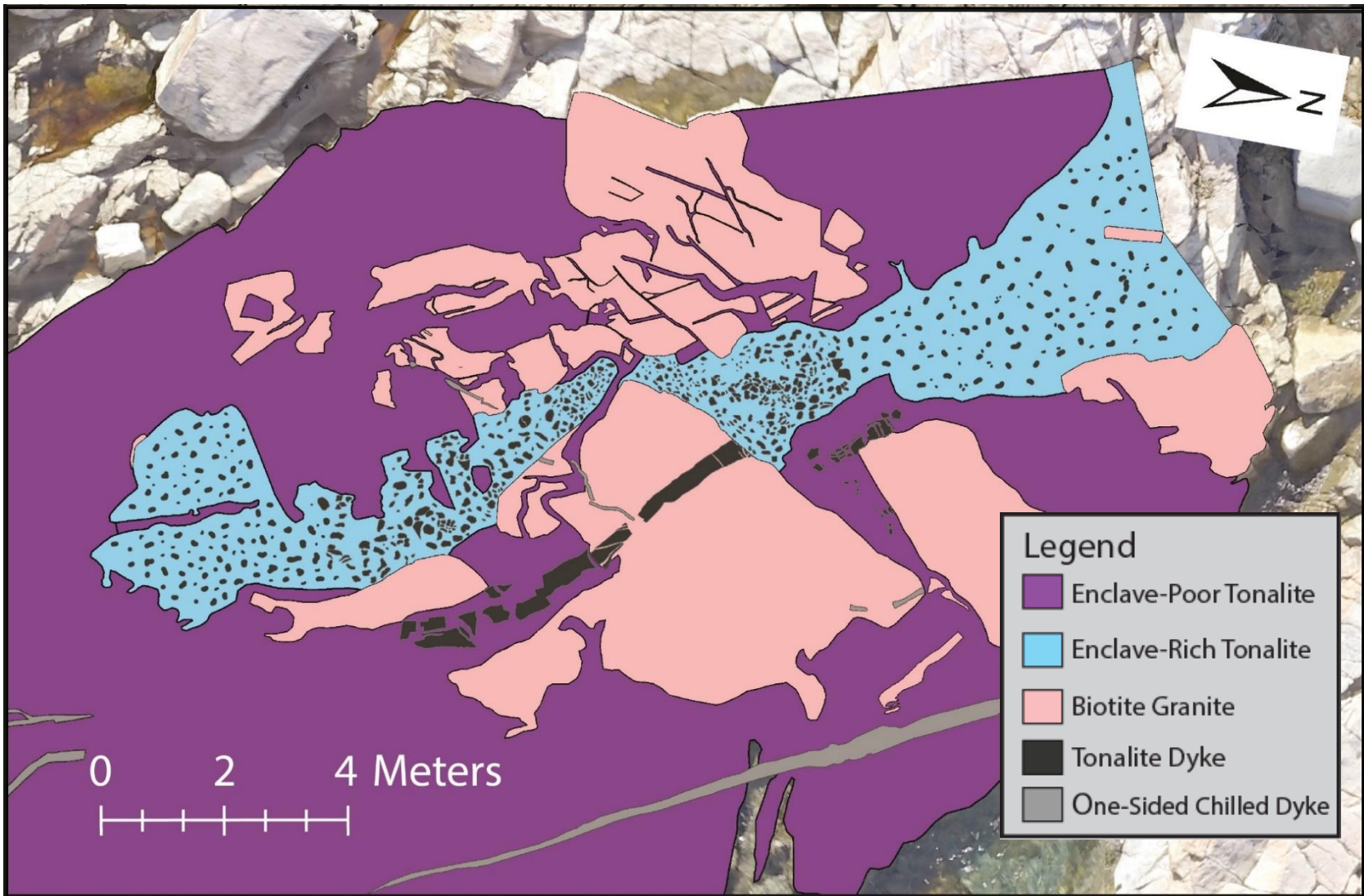


Figure 2.4. Geological map of detailed map area produced in ArcMap. Granite (pink) is interpreted to represent the oldest unit in the map area since it is intruded by both the enclave-poor tonalite (purple) and the enclave-rich tonalite (blue) units, the latter representing the youngest unit in unit in this map. A broken-up synplutonic dyke (black) intrudes both the enclave-poor tonalite and terminates against the enclave-rich tonalite, thus it is interpreted that this dyke intruded before the intrusion of the enclave-rich tonalite but after the enclave-poor tonalite and granite units.

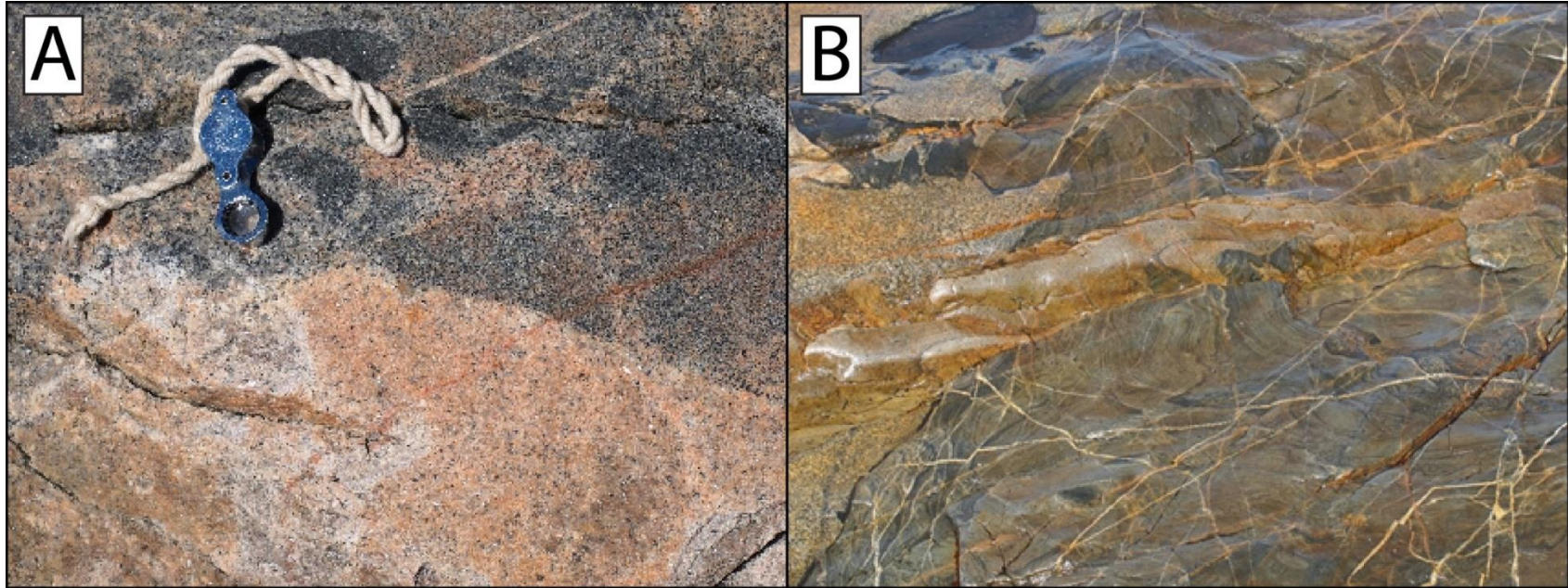


Figure 2.5. Field photographs of boudaries along biotite granite. A) Contact between biotite granite (bottom) and enclave-rich tonalite (top). The irregular nature suggests the biotite granite was partially melting along its contact due to the intrusion of the enclave-rich tonalite. B) Fine-grained angular metasedimentary xenoliths contained within biotite granite suggest a shallow setting for the study area close to walls or roof of the pluton.

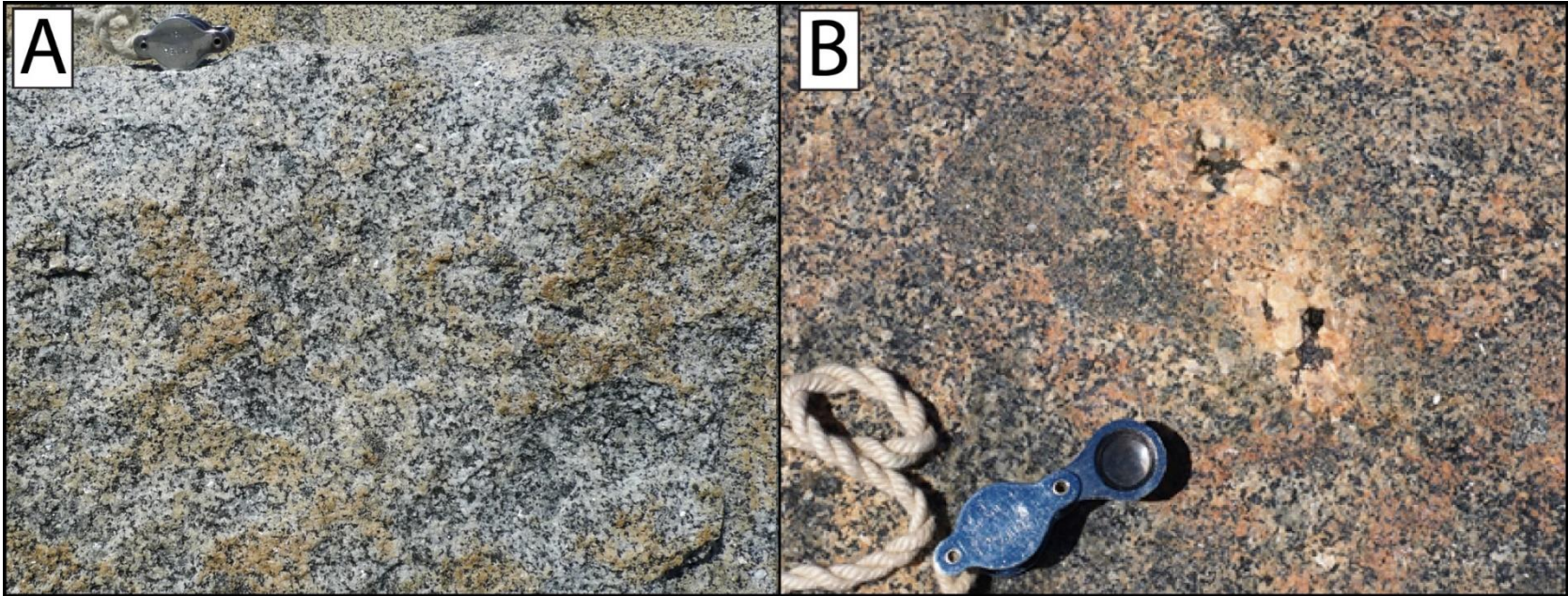


Figure 2.6. Field photographs of enclave-poor tonalite unit. A) Enclave-poor tonalite defined by homogeneous medium-grained plagioclase, quartz, and biotite, with minor pyroxene and hornblende. B) 5-10 cm wide miarolitic cavities are commonly observed in enclave-poor tonalite unit; composed of coarse-grained potassium feldspar, quartz, plagioclase, biotite, and hornblende.

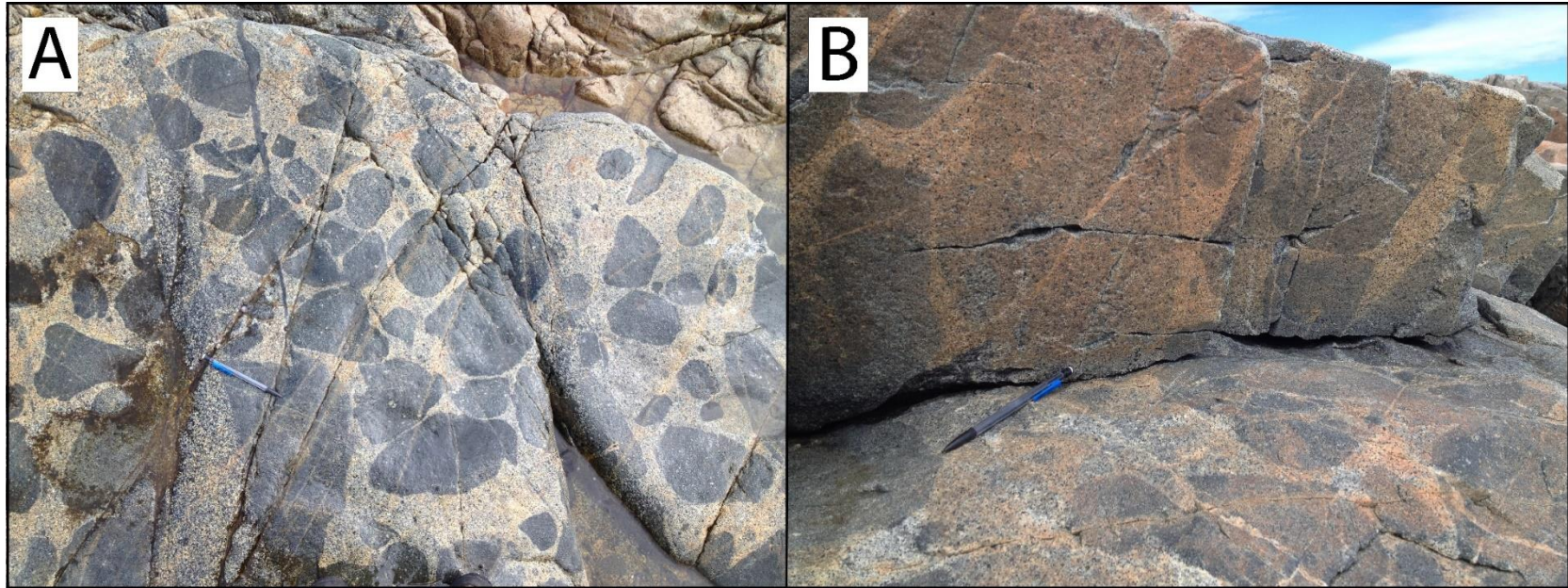


Figure 2.7. Field photographs of enclaves. A) Population of rounded enclaves within enclave-rich tonalite unit in the detailed map area. B) Near vertical elongation direction of enclaves within the enclave-rich tonalite unit in the detailed map area. Multiple populations of enclaves appear to be represented in this region based on differences in mineralogy and grain-size. The nearly vertical stretching direction of enclaves is consistent with other observations suggesting the enclave rich tonalite unit intruded vertically through the enclave-poor tonalite unit in this part of the study area.

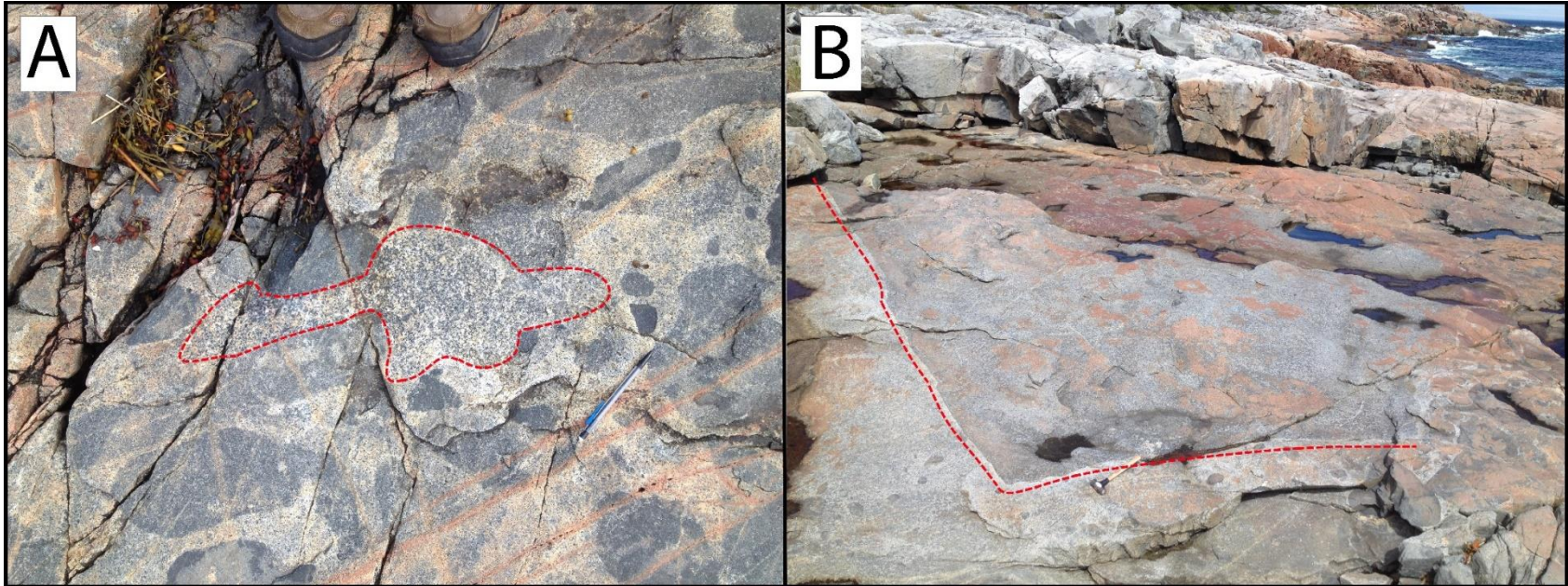


Figure 2.8. Field photographs of enclave-poor tonalite inclusions within enclave-rich tonalite host. A) Small inclusion of coarse-grained tonalite within medium-grained enclave-bearing tonalite. B) Large 3 meter wide angular “block” of coarse-grained tonalite within enclave-bearing tonalite on west side of study area (21N, 709660m E, 5511697m N). Both (A) and (B) may represent examples of stopping of enclave-poor tonalite by enclave-rich tonalite and suggest the enclave-rich tonalite is younger.

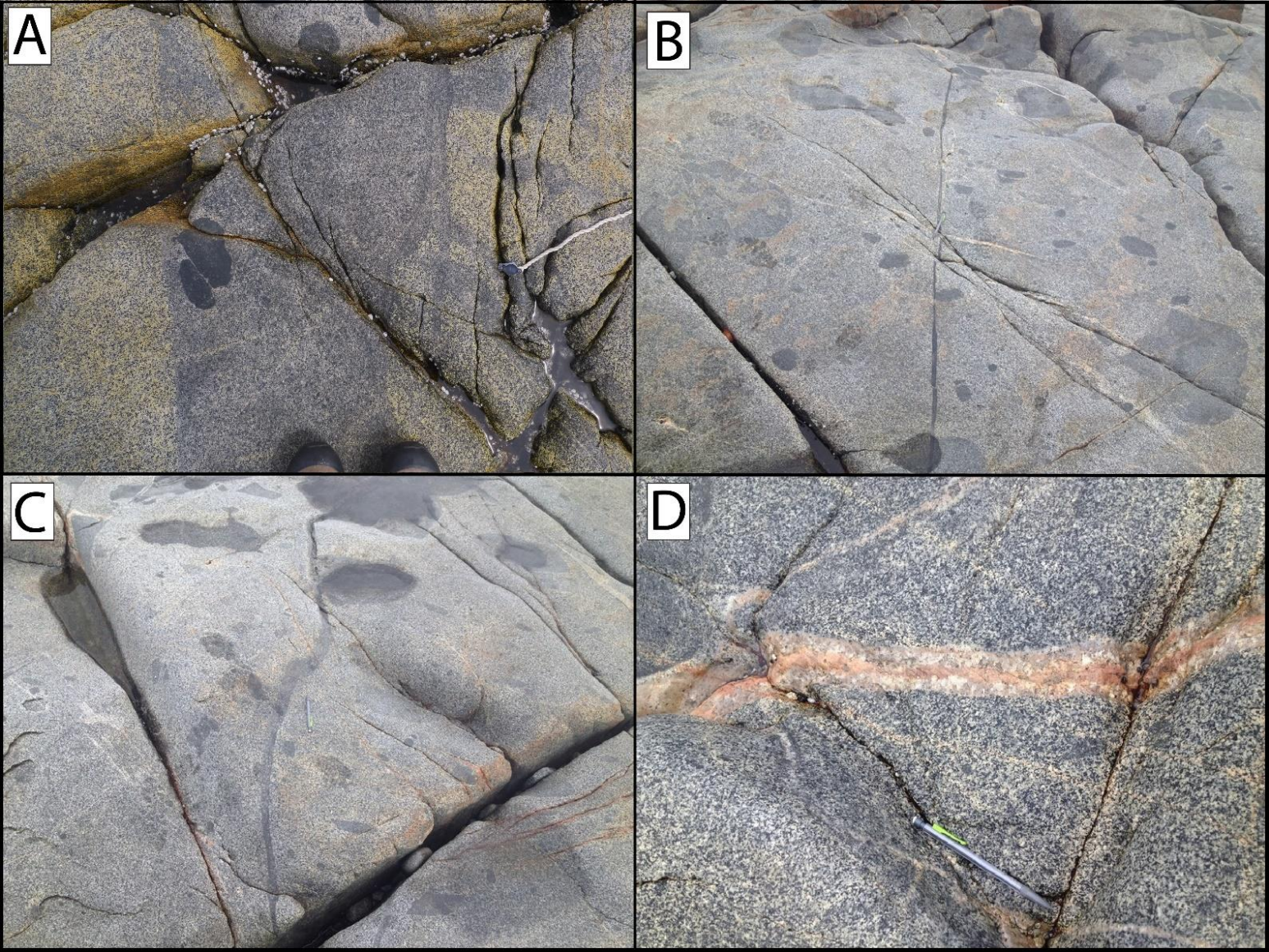


Figure 2.9. Examples of minor dykes located throughout the study area. A) Enclave-bearing tonalite intruding enclave-free tonalite. May represent the intrusion of enclave-bearing magma into a crystal solidification front at the roof of the chamber (Wiebe et al, 1997). B) Thin mafic intrusion into enclave-bearing tonalite host rocks. Slight brittle offset observed in the dyke may represent quenching. C) Thin curved mafic intrusion which likely intruded when the host crystal mush was still mobile. D) Felsic intrusion displaying aplitic cores and pegmatitic rims. May be related to partitioning of fluids a separate phases and being concentrated towards the rim of the intrusion.

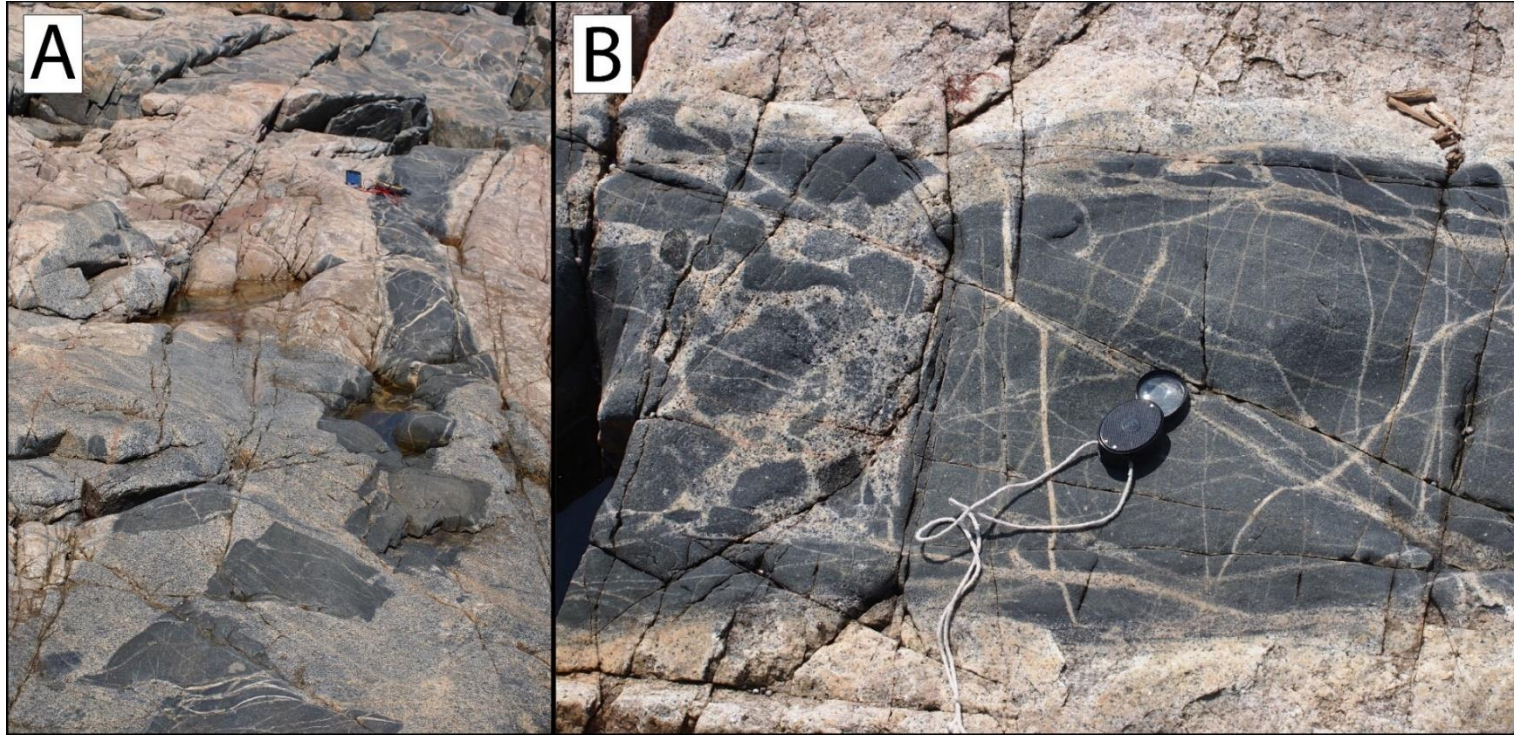


Figure 2.10. Field photographs of broken-up tonalite dyke in the detailed map area (Tonalite Dyke unit in Figure 2.4) that evidence of a relatively high rheological contrast between injecting and host magmas. A) Tonalite dyke pulled apart in quartz diorite unit whereas it is relatively coherent in granite unit. The dislocation of the dyke suggests the quartz diorite was a mobile mush at the time of intrusion that pulled the dyke apart after it quenched. B) Closer examination of same dyke in granite. Liquid from the granite mush has back-intruded the tonalite dyke after quenching and dislocation. This suggests the granite was also not completely crystalline at the time of dyke intrusion.

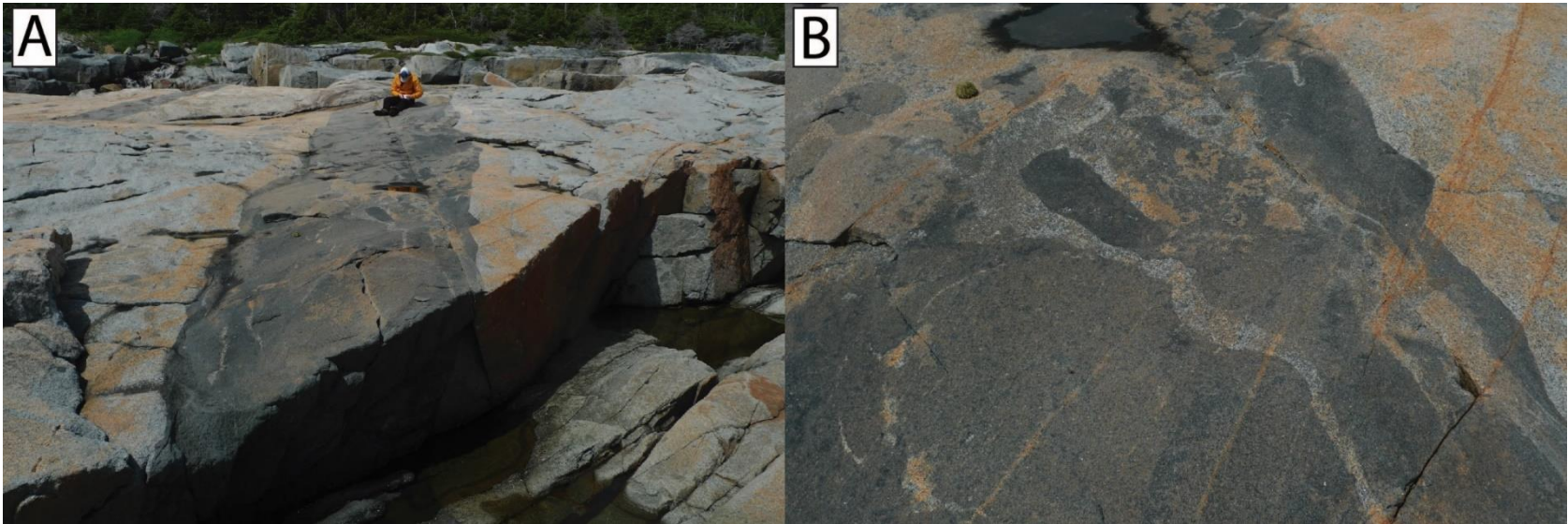


Figure 2.11. Field photographs of a quartz diorite dyke (A in Figure 2.2) that displays evidence of low rheological contrast between intruding and host magmas. A) Dark 2-meter wide quartz tonalite dyke intruding enclave-poor tonalite host on the northern end of the field area. The irregular shared boundary suggests the host was a mush at the time of intrusion. B) Evidence of localized breakup of quartz tonalite dyke into rounded globules, possibly representing a mechanism by which some enclaves were formed.

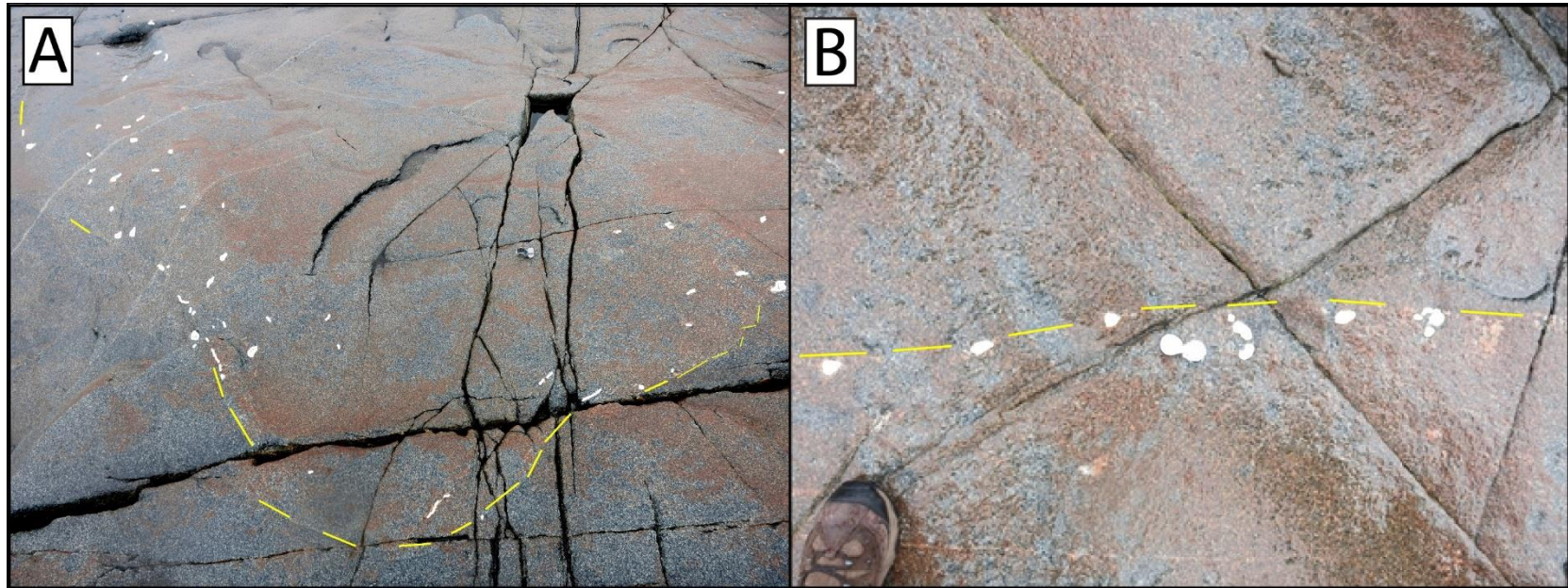


Figure 2.12. Photographs of structures suggesting pulsed input during intrusion of the diorite sill (B in Figure 2.2). A) Subhorizontal surface of the diorite sill (B in Figure 2.2) marked by small felsic segregations occurring along internal boundaries within the sill body. The appearance of felsic segregations suggest incremental pulse-like assembly of the sill. B) Close-up of line of felsic segregations along internal boundary.

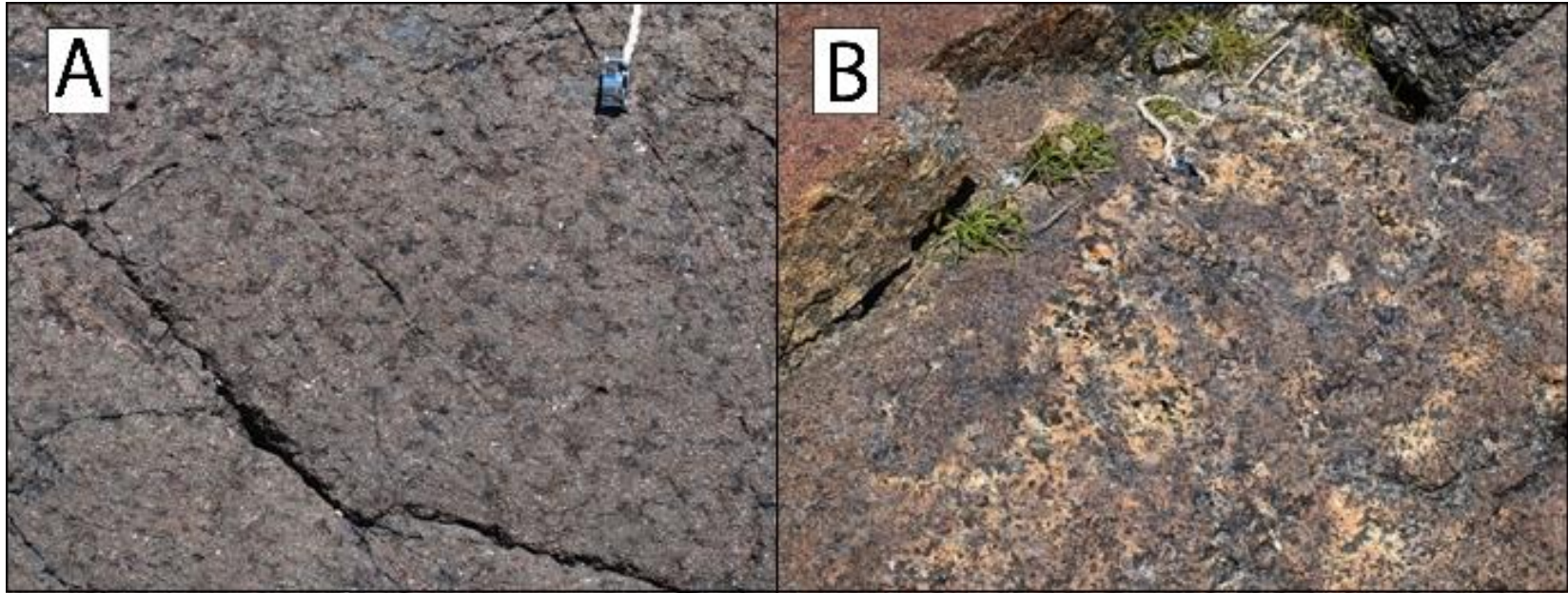


Figure 2.13. Photographs of mafic layered intrusion bordering the eastern end of the study area. A) Mineralogy defined by coarse hornblende oikocrysts. B) Hornblende pegmatite differentiate located towards center of mafic layered intrusion.

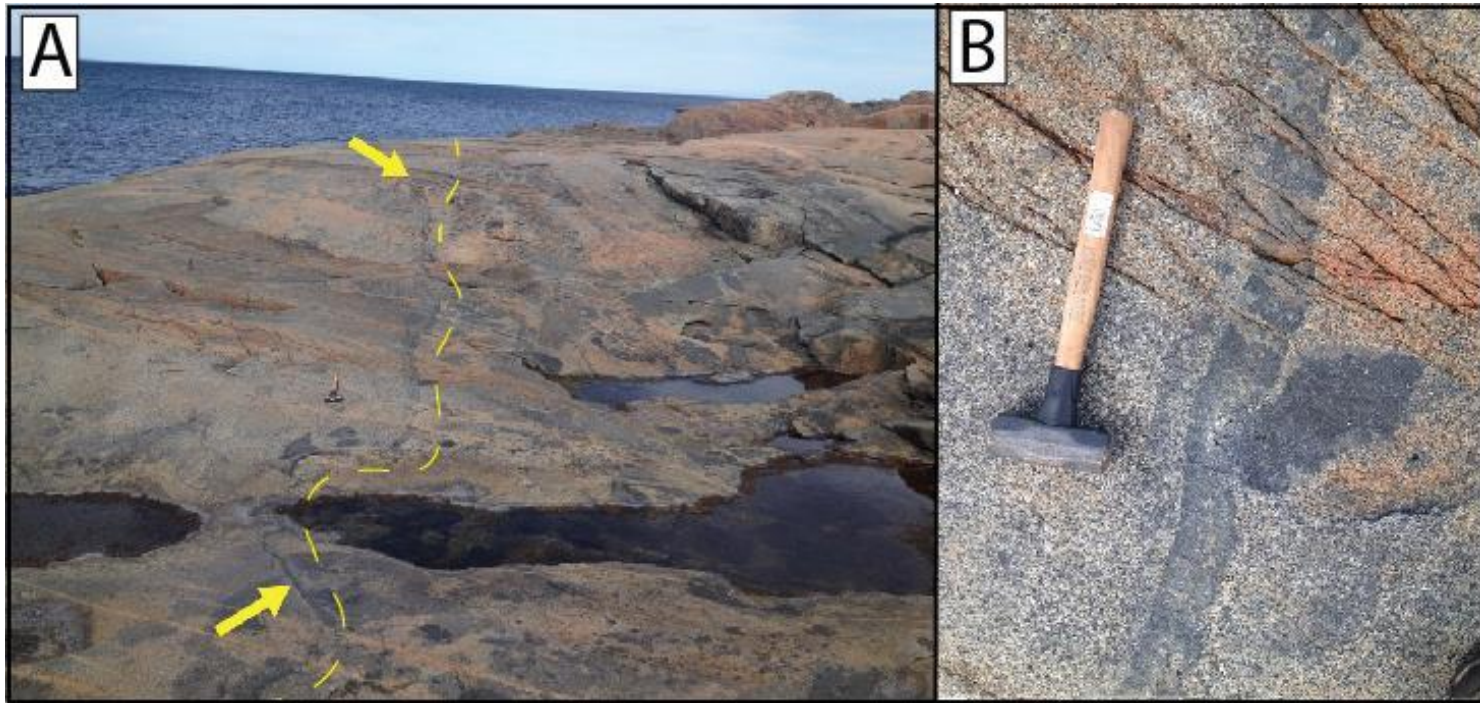


Figure 2.14. Field photographs of a visible contact between the enclave-poor tonalite and enclave-rich tonalite found in parts of the field area. A) Dipping irregular contact between enclave-rich tonalite (right) and enclave-poor tonalite. Contact is located to the left of the yellow line in photo. B) At the boundary (A) clinopyroxene crystals have accumulated as a layer. This layer has a sharp contact against the enclave-poor tonalite, whereas the other contact is cusped. A mafic magmatic enclave is seen impinging on the cusped edge.

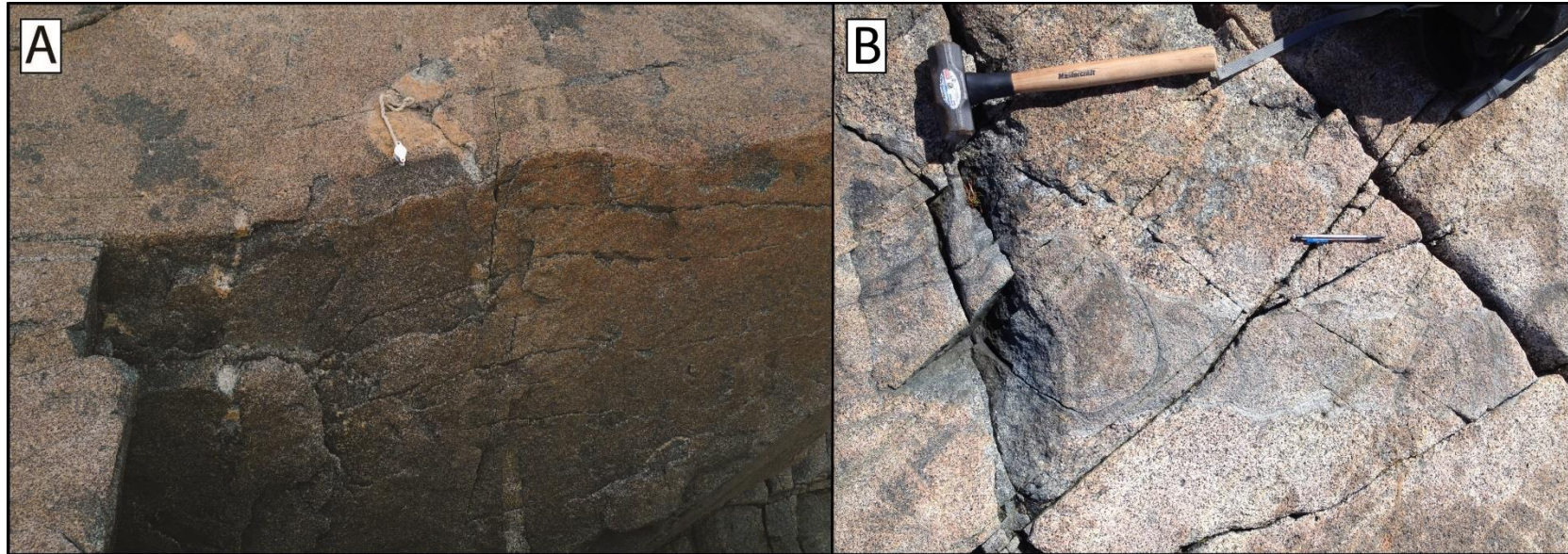


Figure 2.15. Structures suggestive of the movement of liquid and crystals within a mush are observed in the diorite sill (B in Figure 2.2). A) Magmatic pipes interpreted to form by buoyant rise of felsic magma through a more mafic host (Patterson et al, 2009); defines vertical way-up direction in this part of study area (hand lens for scale). B) Migrating magmatic tube structure defined by the buoyant rise of liquid and crystals through a mineralogically similar crystal mush due to processes such as compaction or filter pressing (Patterson et al 2009).

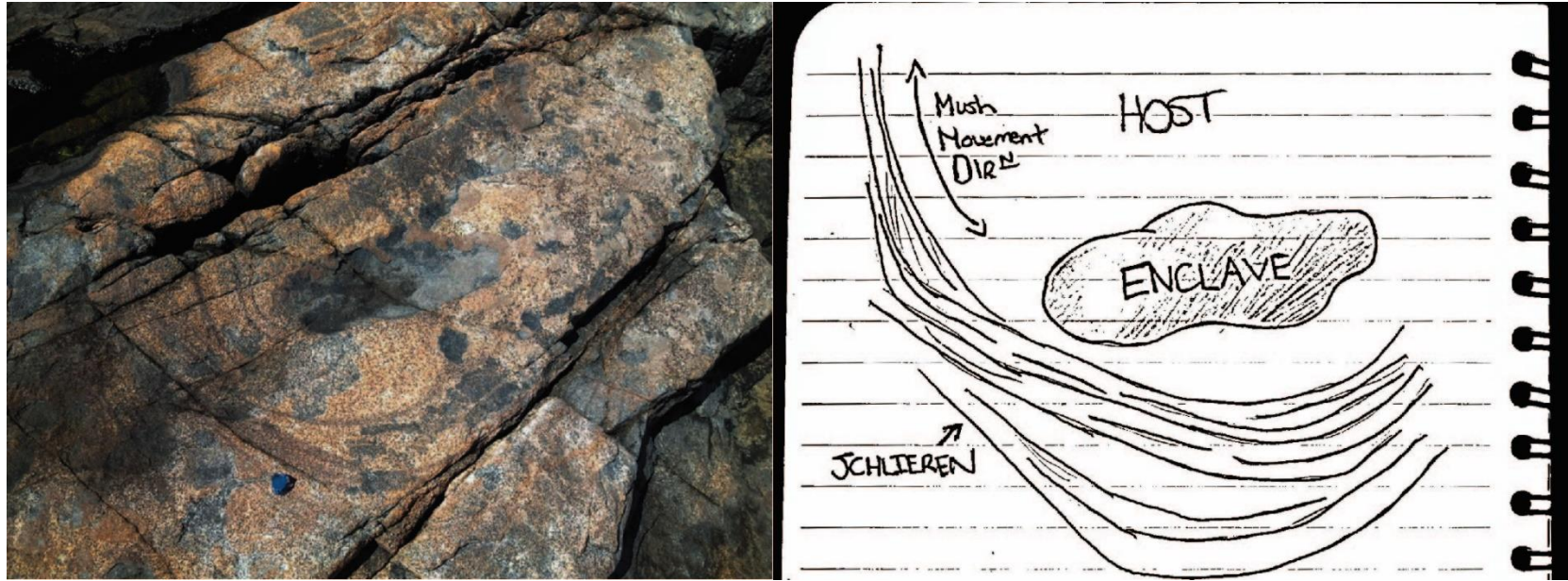


Figure 2.16. Schlieren defined by the alignment of mafic minerals that arise during the movement of crystal-rich magmas, are commonly observed in the enclave-rich tonalite unit. Left) Curved schlieren located near an enclave hosted in the enclave-rich tonalite. The schlieren appears to have formed due to differential motion (sinking, ascension, or lateral motion) between the enclave and host mush). Right) Field sketch depicting original interpretation.

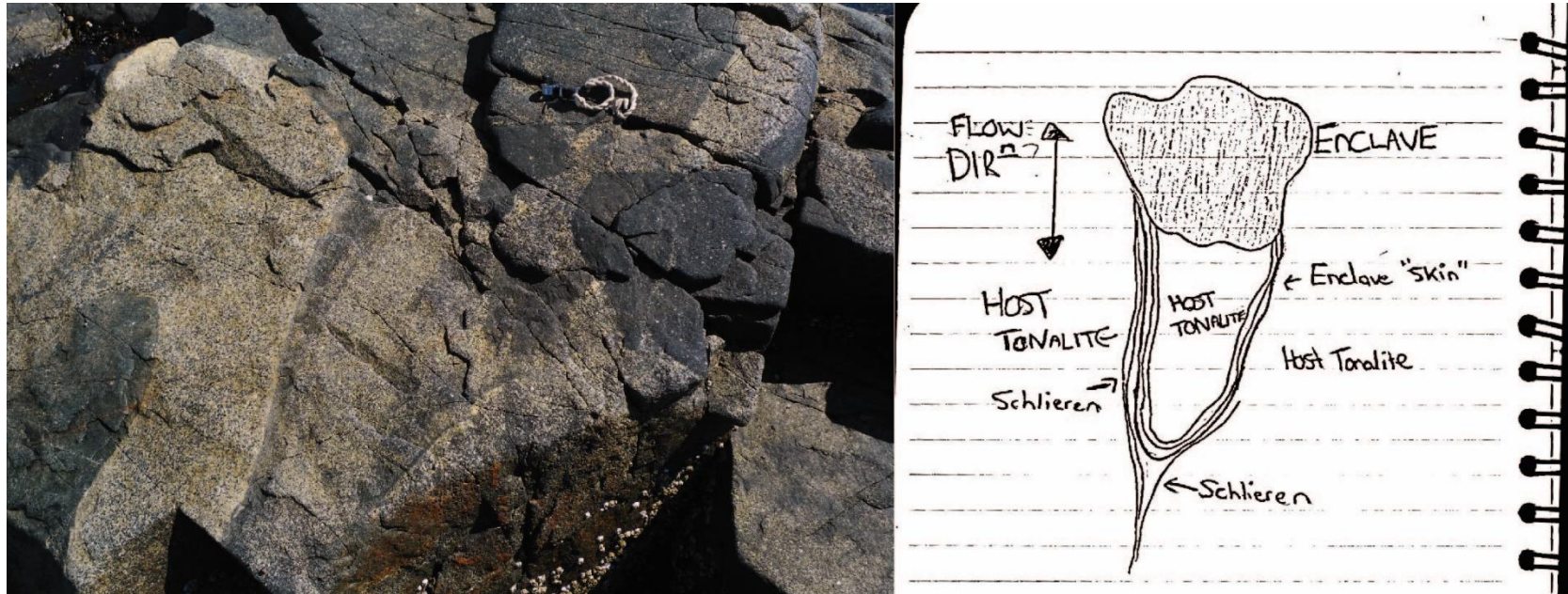


Figure 2.17. Left) Schlieren “tail” partially dragging behind enclave in enclave-rich tonalite mush. The schlieren in this example is abnormally thick and may represent the outer margin of the enclave being separated from the interior during its movement within mush. Right) Field sketch depicting original interpretation.

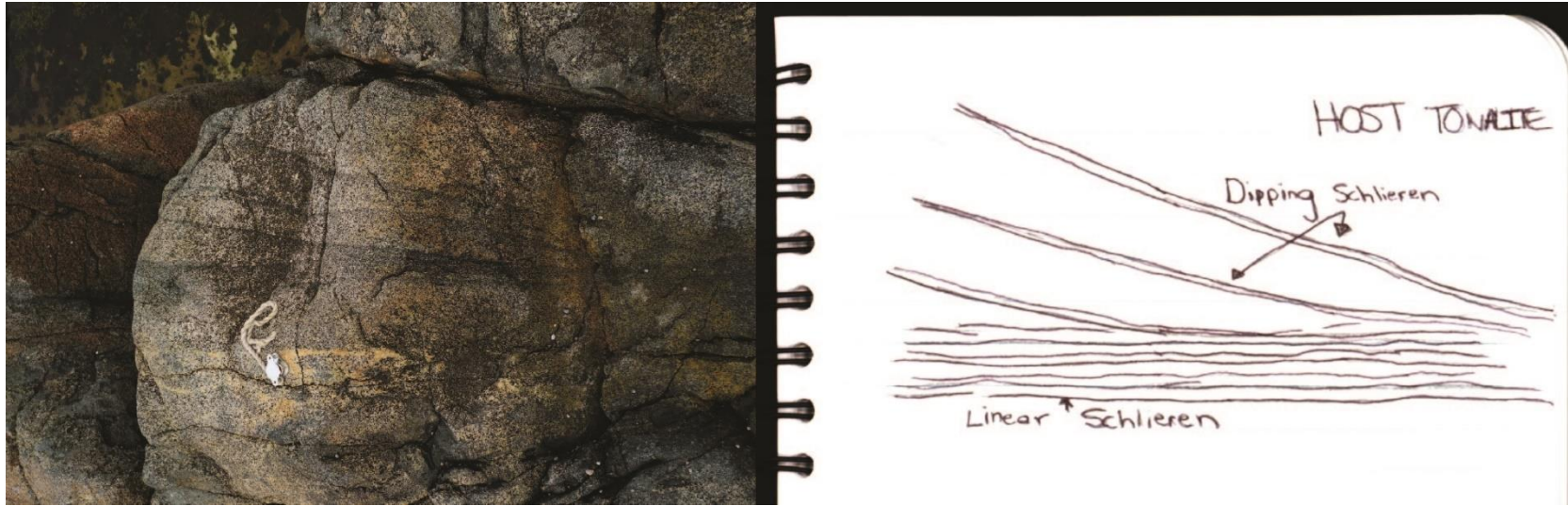


Figure 2.18. Field photograph of schlieren observed in the enclave-poor tonalite unit but are planar. Left) ~1-meter wide planar schlieren set observed in enclave-poor tonalite. The planar geometry and variably dipping beds may be indicative of erosion and deposition of minerals occurring within the host mush. Right) Field sketch depicting original interpretation.

Chapter 3 - Petrography

This chapter reports the results of petrographic examination of rocks from the study area. Various host rocks, enclaves, and dykes were sampled based on size, mineralogy, texture, and location. The general petrographic characteristics of host rock and enclave units are outlined in Table 3.1 at the end of this chapter. A total of eighty-five thin sections were examined (Table B.1 of Appendix B). Most samples were gathered using a hammer and chisel but, due to the limited vertical relief of outcrop in some locations, a portable diamond drill was used to obtain 2-inch diameter core samples of ~3-4-inch length at key locations that occur along flat outcrop. The diamond core drill uses a modified STIHL MS260 chainsaw engine and was invaluable for sampling across important unit contacts, many of which occur along flat outcrop. This chapter is divided into four sections reporting petrographic results for host rocks, enclaves, major dykes/sills, and important contacts. These results will be reported in order of oldest to youngest units.

3.1 Estimating Percentage of Early-Forming Euhedral Crystals

A rough estimate for the crystallinity of key units was obtained by point counting the number of euhedral early-forming crystals in representative thin sections. Plagioclase and clinopyroxene, based on petrographic relationships, are interpreted to be the earliest forming minerals in almost all units. Photomicrographs across the entirety of a thin section were stitched together using Adobe Photoshop. The most euhedral plagioclase

and pyroxene crystals were then outlined and the percent area of the thin section they represent was determined. This technique was applied to the enclave-poor tonalite host (Figure 3.1), the enclave-rich tonalite host (Figure 3.2), and two enclave samples (Figure 3.3 and Figure 3.4).

3.2 Host Rock Petrography

Sampling of host rocks was distributed along the entire length of the field area. A total of thirty-two host rock samples were collected, eighteen of which were thin sectioned. The host rocks are comprised of three main rock types: granite, quartz diorite, and tonalite. Due to high degrees of surface weathering and their overall similarity in appearance, it was not possible to differentiate quartz diorite from tonalite in the field. Instead, intermediate rocks were characterised by the relative abundance of mafic enclaves. As such, two intermediate host units are defined: enclave-rich tonalite (5-20% enclaves) and enclave-poor tonalite (<5% enclaves). All host rocks are lighter in colour and coarser-grained than the MMEs they contain. This lighter colour is attributed to host rocks generally containing lower modal abundances of hornblende compared to the enclaves. In this section, the petrography of three major host rock units will be described: biotite granite, enclave-poor tonalite, enclave-rich tonalite.

3.2.1 *Biotite Granite*

The biotite granite unit outcrops locally in both the central and easternmost parts of the study area. In the east, the unit occurs as a 20-30-meter-wide dyke that cuts the enclave-rich tonalite and locally cuts between the two major tonalite host units. The unit also occurs as a thin gently-dipping sheet in the detailed map area of Figure 2.4. The major minerals comprising this unit are quartz (~40%), potassium feldspar (35-40%), plagioclase (20-25%), and minor biotite (<5%). Quartz, potassium feldspar, and plagioclase are generally anhedral and rounded suggesting the bulk of crystallization occurred at the same time. Quartz generally occurs in coarse-grained clusters and are commonly embayed along shared boundaries with potassium-feldspar and other quartz (Figure 3.5A). Like quartz, both feldspars are commonly rounded and lack euhedral faces (Figure 3.5B).

3.2.2 *Enclave-Poor Tonalite*

The enclave-poor tonalite unit ranges in composition from biotite quartz-diorite to biotite tonalite. It generally has lower SiO₂ contents and a considerably higher proportion of euhedral plagioclase than the enclave-rich tonalite unit (yellow outline in Figure 3.1). In addition to being in the groundmass, plagioclase occur as phenocrysts that are subhedral and tabular (Figure 3.6A). Many crystals display complicated zoning and resorption patterns (Figure 3.6B). However, there is variability in the amount of resorbed plagioclase between thin sections taken from different parts of the unit. The most

common crystals to display internal mottling are plagioclase phenocrysts, which typically contain abundant inclusions of acicular apatite. Groundmass plagioclase is subhedral elongate to tabular and is commonly embayed. Quartz occurs as late interstitial grains or as medium to coarse grained rounded amoeboid crystals. Some quartz display undular extinction suggesting stress after crystallization. The percentage of euhedral early-forming crystals, represented by the resorbed cores in plagioclase, is estimated to be between 15-20% (red outline in Figure 3.1).

Mafic minerals in the enclave-poor tonalite represent approximately 30% of the total modal abundance. Biotite is the most abundant mafic mineral (15%) followed by hornblende (~10%) and clinopyroxene (~5%). Biotite is subhedral elongate and commonly occurs within mafic clusters with hornblende and pyroxene. Biotite commonly contain sagenitic rutile/titanite inclusions and is often found mantling pyroxene or hornblende. Chloritization affects nearly all biotite regardless of sample location. Clinopyroxene is generally anhedral elongate or rounded; some have corroded cores mantled by hornblende and/or biotite whereas others are unaltered. In general, altered clinopyroxene occur in clusters with other clinopyroxene and mantled by hornblende and/or biotite.

3.2.3 Enclave-Rich Tonalite

The enclave-rich tonalite is defined by a high abundance of mafic enclaves that represent 5-20% of the exposed surface area. Petrologically, the unit contains the same

minerals in similar relative abundances to the enclave-poor tonalite. The unit is texturally distinct from the enclave-poor tonalite, particularly in plagioclase, as crystals are generally anhedral and rounded. The dominant minerals include plagioclase and quartz in addition to biotite (~10%), clinopyroxene (<5%), and hornblende (<5%). Using the technique explained in section 3.1, the percentage of euhedral early-forming crystals is estimated to be approximately 20% (see Figure 3.2).

Plagioclase occurs as medium to coarse grained (20-50 μm) crystals that are generally rounded and lack well-defined crystal faces (Figure 3.7A), as opposed to the euhedral plagioclase in the enclave-poor tonalite. The most euhedral crystals generally display a preferred alignment. Patchy zoning and mottled cores are common in plagioclase crystals (Figure 3.7B). Multiple stages of resorption/overgrowth are observed in some plagioclase whereas others show none. Minor clinopyroxene and stubby apatite crystals occur as inclusions in some crystals. Quartz occurs interstitially to larger plagioclase crystals and commonly displays undulose extinction (Figure 3.7C).

The relative abundances and textures of mafic minerals observed in the enclave-rich tonalite are nearly identical to those seen in the enclave-poor tonalite unit. Biotite, pyroxene, and hornblende generally occur together in clusters at low abundances with biotite being the most abundant (~10%). The timing of biotite crystallization appears to be coeval with late plagioclase based on shared anhedral crystal faces. Inclusions in biotite include saogenitic rutile/titanite and rounded Fe-Ti oxides. Minor clinopyroxene occurs as

rounded to elongate anhedral crystals, some of which display a thin hornblende and/or biotite rim (Figure 3.7D).

3.3 Enclave Petrography

Twenty-two enclave samples were thin sectioned to estimate the range in enclave compositions. Samples were chosen based the range of mineralogy and textures that were observed across the entirety of the study area. Samples were initially divided into three groups based on field observations: a) fine-grained dark enclaves with feldspar phenocrysts (Group 1), b) fine-grained dark enclaves that lack feldspar phenocrysts (Group 2), and c) medium-grained enclaves that are similar in colour to surrounding host rock (Group 3). These groupings are consistent with the petrography and each exhibit different mineralogy, textures and grain size.

3.3.1 Group 1 Enclaves

Group 1 enclaves are fine-grained, rounded/ellipsoidal, and are considerably darker than their host rocks. Enclaves are generally stretched in a direction that is parallel to flow foliation in surrounding host rocks. Boundaries between Group 1 enclaves and host rocks are sharp and unchilled. Samples of Group 1 enclaves were obtained in the enclave-rich tonalite in both the central and easternmost part of the field area.

Petrographically, they are characterized by a fine- to medium-grained groundmass containing anhedral rounded plagioclase along with zoned plagioclase phenocrysts. Other distinguishing features include a high abundance of hornblende-mantled clinopyroxene and comparatively low amounts of apatite/Fe-Ti oxide inclusions. The major minerals seen in this group include: quartz (~35%), plagioclase (~30%), hornblende (15%), biotite (10%), clinopyroxene (~5%), and minor orthopyroxene (<5%). Accessory minerals include: apatite, rutile, titanite, zircon, epidote, hematite, ilmenite, and magnetite. Like most intermediate rocks in the study area, enclaves belonging to this group vary slightly in composition from quartz diorite to tonalite. Using the technique described in section 3.1, percentage of euhedral crystals in this group of enclaves is estimated to be between 10-20% (Figure 3.3).

Plagioclase phenocrysts (~1000 μm diameter) are abundant and noticeably larger than groundmass plagioclase (100-250 μm diameter). Phenocrysts commonly contain tiny round clinopyroxene inclusions that are otherwise not found in groundmass plagioclase (Figure 3.8A). The phenocrysts commonly contain irregular mottled cores. Clinopyroxene inclusions are generally restricted to the resorbed regions of plagioclase phenocrysts, and may have crystallized from trapped liquid after plagioclase resorption. (Wiebe, 1968). The unaltered nature of the clinopyroxene inclusions suggests plagioclase shielded them from later hydrous reactions that affected other clinopyroxene in the rock. In some cases, a similar extinction orientation is shared between different clinopyroxene inclusions within the same plagioclase phenocryst, suggesting the inclusions may represent corroded

remnants of originally coarser contiguous crystals. Large embayments occur between phenocrysts and groundmass implying that the latest phase of phenocrysts growth was roughly coeval with groundmass crystallization.

Matrix plagioclase grains are generally rounded to subhedral and do not display obvious elongate habit. Normal and reverse zoning is seen in both the matrix grains and in phenocrysts. Normal zoning likely represents the incomplete reaction between growing crystals and fractionating melt in a cooling magma (Wiebe, 1968). Reverse zoning, however, is related to temperature and pressure increases under water-saturated conditions due to ascent or mafic recharge (Blundy *et al*, 2006; Streck, 2008). Quartz commonly occurs as anhedral interstitial grains, representing the last phase of crystallization, and commonly display undulose extinction (Figure 3.8B).

In order of decreasing modal abundance, the mafic minerals that make up Group 1 enclaves are: hornblende (~15%), biotite (~10%), clinopyroxene (~5%), and orthopyroxene (<5%). Pyroxene are rounded or elongate but are commonly corroded and mantled by hornblende due to hydrous reactions. In general, the thickness of the hornblende mantle increases with grain size of the original pyroxene. Several pyroxene crystals display distinct zonation patterns reflecting complicated growth histories (Figure 3.8C). Biotite occur as pale brown subhedral crystals that contain moderate degrees of subsolidus chlorite alteration. Euhedral faces are usually observed against quartz whereas faces are generally embayed against plagioclase and orthopyroxene. Inclusions of acicular apatite along with rounded epidote, quartz, and ilmenite/magnetite are commonly seen

in biotite. Grains oriented perpendicular to {001} commonly display sagenitic rutile and titanite inclusions, indicating that biotite is oversaturated in Fe and Ti (Figure 3.8D).

3.3.2 *Group 2 Enclaves*

Group 2 enclaves are rounded/ellipsoid shaped blobs that are finer-grained and darker than their hosts and contain unchilled cusped boundaries. This second group of enclaves is characterized by a high abundance of euhedral elongate plagioclase, higher combined modal percentages of hydrous minerals (biotite and hornblende), and larger amounts of apatite/Fe-Ti oxide inclusions in comparison to Group 1 enclaves. Enclaves belonging to this group represent the most common type and are found in both enclave-poor tonalite and enclave-rich tonalite throughout the entire study area. Like Group 1 enclaves, this group exhibits a limited compositional range from quartz diorite - tonalite. Using the technique described in section 3.2, the percentage of euhedral early-forming crystals in Group 2 enclaves is between 25-35%, which are higher than average Group 1 values (see Fig 4.)

Plagioclase and quartz are, as in Group 1, the most common minerals in this group and display the most complicated textures. Plagioclase occurs both in a medium grained groundmass (25-100 μm) and as coarse phenocrysts (200-500 μm). The phenocrysts generally display textures suggestive of disequilibrium crystallization. For example, the phenocryst illustrated in Figure 3.9A displays patchy zoned faces that are cut-off by a non-

zoned twin. Relict euhedral faces can be seen within the interior of coarse plagioclase, but a late anhedral rim usually occurs suggesting the latest phases of plagioclase crystallization occurred at the same time as other minerals in the rock (biotite, hornblende, and orthopyroxene). Like Group 1, many plagioclase phenocrysts contain mottled internal zones that show evidence of resorption (Figure 3.9B). Apart from the rims, plagioclase phenocrysts generally contain fewer clinopyroxene and apatite inclusions than groundmass plagioclase. The groundmass is composed of hypidiomorphic plagioclase that generally display a preferred alignment suggesting flow of the enclave magma.

The enclaves of the Group 2 contain similar modal proportions of mafic minerals to Group 1: hornblende (~20%), biotite (~10%), clinopyroxene (~5%) and orthopyroxene (<5%). All four minerals generally occur in clusters with each other. Hornblende commonly mantles clinopyroxene cores suggesting clinopyroxene was among the earliest forming minerals (Figure 3.9C, 3.9D). Where not mantled by hornblende, clinopyroxene occurs as small round crystals. Clinopyroxene commonly occurs as corroded inclusions in biotite, suggesting it was amongst the earliest phases to crystallize in the enclave magma. Magnetite, ilmenite, and apatite commonly occur as inclusions in clinopyroxene.

Large biotite (up to 3mm) are generally “broken-up” by other minerals including plagioclase, quartz, clinopyroxene, and hornblende. Biotite are generally anhedral but elongate crystals do occur. Crystals are commonly embayed against plagioclase but, in some cases, share euhedral crystal faces. This suggests two generations of biotite

crystallization: the first occurring at the same time as plagioclase (euhedral boundaries) and the second occurring after plagioclase crystallization (anhedral boundaries). Biotite inclusions include: magnetite, titanite, rutile, ilmenite, and apatite commonly occur as inclusions in biotite. Chlorite alteration occurs as a jagged-teeth pattern on some grains. Some crystals contain sagenitic titanite and rutile inclusions.

Hornblende commonly occurs as reaction rims around clinopyroxene but many crystals are solitary and display euhedral crystal faces against biotite and quartz. The solitary crystals are generally more euhedral than those mantling clinopyroxene suggesting the solitary crystals formed first and/or represent complete hydrothermal replacement of clinopyroxene by hornblende. Acicular apatite, ilmenite, and magnetite commonly occur as inclusions. Many crystals have been affected by patchy subsolidus chlorite alteration.

3.3.3 Group 3 Enclaves

The most distinct of the enclave groups is the third group, which is characterized by equigranular unaltered rounded clinopyroxene (Figure 3.10A), low abundances of hornblende, a preferred alignment of euhedral groundmass plagioclase laths, and very high amounts of apatite and Fe-Ti oxide inclusions. This group represents the most mafic (diorite – quartz diorite) enclaves and contain the highest amount of euhedral plagioclase.

Despite being darker, this group is the closest in grain-size to surrounding host rocks when observed in the field and enclaves are generally round.

Groundmass plagioclase display hypidiomorphic elongated habit whereas euhedral phenocrysts are generally tabular. As in the other enclave groups, plagioclase phenocrysts commonly display oscillatory zoning, mottled cores, and embayed margins (Figure 3.10B). In addition, some phenocrysts have rims that are texturally distinct from their cores. For example, pyroxene, Fe-Ti oxide, and apatite inclusions are commonly restricted to the rims of some phenocrysts (Figure 3.10C, 3.10D). Groundmass elongate plagioclase laths commonly display a preferred alignment. Acicular apatite inclusions within groundmass plagioclase occur in much higher abundance than in the other enclave groups.

3.4 Dyke and Sill Petrography

Across the study area exist several dykes and sills that, based on their field and petrographic characteristics, intruded at various times throughout the rheological evolution of the tonalite crystal mush reservoir. This section will examine the petrographic nature of the most prominent dykes and sills in the map area including: a dislocated tonalite dyke in the detailed map area (“Tonalite Dyke” in Figure 2.4), a pair of quartz diorite dykes displaying evidence of enclave formation (A in Figure 2.2), a diorite sill in the west (B in Figure 2.2), and a mafic layered intrusion in the east (C in Figure 2.2).

3.4.1 *Dislocated Tonalite Dyke*

In the detailed map area of Figure 2.4, a broken-up tonalite dyke is seen that had been dislocated after quenching due to movement in the host mush magmas (Figure 2.11A). The dyke is primarily composed of plagioclase, clinopyroxene, quartz, and potassium feldspar. In general, grain size is very fine (15 μm) and equigranular between plagioclase, quartz, and clinopyroxene (Figure 3.11A). Plagioclase and clinopyroxene occur as subhedral rounded to elongate grains. Euhedral faces are most commonly seen against quartz. Both quartz and sparse potassium feldspar occur interstitially between plagioclase and clinopyroxene. Interstitial potassium feldspar may indicate back-intrusion of liquid from the biotite granite through which the sampled part of the dyke is intruding (Figure 3.11B).

3.4.2 *Quartz Diorite Dykes*

A pair of quartz diorite dykes in the northernmost part of study area show local break-up into rounded globules (Figure 2.12A), suggesting a mechanism by which enclaves were formed. The dykes are composed primarily of plagioclase, quartz, biotite, hornblende, and clinopyroxene. Plagioclase occurs both in the groundmass (100-250 μm) and as phenocrysts (1000-1500 μm). The phenocrysts are highly euhedral with elongate or tabular habit and ubiquitously display oscillatory zoning and resorbed cores. Inclusions of clinopyroxene, apatite, and Fe-Ti oxides are commonly seen restricted to the rims of phenocrysts. Some phenocrysts, however, have large core regions that are full of

inclusions (clinopyroxene, Fe-Ti, and apatite), a middle region containing no inclusions, and an inclusion-rich rim. Core regions appear mottled in cross polarized light in comparison to the middle inclusion-free zone (Figure 3.12A). Fe-Ti oxide inclusions in the rim region are fine and generally only found immediately adjacent to the boundary with the core region. The elongate plagioclase phenocrysts display a preferred orientation. Groundmass plagioclase are anhedral and occur within interstitial quartz. High amounts of acicular apatite inclusions are contained within groundmass plagioclase.

The most abundant mafic minerals in dykes are biotite, hornblende, and clinopyroxene. Subhedral biotite is highly abundant in the groundmass is generally found in clusters with other biotite or with hornblende (Figure 3.12B). Crystals are anhedral elongate or rounded and all are at least partially chloritized. Rounded Fe-Ti oxide chadacrysts are commonly found and occasionally occur as “stringer-like” exsolutions along the c-axis in clinopyroxene. Zoning is seen in some of the larger rounded clinopyroxene crystals. Simple twinning is observed in many clinopyroxene crystals.

3.4.3 Diorite Sill

One of the few units in the study area to display a chilled margin is a small diorite sill in the eastern part of the study area (grey unit in Figure 2.2). The sill is composed of primarily of plagioclase and clinopyroxene, some of which are compositionally zoned. The most striking feature of this rock is the very high abundance of opaque minerals

(magnetite, ilmenite, pyrite) which comprise at least 10 % of its modal abundance. The opaque minerals range from rounded to elongate and occasionally display symplectite textures in plagioclase. A very high abundance of acicular apatite is also seen, particularly in the chilled margin of the intrusion, and likely represents quenching of the sill against its host. The center of the sill appears to be slightly more differentiated with higher modal abundances of quartz and lower abundances of clinopyroxene. There are several locations near-circular areas within the section which lack oxide minerals entirely and are composed of quartz and plagioclase. Apatite inclusions are abundant in the center of the sill but generally occur as stubby coarse crystals rather than acicular grains seen in the chilled margin.

3.4.4 Mafic Layered Intrusion

Four samples were taken from the mafic layered sill at the east end of the study area. The base of the intrusion is of troctolite composition and is chiefly composed of olivine, orthopyroxene, and plagioclase (Figure 3.13A). Accessory minerals include clinopyroxene and biotite. Serpentinized disseminated olivine is contained within orthopyroxene and hornblende oikocrysts, suggesting olivine was the earliest mineral to crystallize. Both orthopyroxene and plagioclase commonly occur as coarse euhedral crystals, but plagioclase also occurs interstitially to both olivine and orthopyroxene. Biotite and clinopyroxene both display orange/red colouring in plane polarized light suggesting high Fe and Ti content.

Approximately 50 meters up from the base of the intrusion the textures of the rocks start to become more gabbroic. The cumulate textures in pyroxene and plagioclase at the base of the intrusion are no longer present. Instead, pyroxene occurs as small rounded crystals whereas plagioclase occurs as euhedral elongate laths (Figure 3.13B). Olivine becomes finer-grained, more disseminated, and displays higher degrees of serpentinization. Plagioclase similarly is more altered but still occurs interstitially to olivine. Both biotite and clinopyroxene lose the orange/red colouring seen in the base of the intrusion, suggesting they are not Ti-rich.

3.5 Unit Contact Petrography

Samples were collected across contacts between units to analyze the petrographic nature of mingled boundaries between: 1) enclaves and hosts, 2) dykes and hosts, 3) major host units. Consistent with field observations, the mingled contacts are almost always irregular at the thin section scale and chilled margins are absent in all examined samples (Figure 3.14A). In samples of contacts between enclaves and hosts, the following recurring observations were made: 1) enclaves are always finer-grained than their enclosing hosts with the exception of plagioclase phenocrysts which are approximately the same size, 2) major minerals like plagioclase are generally more rounded/anhedral in enclaves compared to hosts, 3) hornblende is more abundant in enclaves compared to

hosts, and higher amounts of hydrous minerals (biotite and hornblende) in enclaves occur proximal to the boundary with hosts (Figure 3.14B).

In addition to the grain size distinction, enclave-host rock boundaries in thin sections can usually be defined by the appearance of fine-grained inclusions (apatite and Fe/Ti oxides) on the enclave side of the contact but not the host side. Individual minerals that crystallized along this mingled contact can therefore be identified such as biotite that contain abundant titanite, rutile, and apatite inclusions on one side of the crystal but noticeably less on the other side (Figure 3.14C, 3.14D). Coarse-grained minerals such as plagioclase and biotite are generally elongated parallel to the contact itself.

In rare cases, crystals may have been displaced from one unit and incorporated into the other. Evidence of this is seen in the boundary between the enclave-poor tonalite and biotite granite, where interstitial potassium-feldspar is observed on the tonalite side of the boundary proximal to the boundary. Since potassium-feldspar is not observed in any samples taken from the interior of the enclave-poor tonalite unit, a possible explanation is that it was derived from the liquid from the granite during mingling of the two units. In addition to potassium-feldspar, fine-grained muscovite is seen in the tonalite near the mingled contact whereas it is otherwise absent in the rest of the enclave-poor tonalite unit.

3.6 Discussion

Petrographic examination of enclaves, host rocks, and dykes reveals a multi-stage crystallization history for many of these rocks. In nearly all units, early crystals such as plagioclase and clinopyroxene display textures suggesting changing liquid environments including: resorption/overgrowth sequences, patchy zonation, and inclusions being restricted to particular zones of a crystal (Chen *et al*, 2009). These textures indicate that both enclaves and host rocks experienced mixing earlier in their magmatic histories. Resorbed cores in plagioclase reflect rapid changes in temperature during crystallization. The variability in the amount of resorbed plagioclase within the enclave-poor tonalite may reflect heterogenous heat distribution throughout the crystal mush after mafic recharge (Burgisser and Bergantz, 2011).

Despite being compositionally similar, enclaves and host rocks can be distinguished due to enclaves always containing less silica and being finer-grained. On average, enclaves are 4% less silica-rich than their enclosing hosts. These observations fit the criteria for the definition of a mafic magmatic enclave as being “igneous bodies that are more mafic and finer-grained than their igneous hosts” (Barbarin, 2005). Enclaves almost ubiquitously contain higher modal abundances of hornblende than their hosts, explaining their darker colour in the field.

Enclaves and hosts are also characterized based on their estimated crystallinities. This was done by point counting the number of euhedral early forming minerals

(plagioclase and clinopyroxene) representing a rough estimate of the proportion of crystals to melt in the mush. It is important to note that this way of estimating the crystallinity, due to the high internal complexity of the units, is not an accurate representation of the crystallinity at the time of emplacement for each unit but provides a qualitative petrographic property that can be distinguished between them. The enclaves, which are expected to have cooled rapidly once they were enclosed in a cooler host at shallow crustal depths, rather than the larger host rock units which may have been reheated due to mafic recharge and were likely affected by crystal settling and compaction (Marsh, 2002; Streck, 2008). Processes such as crystal settling and compaction appear to have been particularly important in the enclave-poor tonalite unit, based on its high quantity of euhedral crystals. For this reason, the volume of resorbed plagioclase cores in host rocks are interpreted to be a better estimate of the crystallinity at the time of emplacement. The enclave-rich tonalite and enclave-poor tonalite are estimated to have had similar crystallinities (approx. 15-20%) based on the volume of clinopyroxene and resorbed plagioclase cores, interpreted to be the earliest forming minerals in both units.

Enclaves can be grouped based on petrographic observations including mineralogy, mineral textures, and estimated emplacement crystallinity. This suggest multiple enclave populations occur throughout Wild Cove East and represent multiple distinct magmas that existed at deeper crustal levels. A process such as convection likely acted to stir the different enclave populations together and carry them to the current

interpreted shallow level (Hodge *et al*, 2012). Based on their estimated emplacement crystallinity, possible mechanisms for enclave formation include: 1) the disaggregation of a previously existing crystal mush due to forceful injection of new magma, or 2) the breakup of crystal-poor mafic dykes due to rheological instability as they intrude a more viscous felsic magma (Wiebe *et al*, 1997). The first scenario may represent the more crystalline enclaves of Group 2 and Group 3 whereas the latter may better estimate the process by which the Group 1 enclaves were formed.

Several processes that occurred during mingling of the units may be indicated based on petrographic observations. All mingled contacts between enclaves, hosts, and dykes are highly irregular, which is consistent with field observations. It appears that the transfer of liquid, or even crystals, across the contact from one unit to the other may have occurred based on the appearance of minerals at the mingled contact that don't occur in the interior of the unit. This is consistent with the back-intrusion of younger units by liquid from older units that is observed at the field scale.

The diffusion efficiency of particular elements can similarly be estimated based on petrographic observations. In several cases in which minerals appear to have crystallized across mingled contacts, there is a difference in the mineral inclusions that occur on one side of the boundary versus the other. Examples of this include apatite in plagioclase and rutile in biotite, suggesting that crystallization was faster than diffusion of elements such as phosphorus and titanium. Volatiles such as water, however, appear to have been present in abundance at unit boundaries during mingling based on higher modal

abundances of biotite and hornblende in enclaves close to the mingled boundary with its host.

Table 3.1. Petrographic features of key units in study area

	Biotite Granite	Enclave- Poor Tonalite	Enclave-Rich Tonalite	Group-1 Enclaves	Group-2 Enclaves	Group-3 Enclaves
Dominant Minerals	Qtz (40%), Kfs (35%), Pl (25%), Bt (<5%)	Pl (75%), Qtz (10%), Cpx (10%) Bt (5%), Hbl (<5%)	Pl (75%), Qtz (20%), Bt (5%), Cpx (<5%), Hbl (<5%)	Qtz (35%), Pl (30%), Hbl (15%), Bt (10%), Cpx (5%), Opx (<5%)	Pl (40%), Qtz (25%), Hbl (20%), Bt (10%), Cpx (5%), Opx (<5%)	Pl (75%), Cpx (15%), Bt (5%), Opx (5%), Qtz (<5%)
Accessory Minerals	Py, Fl, Zrn,	Mag, Ilm, Ap, Zrn	Mag, Ilm, Zrn	Ilm, Mag, Rt, Ttn, Ap, Zrn	Ilm, Mag, Rt, Ttn, Ap, Zrn	Ap, Ilm, Mag, Rt, Ttn, Zrn
Grain Size	Medium- grained	Medium- grained	Medium- grained	Fine- grained	Fine-grained	Fine-grained
Estimated Crystallinity	N/A	20 %	50% (xtals) 20% (cores)	15 %	30 %	35 %

Mineral abbreviations (Kretz, 1983): Qtz = quartz, Kfs = potassium feldspar, Pl = plagioclase, Hbl = hornblende, Cpx = clinopyroxene, Opx = orthopyroxene, Bt = biotite, Py =

= pyrite, Fl = fluorite, Zrn = zircon, Mag = magnetite, Ilm = ilmenite, Ap = apatite, Rt = rutile,
Ttn = titanite.

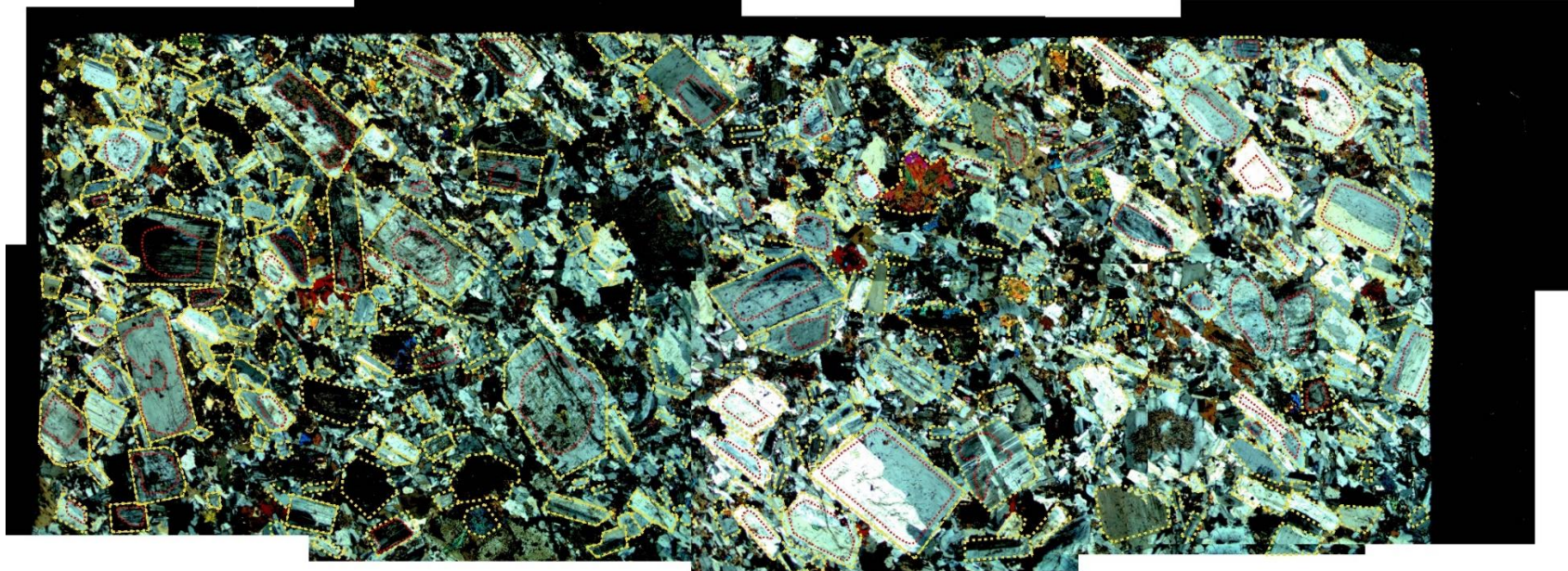


Figure 3.1. Euhedral plagioclase and pyroxene in enclave-poor tonalite estimated to represent the proportion of euhedral early-forming crystals. A high proportion of euhedral crystals (~50 %) are observed (yellow outline). Resorbed cores in plagioclase (example in Figure 3.3B), are interpreted to represent changes in crystallization environments (i.e. pressure, temperature, or chemical environments).

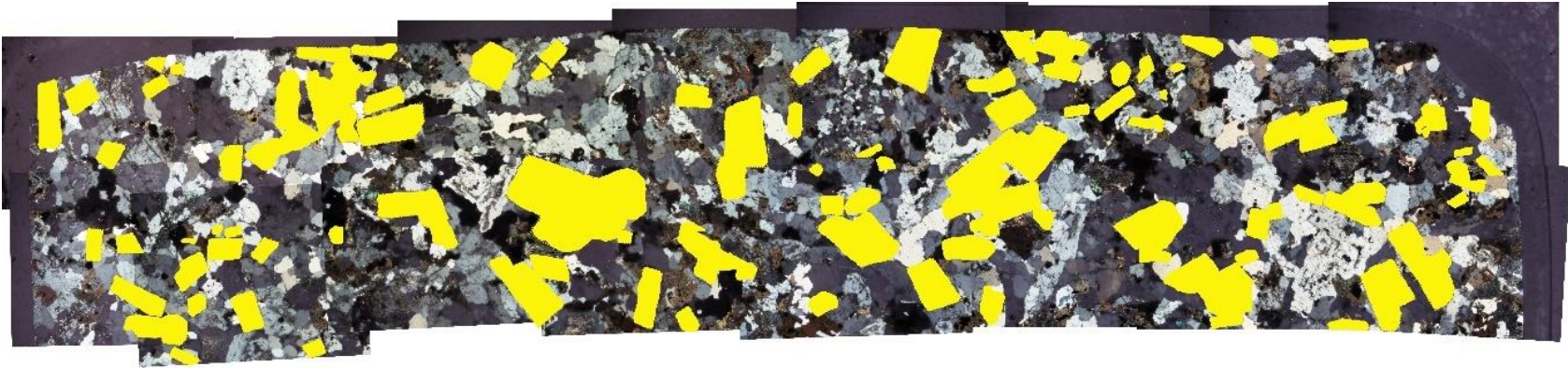


Figure 3.2. Euhehedral plagioclase and pyroxene in enclave-rich tonalite. The percentage of euhehedral crystals is approximately 20% suggesting the earliest crystals were in suspension and could move freely relative to each other (Marsh et al, 2002).

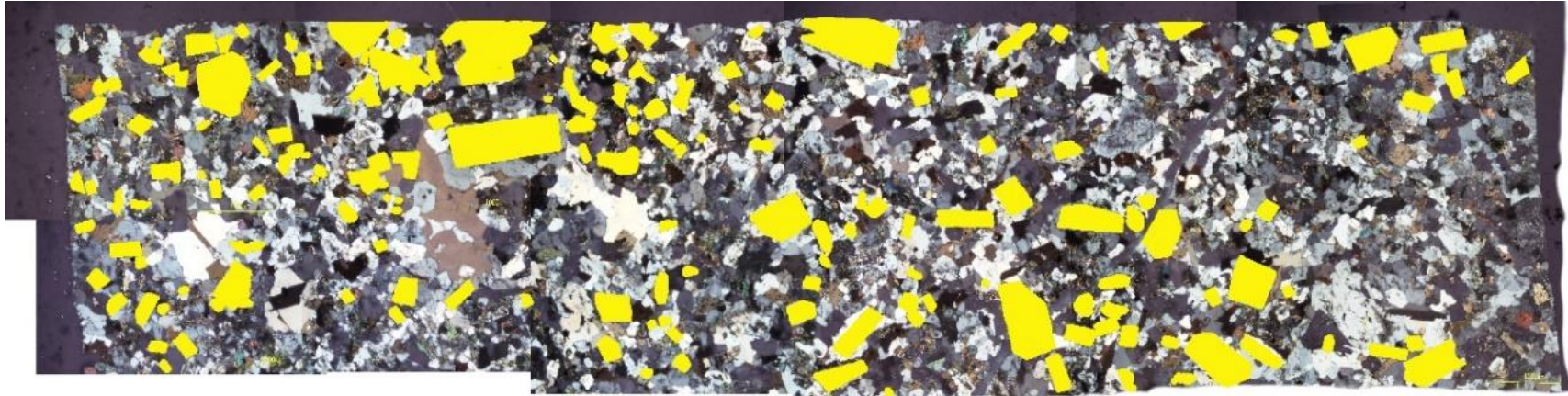


Figure 3.3. Euhedral plagioclase and pyroxene in Group 1 biotite hornblende tonalite enclave. The proportion of early forming crystals to melt was approximated by point counting the number of euhedral plagioclase and clinopyroxene in a representative thin section. The crystallinity is estimated to be between 10-20%, suggesting the early crystals were suspended in the melt and could move freely relative to one another (Marsh, 2002).



Figure 3.4. Euhedral plagioclase and pyroxene in Group 2 biotite hornblende quartz diorite enclave. The proportion of crystals to melt was estimated by point counting the number of euhedral early forming crystals in a representative thin section. The estimated crystallinity for this group ranges from 25-35%, which is higher than the estimated values for group 1 enclaves.

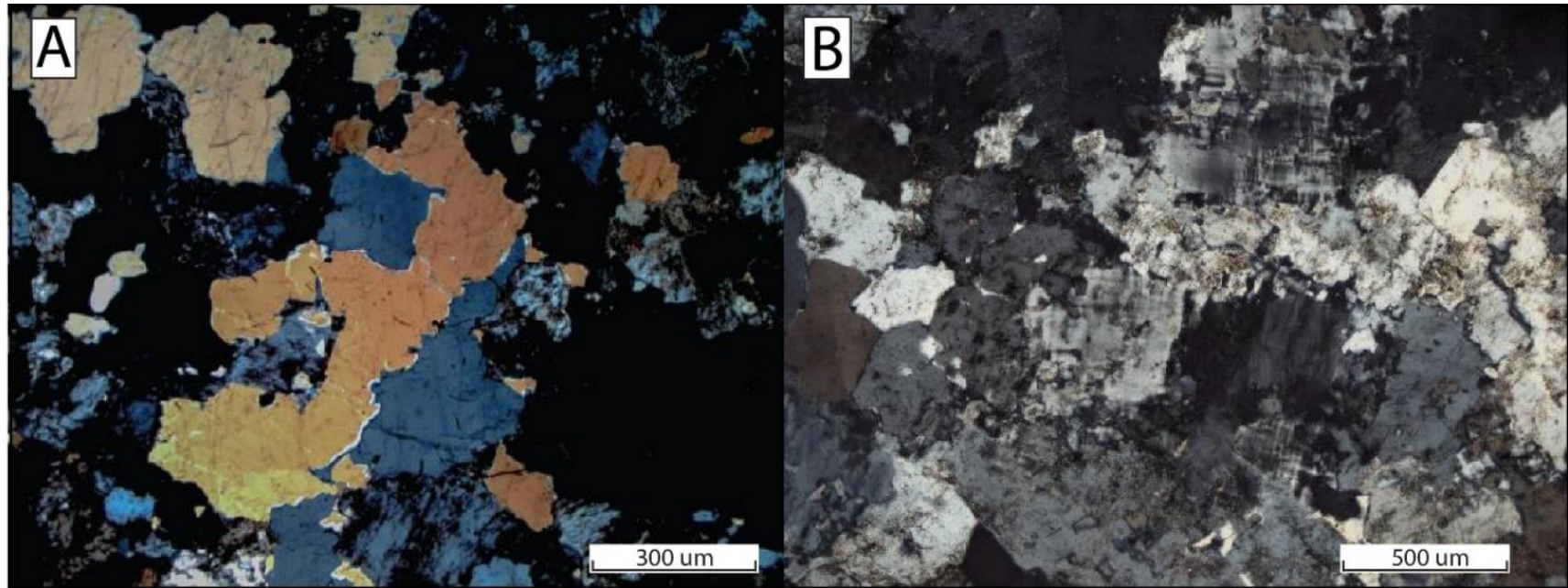


Figure 3.5. Photomicrographs of textures in the biotite granite unit. A) Coarse embayed quartz in granitic host rock. B) Anhedral groundmass of plagioclase, potassium feldspar, and quartz.

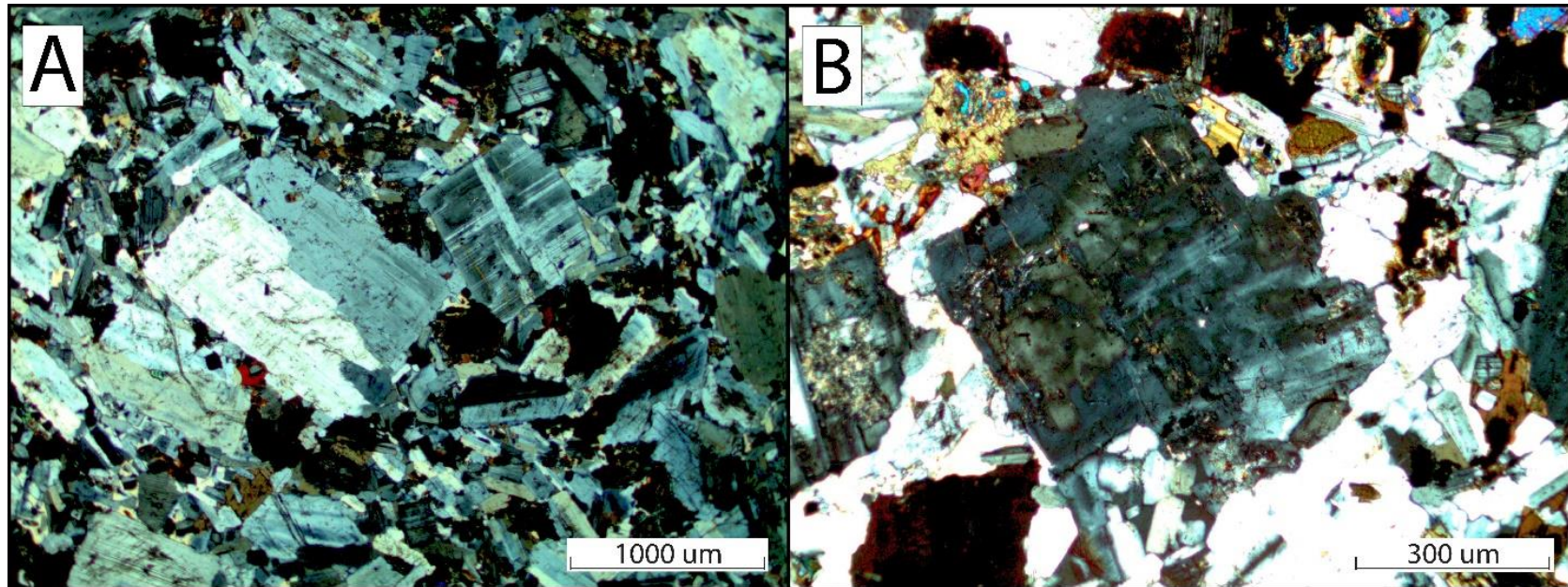


Figure 3.6. Photomicrographs of textures in the enclave-poor tonalite unit. A) High proportion of euhedral crystals in the enclave-poor tonalite host. Euhedral plagioclase occurs as both elongate laths in the groundmass and tabular phenocrysts. B) Groundmass plagioclase displays evidence of core resorption and indicates rapid changes in crystallization environments.

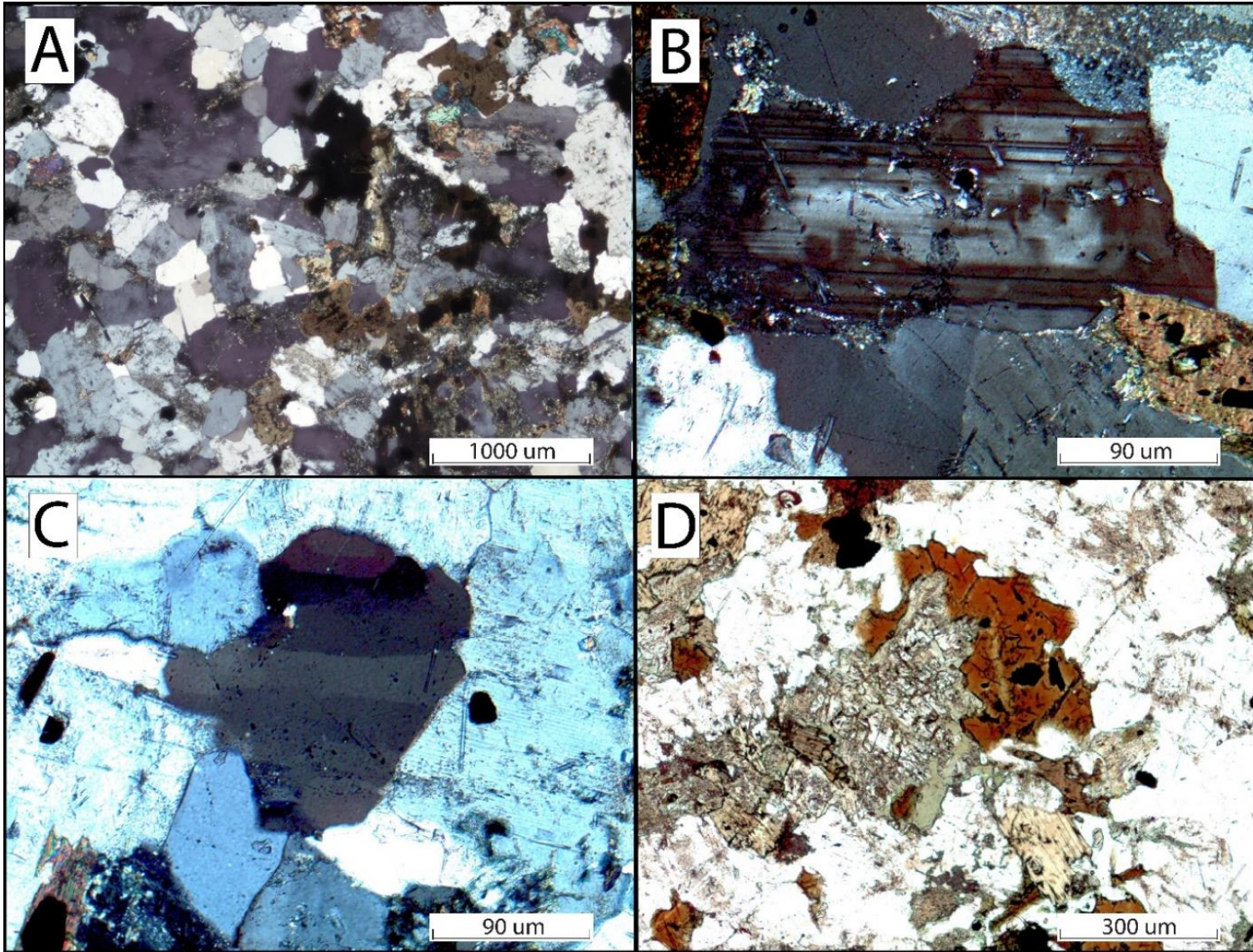


Figure 3.7. Photomicrographs of textures in enclave-rich tonalite unit. A) Overall lack of euhedral faces in early forming minerals such as plagioclase and clinopyroxene. B) Resorbed cores in groundmass plagioclase reflecting rapid changes in crystallization environments during early plagioclase growth. C) Undulose extinction in quartz suggesting strain after crystallization. D) Mafic cluster with relict clinopyroxene core being mantled by hornblende and biotite.

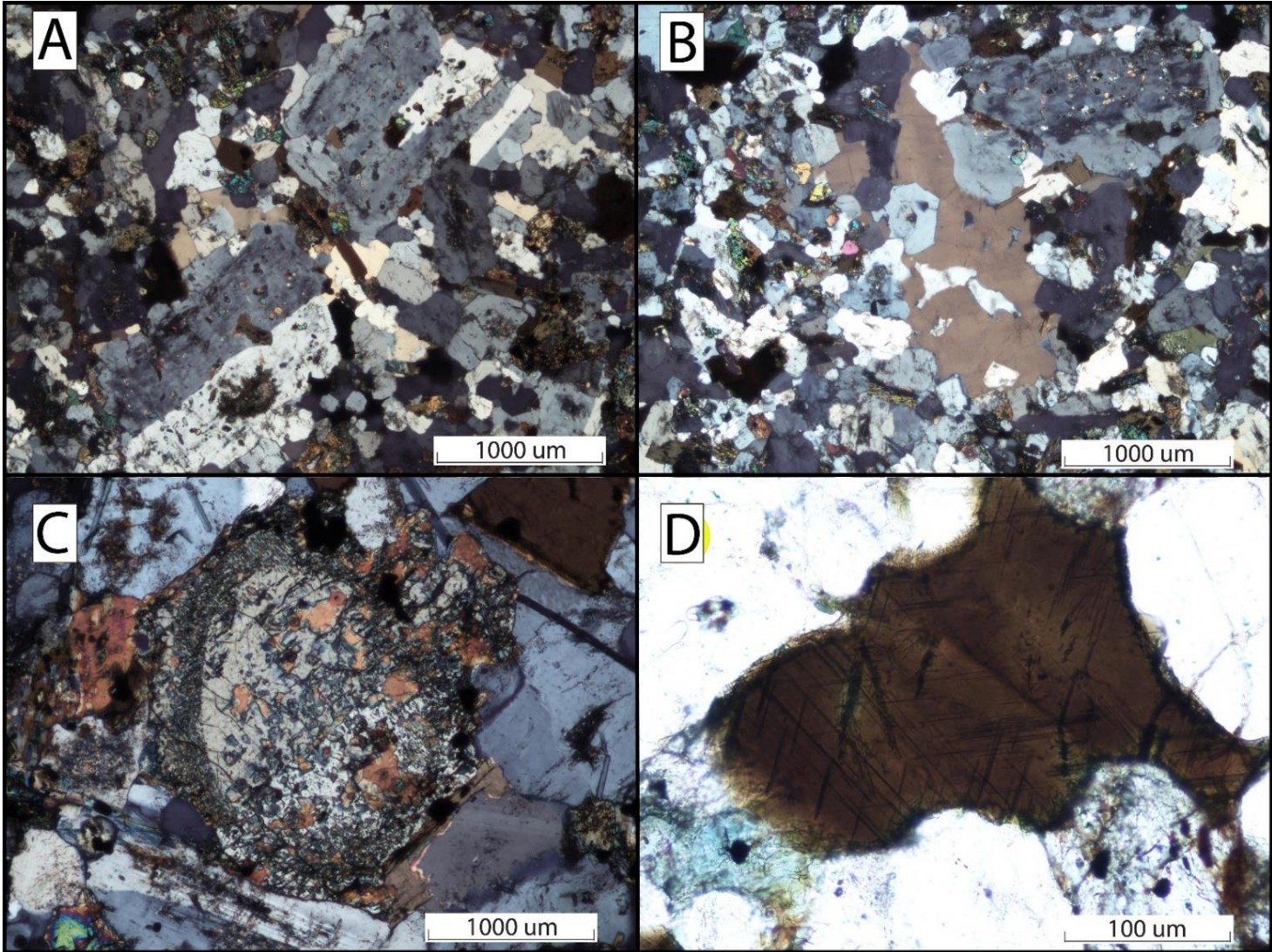


Figure 3.8. Photomicrographs of textures in Group 1 enclaves. A) Plagioclase phenocryst containing clinopyroxene inclusions that are restricted to resorbed regions in plagioclase. The plagioclase inclusions, based on similar extinction angles, are interpreted to be resorbed remnants of earlier formed crystals. The anhedral rims in plagioclase phenocrysts suggest coeval crystallization with groundmass plagioclase. B) Undulose extinction in phenocrystic quartz that is distinct from surrounding interstitial quartz. C) Compositionally zoned clinopyroxene. D) Sagenitic rutile and titanite inclusions within biotite.

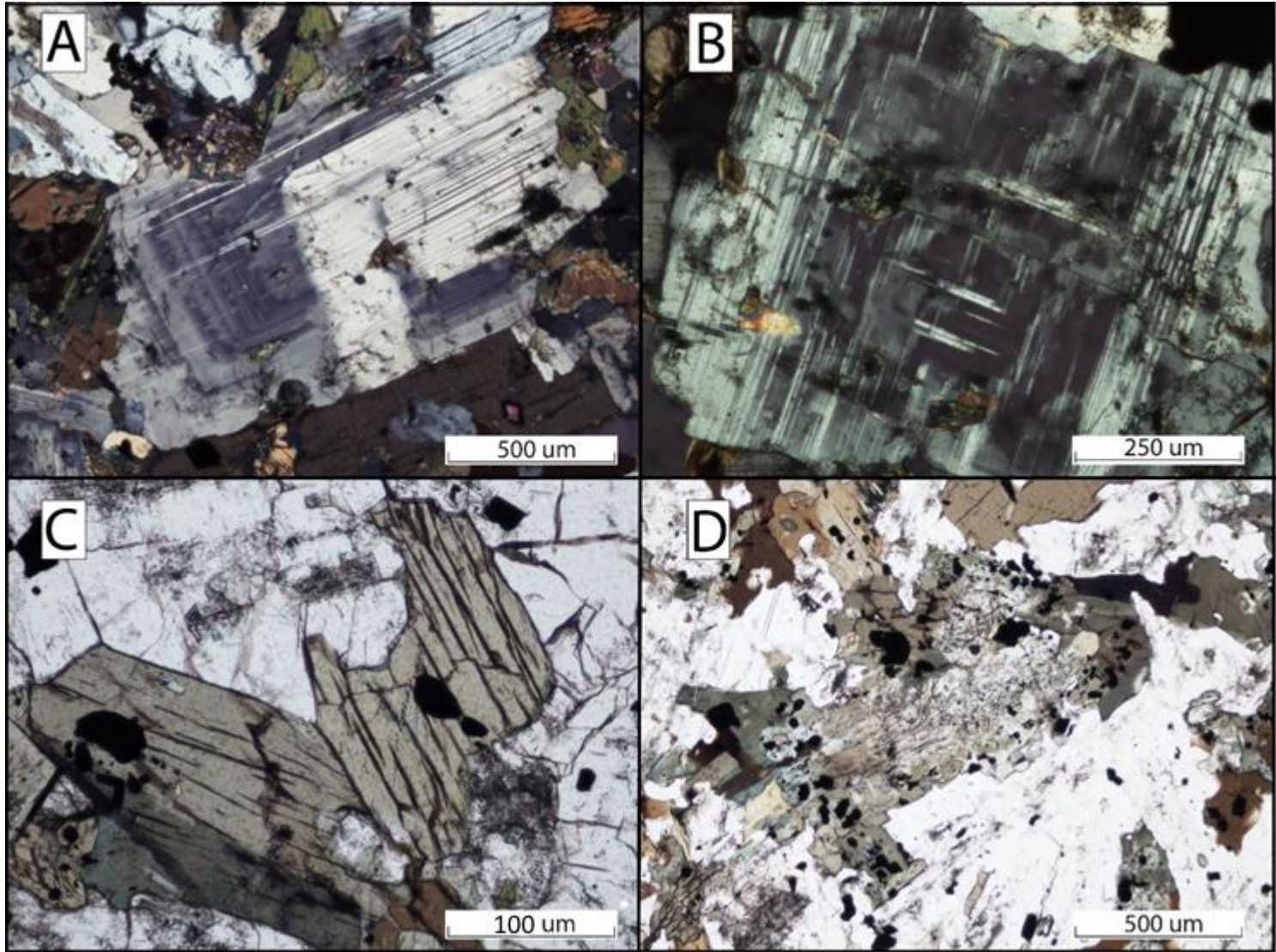


Figure 3.9. Photomicrographs of textures in Group 2 enclaves. A) Oscillatory zoned plagioclase phenocrysts with multiple generations of albite twinning overgrowth. Early euhedral cores can be distinguished based of the zoning patterns in the interior of the crystal. The crystallization of the anhedral rim appears to have been approximately coeval with the groundmass. B) Mottled core in plagioclase phenocryst reflects resorption of early plagioclase possibly due to the exchange of liquid from an hotter injected magma or due to convection carrying the crystals to new thermal environments (Wiebe et al, 1997). C) Hornblende forming by near complete replacement of clinopyroxene during late magmatic reaction. D) Corroded clinopyroxene core mantled by hornblende.

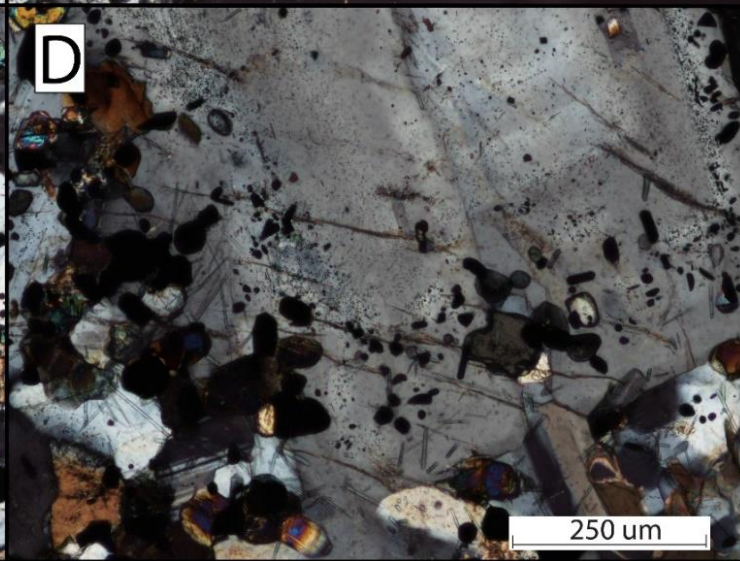
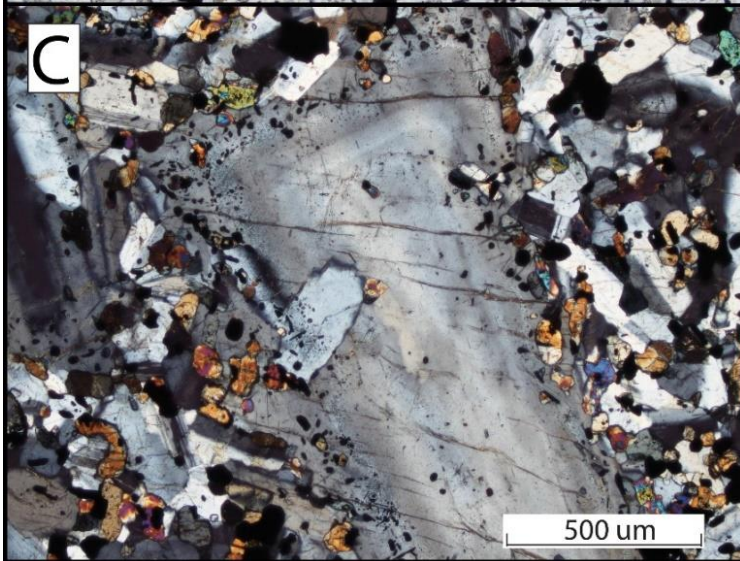
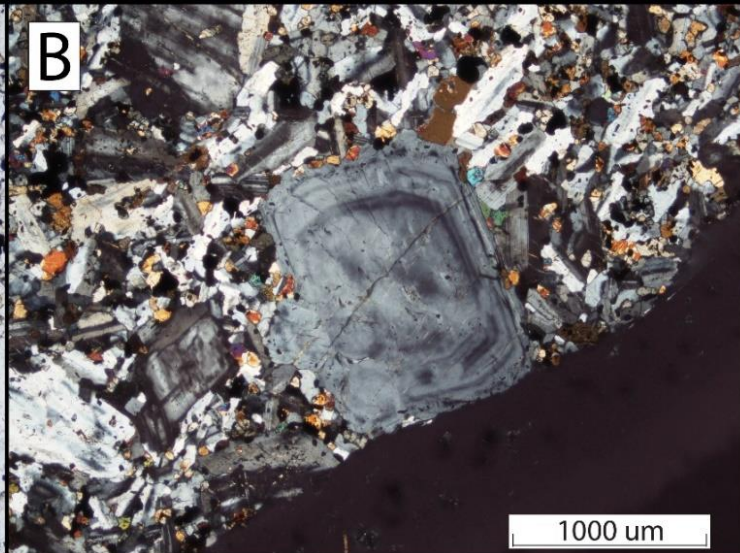
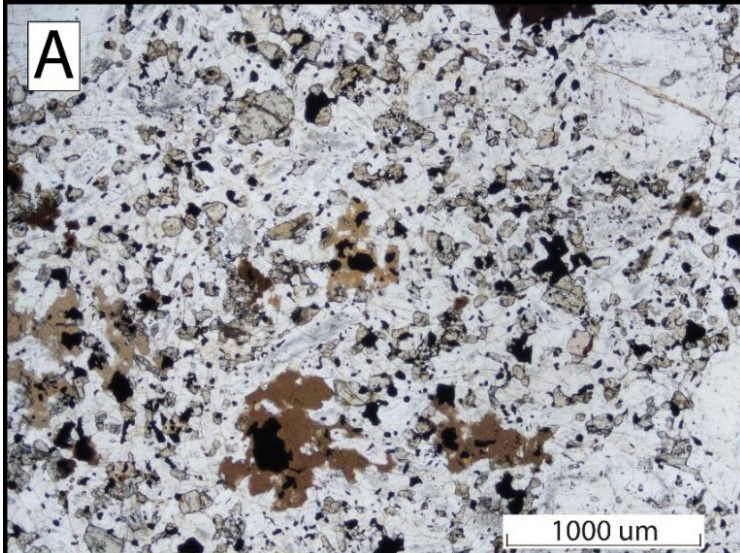


Figure 3.10. Photomicrographs of textures in Group-3 enclaves. A) High modal abundance of fine-grained rounded clinopyroxene that, unlike clinopyroxene in Groups 1 and 2, lack evidence of hornblende replacement. B) Patchy zoning overprinted by oscillatory zoning in plagioclase phenocryst. The patchy zones reflect rapid changes in crystallization environments whereas the oscillatory zones reflect changes in diffusive rate of elements. C) Clinopyroxene, apatite, and Fe-Ti oxide chadacrysts restricted to outermost rim of zoned plagioclase phenocrysts representing changing liquid environments throughout crystallization history. D) Multiple stages of oxide mineralization occurring immediately adjacent to new growth regions in plagioclase phenocrysts.

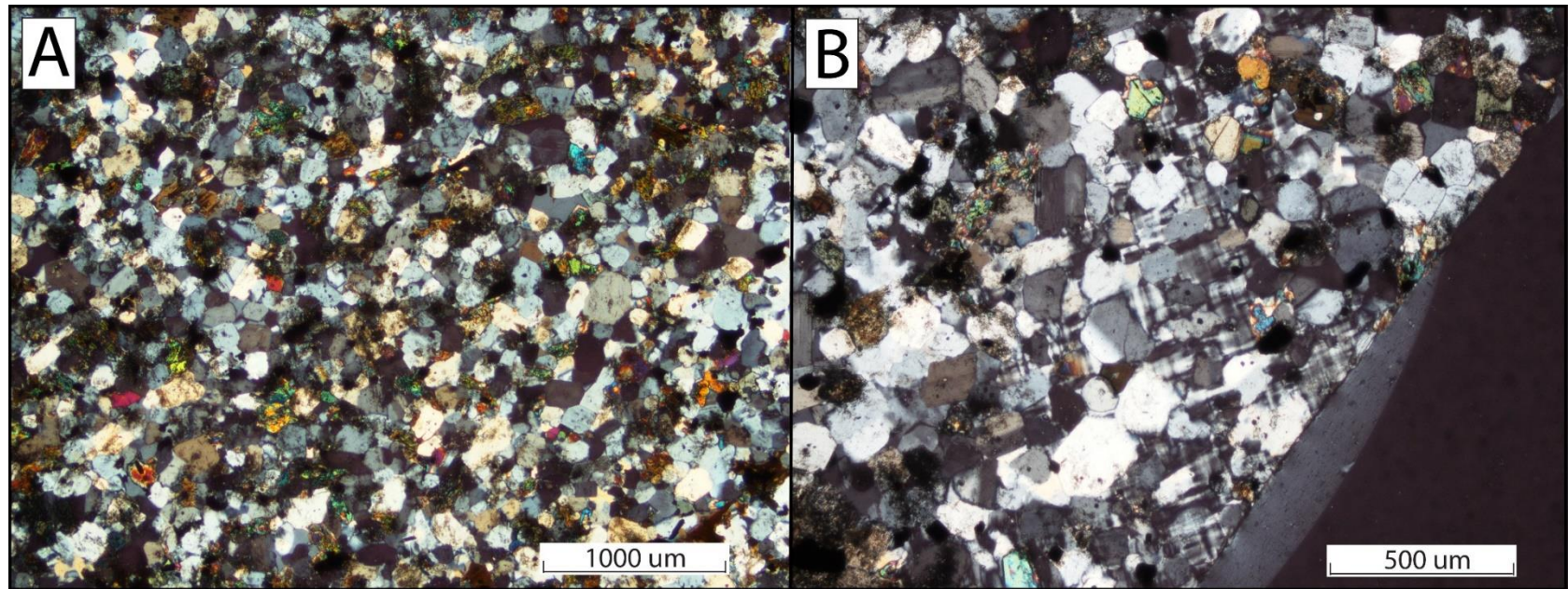


Figure 3.11. Photomicrographs of textures in broken-up tonalite dyke (Tonalite Dyke unit in Figure 2.4). A) Fine-grained equigranular groundmass composed of clinopyroxene, quartz, and plagioclase in broken up syn-plutonic tonalite dyke. Equigranular texture suggests all major minerals had coeval crystallization. B) Interstitial optically continuous potassium feldspar in tonalite dyke. May represent liquid from biotite granite back-intruding tonalite dyke after quenching.

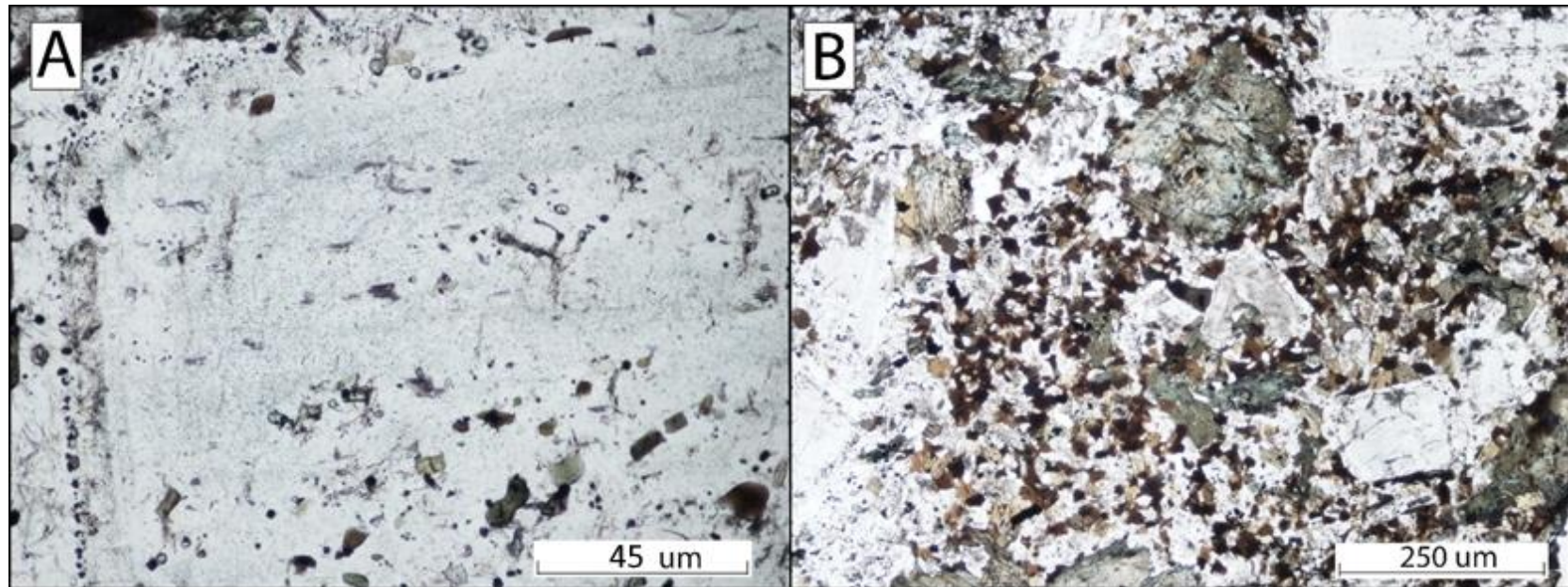


Figure 3.12. Photomicrographs of textures in quartz diorite dykes. A) Compositional zoning in plagioclase phenocrysts with high inclusion abundance (clinopyroxene, apatite, and Fe-Ti oxides) occurring within core and rim regions whereas the middle region largely lacks inclusions. Indicates changing liquid compositions over the crystallization history of this mineral. B) High abundance of biotite contained within groundmass.

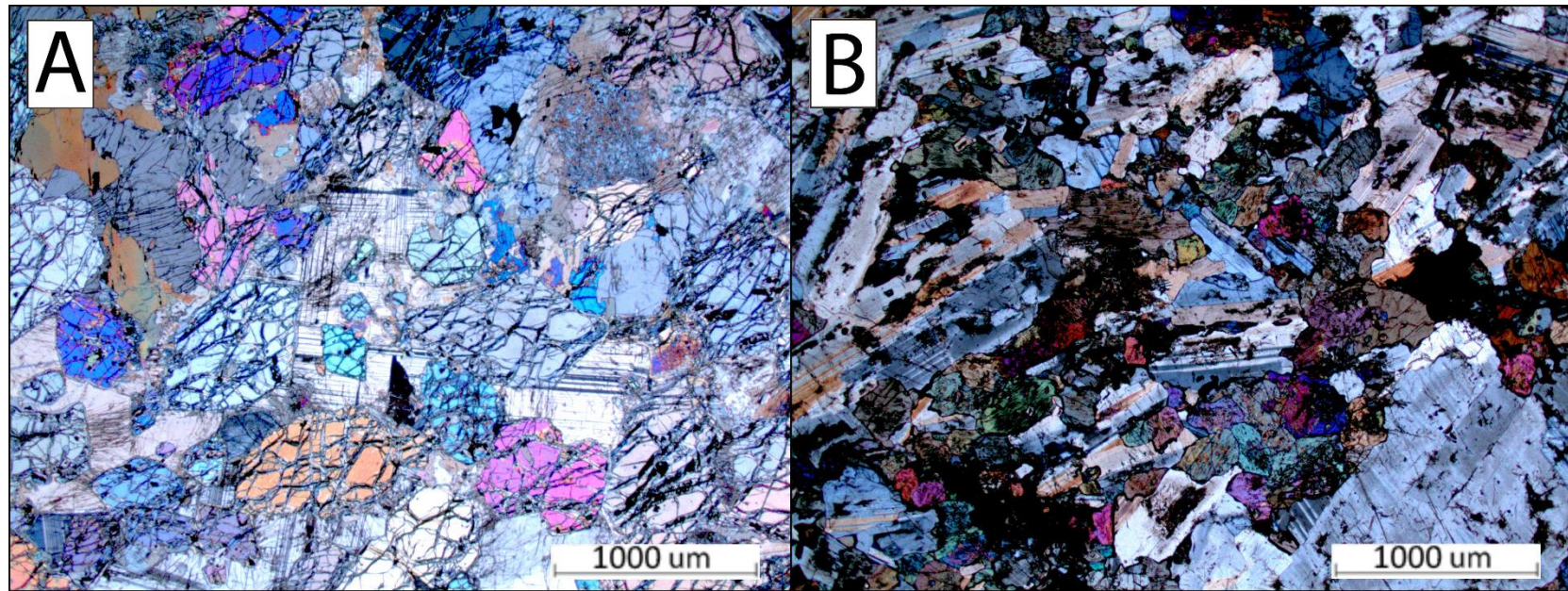


Figure 3.13. Photomicrographs taken from the mafic layered intrusion bordering the eastern end of the study area. A) The bottom of the intrusion is characterized by coarse serpentinized olivine, cumulate plagioclase, and orthopyroxene. B) The middle of the intrusion is characterized by finer-grained olivine, pyroxene, and elongate plagioclase laths.

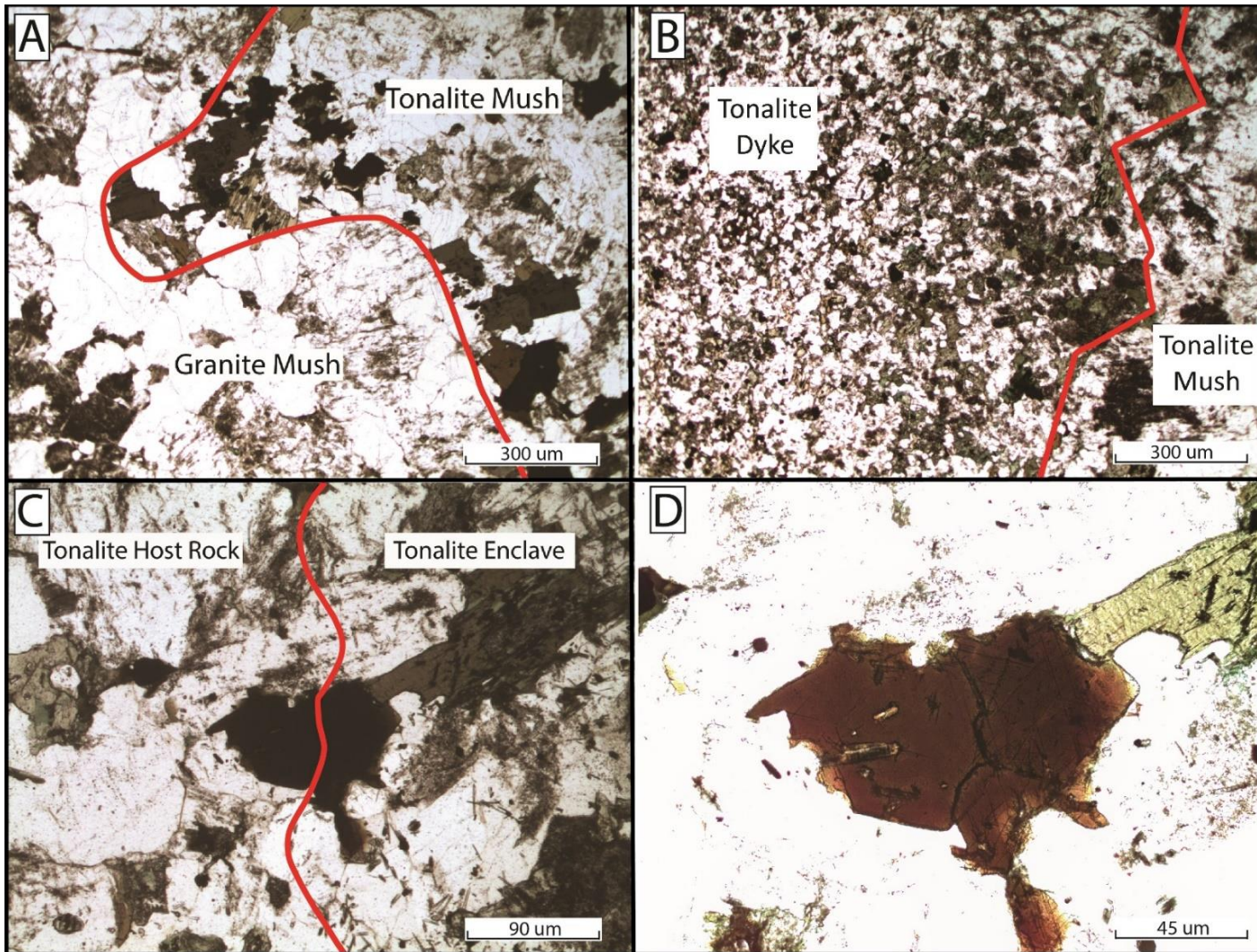


Figure 3.14. Photomicrographs of mingled contacts between units. A) Irregular unchilled boundary between granite mush and enclave-rich tonalite mush. B) Contact between disaggregated tonalite dyke; abundance of hydrous minerals in tonalite dyke increases closer to the boundary with the tonalite mush. C) Crystallization of biotite occurring across boundary between tonalite host mush and tonalite enclave, boundary defined by difference in abundance of acicular apatite inclusions in enclave (high) vs host rock (low). D) Increased magnification image of biotite displaying sagenitic rutile on only one side of boundary suggesting crystallization rate was faster than diffusion rate of titanium across contact.

Chapter 4 – Geochemistry

Whole rock and mineral chemical analyses were carried out to assess the compositional range of the mingled magmas and test the range of composition of complex minerals which appear to have undergone more than one episode of crystallization. This chapter will discuss the results of geochemical analyses of units in the study area including enclaves, host rocks, dykes, and sills. The major and trace element compositions of selected units were analyzed using ICP-MS and individual minerals were examined using the electron probe micro-analyzer (EPMA). The results of these analyses will be presented and the implications they have on the tectonic setting and magmatic history of the study area will be discussed.

4. 1. ICP-MS Major and Trace Element Results

4.1.1 Methods

Major and trace element compositions of selected enclaves, host rocks, and dykes were determined at ActLabs Laboratories Ltd (Ancaster, Canada). A total of nine host rocks, six enclaves, and three dyke samples were chosen for ICP-MS analysis to characterize major and trace element compositions. Sample preparation was done using equipment at Memorial University including an agate mill for powdering samples. The mill was cleaned using silica sand between samples to eliminate any possible effects of cross-contamination. Prepared pulps were packaged and mailed to ActLabs headquarters in

Ancaster, Ontario, where the 4Litho – Lithium Metaborate/Tetraborate Fusion – ICP and ICP/MS analytical methods were used. The procedure is a combination of packages Code 4B (lithium metaborate/tetraborate fusion ICP whole rock) and Code 4B2 (trace element ICP/MS). The following information about the procedure was obtained from the ActLabs web page: *Fused samples are diluted and analyzed by Perkin Elmer Sciex ELAN 6000, 6100, or 9000 ICP/MS. Three blanks and five controls (three before sample group and two after) are analyzed per group of samples. Duplicates are fused and analyzed every 15 samples. Instrument is recalibrated every 40 samples.* The datasets were plotted on major and trace-element diagrams to assess trends and compare rock compositions. The detailed results for ICP-MS analysis are reported in Tables C.1-C.3 of Appendix C.

4.1.2 Major and Trace Element Geochemistry

Most of the major elements (MgO, FeO^T, CaO, Na₂O, P₂O₅, TiO₂) form tight linear trends on Harker diagrams with increasing SiO₂ between mingled enclaves and host rocks (Figure 4.1). In the past, it has been suggested that linear trends in major elements may be indicative of magma mixing but it is now generally interpreted to be the product of multiple processes including fractional crystallization, assimilation, recharge, diffusion, and mixing (Tindle, 1991). Many of the major elements (eg. MgO, CaO, FeO^T) display a linear negative slope with increasing silica content, a trend commonly observed in calc-alkaline rocks (Tindle, 1991). This is consistent with all mingled units plotting in the calc-

alkaline fields of both the AFM ternary plot (Figure 4.2) and the Th-Hf-Ta diagram (Figure 4.3) of Pearce (1982).

In general, enclaves show higher amounts of MgO and FeO^T relative to their intermediate host rocks and the total alkalis (K₂O + Na₂O) are similar between enclaves and hosts. Most analyzed samples including host rocks, enclaves, and dykes plot within the four andesite fields of the Na₂O + K₂O vs. SiO₂ plot of Lebas *et al* (1986) (Figure 4.4). Host rocks generally plot within the andesite fields apart from two samples that plot in the dacite field. Groups 1 and 2 enclaves plot in the trachy-andesite to andesite fields whereas Group 3 enclaves plot in the basaltic andesite field. These results are consistent with petrographic observations suggesting Group 3 enclaves comprise the most mafic enclaves in the study area.

Linear trends in trace elements with increasing SiO₂ are a preferred indication of magma mixing (Tindle, 1991). Various trace elements in enclaves, host rocks, and dykes were plotted against SiO₂ in order of increasing incompatibility (from top-left to bottom-right) (Figure 4.5). In general, enclaves and host rocks have similar abundances of both incompatible elements (eg. Rb, Ga) and compatible elements (e.g. Sr, Y). Distinct trends with silica content are not observed for most trace elements. However, minor trends are observed in some trace elements within specific enclave groups. For the most incompatible elements, Rb and Ba, a positive trend is observed in Group 3 enclaves while a scattered non-definitive trend is observed in the Group 2 enclaves. A strong decrease in V is observed with increasing SiO₂ in host rocks, enclaves, and dykes which is consistent

with trends commonly seen in calc-alkaline magmas due to magnetite fractionation (Winter, 2001). Rb and Ba are commonly excluded from most minerals but are included in micas and potassium feldspar (McBirney, 2007), and this is consistent with the most biotite-rich samples of both enclaves and host rocks displaying the highest Rb and Ba abundances. An increase in Ba/Sr with increasing SiO₂ is observed in all units, correlative with increasing abundance of plagioclase and a lack of orthoclase crystallization (Figure 4.6). High field-strength elements such as Zr, Nb, and Ta are generally incompatible in most common igneous minerals but can be incorporated into accessory minerals such as zircon, apatite, magnetite, and ilmenite. Accordingly, Nb is concentrated in units that contain the highest abundances these minerals (McBirney, 2007). This relationship is observed in the decreasing trends of both Nb and P₂O₅ with increasing SiO₂ and the positive correlation between Nb and P₂O₅ (Figure 4.7).

Rare earth elements (REEs) for analyzed enclaves, host rocks, and dykes display similar trends when plotted normalized to chondrite compositions (Figure 4.8). All groups are enriched in light REEs (LREE) (50-150x chondrite) compared to heavy REEs (HREEs) (9-18x chondrite), likely reflecting low degrees of partial melting of an enriched mantle source or crustal assimilation (Winter, 2001). REE concentrations in host rocks, enclaves, and dykes appear to generally be a function of SiO₂ content, with the most SiO₂-rich samples displaying the highest REE concentrations. Of the thirteen analyzed samples, notable negative Eu anomalies are only observed in one Group 1 enclave and a syn-

plutonic tonalite dyke suggesting most magmas were not separated from their earliest phases of plagioclase crystallization (McBirney, 2007).

All units display enrichment of large ion lithophile elements LILEs (K, Rb, and Ba) relative to high field strength elements HFES (Ta to Yb), a chemical signature common to subduction-related magmatism (Winter, 2001; Figure 4.9). However, Ta and Nb are enriched 2-7 times relative to MORB in all units whereas typical arc patterns show depletion (or only minor enrichment) of these elements compared to MORB. (Figure 4.10). When normalized to average continental crust (Taylor and McLennan, 1985), most incompatible elements show values close to those for average continental crust, except for a slight depletion in LILEs (Fig. 4.11). Together, these results suggest rocks from Wild Cove East have arc-related geochemical signatures and have been contaminated by upper continental crust.

4.2 Analysis of main rock forming minerals

4.2.1 Methods and sample selection

Twelve thin sections were analyzed using the Electron Microprobe Micro-analyzer (EPMA) at Memorial University to determine the compositions of major minerals. The instrument is a JEOL JXA-8230 model that uses a tungsten filament to produce an electron beam which is focused as small spots on the samples. A beam current of 20 nA was used with an accelerating potential of 15 kv. The EPMA uses both wavelength dispersive

spectrometry (WDS) and energy dispersive spectrometry (EDS) to determine mineral compositions. Four spectrometers are used at any time for WDS analysis. Standards provided from Astimex were analysed to determine accuracy of results. Prior to analysis, the surface of each thin section was cleaned using ethanol and coated with a thin layer (200 angstroms) of carbon to allow for optimal dispersal of the electron beam. A 3-micron diameter beam was used for plagioclase, pyroxene, and olivine whereas a 1-micron diameter beam was utilized for biotite and hornblende. The detailed results for each EPMA analysis are reported in Tables C.4-C.24 of Appendix C.

Three enclaves were analyzed using the EPMA, one from each of the petrographically defined groups. The goals of these analyses were to determine a) if distinct mineral compositions are observed between the three groups, and b) if enclave mineral compositions are similar or distinct from those in the enclosing host rocks c) if multiple crystal populations are present within individual units. In addition, minerals displaying distinct textures such as internal mottling in plagioclase and zoning in clinopyroxene were examined. Prior to EPMA analyses, targets were selected following petrographic examination of representative thin sections that had the best chance of providing answers to these questions.

A sample from each of the major intermediate host rock units was chosen for EPMA analysis to determine the compositions of major minerals and compare the results to those obtained from enclave minerals. In addition, two samples that each represent

the boundary between two host units were analyzed. One of these samples was defined by a thin dark anastomosing contact (Figure 2.10) and one was not.

Three important intrusions were selected for EPMA analysis: a pair of quartz diorite dykes located in the northernmost part of the study area (A in Figure 2.2), a diorite sill containing magmatic pipes and tubes (B in Figure 2.2), and a mafic layered intrusion bordering the eastern end of the study area (C in Figure 2.2). The compositions of major minerals including plagioclase, pyroxene, biotite, and hornblende were determined in each unit.

4.2.2 Plagioclase Compositions

Ternary plagioclase diagrams for host rocks, enclaves, and dykes/sills were produced using IgPET. A distinct compositional range is observed within each of the three petrographically defined enclave groups (Figure 4.12A). Specifically, all three groups have distinct plagioclase core compositions but similar oligoclase rim compositions. Group 1 and Group 2 enclaves both contain plagioclase cores of andesine compositions. However, Group 2 andesine are generally more Ca-rich than andesine in Group 1 enclaves. The most compositionally primitive plagioclase cores are found in the Group 3 enclaves, which are generally of labradorite composition.

Plagioclase compositions for the two major intermediate host rock units were similarly plotted on a ternary plot using IgPET (Figure 4.12B). Plagioclase in both the

enclave-rich and enclave-poor tonalite units generally contain cores of andesine composition and rims of oligoclase composition. Some crystals in both units display an opposite trend, however, with oligoclase cores and andesine rims. Although the rim compositions are similar between the two units, the cores for the enclave-rich tonalite have a more restricted range and are Ca-poor compared to the enclave-poor tonalite unit. Plagioclase crystals found in the contact between the two units are of andesine composition but are more calcium-rich than majority of the analyzed minerals from the two tonalite units.

Both the diorite sill and the quartz diorite dyke display a wide range in plagioclase composition from labradorite to oligoclase that can be seen in individual crystals (Fig. 4.12C). This is comparable to the combined compositional range of all analyzed host rocks and enclave in the study area. The mafic layered intrusion in the east displays the most Ca-rich plagioclase in the study area: its base nearing bytownite composition (An_{68-66}) and labradorite (An_{51-58}) composition in the middle (Figure 4.12D).

4.2.3 Pyroxene Compositions

Pyroxene compositions were determined in samples from each of the enclave groups. Multiple grains were selected from representative thin sections including: pyroxene mantled by hornblende, pyroxene lacking hornblende rims, pyroxene occurring as inclusions in plagioclase, and pyroxene displaying compositional zoning. Compositions

from EPMA analysis were plotted in a pyroxene quadrilateral using IgPET (Figure 4.13). Pyroxene compositions of all groups generally plot in the Ca-Mg rich end of the augite field (Figure 4.13A). There are exceptions, however, including: 1) a zoned enclave clinopyroxene that displays a Ca-poor augite core and a Ca-rich augite rim, and 2) a zoned enclave pyroxene containing enstatite core and a Ca-poor augite rim. Overall, there is a high degree of overlap in clinopyroxene composition between the three enclave groups.

Many of the analyzed host rocks pyroxene grains similarly plot in the Ca-rich augite field (Figure 4.13B). Pyroxene grains from contact between the two major host units, however, are generally of diopside composition and pyroxene in the enclave-rich tonalite immediately adjacent this contact plot in the Ca-poor augite field. A distinction is seen between the composition of pyroxene that exists as corroded cores in hornblende (Ca-poor augite) and those that are separate crystals (Ca-rich augite) in both host units. A trend is seen across two clinopyroxene grains that oscillate from Ca-rich to moderately Ca-rich augite from core to rim. Corroded pyroxene cores in the quartz diorite dyke (A in figure 2.2) are of enstatite composition (Figure 4.13C). Pyroxene inclusions in plagioclase are generally of Ca-rich augite composition but, in some cases, contain a pigeonite core and a Ca-poor augite rim. In the diorite sill (B in Figure 2.2), both Ca-rich augite and Ca-poor augite populations are observed. Pyroxene in the mafic layered sill (C in figure 2.2) includes enstatite at the base and Ca-rich augite/diopside at the middle (Figure 4.13D).

4.2.4 Biotite and Hornblende Compositions

Due to the overall similarity between samples, biotite was only analyzed in two enclave samples and their corresponding host rocks. The average range in TiO₂ is 3.0-4.5 wt % in enclaves and 3.5-5.0 wt % in host rocks. There is only a modest change in Mg # from core to rim in each of the analyzed minerals. The biotite Mg # is comparable between both all samples. Hornblende generally occurs as both solitary crystals and as reaction rims on pyroxene in all units. The compositions of hornblende in these two positions were found to be nearly identical in the two enclave samples (see Table C.7 in Appendix C).

4.2.5 Plagioclase Feldspar Chemistry

EPMA traverses were conducted across select enclave-hosted plagioclase that display unusual mottling and zoning patterns. In a Group 1 tonalite enclave, plagioclase grains were analyzed that are composed of two zones: a mottled andesine (An₃₂) core, and an oligoclase (An₂₂) overgrowth/rim (Figure 4.14). Small clinopyroxene inclusions are restricted to the core regions of An₃₂ in both crystals and, based on similar extinction angles among multiple pyroxene inclusions, these appear to be corroded remnants of original coarser-grained pyroxene. The inclusions become more Fe-rich towards the rim of the plagioclase phenocryst (Mg₇₄ → Mg₇₃ → Mg₇₁). Rapid decompression of a magma has been proposed by previous studies as a process which can lead to resorption of early

forming minerals (Nelson and Montana, 1992). This may explain the resorption of early andesine cores inclusions and subsequent overgrowth by oligoclase rims.

Two plagioclase phenocrysts in a Group 2 tonalite enclave were similarly examined. Both crystals display a compositional range from An₄₅₋₂₅ and, like Group 1, are composed of mottled andesine cores and oligoclase rims. Abrupt peaks and valleys in An content across both traverses correlate with patchy zoning in the mineral that is seen in both crossed polar microscopy and backscatter images (Figure 4.15). In both grains, the lowest Ca-content is located at the rims suggesting the latest crystallization was from an evolved liquid. The zoning in both plagioclase grains indicates the earliest crystallizing phase was andesine (An₄₅₋₄₀) which was later corroded and overgrown by an oligoclase rim (An₂₅). The mottled shape of the andesine cores likely records a period of non-crystallization and partial resorption of the core (Wiebe, 1968). The outermost parts of resorbed andesine cores are slightly more calcic than the innermost regions and may represent an earlier mixing event or build-up of compatible Ca as the volume of feldspar decreased due to resorption which affected these crystals (Wiebe, 1968).

Core and rim EPMA analyses were conducted on plagioclase crystals in both the enclave-rich tonalite and enclave-poor tonalite unit (Appendix C.7). Plagioclase crystals were analysed from a core taken between the contact between the two units. A wide range in core compositions is observed in single thin sections for both units: with a range of An₄₄₋₂₆ in the enclave-poor tonalite, and a range of An₃₃₋₁₉ in the enclave-rich tonalite. In some cases, plagioclase cores displaying resorption textures are more An-rich than their

respective rims whereas in others they are less An-rich than the rims. A narrow rim compositional range of An₂₁-An₁₉ is observed in the enclave-rich tonalite units.

Plagioclase grains displaying disequilibrium textures were examined in samples taken from a quartz diorite dyke in the northernmost part of the field area. This dyke is characterized by containing rounded globules within its margins and provides evidence in the study area of a potential enclave-forming processes. The range of An₅₀₋₃₀ is seen in two analyzed plagioclase phenocrysts, values which are close to those observed in Group 3 enclave phenocrysts. Oscillations between An₅₀₋₃₀ occur in the mottled regions of both crystals and represent the core and overgrowth regions, respectively. Plagioclase of Figure 4.16A is mottled across its entirety and this is reflected in the oscillating peak and valleys in An # from core to rim. A separate plagioclase (Figure 4.16B) displays a more complicated history with early resorption of an oligoclase core (An₃₀), followed by prolonged crystallization of labradorite (An₅₀) beginning midway through the traverse and finally crystallization of an oligoclase rim (An₃₀). Petrographic observations reveal that pyroxene inclusions are restricted to the mottled oligoclase core and rim of the mineral. The early oligoclase core appears to have been resorbed due to injections of a more mafic magma that crystallized labradorite and not pyroxene.

4.2.6 Zoned Pyroxene Chemistry

Like plagioclase, pyroxene is interpreted based on petrography, to be among the earliest minerals to have crystallized in all units and thus has the potential to record early magmatic events. EPMA traverses were conducted across selected clinopyroxene crystals in enclaves and dykes that display textures suggesting changing crystallization environments including irregular zoning patterns and distinct rim overgrowths. Coarse clinopyroxene crystals were analyzed in 10-20 point traverses from core to rim and spot analyses at the core and rim were conducted for fine-grained crystals.

A clinopyroxene from a Group 1 tonalite enclave was analyzed that displays three compositional zones suggestive of crystallization under changing conditions: a Ti-rich core, a depleted zone, and a Cr-rich rim (Figure 4.17). The Ti-rich composition of the core is titanite, a mineral generally derived from alkaline magmas (Leung, 1974). There exists a gradual decrease from Mg_{81} to Mg_{72} away from the core until a sudden increase to Mg_{76} occurs across a visible boundary close to the rim. At the same point, a significant increase in Cr from low values to nearly 500 ppm occurs close to the rim region of the crystal. Since chromium is typically enriched in mafic magmas, the replenishment observed at the rim suggests late crystallization from a more primitive (mafic) magma (Streck, 2008). Thus, this crystal appears to have had a complex magmatic history involving: 1) early crystallization from a Ti-rich alkaline magma, 2) a period of fractionation

to form the middle zone, 3) late crystallization from a mafic magma, and 4) incorporation into tonalite crystal mush.

Several zoned clinopyroxene grains were similarly examined in a quartz diorite dyke (A in Figure 2.2) that potentially displays evidence of enclave formation. One pyroxene oscillates between Mg_{76-71} from core to rim suggesting either changing pressures or minor mafic recharge (Streck, 2008; Figure 4.18). The increase in Mg # towards the rim of the crystal is accompanied by a significant rise in Cr by almost 400 ppm. The change in element abundances from core to rim in this crystal suggest changing crystallization environments due to mafic enrichment or decompression during rise of the dyke (Nelson and Montana, 1992).

4.2.7 Evidence of Magma Mixing and Crystal Transport

The occurrence of crystal populations with contrasting compositions in the same rock, particularly plagioclase, has been reported in previous studies on magma mingling and enclave formation (Wiebe, 1968; Astbury *et al*, 2016). Two plagioclase phenocrysts displaying distinct core compositions occur in the same thin section from a Group 2 enclave (Figure 4.14). Both crystals have a similar overall range in anorthite composition, ranging from An_{50-20} . However, the core compositions of the two crystals are on opposite ends of that range, with the first phenocryst containing a core of An_{50} and the second containing a core of An_{23} . Although these crystals are now adjacent to one another, early

crystallization in each must have taken place under separate and very different conditions (Wiebe, 1968). The two crystals also display distinct trends from core to rim: the first crystal experiences a gradual rise in An content followed by a decrease back to core-values, whereas the second crystal displays a modest depression followed by an increase to core values followed by a significant decrease proximal to the rim. The abrupt peaks and valleys in An content across the traverse appear to be correlated with patchy zoning and mottling within plagioclase. Since the rim value of both phenocrysts are similar, the latest stage of crystallization in each was likely under similar conditions. These two crystals may represent the end-members of an early mixing event and suggest the displacement of crystals from one magma to another may have occurred (Wiebe, 1968).

Crystal capture and displacement is also suggested by the occurrence of pyroxene with unusual compositions in some enclave rocks. The zoned Group-1 tonalite enclave pyroxene referred to in Figure 4.17, for example, display primitive cores (Mg_{80-76}) compared to the average compositional range of other pyroxene in the same thin section (Mg_{73-71}). Similarly, an anomalous pyroxene from a Group-3 quartz diorite enclave displays more evolved compositions (Mg_{60} core, Mg_{65} rim) compared to the range for other analysed pyroxene in the same rock (Mg_{73}). These anomalous compositions are represented by the star symbols in Figure 4.19.

4.2.8 Comparison of Phenocryst Rims to Groundmass Plagioclase in Enclaves

The compositions of plagioclase phenocrysts rims were compared with groundmass plagioclase in the same rock to determine their relative timing of crystallization. In a Group 1 biotite tonalite enclave, the cores of two plagioclase grains in the groundmass were determined to be An₁₉ and An₂₀ respectively. In the same thin section, the rims of two plagioclase phenocrysts contain a composition of An₂₀ and An₂₂ respectively. This suggests that the nucleation and crystallization of groundmass plagioclase occurred at similar temperatures to rim crystallization in plagioclase phenocrysts. Similarly, the rims of phenocrysts in Group 3 enclaves display overlap in compositional range (An₂₉₋₂₈) to groundmass plagioclase (An₂₉₋₂₆). Increased nucleation rate during groundmass plagioclase crystallization may be due to a combination of decreased pressure due to rise of the magma and an increase in volatiles (Wiebe, 1968). A summary of the range in plagioclase compositions for both groundmass and phenocrysts is shown by Figure 4.19.

4.2.9 Comparison of Enclave and Host Rock Plagioclase

Plagioclase in host rock samples was analyzed and compared with the results from enclaves to determine chemical similarities that may have resulted due to prolonged mingling of the different magmas. Two enclave-host rock pairs were analyzed: 1) enclave-rich tonalite host rock and Group 1 tonalite enclave, and 2) enclave-poor tonalite and

Group 2 quartz diorite enclave. Samples of enclaves and host rocks were taken several meters apart from each other.

In the first example, plagioclase crystals in the enclave-rich tonalite host were compared to those of approximately the same size in a nearby Group 1 enclave. The range of An content is similar in plagioclase of both rocks, with core values of $\sim\text{An}_{25}$ and rim values of $\sim\text{An}_{20}$. The An content of the rim in both the host rock and enclave plagioclase is similar at $\sim\text{An}_{20}$, but the core values of the enclave phenocryst are higher ($\sim\text{An}_{33}$) than the cores of the host rock crystals (An_{26-24}) suggesting that initial growth of plagioclase phenocrysts occurred in a more primitive Ca-rich magma. However, the similar rim compositions suggest that the latest stage of crystallization took place at similar temperatures in the enclave and its host.

In the second example, a similar comparison was made between a sample taken from the enclave-poor tonalite host unit and an enclosed quartz diorite Group 2 enclave. There exists a greater range in An content between the rims of plagioclase in the enclave and host than in the previous example, particularly in the phenocrysts of the two minerals (An_{33-30} rims in enclave and An_{25-20} rims in host). Thus, it appears that the latest stages of plagioclase crystallization in the enclave and host rock were not at similar temperatures. The lower An contents in the enclave are consistent with late crystallization from a more evolved liquid than experienced by the host rock.

There is little to no correlation between the core compositions of plagioclase phenocrysts in enclaves and the enclave-rich tonalite unit. Core values were compared

between a Group 1 enclave and its enclosing enclave-rich tonalite host. The core values of the enclave phenocryst are higher (An_{34-32}) than the cores of the host rock crystals (An_{26-24}) suggesting that growth of enclave plagioclase phenocrysts occurred in a slightly more primitive magma than in the hosts. Limited compositional overlap exists between cores of phenocrysts in Group 1 enclaves and the enclave-poor tonalite unit (Figure 4.19).

4.3 Discussion

The geochemistry of mingled rocks has important implications for the magmatic processes by which they were formed. A protracted history of magma and mineral evolutions can be deduced from combined ICP-MS and EPMA data. Major and trace element plots suggest that crystal fractionation was not the only processes that affected these rocks but likely acted in addition to assimilation, partial melting, and magma mixing. All units share similar trends with respect to their trace element compositions and the range in concentrations appear to be largely related to mineralogy and SiO_2 content. This may be related to variable degrees of mixing and hybridization between different mantle and crustal derived end-members (Wiebe *et al*, 1997).

In addition to the ubiquitous calc-alkaline signatures exhibited by all mingled units, many trace element ratios appear to be very close to average upper continental crust. This is consistent with interpretations from previous studies that the Fogo Batholith was emplaced due to dextral related movement along the Dog Bay Line, possibly reactivated

during extensive strike-slip motion in the early Devonian Acadian (Williams *et al*, 1993). The Dog Bay Line is bounded by rocks representing the Popelogan-Victoria arc to the west and Ganderian crustal rocks to the east (Van Staal, 2012). Mantle derived melts that partially melted, mixed and hybridized with accreted arc and continental material at the base of the crust may have led to the formation of andesite-dacite magmas that represent the units in the study area.

Trace element plots, although displaying similar trends between host rocks and enclaves, reveal multiple enclave populations are represented in the study area. This is evidenced by distinct linear trends in certain incompatible elements (ex. Rb, Ba, Sr) between different enclave populations when plotted against SiO₂. Similarly, unique compositional ranges of plagioclase exist in each of the three enclave groups (Figure 4.12B, 4.19). These results are consistent with field and petrographic observations suggesting enclaves in the study area represent multiple intermediate injections that mingled with crystal mushes of similar intermediate composition in a shallow crustal magma chamber.

Individual minerals, particularly plagioclase and pyroxene (interpreted to be the earliest forming minerals in all units), reveal complicated crystallization histories reflecting changing thermal and chemical conditions. Enclaves, in all three groups, generally contain mottled plagioclase with An-rich core/An-poor rims suggesting resorption occurred due to decompression melting during magma ascent (Nelson and Montana, 1992). Host rocks, however, display a mixture of resorbed plagioclase crystals with either An-rich cores/An-

poor rims or An-poor cores/An-rich rims, implying crystals were affected by both decompression melting and mafic recharge. Evidence of mafic recharge is also seen in zoned clinopyroxene crystals in enclaves where abrupt increases in Mg # and Cr₂O₃ are observed at the rims.

Unique plagioclase and pyroxene crystals with unusual compositions occur in both enclaves and host rocks suggesting crystal capture and displacement. It is unlikely that the anomalous crystals in enclaves were derived from the current host rocks, or vice-versa, due to the discrepancy in core compositions between enclave-host rock pairs. Instead, crystal displacement likely took place during an earlier mixing events at deeper levels in the crust where average magma viscosities were lower. Together, the geochemical evidence suggests host rocks and enclaves are composed of crystals that had unique histories involving transportation and displacement between multiple magmas and mush-like reservoirs during their ascent through the crust.

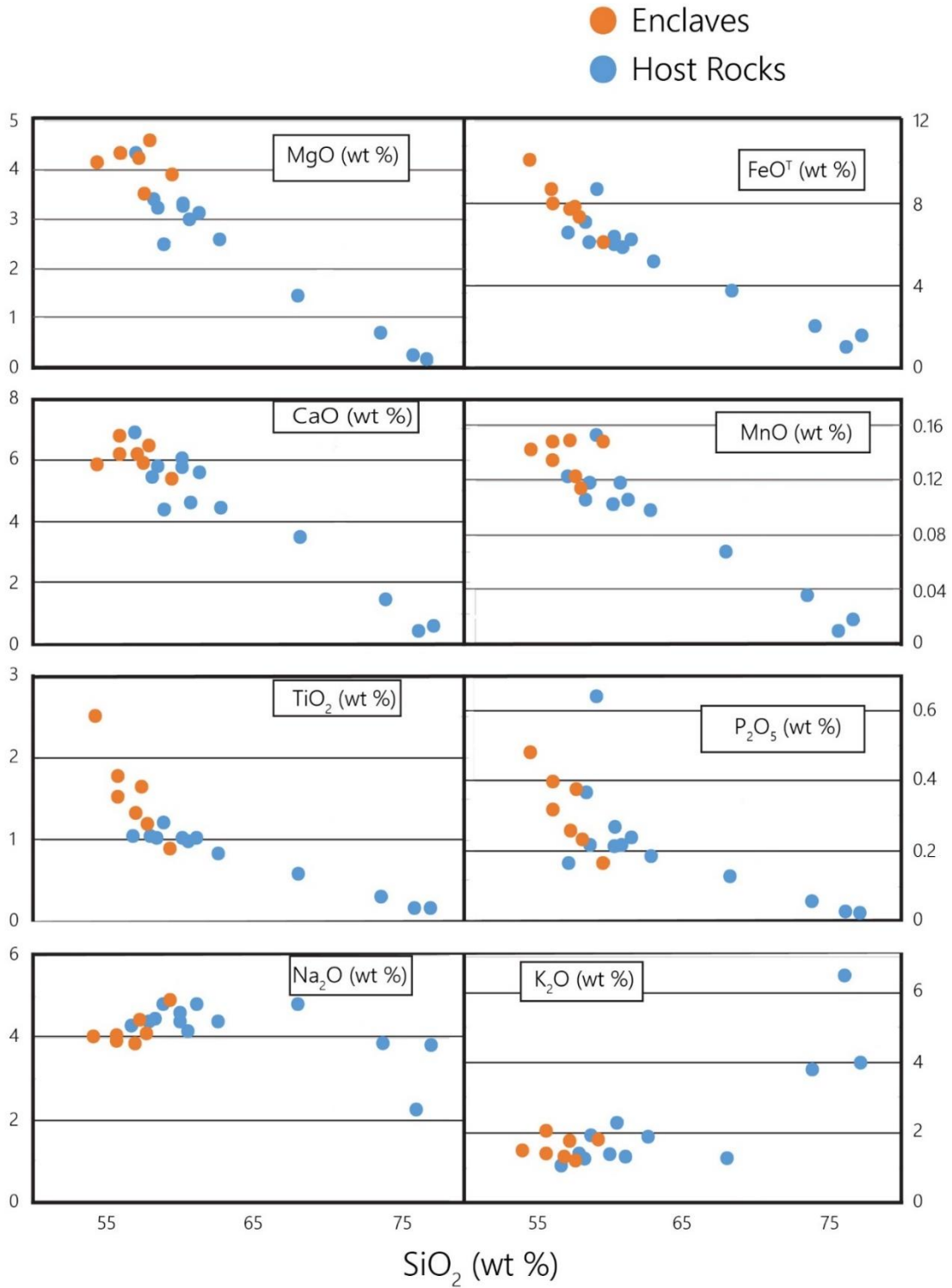


Figure 4.1. Major element Harker diagrams for enclaves and host rocks displaying mingling relationships in the study area.

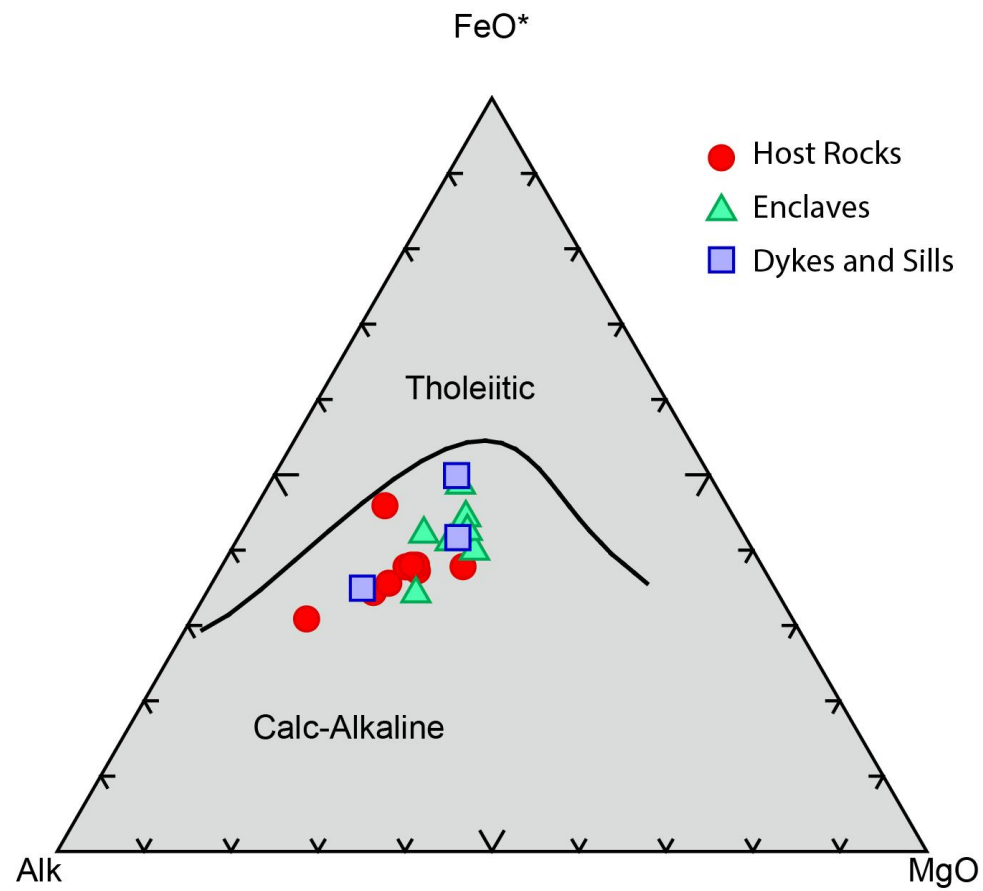


Figure 4.2. AFM diagram for host rocks, enclaves, and dykes/sills that display mingling relationships in the study area. A calc-alkaline signature is displayed by all units, reflecting input from continental material.

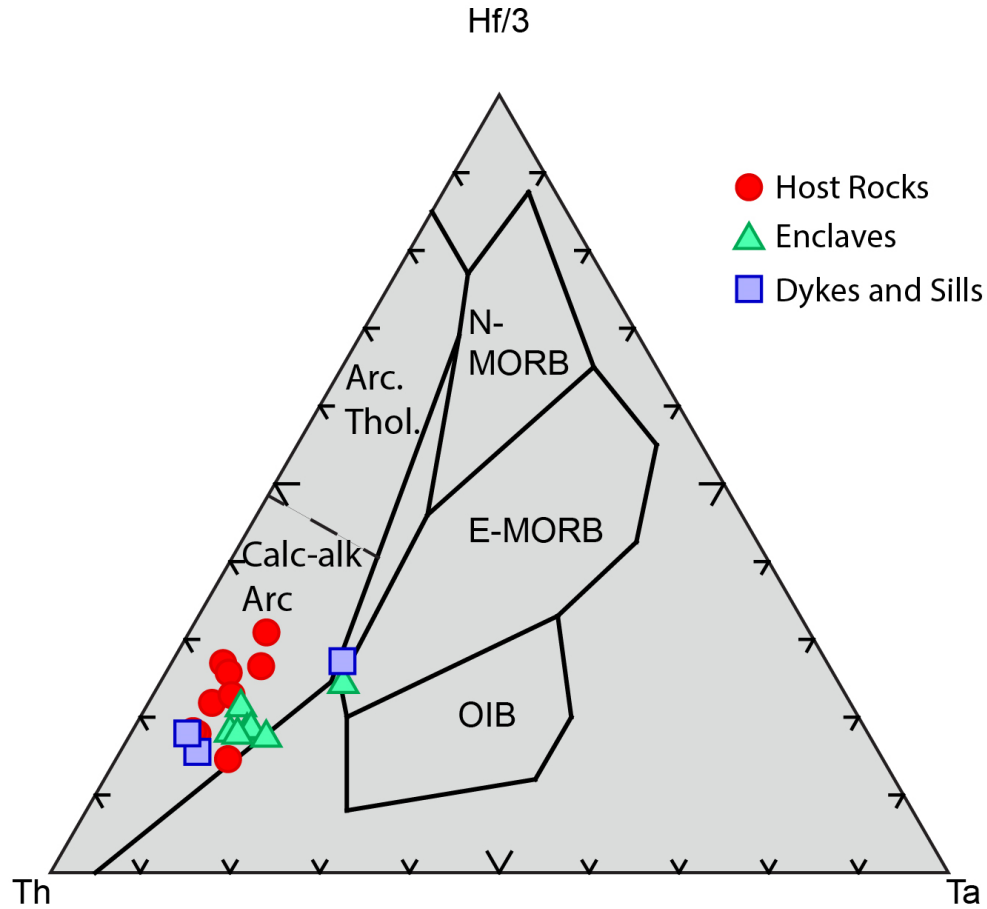
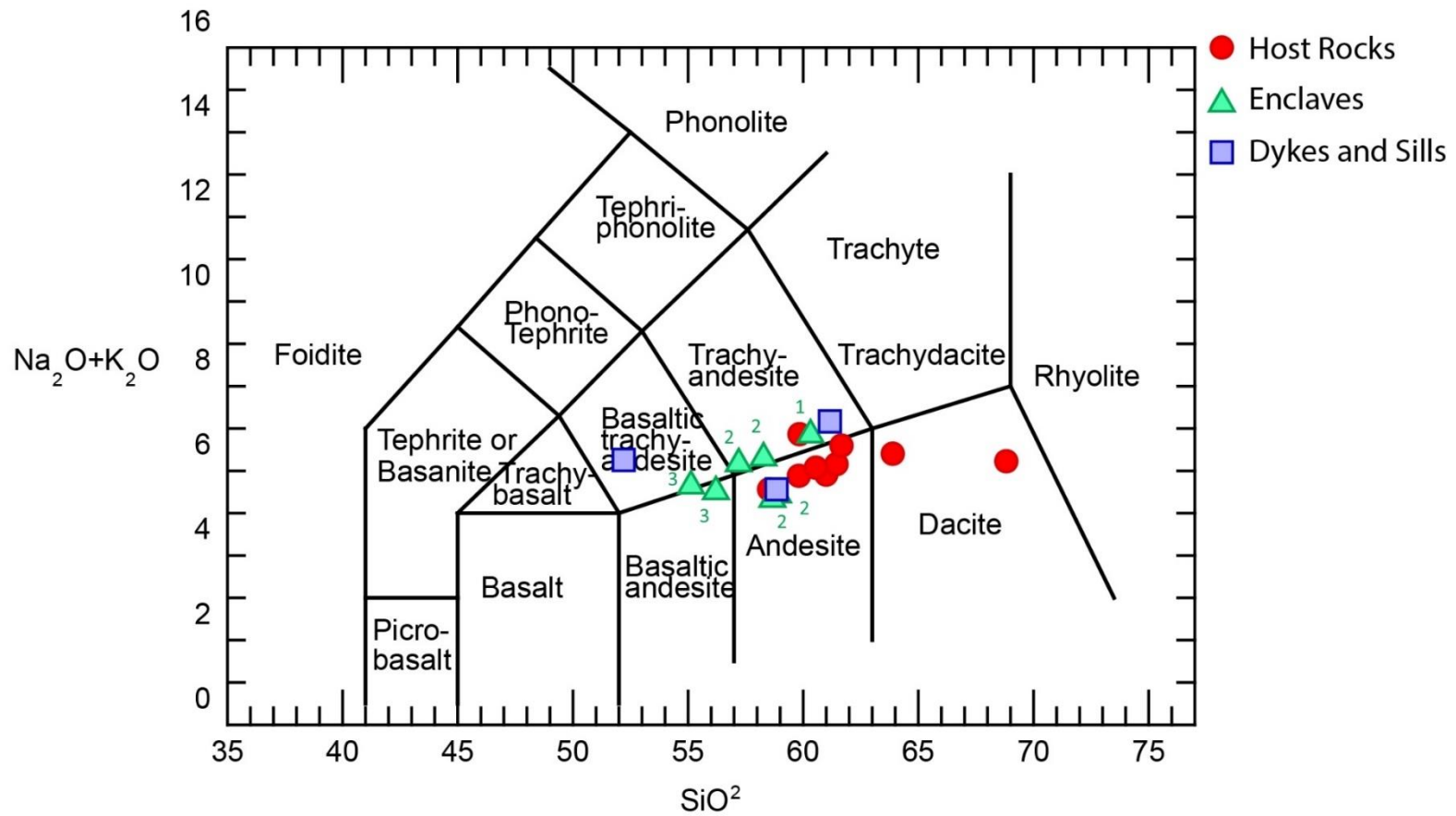


Figure 4.3. Th-Hf-Ta plot of Wood (1980) for selected host rocks, enclaves, and dykes/sills. N-MORB = normal, depleted mid-ocean ridge basalt, E-MORB = enriched mid-ocean ridge basalt, OIB = ocean island basalt, Arc Thol. = volcanic arc tholeiite, Calc-Alk Arc = calc-alkaline volcanic arc basalt.



(Lebas et al, 1986)

Figure 4.4. TAS (total alkalis vs. silica) plot following Lebas et al. (1986) for mingled host rocks, enclaves (numbered by group), and dykes/sills in the study area.

- 1 - Group 1 Enclaves ● Enclaves
- 2 - Group 2 Enclaves ● Host Rocks
- 3 - Group 3 Enclaves ● Dykes and Sills

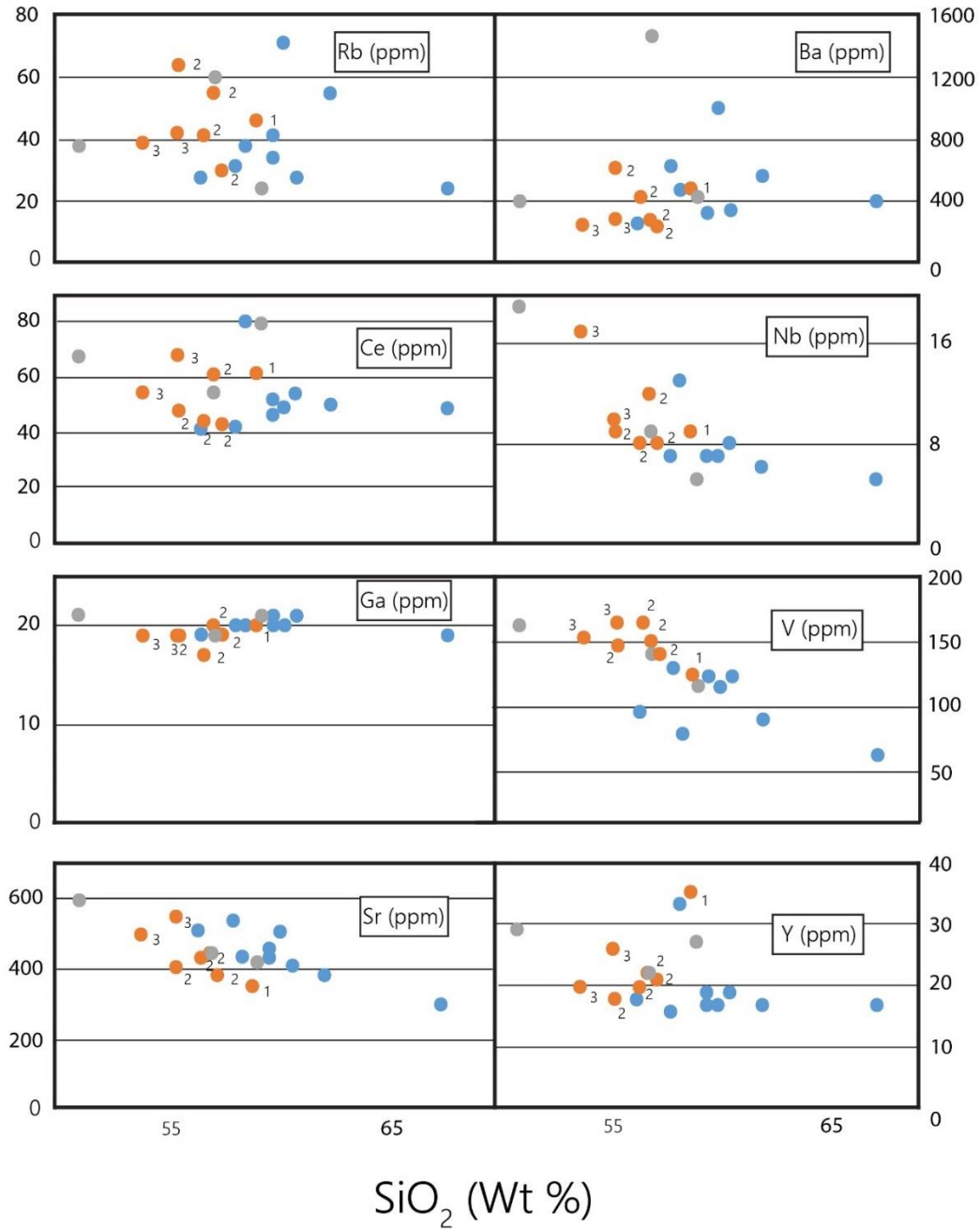


Figure 4.5. Trace element Harker diagrams for enclaves, host rocks, and dykes that display mingling relationships in the study area.

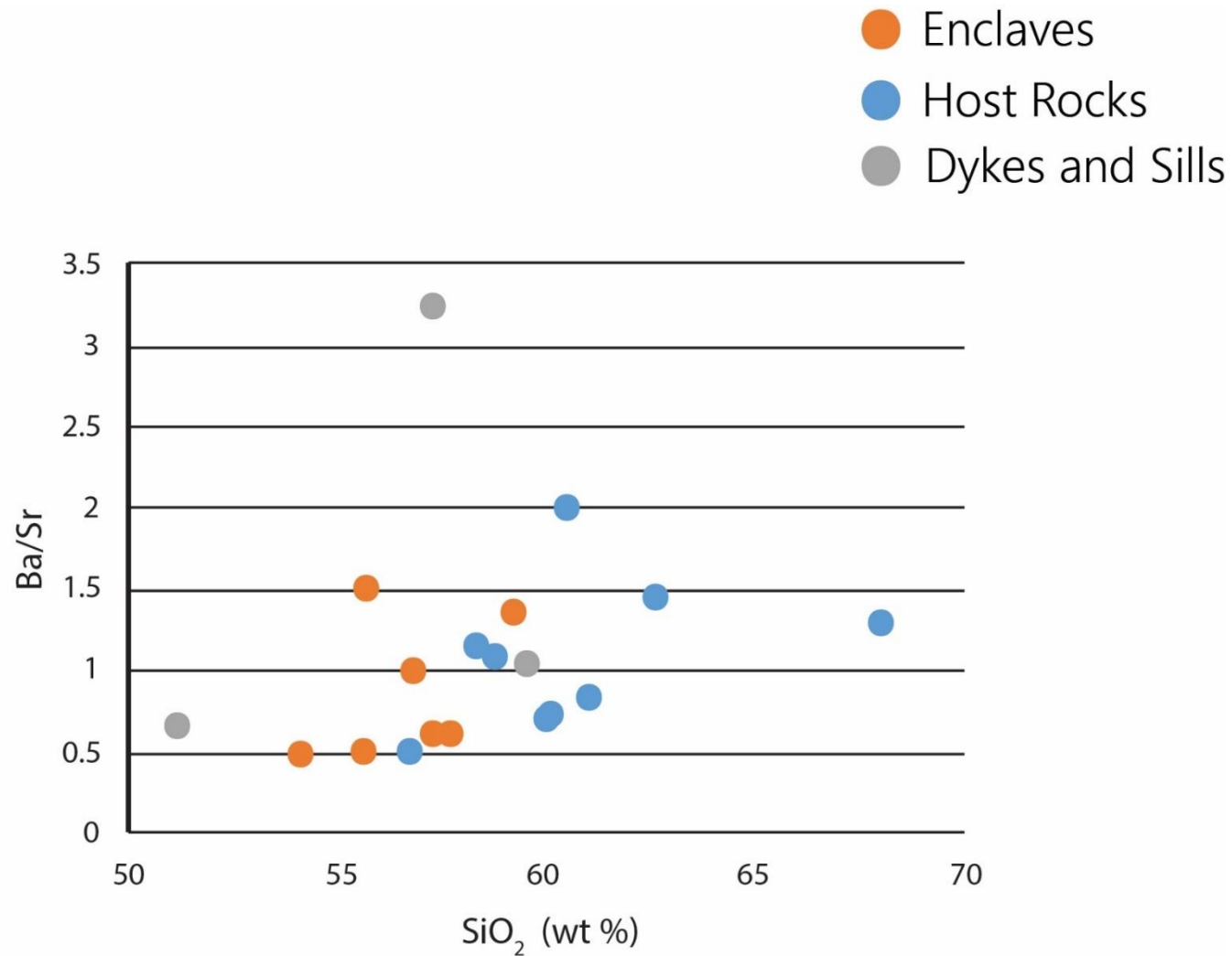


Figure 4.6. Plot of Ba/Sr vs SiO₂ for selected host rocks, enclave and dyke/sills. All units display increasing Ba with SiO₂ suggesting increasing abundance of plagioclase and lack of orthoclase crystallization (McBirney, 2007).

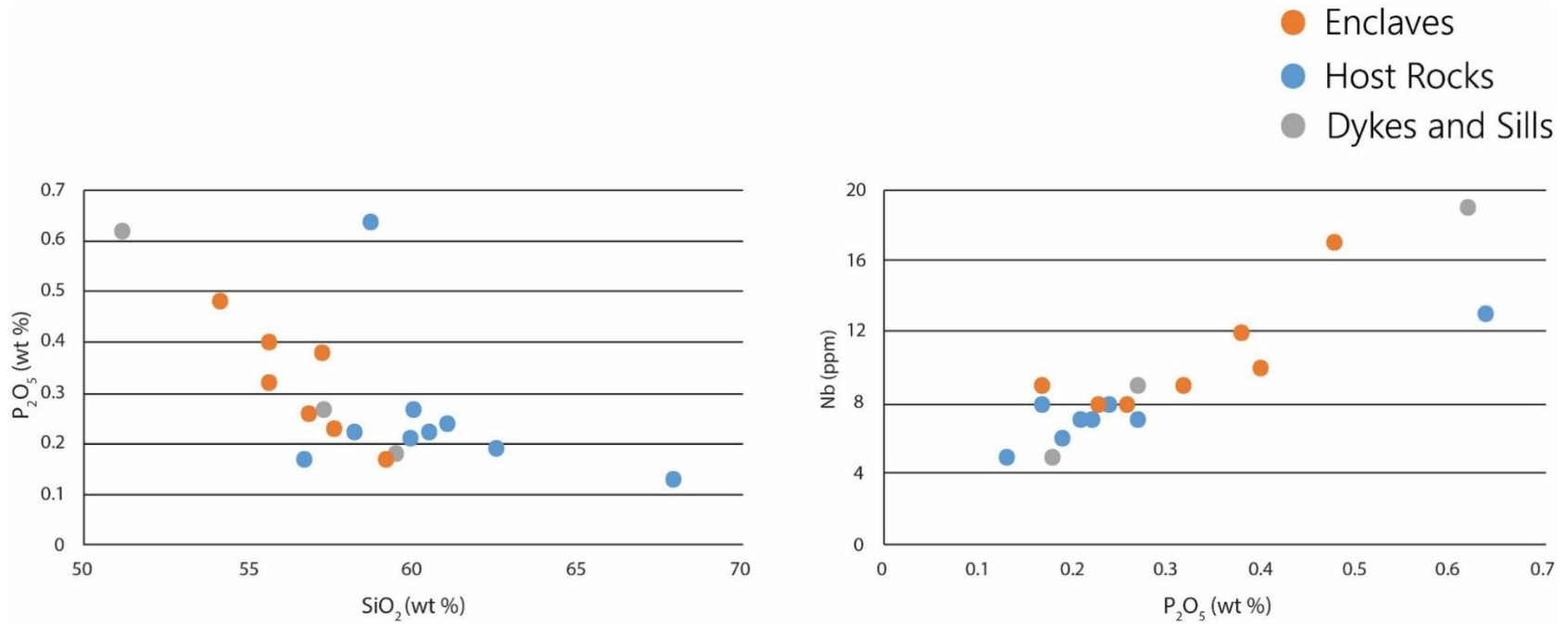


Figure 4.7. Plots displaying negative correlation of P_2O_5 with SiO_2 and a positive correlation of P_2O_5 with Nb. Combined with the negative correlation between SiO_2 and Nb (Figure 4.5), these relationships suggest Nb in enclaves, host rocks, and dykes is incorporated into accessory minerals such as apatite.

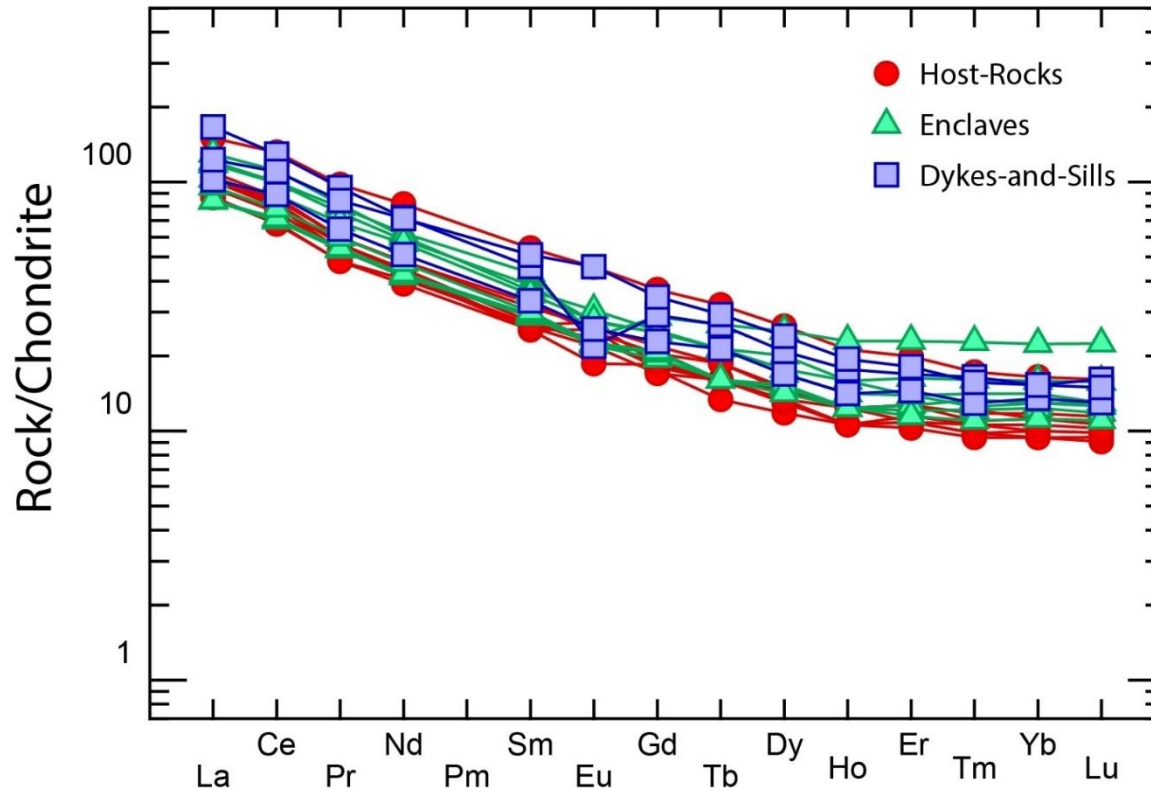


Figure 4.8. Chondrite-normalized REE patterns for host rocks, enclaves, dykes, and sills at Wild Cove East that display mingling relationships. The highest concentration of rare earths in the enclaves are a function of SiO_2 content, with the most silica-rich enclaves displaying the most REEs and the most silica-deficient enclaves displaying the lowest concentrations. This relationship is not observed in the host rocks however as the highest SiO_2 host displays the lowest concentrations of REEs. Therefore, REE concentrations, at least in the host rocks, are not solely a function of fractional crystallization (Winter, 2001).

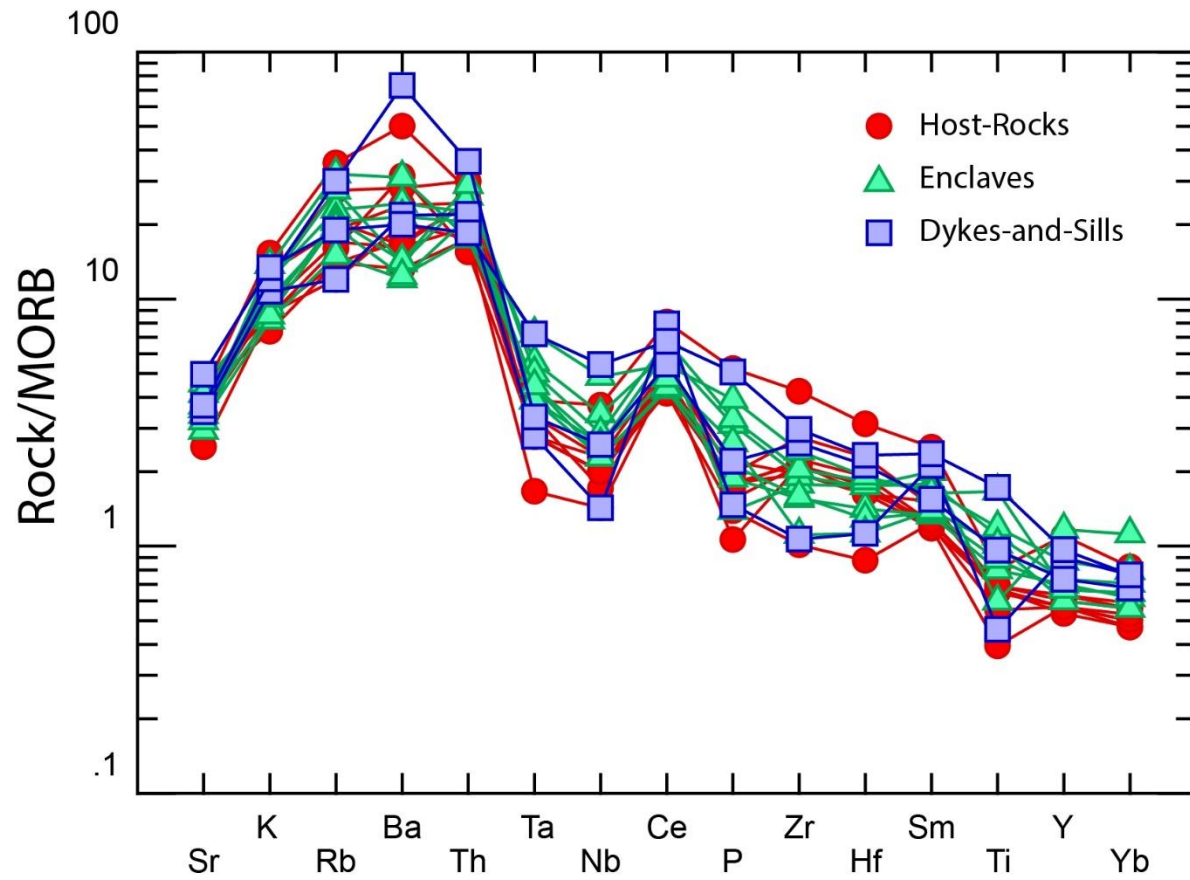


Figure 4.9. MORB-normalized REE plots for host rocks, enclaves, dykes, and sills that display mingling relationships in the study area. All units display enrichment of LIL elements (Sr, K, Rb, and Ba) relative to HFE elements (Ta-Yb), a chemical signature common subduction-related magmatism (Winter, 2001).

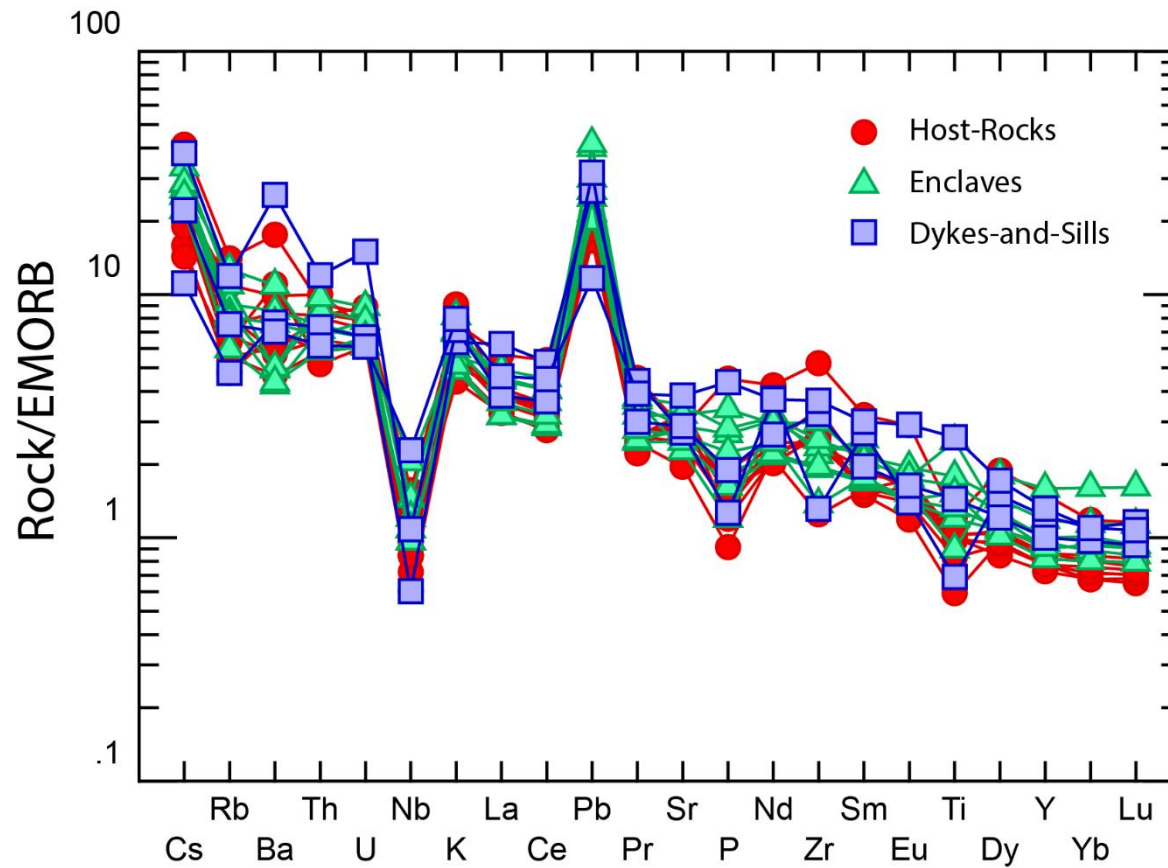
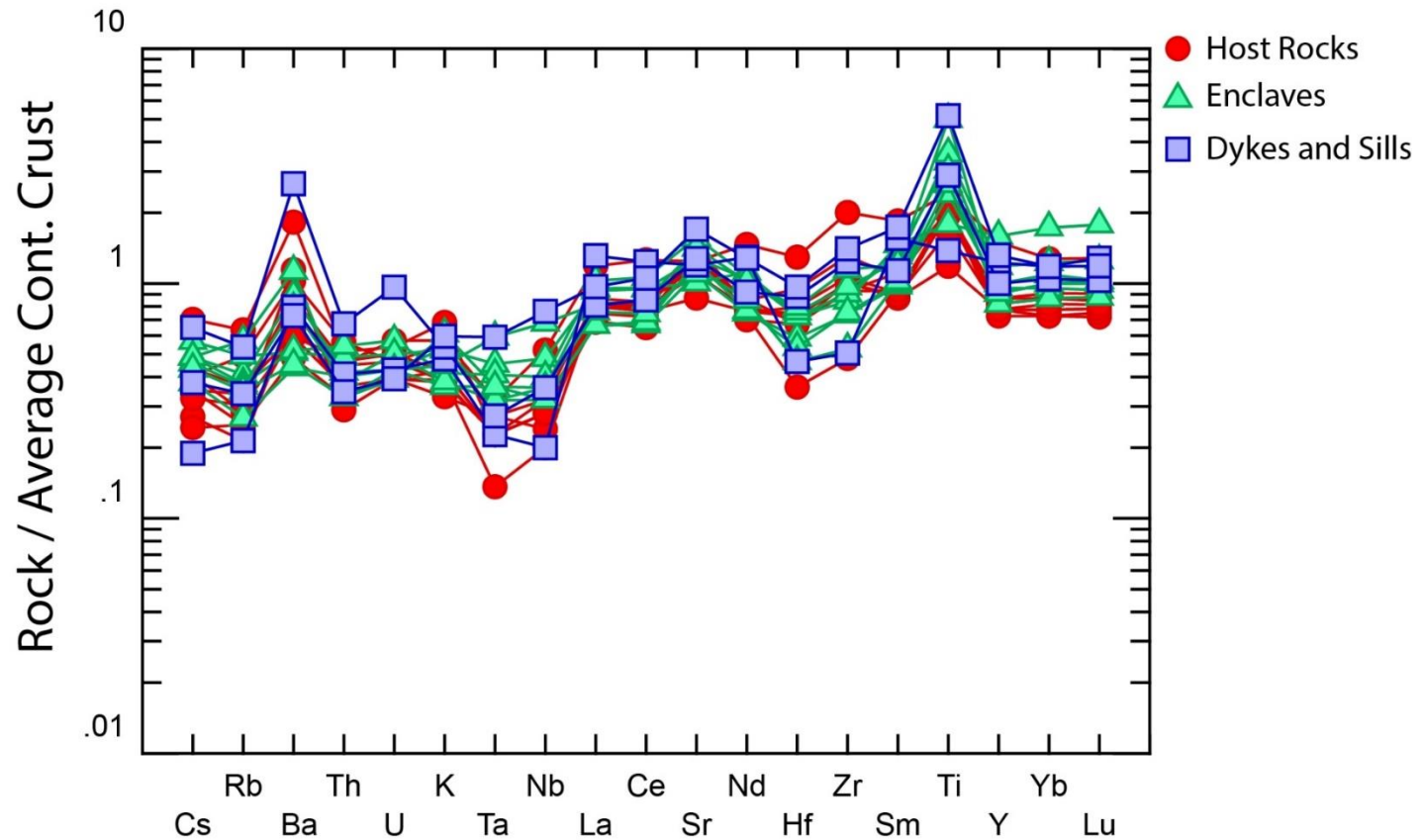


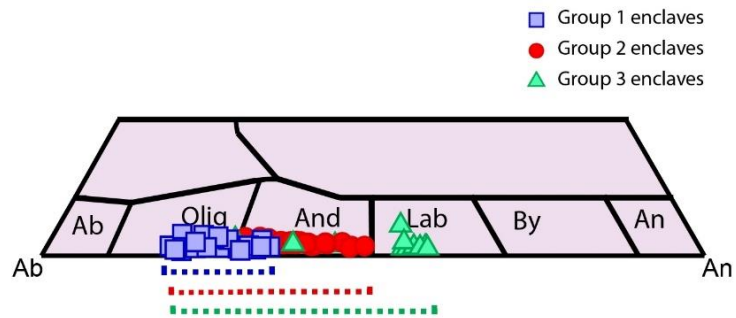
Figure 4.10. EMORB-normalized multi-element plot for host rocks, enclaves, dykes, and sill that display mingling relationships in the study area (Sun and McDonough, 1989). Elements are in order of increasing compatibility from left to right. All units are enriched in LIL, particularly in the most incompatible elements (Cs, Pb, K) (Winter, 2001). The spiked section pattern is consistent with subduction or plate margin settings (Winter, 2001).



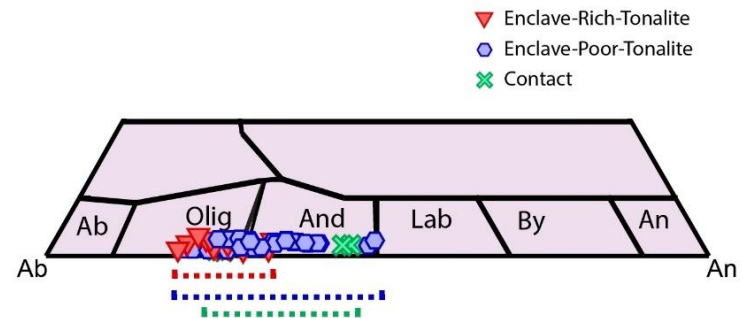
(Taylor and McLennan, 1985)

Figure 4.11. Plot of incompatible elements normalized to upper continental crust for selected host rocks, enclave, and dykes/sills (Taylor and McLennan, 1985) showing nearly identical values except for slight depletion in large ion lithophile (LILE) enrichment and negative Ta-Nb anomaly, a typical signature of arcs.

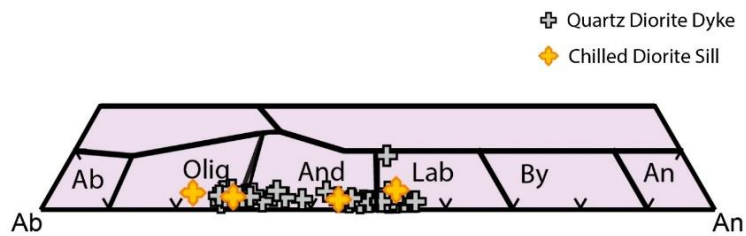
A. Enclave Plagioclase Compositions



B. Host Rock Plagioclase Compositions



C. Dykes and Sills Plagioclase Compositions



D. Layered Mafic Intrusion Plagioclase Compositions

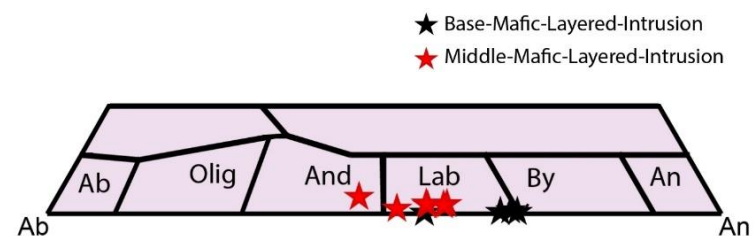
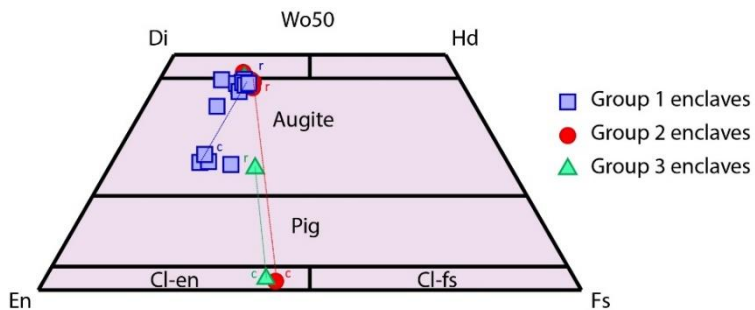
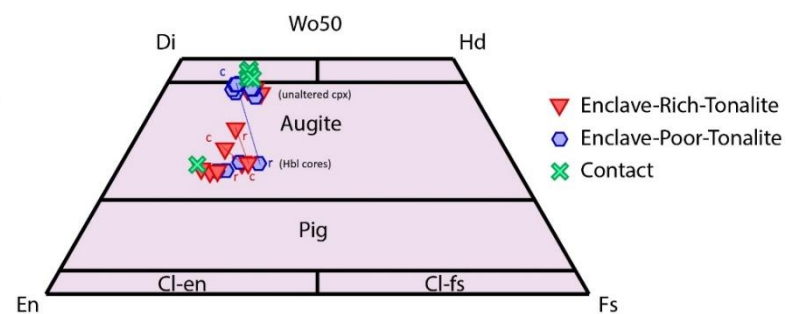


Figure 4.12. Feldspar ternary plots of selected host rocks, enclaves, and dykes/sill in the study area. A) Feldspar ternary plot of enclave populations at Wild Cove. Despite similar rim compositions in all groups, a distinct range in core composition is observed in each. Rims generally display more evolved compositions than cores but in some cases the cores are more evolved than the rims. B) Feldspar ternary plot of the two intermediate host rock units and the contact between them. Considerable overlap is observed between the host units but the most Ca-rich plagioclase compositions are observed in the enclave-poor tonalite. Plagioclase in the contact have higher An content than in the enclave-rich tonalite and are comparable to the most primitive plagioclase in the enclave-poor tonalite. C) Feldspar ternary plot of quartz diorite dyke in the northernmost part of the study area and the diorite sill. The overall range in both units is comparable to the combined range observed in all nearby host rocks and enclaves. D) Feldspar ternary plot of mafic layered intrusion located in easternmost part of study area. The base of the sill is composed of labradorite-bytownite and is the most primitive of all analyzed plagioclase. The middle of the sill is composed of andesine-labradorite.

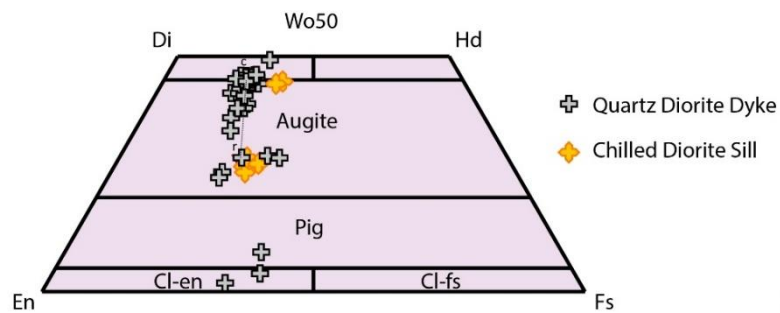
A. Enclaves Pyroxene Compositions



B. Host Rock Pyroxene Compositions



C. Dykes and Sills Pyroxene Compositions



D. Mafic Layered Intrusion Pyroxene Compositions

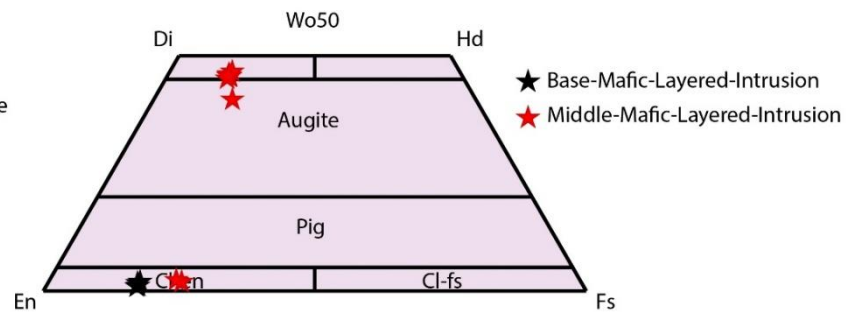


Figure 4.13. Pyroxene quadrilateral plots for selected host rocks, enclaves, and dykes in the study area; A) Pyroxene quadrilateral plot of mafic magmatic enclaves of Wild Cove East. Most analyzed pyroxene, regardless of group, plot in the Ca-rich end of the augite field. A trend is observed in a zoned Group 1 clinopyroxene from Ca-poor augite at the core to Ca-rich augite at the rim. Several pyroxene inclusions in plagioclase plot in the enstatite field whereas others plot in the Ca-poor augite field. B) Pyroxene quadrilateral plot of host rocks in the study area. Like the enclaves, many of the analyzed host rock pyroxene plot in the Ca-rich augite field. Pyroxene from the contact between the two intermediate host units are generally of diopside composition. Analyzed enclave-rich tonalite pyroxene immediately adjacent to this contact, however, plot in the Ca-poor augite field. Pyroxene that are now corroded cores in hornblende, from both host rock units, similarly plot towards the Ca-poor end of the augite field. C) Pyroxene quadrilateral plot of quartz diorite dyke located in northernmost end of field area and the diorite sill. A trend is seen across two pyroxene grains that oscillates from Ca-rich to moderately Ca-rich augite. In the diorite sill, one corroded pyroxene core displays Ca-rich augite/diopside composition whereas other corroded pyroxene displays Ca-poor augite composition. D) Pyroxene in the mafic layered sill includes enstatite at the base and Ca-rich augite/diopside at the middle.

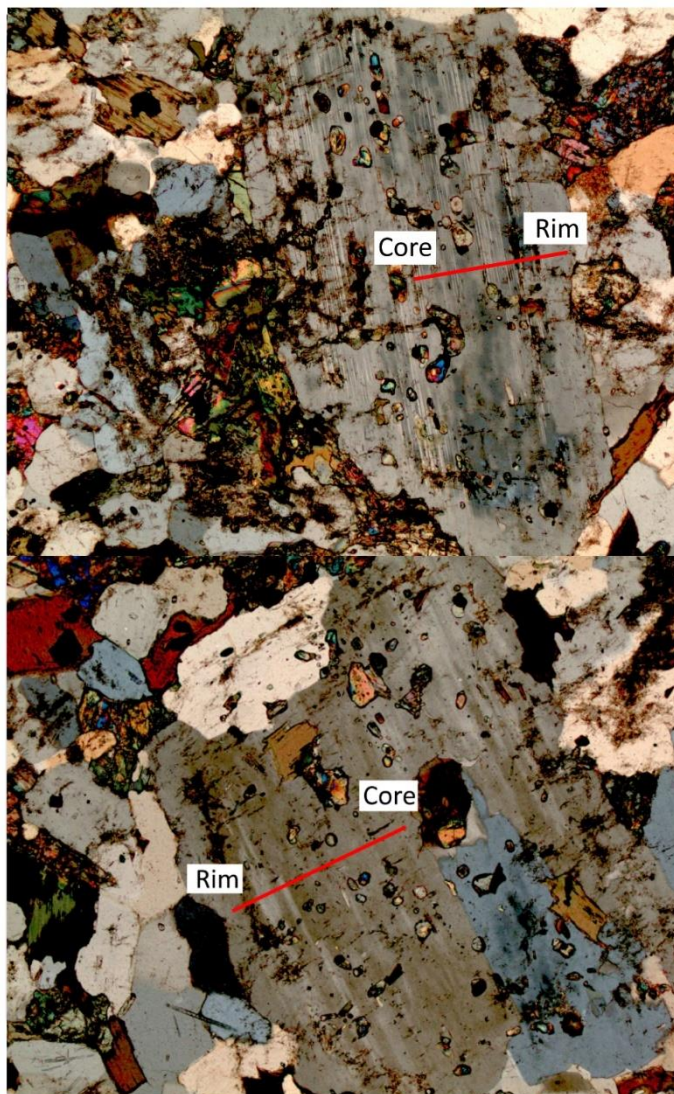
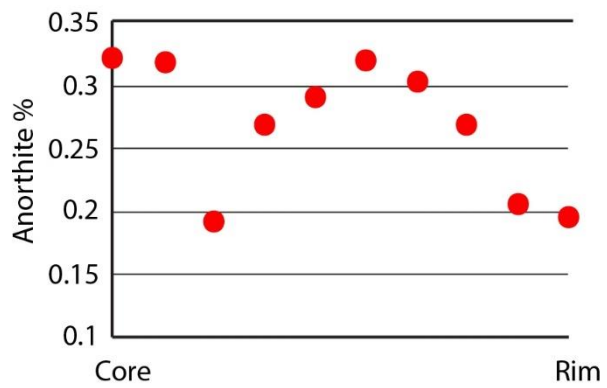
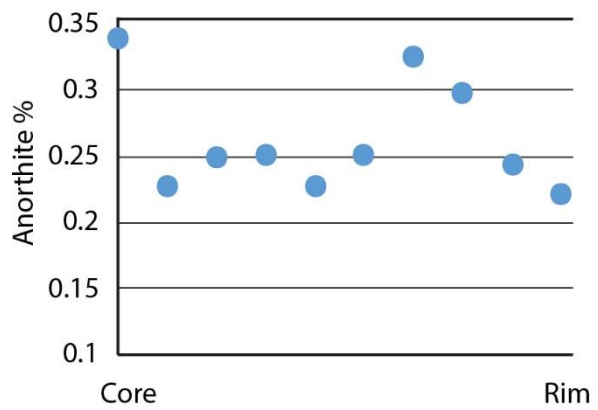
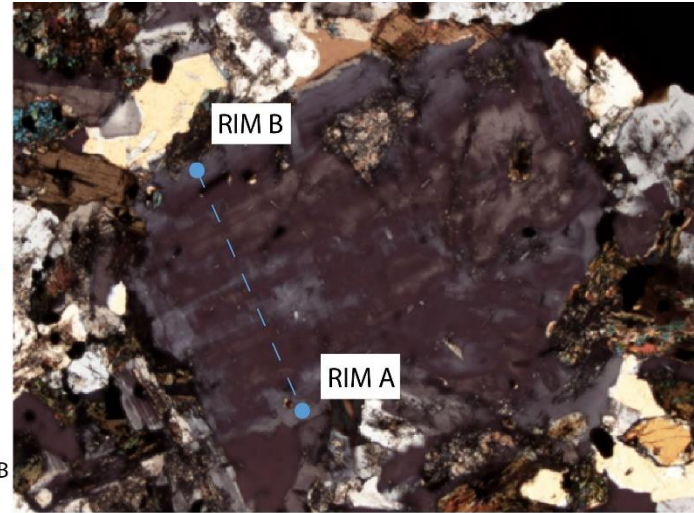
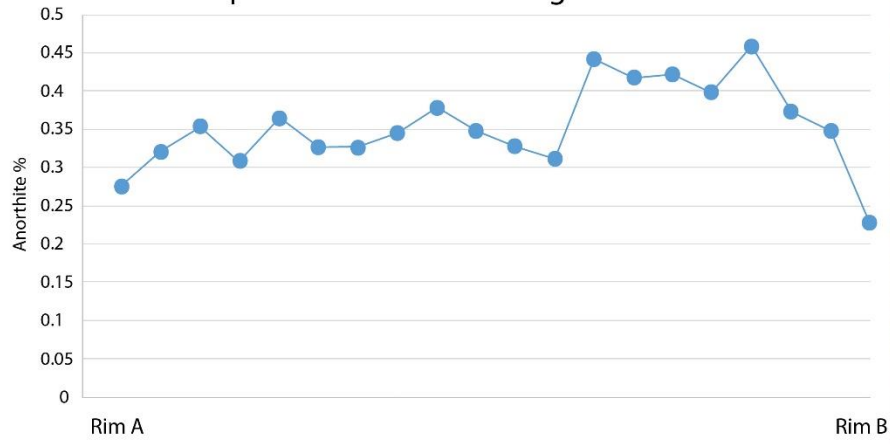


Figure 4.14. EPMA traverse across a resorbed plagioclase phenocryst contained in Group 1 tonalite enclave. Two distinct zones are observed in both crystals: a resorbed An₃₅ andesine core and an An₂₀ oligoclase overgrowth/rim. Fine rounded clinopyroxene inclusions are restricted to the andesine core regions of both crystals. Mottling and resorption of the core by a more albite-rich phase may be due to decompression melting (Nelson and Montana, 1992). Resorption of clinopyroxene inclusions also likely occurred, based on the similar extinction angles between separate inclusion populations.

Group 2 Enclave Mottled Plagioclase A



Group 2 Enclave Mottled Plagioclase B

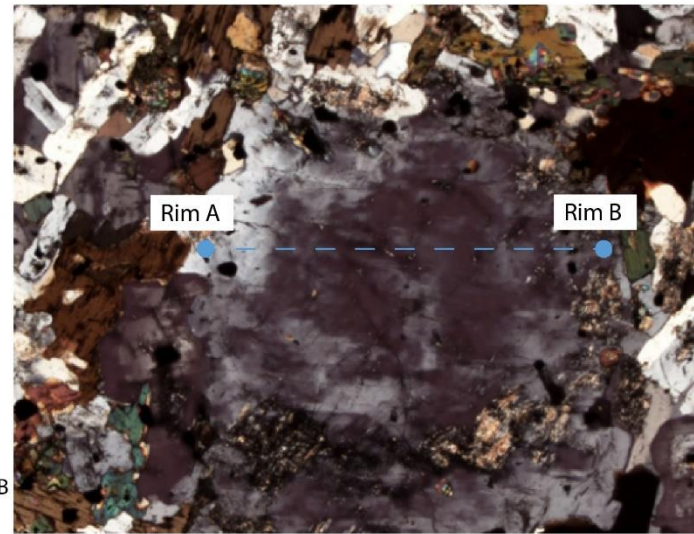


Figure 4.15. EPMA traverse across two resorbed plagioclase phenocrysts contained within a Group 2 biotite tonalite enclave. Both crystals display a compositional range of An₂₅-An₄₅ with andesine cores and oligoclase rims. Abrupt peaks and valleys in An % across traverse correlate with patchy zoning in the mineral. Rim compositions and extinction colour are identical to irregular embayments which truncate mottled cored regions. The outermost parts of corroded cores are more calcic than the innermost regions and may represent an earlier mixing event that affected these crystals (Wiebe, 1968).

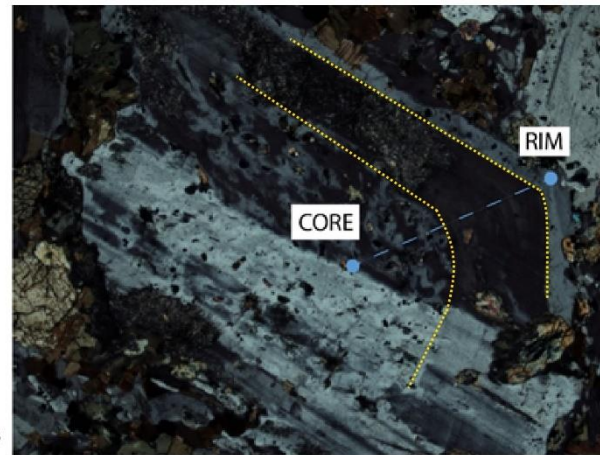
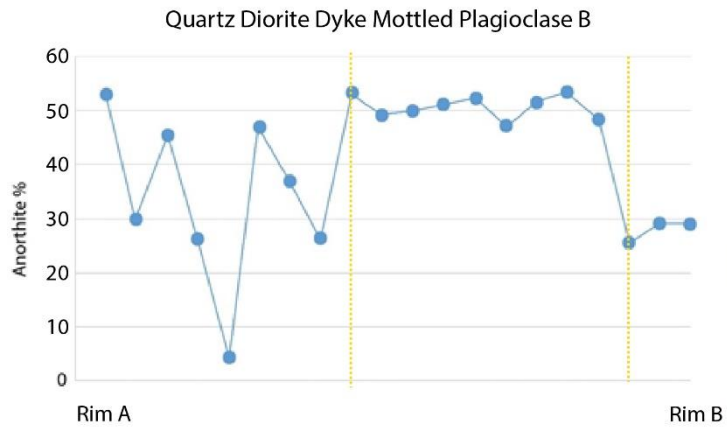
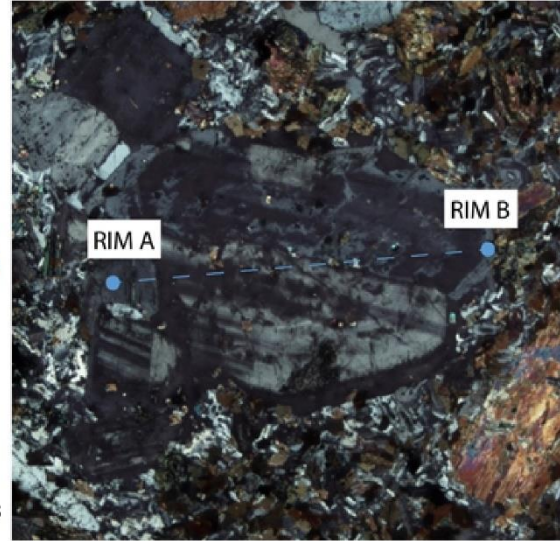
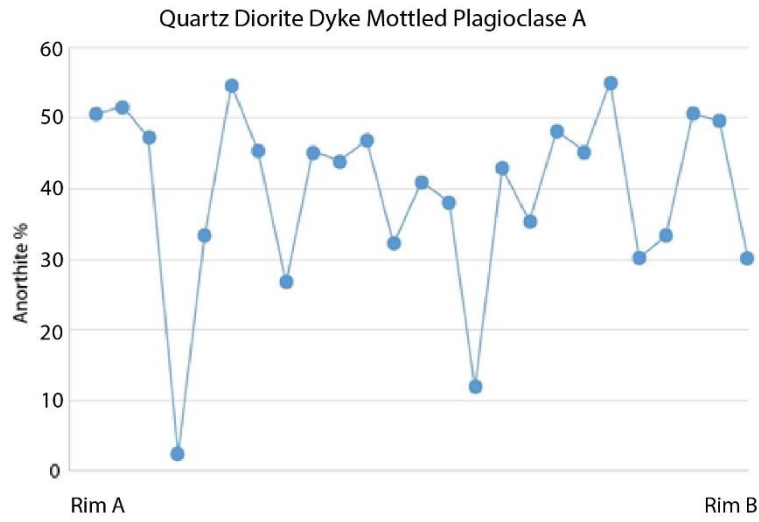


Figure 4.16. EPMA traverse across two resorbed plagioclase phenocrysts contained within a quartz diorite dyke that located at the northernmost end of the study area. These dykes preserve evidence break-up into rounded globules due to interactions with host material, a possible mechanism by which some of the enclaves were formed. Both crystals display a compositional range of An_{50} - An_{30} , and oscillations between these two end-member compositions are observed within the mottled regions of the crystal. The abrupt change from An_{30} at the core to An_{50} towards the rim can be explained by injection a hotter and more primitive magma. Hybridization between host and injected magma may have resulted in the formation of An_{30} rims (Andrews et al, 2008). In (A), the mottled region extends across the entire length of the crystal whereas in (B) contains mottled textures only in the core regions. Pyroxene and Fe-Ti oxide inclusions are restricted to the mottled oligoclase interior.

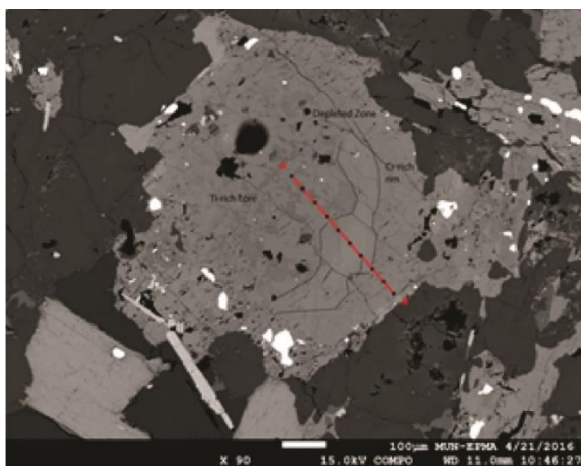
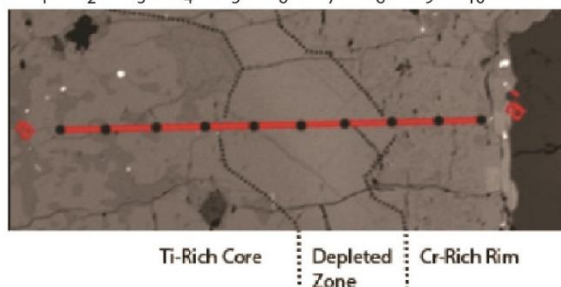
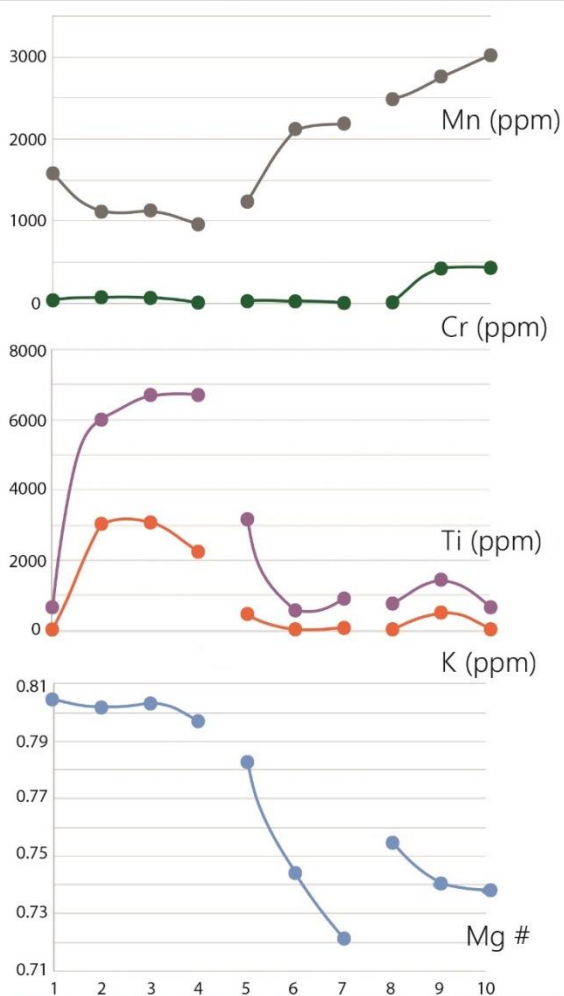


Figure 4.17. A Group 1 enclave clinopyroxene displaying three distinct compositional zones was analyzed using the EPMA to assess its history. A ten-point traverse was conducted from core (a) to rim (a') as seen in the backscatter image to the left.



The core of the crystal is enriched in TiO_2 and K_2O . This is correlated with the presence of Ti-bearing minerals such as ilmenite in the core (oxide minerals are coloured white in the backscatter image above). The core is titanite (Leung, 1974), a mineral that generally crystallizes from alkaline magmas.

Mg # is high in the core region but decreases towards the edge of the middle depleted zone of the mineral. A significant increase of Mg # and Cr_2O_3 occurs at the outer zone. Since Cr is typically enriched in mafic magmas, this suggests the overgrowth crystallized from a more mafic magma.

The compositional trends suggest a four-stage history:

1. First crystallization from a Ti-rich alkaline magma.
2. Fractionation of alkaline magma to form middle zone.
3. Late crystallization from a more mafic Cr-rich magma.
4. Incorporation into tonalite crystal mush.

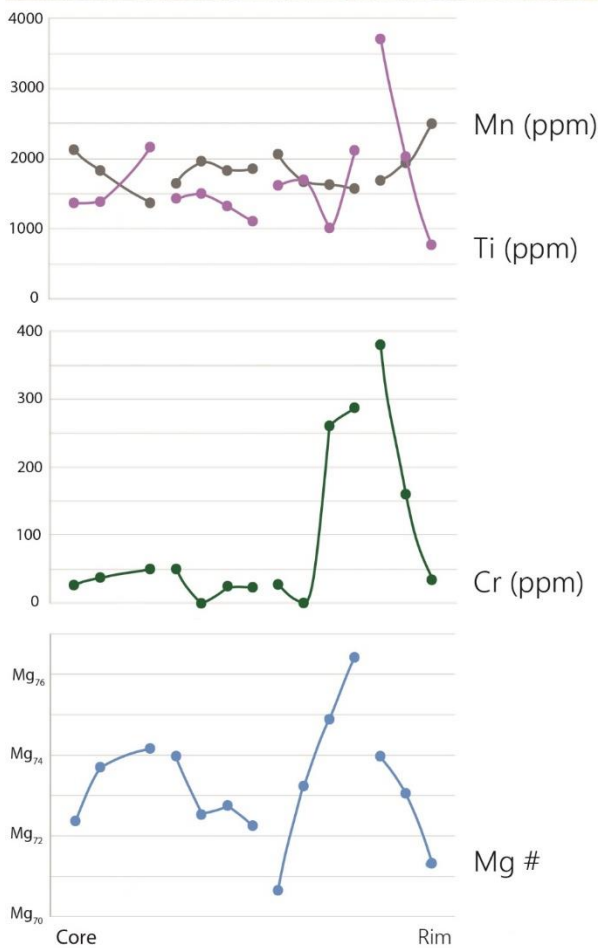
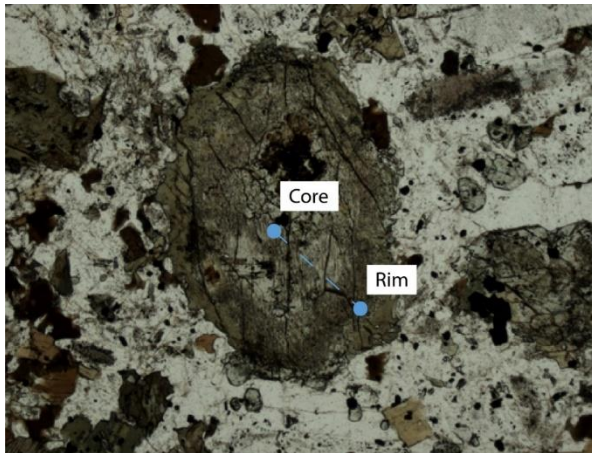


Figure 4.18. EPMA traverse across pyroxene in quartz diorite dyke in western part of study area that display evidence for MME formation. 15 points were analyzed from core to rim. A narrow range in Mg# is seen from Mg₇₆ – Mg₇₁ which sinuously oscillates between endmembers across the traverse. The second peak in Mg# at points 11-13 is accompanied by a rise in C₂O₃ from nearly zero to almost 400 parts per million. Similarly, a rise in Ti is observed in this region from around 2000 ppm to almost 4000 ppm.

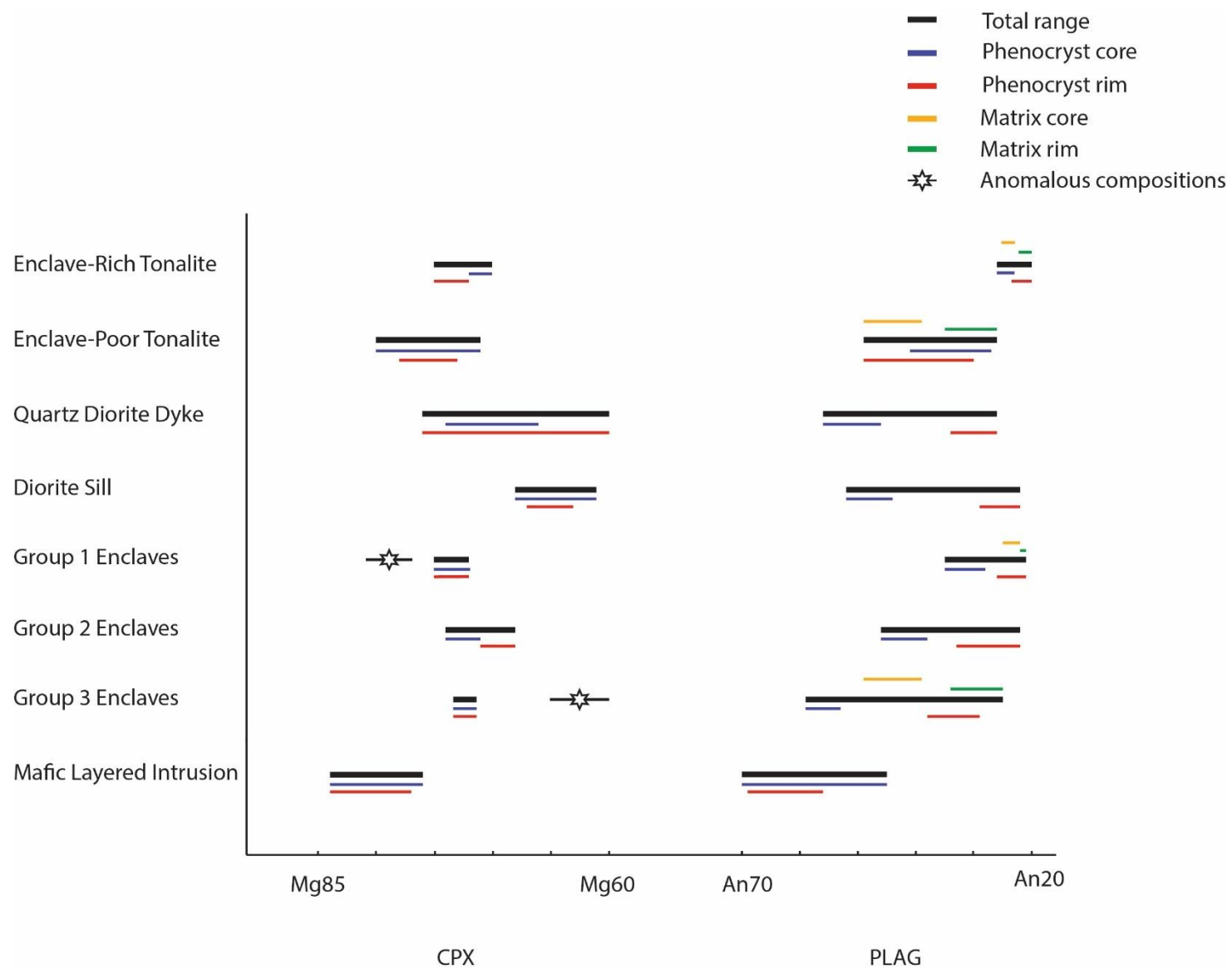


Figure 4.19. Summary plot displaying range in composition of pyroxene and plagioclase in major units. Lines with stars represent anomalous mineral compositions that are unusual compared to the rest of the rock such as: 1) Mg₈₀–Mg₇₆ core of corroded pyroxene in a group 1 enclave (reported in Figure 4.17), and 2) Pyroxene in Group 3 enclave with an Mg₆₅ core and Mg₆₀ rim.

Chapter 5 – Physical Properties of Crystal Mushes

This chapter will discuss the rheological properties of various units in the study area including host rocks, enclaves, and dykes. The relative rheology of magmas has a significant influence on the types of interaction that will take place between different magmas (i.e. mingling vs mixing). Physical properties including temperature, density, and viscosity will first be defined and their implications for magmatic processes will then be discussed.

5.1 Temperature and heat transfer in magma bodies

5.1.1 Liquidus and solidus temperatures

At temperatures above the liquidus, magmas are entirely molten and no crystals exist in suspension. Crystallization begins as magmas cool below the liquidus and continues until the solidus (100% crystalline) is reached. The rate of crystallization generally does not increase linearly with increasing temperature, particularly in intermediate and felsic magmas (refer to Figure 1.6). Basaltic magmas have higher solidus temperatures (~1300 °C liquidus and ~950 °C solidus at 10 kb [~35 km depth], respectively) than granitic magmas (~1200 °C liquidus and ~650 °C solidus at 10 Kb [~35 km depth], respectively), and therefore begin crystallizing at higher temperatures (Stern *et al*, 1975). Granitic magmas, having a wide range between liquidus and solidus, can stay partially molten over a large temperature range. The temperature range between liquidus and

solidus for a typical tonalite was assumed to be 1050 – 850 °C based on experiments by Stern *et al* (1975). The rate of crystallization during this temperature interval was estimated by Bachmann and Huber (2016) to be 1000 °C = 10 vol % crystals, 950 °C = 30 vol % crystals, 900 °C = 50 vol % crystals. The addition of water acts to lower the liquidus and solidus temperatures in all magmas. The solubility of water is generally higher in felsic magmas and has a strong dependence on pressure (Burnham, 1980).

Magmas generally behave as crystal mushes when crystal proportions are at approximately 25-50% (Marsh, 1981). Beyond 50% crystallinity, magmas reach a maximum packing of crystals that form a strong interlocking network and causes them to behave as partially molten solids (Marsh, 1981). At lower crystallinities, the magma does not form a fully interlocking framework and instead behaves as a mush in which crystals are unable to move freely relative to one another (Marsh, 2002). Below 25% crystallinity, the crystals are suspended in the melt and can move independently by processes such as crystal settling (if crystals are denser than surrounding melt) or by magmatic turbidites (Irvine *et al*, 1998). Mafic magmas form permeable monomineralic strings (primarily plagioclase and pyroxene) that provide strength to a mush even at low crystallinities (Philpotts and Carroll, 1996). Compaction or filter pressing of a crystal mush, particularly at low crystallinities (< 35% in basalts), can result in the separation of interstitial liquid from the crystal framework (Philpotts and Carroll, 1996).

5.1.2 Heat transfer in magma reservoirs

Crustal magma chambers represent highly complex thermodynamic systems in which the overall energy balance is reliant on multiple processes. The cooling rate of a pluton depends primarily on the thermal conductivities and latent heat of crystallization of both the magma body and wall rocks (Nabelek *et al*, 2012). Heat is lost immediately after emplacement of a magma body by conduction to surrounding country rocks (Bachmann and Huber, 2016). Consequently, the length of time magmas remain entirely molten is limited. Steady-state conduction is governed by Fourier's Law ($q=k\Delta T/\Delta z$), which states that heat travels proportional to a gradient from high temperature to low temperature, where k = thermal conductivity (W/mC). Heat flux (q) increases with increasing temperature gradient (ΔT) and decreases with increasing width of the gradient (Δz). When integrated to a homogenous material of 1-D geometry between two endpoints at constant temperature, heat flow rate is given by:

$$\frac{Q}{\Delta t} = -kA \frac{\Delta T}{\Delta x}$$

where A is the cross-sectional surface area, ΔT is the temperature difference between two ends, and Δx is the distance between two ends.

Heat transfer from a magma chamber changes with time and is therefore not steady-state. The temperature gradient (dT/dz) will become less with increasing time as the magma body and surrounding rocks become similar in temperature. When magma is emplaced into cool country rock, the initial temperature gradient is high and heat transfer

is rapid. However, the temperature gradient and the heat transfer rate decrease immediately after heat is transferred from the magma into the country rocks. A simple cooling timescale for a magmatic body is modelled by:

$$\tau = \frac{D^2}{4\kappa}$$

Where D is the length scale (e.g. width of a dyke, radius of a sphere). Thus, the cooling rate is longer for larger magma bodies and is inversely proportional to thermal diffusivity, κ , which is given by:

$$\kappa = \frac{k}{\rho c_p} \left(\frac{m^2}{s} \right)$$

Where k is thermal conductivity (W/mK), and ρ is density (kg/m³). The specific heat capacity c_p (J/kg/°C) is the ability of a material to store heat.

The cooling rate of magmas decreases as the temperature contrast between the magma and country rock becomes smaller. In addition, processes such thermal convection and mafic recharge will act to decrease, or even reverse, the cooling rate in magma reservoirs (Bachmann and Huber, 2016). Therefore, magmas tend to stay at near-solidus temperatures for long periods (Bachmann and Huber, 2016). Energy supplied from fresh magmatic injection can cause remelting of the mush and the formation of a melt-rich mobile layer (Burgisser and Bergantz, 2011; Zavala *et al*, 2011). Another consequence

of these processes is the unlikelihood that thermal diffusion ever reaches equilibrium at the reservoir-scale in open magma chamber systems (Bachmann and Huber, 2016).

As contact aureoles between magmas and surrounding wall rocks get hotter the amount of heat that is transferred across the contact decreases since thermal diffusivity decreases with increasing temperatures in rocks (Nabelek *et al*, 2012). In turn, this acts to decrease the cooling rate of the pluton. The temperature dependence of thermal diffusivity can act to more than double the crystallization time in magma intrusions and keep them as mush-like fluids for an extended period. A study by Nabelek *et al* (2012) determined, assuming the temperature dependence of thermal diffusivity, that a sill as thick as 50 meters can remain in a mobile mushy state for nearly 33 years after emplacement of a single batch of melt. Assuming there is no change in thermal diffusivity, the timescale would be reduced to approximately 19 years ($D^2/4\kappa = 2500/4 \times 10^{-6}$).

The thermal evolution of a mafic body that is entirely enclosed in a felsic host, such as a magmatic enclave, varies depending on the size of the body and the temperature difference between the two magmas. The heat equation indicates that the cooling rate of an enclosed mafic body is related to the inverse square of its diameter and therefore larger bodies will take a longer time to reach thermal equilibrium with a granitoid host (Fernandez and Barbarin, 1991). If thermal equilibrium is achieved quickly between small mafic blobs and a felsic host, the blobs will become rigid and chemical exchange between the two magmas will be strongly limited (Fernandez and Barbarin, 1991).

5.2 Rheological properties of magmas

5.2.1 Viscosity

Viscosity is an important control on the physical transport of lithospheric silicate melts and is dependent on both temperature and magma composition. It is defined as a measure of the internal friction within fluids that arises due to collisions at the molecular scale (Clemens and Petford, 1999). Among the earliest models for measuring magma viscosity were those conducted by Bottinga and Weill (1972), who estimated the influence of major oxide composition. Shaw (1965) modelled viscosity by the degree of polymerization (R) in a magma, a measure of the cation to oxygen proportion in the melt.

An important modifier of polymerization in magmas is water, which has a significant impact on magma viscosity. The addition of only a few weight percent water can decrease the viscosity by multiple orders of magnitude. As such, a wide range in viscosities is observed between anhydrous and mafic melts from 10^7 to 10 Ns/m². In general, temperature and water content are interdependent in granitic magmas due to magmas have a higher solubility for water at lower temperatures.

In addition to water, magma viscosity is highly dependent on the amount of crystals suspended in the melt. While the effects of water (decrease viscosity increase with cooling) and temperature (increase viscosity with cooling) counterbalance each other to some extent, increased crystal content during cooling will act to increase magma viscosity to very high values (e.g., Clemens and Petford, 1999). The physical effect of

crystals, assumed to be spherical shapes of equal size, is best modelled by the Einstein-Roscoe equation:

$$\eta_r = \frac{\eta_{mix}}{\eta_{melt}} = \left(1 - \frac{\phi}{\phi_0}\right)^{-2.5}$$

where ϕ is the crystallinity and ϕ_0 is the maximum packing fraction. When magmas exceed crystallinities of 20-25 vol%, they first behave like Bingham fluids that possess a yield strength and the rheology becomes non-Newtonian as a semirigid crystal network begins to form in the crystal mush (Clemens and Petford, 1999; Getson and Whittington, 2007).

5.2.2. Density

Magma density depends on several variables including: composition, water content, crystallinity, and temperature. Mafic magmas ($\sim 2.9 \times 10^3 \text{ kg/m}^3$ at room temperature) are denser than felsic magmas ($\sim 2.5 \times 10^3 \text{ kg/m}^3$ at room temperature). When felsic magma underlays mafic magma, as can be the case during mafic recharge events, the difference in density can lead to the formation of Rayleigh-Taylor instabilities at the boundary between the two magmas. Features such as load or flame structures can arise from these density instabilities due to the sinking of mafic magma or the buoyant rise of felsic magma (Wiebe and Collins, 1998). During crystallization, minerals generally sink because their individual densities are greater than the surrounding melt. An exception to this case is plagioclase feldspar, which is often less dense than a mafic melt

and therefore floats. The sinking/rising of crystals in a melt can be modelled using Stokes velocity:

$$v = \frac{2(\rho_{crystal} - \rho_{melt})}{9\mu} gR^2$$

where μ is the dynamic viscosity (kg/m.s) and R is the radius of the crystal.

Previous studies have suggested that magmatic enclaves of diameters greater than a few centimeters should sink faster than the rate of ascent of a newtonian granitoid host magma, estimated to be 13.1^{-3} - 145 cm/yr (Mahon *et al*, 1988). It is generally accepted, however, that most magmatic reservoirs largely exist as crystal mushes and therefore do not behave as newtonian fluids but rather as pseudo-plastic or visco-plastic bodies. Thus, to prevent enclaves from sinking during ascent the granitoid mush must have a high yield strength which, for a visco-plastic body, can be estimated by the volume fraction of crystals. A study by Fernandez and Barbarin (1991) estimated that a crystallinity of about 30% is needed to avoid sinking of enclaves in granitoid magmas.

5.2.3. Estimated Viscosities and Densities using KWare MAGMA

The effects of temperature and crystallinity on both viscosity and density were modelled for samples from Wild Cove East representing three enclave groups and major host rock units. Rheological properties were determined using KWare MAGMA, a software that uses user-entered oxide weight percentages, temperature, pressure, crystal volume

percentage, and crystal size parameters to calculate viscosity, density, and silicate classification. Effective viscosities are calculated to estimate the effect of crystals and vesicles on viscosity by the following equations:

$$\eta' = \eta (1 - R\phi)^{-2.5} \quad (\text{Bottinga-Weil estimation})$$

and

$$\eta' = \ln \eta + \frac{\alpha D}{[(\phi'/\phi)^{1/3} - 1]} - 0.15 \quad (\text{Shaw estimation})$$

Where η' is the effective viscosity, η is the liquid viscosity, ϕ is the volume fractions of crystals (and vesicles), R is the volumetric ratio of solids at maximum packing, ϕ' is the concentration of crystals (and vesicles) at maximum packing, and α is a constant that varies with mean diameter D . The program follows McBirney and Murase (1984) and uses $\alpha = 0.011$ and $R(\phi') = 1.0$. The development of the program was completely solely by Ken Wohletz at the Los Alamos National Laboratory of the University of California.

A gradual decrease in viscosity with increasing temperature is observed in representative host rocks and enclaves, assuming magmas are crystal-free and at constant pressure at 1km depth (=500 bars; Figure 5.2). Viscosity depends on SiO₂ content, with the most silicic units displaying the highest viscosities and all units displaying similar trends. The viscosities of all enclave samples are nearly two orders of magnitude less than the that estimated for the enclave-rich tonalite unit. The same conditions were imposed to calculate density, which decreases with increasing temperature in all units (Figure 5.3). Density is negatively correlated with silica content, with the most mafic units displaying

the highest densities. Enclaves display similar or higher estimated densities than the host rocks.

The effects of changing crystallinity on both magma viscosity and density were similarly examined using KWare MAGMA. In Figure 5.3, host rock and enclave viscosities were estimated under changing crystallinity and constant temperature (=1000 °C), pressure at 1km depth (= 500 bars), and spherical crystal size (= 0.5 mm). This is only intended to isolate the effect of crystallinity of viscosity and does not represent realistic conditions within the earth. All units show an increase in viscosity by roughly an order of magnitude with each 10% increase in crystallinity. At around 50% crystallinity, interpreted to be the rheological “lock-up” point by Huber, Bachmann, and Manga (2009), the rate of viscosity change is increased significantly. Under the same conditions, density increases linearly with crystallinity (Figure 5.4).

Since crystallinity will undoubtedly change with temperature, it is unrealistic to suggest the two properties will ever change independent of each other. Using the tonalite crystallization rate by Stern *et al* (1975) and Bachmann and Huber (2016), the effect of temperature-dependent crystallinity on viscosity was estimated (Figure 5.5). A significant viscosity increase occurs at 900 °C, the temperature at which intermediate magmas are estimated to be 50% crystalline. All enclave samples show lower viscosities than hosts at temperatures close to the liquidus except for a Group 1 enclave displays a higher viscosity than the hosts at temperatures below 900 °C.

It is important to note that the viscosities and densities estimated from KWare MAGMA are only first-order estimates. Some questionable values were produced by the software such as the trend of the Group-3 enclave in Figure 5.5, which displays a lower viscosity at 850 °C (solidus) than 900 °C. Similarly, there are discrepancies between density estimates made by the software and those calculated for the same samples using specific gravity, particularly under near solidus conditions (Table D.1 of Appendix D). These unusual results may be due to errors or bugs in the software. Therefore, the usage of KWare MAGMA appears to be only suitable for approximating and comparing magma viscosity and density but the absolute results should not be reported.

5.2.4 Cooling Rate Modelling Using KWare 3DHEAT

The cooling rates of magma bodies under specific conditions were modelled using KWare 3DHEAT, a software built to model both conductive and convective heat flow for various rock and magma properties. The program is designed around Fick's second law of diffusion and provides a user interface that allows the design of a computational mesh representing rock properties, geometry, and magma body emplacement. The modeling calculates the nonlinear effects of heterogeneous media, latent heat, temporal, spatial, and thermally varying properties using the following equation:

$$\frac{\partial T}{\partial t} = \nabla \cdot (\kappa \nabla T) - \mathbf{u} \cdot \nabla T + q$$

where T is temperature, t is time, k is the diffusivity coefficient, u is the convective velocity vector, and q represents heat sources/sinks (latent heat).

Initial conditions use a designated regional thermal gradient and continuous or symmetrical thermal gradients are assigned along the boundaries. Convective heat transfer in the magma is calculated as a function of temperature and composition. Magma properties including density, porosity, heat capacity, initial temperature, thermal conductivity, and crustal depth are assigned by the user before the calculation is run. For this study, two scenarios were modelled using 3DHEAT: A) the equilibration rate of enclaves in a compositionally similar host and B) the cooling rate of a 1-km thick homogenous intermediate body at approximately 1-km crustal depth.

The first case models the three-dimensional equilibration rate of intermediate crystal-poor blobs in an intermediate crystal-rich host at shallow crustal level. To get an upper limit on the equilibration rate, blobs were inputted at the approximate size of the largest enclaves in the study area (1 m x 40 cm x 40 cm). The equilibration rates were modelled in 1050 °C and 950 °C intermediate hosts, the temperature conditions estimated by KWare MAGMA (based on major oxide chemistry and estimated emplacement crystallinity) for the enclave-rich and enclave-poor tonalite units, respectively. The initial temperature of the intermediate blobs in both models is 1100 °C, the temperature 3DHEAT assumes typical intermediate magmas are at their liquidus. Heat lost to the crust was neglected in these models due to the small size of the blobs relative to the overall

system. The initial conditions of the enclave cooling models in both the enclave-rich tonalite and enclave-poor tonalite is provided by Figure 5.7. The results suggest nearly identical temperatures between blob and host are achieved in ~8.2 days for the enclave-rich tonalite compared to ~82 days for the enclave-poor tonalite.

The second scenario models the cooling times of homogenous magma bodies at approximately 1-km depth. The cooling times of a 1km thick 1050 °C intermediate body and a 1km thick 950 °C intermediate body were tested, interpreted to be the approximate temperature conditions of the enclave-rich tonalite and enclave-poor tonalite units respectively. The effects of conduction, convection, and latent heat are considered by KWare 3DHEAT in this model. The results suggest the estimated cooling time of the enclave-rich tonalite magma is ~74 kyrs compared to ~49 kyrs for the enclave-poor tonalite magma, both of which are longer than the cooling rate of ~ 8 kyrs estimated by $\tau = D^2/4 \kappa$ for a 1-km thick body. Mafic recharge, a process that evidently took place at Wild Cove East, along with ground water circulation are additional factors that may influence cooling times of shallow magma bodies (Bachmann and Huber, 2016).

5.3 Discussion

The calculated viscosity and density properties of host rocks and enclaves, despite being only first-order approximations, may have implications for the types of interactions that can take place between magmas. Previous models have suggested that magma

mingling takes place when the rheological properties of two co-existing magmas, particularly viscosity, are distinct enough to prevent mixing from occurring (e.g., Barbarin, 1991). Based on the results from KWare MAGMA, enclaves from all three groups have noticeably lower viscosities than the intermediate host rocks that contain them, favoring mingling as opposed to mixing. The lower viscosity of the enclaves is consistent with the model by Barbarin (1991) of enclaves representing the break-up of crystal-poor mafic dykes as they intrude a more viscous felsic magma. Magma viscosity increases significantly with increasing crystallinity in all units, and the most dramatic increase occurs at crystallinities greater than 50%, interpreted to be the rheological “lock-up” point. Thus, a significant viscosity difference exists between intermediate magmas at the liquidus and intermediate magmas that are partially crystalline (i.e. a crystal mush). This may account for why mixing did not occur between host mush units and enclaves at Wild Cove East, despite compositional similarity between nearly all rocks.

The results of both KWare MAGMA and specific gravity suggest enclave densities are either equal to or greater than the host rocks that contain them. This supports the sinking of enclaves shortly after intrusion into the host tonalite magmas. However, per Fernandez and Barbarin (1991), sinking of enclaves cannot occur if the host magma contains a high yield strength, which typically arises when magmas reach crystallinities of around 30 percent. Therefore, if the tonalite mush units of Wild Cove East had a sufficient yield strength and enclaves are comparatively crystal-poor, movement within the host mush would result in parallel movement in the enclaves.

Based on modelling using KWare 3DHEAT, the timescales of cooling for both enclaves and host rocks can be estimated. An intermediate blob with dimensions approximately equal to that of the largest enclaves in the study area (1 m x 40 cm x 40 cm) reaches thermal equilibrium with an intermediate host on the order of tens of days. This is significantly shorter than the estimated multiple tens of thousands of years it takes for intermediate magma (at the approximate size and temperature of host tonalite units in the study area) to cool to solidus temperatures at 1-km crustal depth. The longer cooling time estimated by KWare 3D heat for a 1-km wide intermediate body at 1-km depth compared to the diffusion equation may be related to latent heat, which can act to buffer cooling rates in crystal mushes (Huber *et al*, 2009). Assuming an open system that is susceptible to thermal recharge by intermittent injections of mafic magma, as is evident in Wild Cove East, cooling likely takes over a hundred thousand years. It is estimated that, upon break-up, intermediate enclaves will quickly equilibrate to the temperature of their host and will together cool and crystallize for a much longer period.

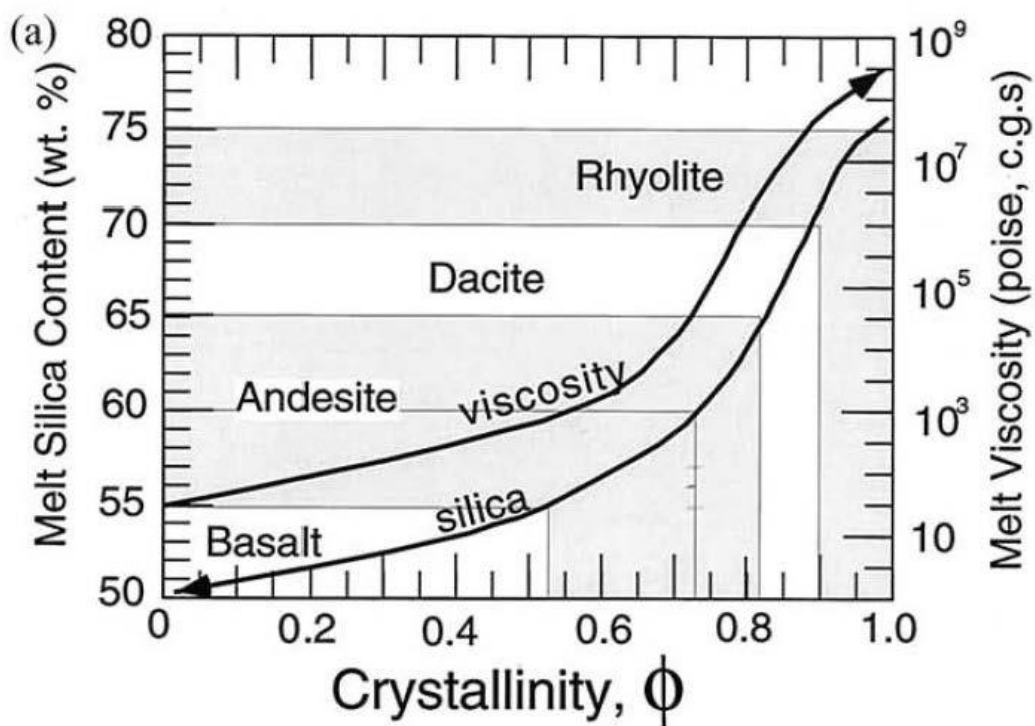


Figure 5.1. Change in melt silica content and melt viscosity with increasing crystallinity as calculated for a magma of tholeiitic composition by MELTS (Marsh, 2002)

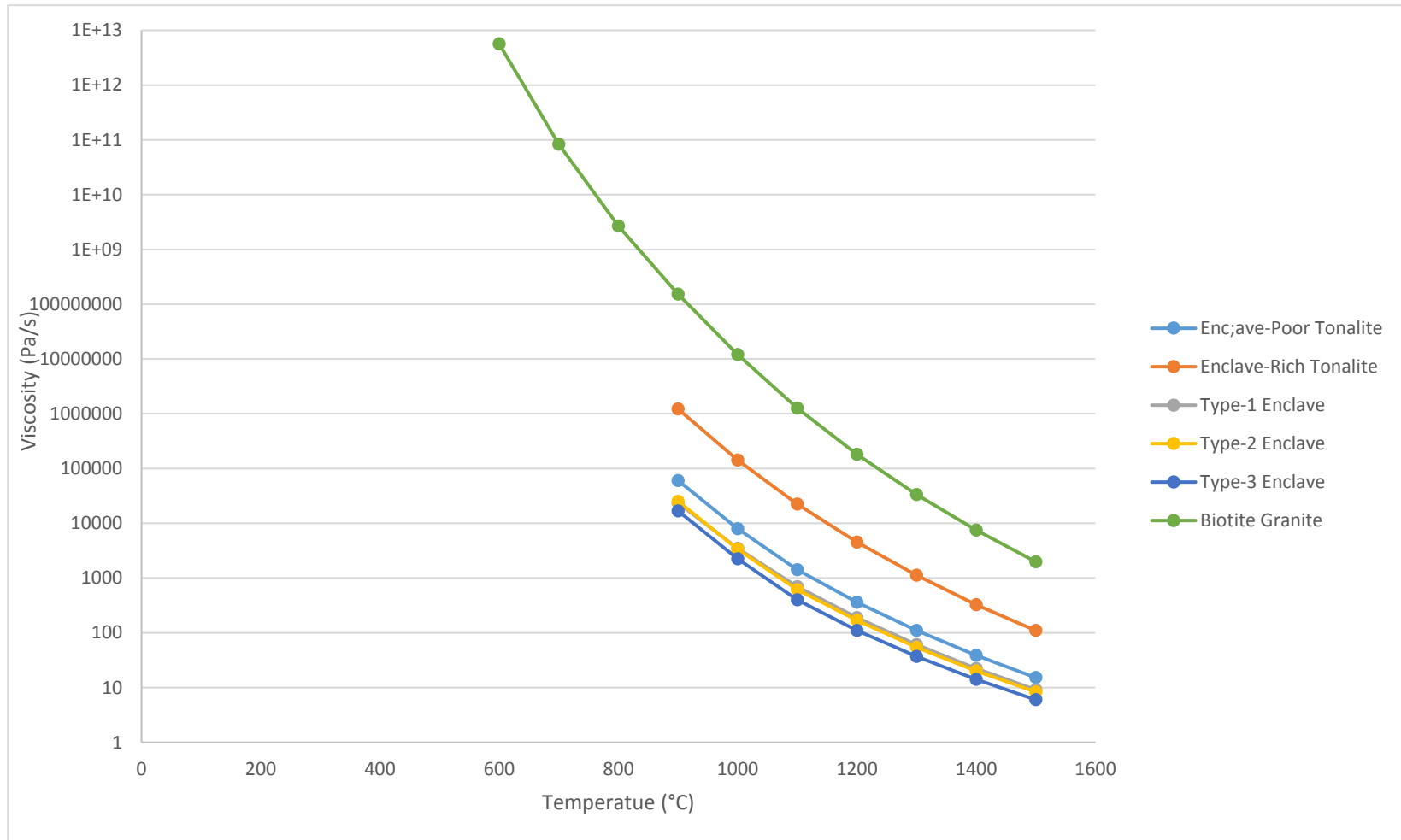


Figure 5.2. Relationship between temperature (°C) and viscosity (Pa/s) assuming constant pressure (=500 bars) and zero crystallinity. Viscosity values were calculated using MAGMA software.

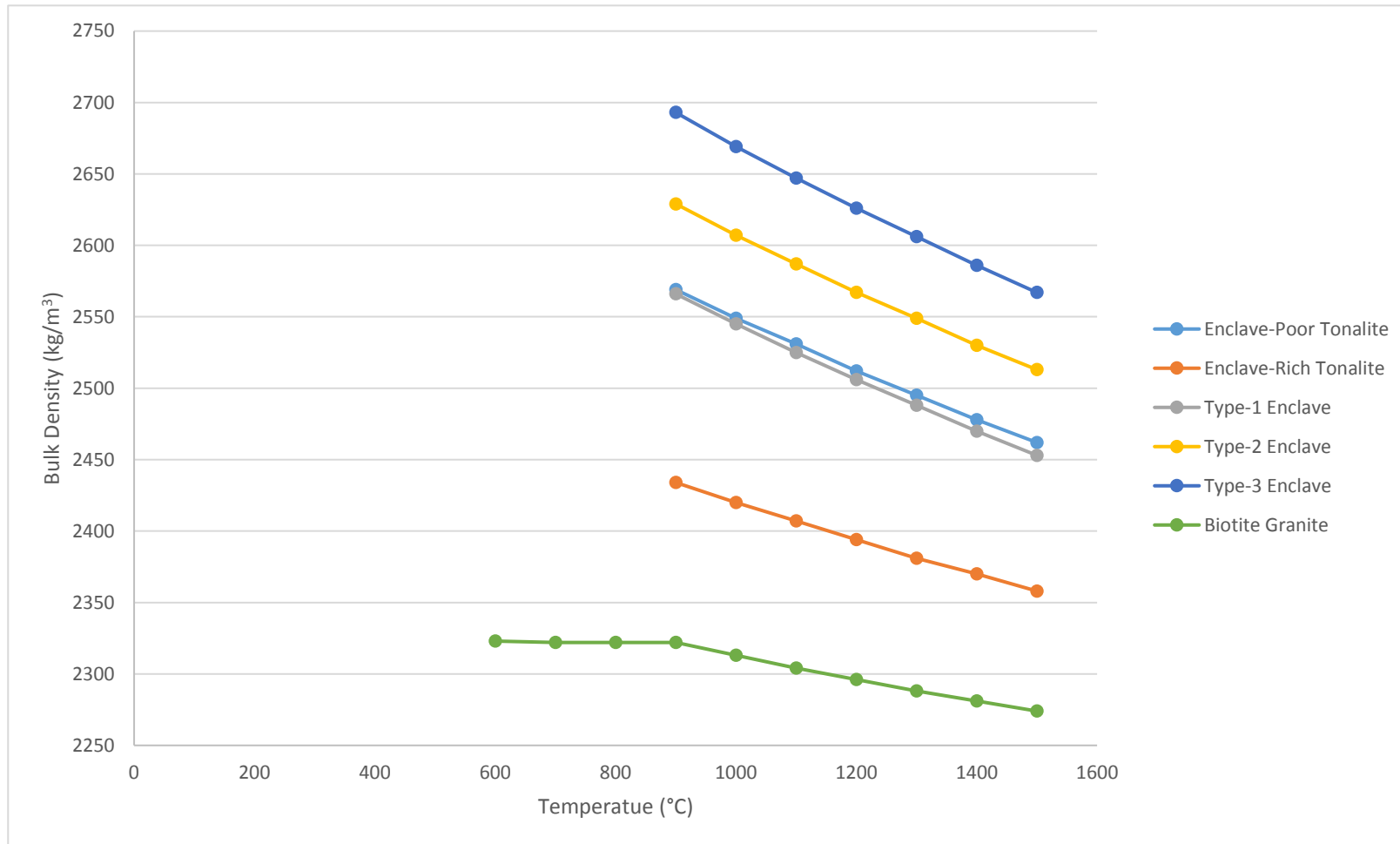


Figure 5.3. Relationship between magma density (kg/m³) and temperature (°C) assuming constant pressure (=500 bars) and zero crystallinity. Density values were calculated using MAGMA software.

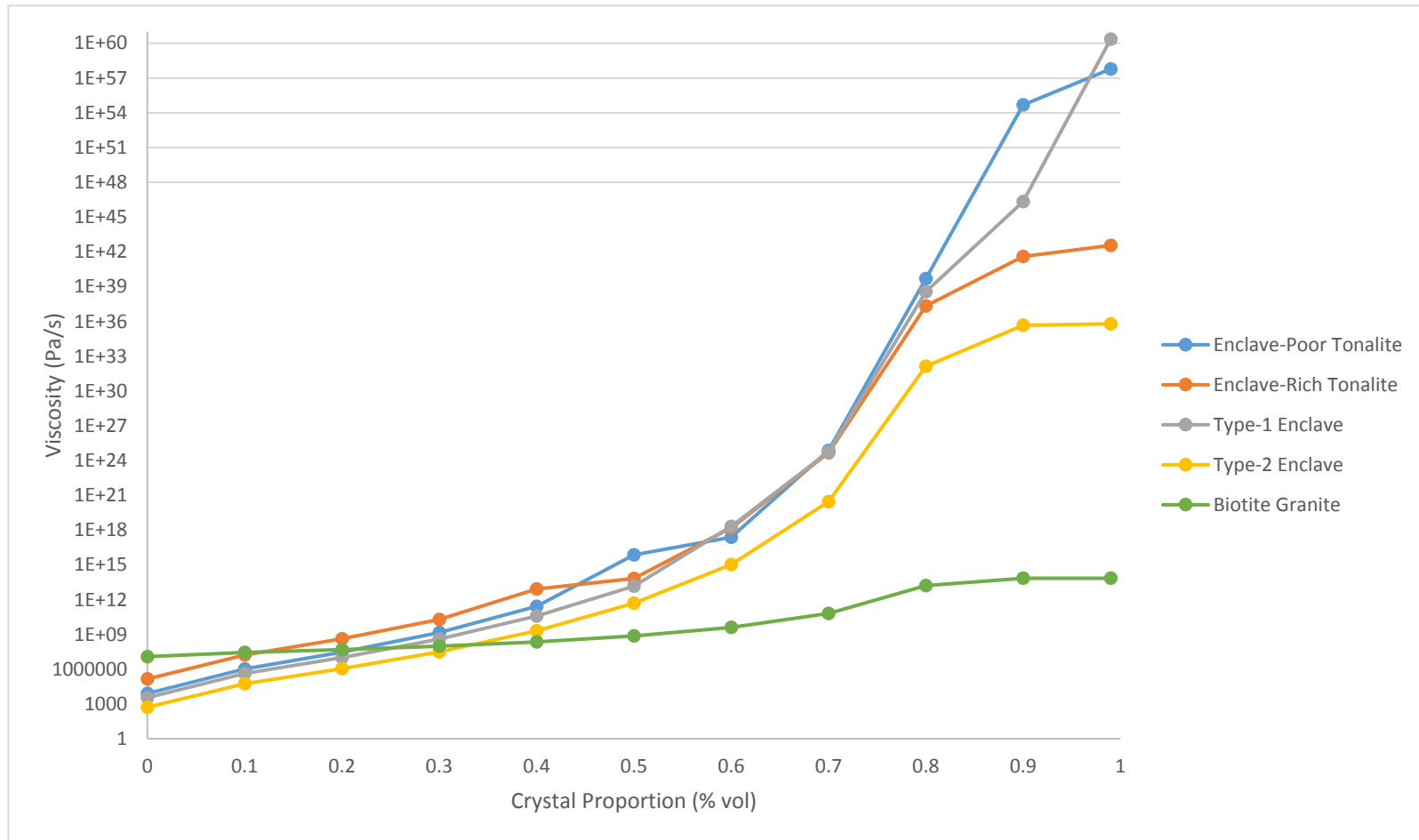


Figure 5.4. Relationship between magma viscosity (Pas) and crystallinity (vol %) assuming constant temperature (=1000 °C), pressure (=500 bars), and crystal size (=0.5 mm). Viscosity values were calculated using MAGMA software. Intended to isolate the effect of crystallinity on viscosity and does not represent realistic conditions in the earth.

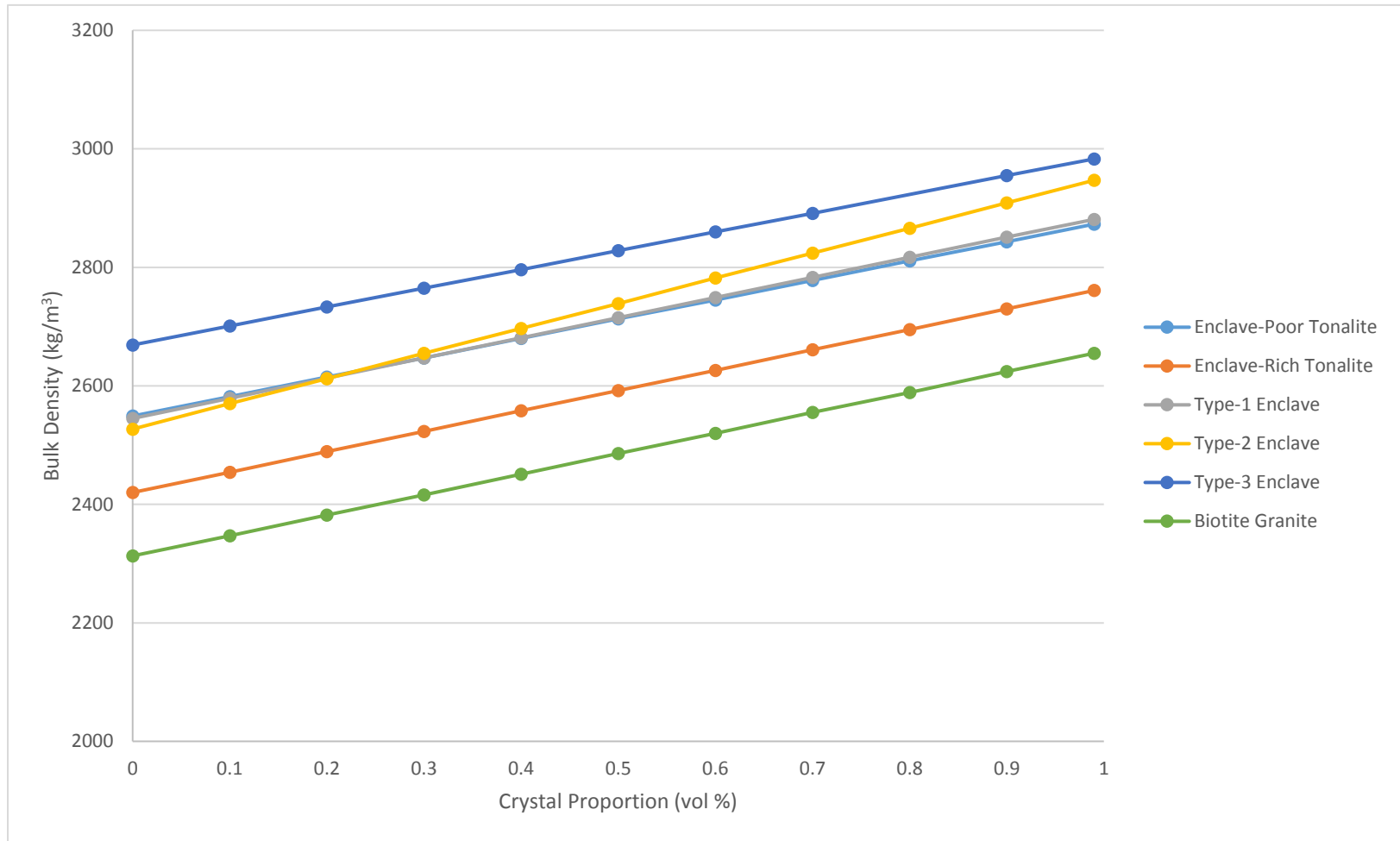


Figure 5.5. Relationship between density (kg/m^3) and crystallinity (vol %) assuming constant temperature ($=1000\text{ }^\circ\text{C}$), pressure ($=500\text{ bars}$), and crystal size ($=0.5\text{ mm}$). Density values were calculated using the program MAGMA. Intended to isolate the effect of crystallinity on density and does not represent realistic conditions in the earth.

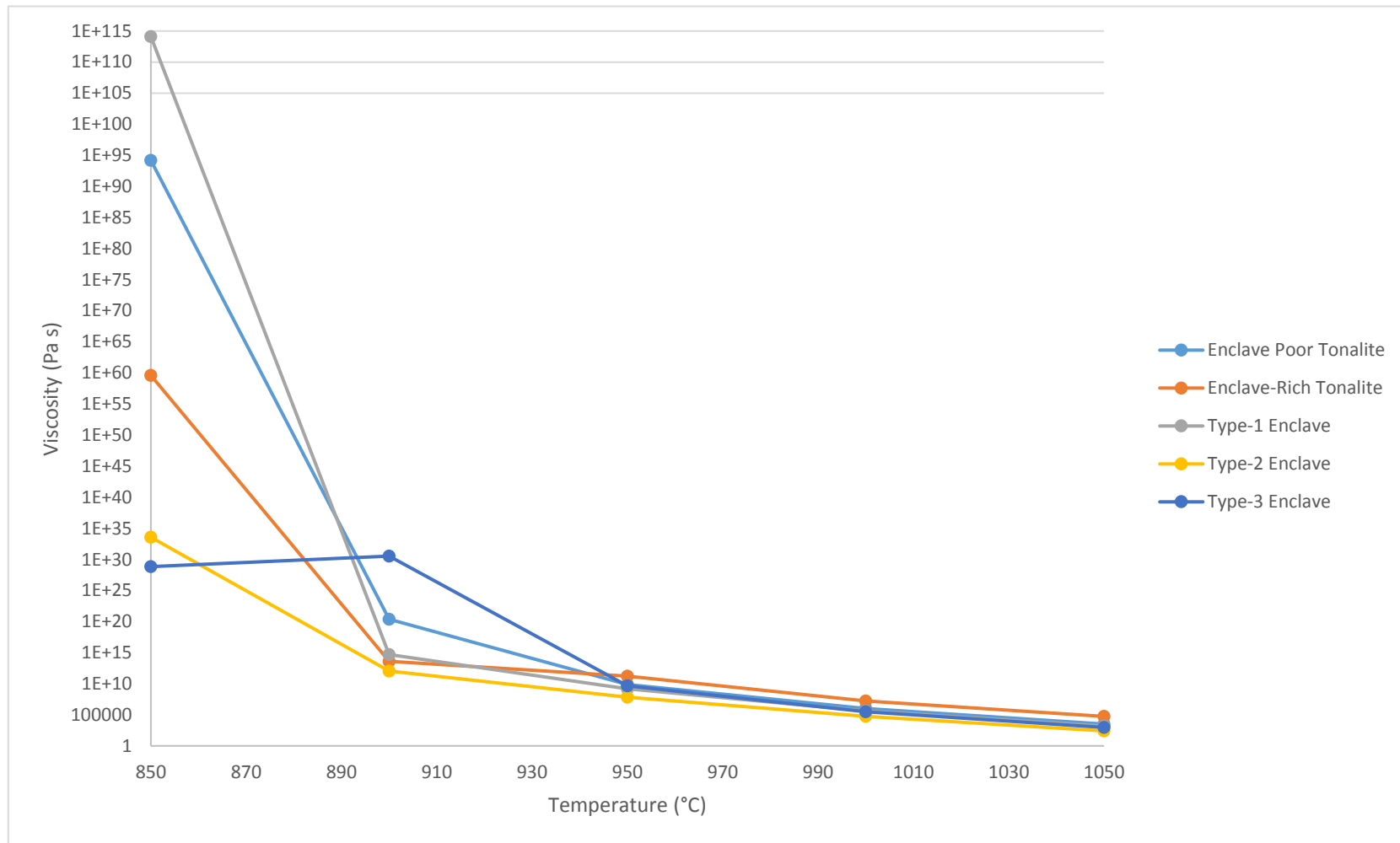


Figure 5.6. Relationship between viscosity (Pa s) and temperature (°C) assuming constant pressure (=500 bars), crystal size (=0.5 mm), and crystallinity changes with temperature. Average tonalite liquidus and solidus temperatures are estimated at 1050 and 850 °C respectively (Stern et al, 1975). Relative change in crystal proportion with temperature for andesite magma is estimated from Bachmann and Huber, 2016 (1000 °C = 10% xtals, 950 °C = 30% xtals, 900 °C = 50% xtals).

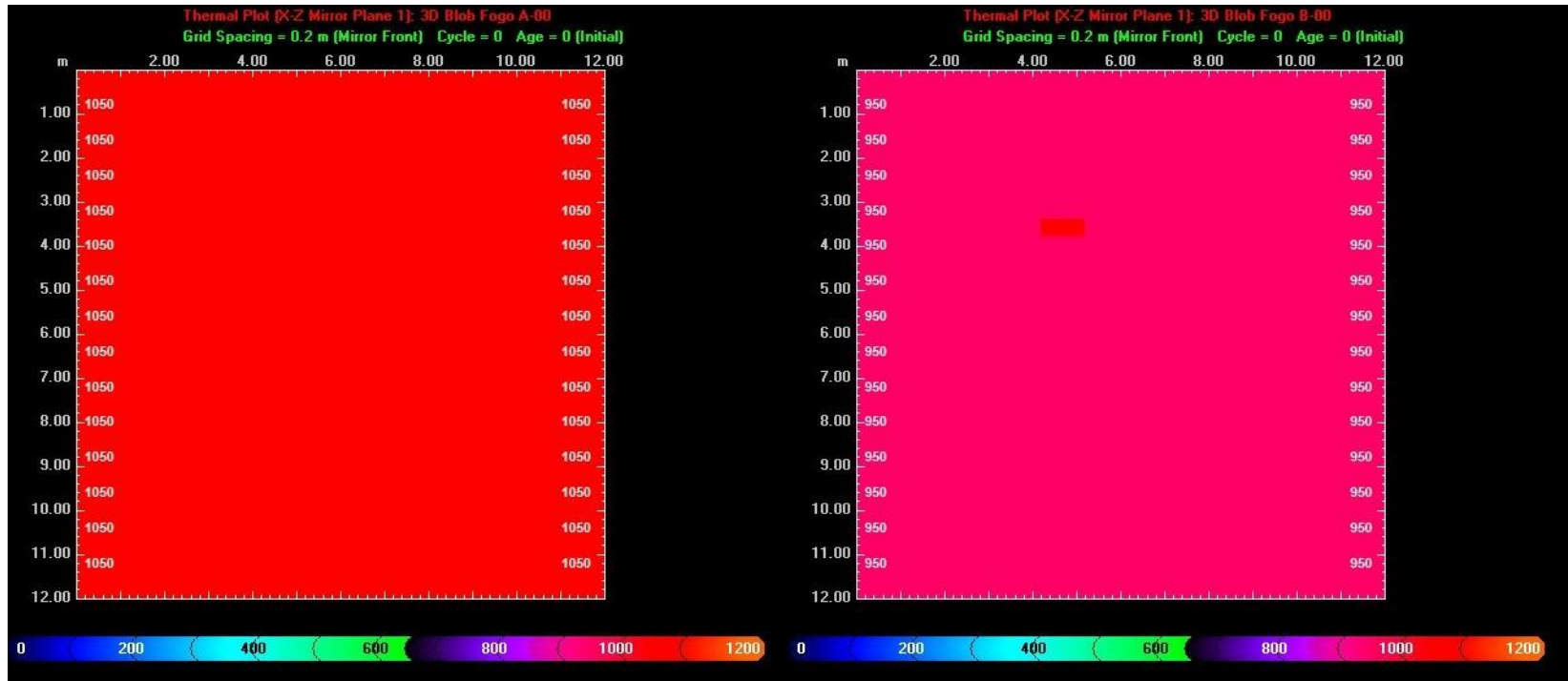


Figure 5.7. Initial conditions for 3DHeat model for three-dimensional cooling of an 1100°C intermediate enclave (1m x 40cm x 40cm) in 1050°C and 950°C host magmas estimated to be the approximate conditions of the enclave-rich tonalite and enclave-poor tonalite units, respectively.

Chapter 6 – U-Pb Zircon Geochronology

This chapter will discuss the sampling, methods, and results of U-Pb geochronology for selected rocks in the study area. Based on previous field and petrographic observations, it is apparent that most of the units at Wild Cove East mingled at similar temperatures as crystal mushes and must be similar in age. The results of U-Pb zircon analysis will reveal the age relationship between the units and how they compare to previous zircon ages obtained on Fogo Island.

6.1 Methods

Parts of the following procedures were carried out by the author, Amanda Langille, or Gregory Dunning at Memorial University of Newfoundland. Before measurement in the thermal ion mass spectrometer (TIMS), zircons must be separated in a series of careful processes. Initially, around 20 Kg of each rock sample was obtained from the field. Large samples were broken down in to smaller pieces (no more than several inches in size) using a hydraulic splitter, and the small pieces were then put into a jaw crusher which further breaks down the rock into fine chips. A fine-grained powder is then produced using a disc mill. The process of zircon separation begins by running the powdered rock across a wifley table under a smooth flow of water to separate heavy minerals from lighter minerals. Thorough cleaning using an air hose and alcohol is essential throughout each crushing process to prevent any cross-contamination between samples.

The heavy minerals were sieved to remove any larger pieces and strongly magnetic minerals were removed by a handheld magnet after sieving. The samples were then passed through methylene iodide, which has a density of 3.32 g/cm, to separate dense minerals such as zircon. The dense mineral separate is then passed several times, at increasing tilt and magnetic field strength, through a Franz magnetic separator which separates minerals based on their magnetic susceptibilities. Zircons are then picked using tweezers from the Franz separate under a binocular microscope. To ensure the best results, euhedral zircons that lack inclusions are selected. Selected zircons are mounted in epoxy and polished down to their centers to be mapped using the scanning electron microscope (SEM). These maps can be used to identify internal corrosion or growth zoning within individual zircons.

The zircons selected for U-Pb TIMS geochronology are first annealed at 1000 C for 36 hours and then etched in concentrated hydrofluoric acid in a pressure bomb at 200 C for several hours. Combined, these procedures remove parts of the crystal that may have experienced Pb loss. Etched zircons are then washed using distilled nitric acid, double distilled water, and acetone before loading in Krogh-type TEFLON dissolution bombs. A mixed $^{235}\text{U}/^{205}\text{Pb}$ tracer of known concentration is added in proportion to the sample weight, along with 15 drops of distilled hydrofluoric acid, before the bomb is sealed and put in an oven at 210 °C for 5 days. This results in complete dissolution of the zircon crystals.

Following dissolution, standard column ion exchange techniques are used to remove U and Pb from the solution. The dissolved zircon solutions, already mixed with tracer solution, are put in a resin-filled TEFLON column. Specific elements are then removed from the solution by washing the column with HCl at appropriate rates and amounts. Ions are removed from the column based on their affinity to either the solvent or the resin in the column. The steps are designed so that HCl will first remove Zr, Si, and REEs from the solution, leaving behind Pb and U in the column. Water is then passed through the column and to remove the remaining Pb and U, which is collected in a small beaker. After adding one drop of ultrapure phosphoric acid, the U/Pb solution is dried down to a single drop on a hotplate.

Following ion exchange, analysis using the MAT 262 TIMS is completed. The U/Pb solution is loaded onto an outgassed rhenium filament with silica gel and dilute phosphoric acid and dried. The loaded filament is mounted on a magazine and is pumped down to a high vacuum in the turret of the mass spectrometer. The filament is heated by an electric current resulting in the ionization of the solid sample.

For the present work, the faraday cups are calibrated with NBS 981 lead standard and the ion-counting secondary electron multiplier is calibrated against the faraday cup through measuring a known Pb isotopic ratio. The method used to collect isotopic ratios was dictated by the signal strength of the Pb and U in the samples. Smaller samples were measured by peak jumping on the secondary electron multiplier whereas ratios in larger samples were determined by simultaneous measurement using four faraday cups. Data

sets were measured in the temperature range of 1400 to 1550 C for Pb and 1550 to 1640 C for U. The best data sets were combined to produce a mean value for each ratio.

Corrections for Pb and U fractionation of 0.1 ‰/amu and 0.03 ‰/amu, respectively, were completed for the measured ratios based on volumes obtained by measurement of NBS standards. In addition, corrections were made for laboratory procedure blanks (1-2 picograms for Pb, 0.3 picograms for U) and the two-stage model of Stacey and Kramers (1975) was used to calculate the composition of common Pb above the laboratory blank. The decay constants of Jaffey *et al* (1971) were used for calculating the ages.

The isotopic ratios were calculated and are reported with two-sigma uncertainties. The age of each rock is reported as the weighted average of the $^{206}\text{Pb}/^{238}\text{U}$ ages calculated using ISOPLOT, and the uncertainty is reported at the 95% confidence interval. To determine accuracy of the procedure, nine U/Pb analyses of the TEMORA zircon standard (Black *et al*, 2003) were conducted at the time of sample measurement and using the same detector and measurement conditions (Sparks and Dunning, 2015).

6.2 Results

Zircon crystals from four units were dated including: enclave-poor tonalite (BG06-20A), biotite granite (BG0621A), diorite sill (072001), and chilled diorite dyke (16070803). A full report of the results is presented in Table 6.1.

6.2.1 Biotite Granite

Clear euhedral prismatic zircons were obtained from the biotite granite (BG06-21A) unit that range in size from 50-100 μm . Three of the most euhedral grains were selected for U-Pb zircon TIMS analysis. The analyzed fractions Z1 and Z2 show significant overlap and yield a concordant $^{206}\text{Pb}/^{238}\text{U}$ age of 410 \pm 1.4 Ma at the 95% confidence interval (Figure 6.1). Fraction Z3 displays evidence of an older component and was therefore excluded during age calculation of this rock. Zircons selected for CL imaging display complicated igneous growth zoning in most of the crystals (Figure 6.2C). In many cases, multiple growth zones which truncate previous zones are observed. Some crystals display bright cores and dark rims whereas other grains contain darker cores and bright rims.

6.2.2 Enclave-Poor Tonalite

The enclave-poor tonalite (BG06-20A) yielded clear subhedral prismatic to elongate zircons some of which display grain tips. Four of the most euhedral grains ranging in size from 50-100 μm were selected for U-Pb zircon TIMS analysis. All fractions (Z1, Z2, Z3, and Z4) tightly overlap and yield a concordant $^{206}\text{Pb}/^{238}\text{U}$ age of 408.2 \pm 1 Ma, at the 95% confidence interval (Figure 6.1). All crystals selected for CL imaging display igneous growth zoning, some of which contain dark cores and lighter rims. Oscillatory zoning is observed through the entirety of some crystals and is restricted to particular regions of

other grains. An imaged zircon displays evidence of partial resorption of the core followed by multiple sequences of overgrowth (top right of Figure 6.2B).

6.2.3. Diorite Sill

The diorite sill (072001) yielded abundant large (300-500 μm) elongate to prismatic zircons. Both euhedral zircons displaying grain tips and cracked/broken grains were observed. All analyzed fractions (Z1, Z2, Z3, and Z4) tightly overlap and yield a concordant $^{206}\text{Pb}/^{238}\text{U}$ age of 409 \pm 1.1 Ma. The grains generally display simple igneous zoning in CL imaging. Several grains display more complicated zoning patterns but these are not representative of the majority (Figure 6.2A).

6.2.4 Chilled Diorite Dyke

Clear euhedral elongate to prismatic zircons were obtained from a chilled diorite dyke (16070803). This minor intrusion is the only unit in the study area to display a straight chilled margin and is therefore interpreted to be the youngest unit in the study area. Five of the most euhedral representative zircons were selected for U-Pb zircon TIMS analysis. A concordant $^{206}\text{Pb}/^{238}\text{U}$ age of 407.9 \pm 0.9 Ma was determined from all tightly overlapping fractions (Z1, Z2, Z3, Z4, and Z5). The measured $^{208}\text{Pb}/^{206}\text{Pb}$ ratio in zircons from this sample (0.2010 -0.2486) are on average higher than those observed in the other samples, suggesting a different melt source compared to other rocks. CL imaging reveals

many of the grains display complicated igneous zoning (Figure 6.2D). Grains generally contain dark embayed core regions suggesting resorption along with lighter rim regions.

6.3 Discussion

The U/Pb zircon ages determined from these four rocks overlap at the 95% confidence interval and suggest that the units likely crystallized very close together or overlap in time. This is evidenced by the calculated ages of the biotite granite unit (410 +/- 1.4 Ma), the enclave-poor tonalite (408.2 +/- 1 Ma), and the diorite sill (409.3 +/- 1.1 Ma). The ages of these three units overlap within error, consistent with field and petrographic observations such as the irregular margins between the granite and tonalite, back-intrusion of younger units by older units, or the occurrence of magmatic pipes/ladder structures in the diorite sill, that suggest units mingled as crystal mushes. Due to the inherent limitations involving the resolution of the TIMS detector, the ages can only be resolved to roughly a million years, and therefore the measurements cannot resolve small age differences between these units if they exist. The 407.9 +/- 0.9 Ma U/Pb age of the chilled diorite dyke provides a younger age limit for magmatism in the study area, this dyke being the only unit that displays a straight chilled margin.

The 408.2 +/- 1 Ma U/Pb zircon age derived from the enclave-poor tonalite closely agrees with a previous age of 408 +/- 2 Ma U/Pb zircon age derived from a quartz diorite of the Wild Unit (Aydin ,1994). The 410 +/- 1.4 Ma U/Pb zircon age for biotite granite is

significantly younger than a previous age of 420 ± 2 Ma from a monzogranite of the Fogo Suite, located east of Wild Cove East (Aydin, 1994). This latter age was not based on concordant data, however.

Several zircons in the biotite granite, enclave-poor tonalite, and chilled diorite dyke display evidence of resorption and growth zoning and potentially highlight the age complexity that can occur within single zircons. Anhedral cores, if not inherited, may suggest thermal rejuvenation took place in the mush (Miller *et al*, 2007). In addition, some zircon crystals display up to three zones of resorption/overgrowth whereas as other crystals in the same rock display none, suggesting zircons did not experience the same crystallization histories despite being in the same rock. This is consistent with the heterogeneity in textures and chemistry observed in major minerals like plagioclase and clinopyroxene within single thin sections. Due to the refractory nature of zircon, these may suggest significant differences in temperature existed in different parts of the mush reservoir and/or zircons were displaced between multiple magmas throughout their crystallization histories (Storm *et al*, 2011).

TABLE 6.1. U-Pb Zircon Data from Rocks of Wild Cove East

Fraction	Concentration Weight [mg]	Concentration		Measured		Corrected Atomic Ratios *						Age [Ma]			
		U [ppm]	Pb rad	total common Pb [pg]	206Pb 204Pb	208Pb 206Pb	206Pb 238U +/-	207Pb 235U +/-	207Pb 206Pb +/-	206Pb 238U	207Pb 235U	207Pb 206Pb			
BG06-20A - Enclave-Poor Tonalite															
Z1 1 clr prm	0.002	1022	73.2	4	2344	0.2174	0.06538	28	0.4963	28	0.05505	26	408.1	409	414
Z2 1 clr prm	0.002	1538	107.6	3	3641	0.1841	0.06560	36	0.4975	28	0.05501	16	409.5	410	412
Z3 1 clr prm	0.002	1218	84.1	4	2758	0.1728	0.06532	32	0.4957	28	0.05504	18	407.8	409	414
Z4 3 clr euh prm	0.006	718	49.5	6	2941	0.1737	0.06529	36	0.4964	28	0.05514	14	407.6	409	418
BG06-21A - Biotite Granite															
Z1 2 clr euh prm	0.003	192	13.8	7	341	0.2097	0.06582	36	0.4999	60	0.05508	56	410.8	412	415
Z2 2 clr euh prm	0.003	238	16.1	8	366	0.1445	0.06563	32	0.4985	52	0.05509	54	409.6	411	416
Z3 4 clr euh prm	0.006	399	27.6	6	1557	0.1556	0.06633	30	0.5103	26	0.05580	24	413.9	419	444
F0720-01 - Chilled Diorite Sill															
Z1 5 clr euh prm	0.015	1142	78.2	7	9759	0.1615	0.06545	54	0.4963	36	0.05500	22	408.7	409	412
Z2 1 clr euh prm	0.003	532	36.5	1	6209	0.1637	0.06541	40	0.4941	28	0.05479	20	408.4	408	403
Z3 5 clr euh prm	0.015	918	64.1	6	9131	0.1808	0.06565	30	0.4982	18	0.05503	18	409.9	410	414
Z4 1 clr euh prm	0.003	770	53.5	5	1823	0.1769	0.06558	40	0.4965	36	0.05490	30	409.5	409	408
F160708-03 - Chilled Diorite Dyke															
Z1 2 clr euh prm	0.004	193	13.6	3	1090	0.2010	0.06527	28	0.4948	32	0.05498	30	407.6	408	411
Z2 4 clr euh prm	0.008	190	13.5	3	1940	0.2105	0.06530	40	0.4953	34	0.05501	28	407.8	409	413
Z3 1 clr euh prm	0.002	303	21.7	3	778	0.2144	0.06537	58	0.4963	72	0.05506	70	408.2	409	415
Z4 1 clr euh prm	0.002	654	47.6	2	2342	0.2393	0.06534	48	0.4951	40	0.05496	28	408.0	408	411
Z5 1 clr euh prm	0.002	259	19.0	4	526	0.2486	0.06541	34	0.4956	54	0.05496	52	408.4	409	411

Notes: Sample locations: BG06-20A = 21N 709963 5511638, BG06-21A = 21N 709685 5511645, 072001 = 21N 707689 5511688, 16070803 = 21N 710176 5511484

Z=zircon, 1,3,4 =number of grains, clr=clear, prm =prism, euh=euhedral.

All zircon was chemically abraded (Mattinson, 2005). Weights were estimated so U and Pb concentrations are approximate.

* Atomic ratios corrected for fractionation, spike, laboratory blank of 2 picograms of common lead, and initial common lead at 410 Ma calculated from the model of Stacey and Kramers (1975), and 0.3 picogram U blank. Two sigma uncertainties are reported after the ratios and refer to the final digits.

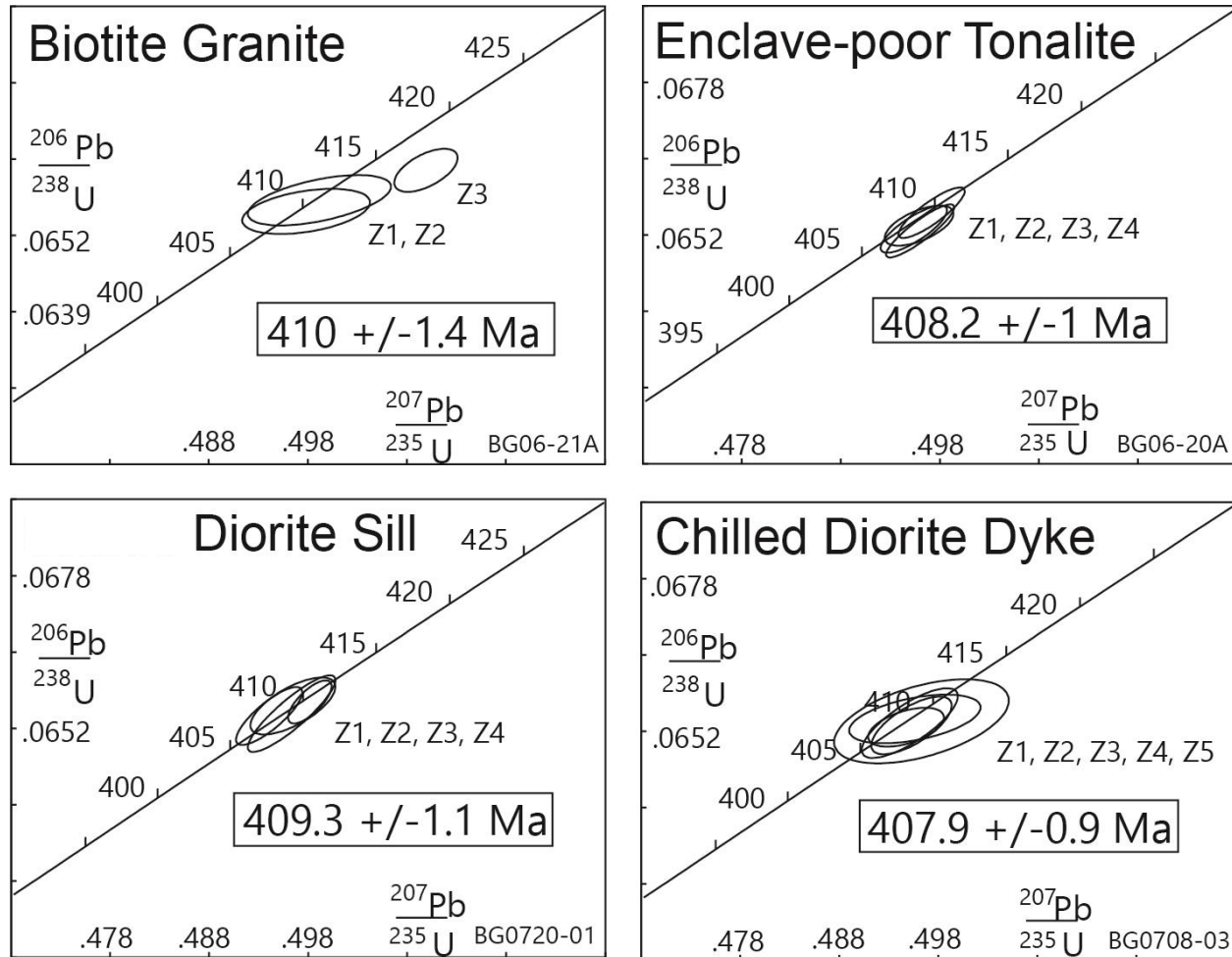


Figure 6.1. Concordia diagrams of U/Pb results of zircon analyses from samples from Wild Cove East. Error ellipses are at the two-sigma level. Refer to Table 1 for sample locations and descriptions

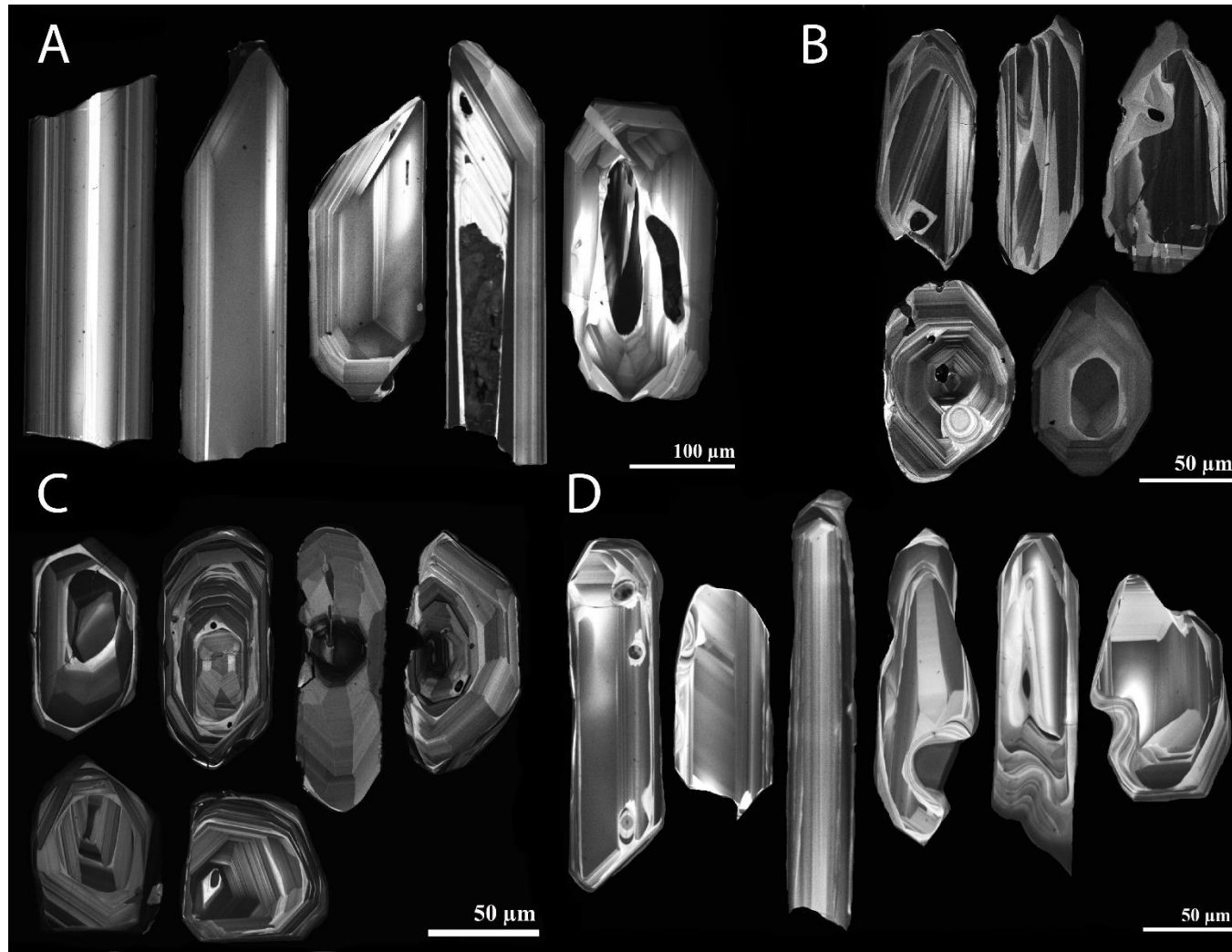


Figure 6.2. Cathodoluminescence images of zircon crystals representative of the type analyzed from each sample. A. Diorite Sill, B. Enclave-Poor Tonalite, C. Biotite Granite, D. Chilled Diorite Dyke.

Chapter 7 – Summary and Conclusions

This project involved the detailed investigation of mingled intermediate rocks from Wild Cove East, Fogo Island. The units were studied at multiple scales including the field scale, thin section, and mineral scale to assess the nature of interaction between multiple crystal mushes, including melts and crystals. Key findings from this study are summarized below.

7.1 Tectonic Setting

The 7-km thick gabbro-diorite-tonalite-granite Fogo Batholith is interpreted to have intruded during widespread strike-slip deformation which affected Central Newfoundland in the Silurian-Devonian (Currie, 2003). New U-Pb zircon ages from Wild Cove East (410 +/- 1.4 Ma for the biotite granite unit and a 408 +/- 1 Ma for the enclave-poor tonalite unit) correlate with nearby Early Devonian intrusions, including the 408 +/- 2 Ma Loon Bay intrusive suite, the 422 +/- 2 Ma Long Island pluton and others (Elliot *et al*, 1991; McNicoll *et al*, 2006; Figures 1.4, 6.1). The ages and field relationships of these units bracket a strike-slip event in the early Acadian orogeny related to dextral-transtensional movement along the Dog Bay Line (Currie, 2003). The variety of rock compositions in Wild Cove east, ranging from gabbro to granite, likely reflect varying degrees of melting before emplacement at the current interpreted shallow level.

To account for our combined field, petrographic, and geochemical observations, a simple model, such as that by Burgisser and Bergantz (2011) is favoured. This model suggests highly viscous crystal mushes can be rapidly remobilized due to reheating from below by fresh magmatic intrusions. Heat provided from the recharging magmas causes the overlying mush network to destabilize and the formation of a mobile layer at the base of the crystal mush. More specifically, the fluidized layer is formed by the propagation of granular-fluid stresses associated with the intrusion of a hot melt from below, which creates localized faulting in the mush (Schleicher et al, 2016). The new mobile layer, being hotter and less dense than the overlying much, will eventually penetrate the mush in a process called “unzipping” due to increasing Rayleigh-Taylor instabilities between the two layers (Burgisser and Bergantz, 2011). The resultant rapid overturn creates strong mixing in the mid-crust and can lead to the juxtaposition of crystals and magmatic material with contrasting chemistries, textures, and ages (Figure 7.1; Burgisser and Bergantz, 2011; Schleicher et al, 2016).

7.2 Mingling of Compositionally Similar Crystal Mushes

The rocks of Wild Cove East represent a small multi-component crystal mush reservoir that existed as an open-system at shallow depth. Field evidence for mingling of multiple crystal mushes include: the irregular nature of boundaries between units, the occurrence of schlieren in intermediate host rocks, the presence of magmatic tube and

pipe/ladder structures in mingled intrusions, the back-veining of younger units by liquid from older units, and the overlap in U-Pb zircon ages of the units. Structures such as metasedimentary xenoliths and miarolitic cavities are abundant and suggest reservoir storage occurred close to the walls or roof of a pluton at depths not much greater than 1-km (Burnham and Ohmoto, 1980; Peretyazhko, 2010).

The setting of a shallow open intermediate magma chamber lends itself to multiple types of interactions between mushes and intrusions. Intermediate rocks have a wide temperature interval between liquidus and solidus temperatures and can therefore, in theory, exist as crystal mushes for a long period. Furthermore, recharge of the reservoir by hot intrusions at depth could supply sufficient heat to preserve, or even re-dissolve, existing crystal mush. The intrusion of the 200-meter wide troctolite-gabbro mafic layered intrusion located at the eastern end of the study area, which lacks a noticeable chilled margin, potentially represents an example of a late recharge event that took place closer to the current interpreted shallow level. Additionally, located a few kilometers to the east are a series of layered gabbros belonging to the Tilting Layered Suite (Aydin, 1994) that overlap in age with the rocks of Wild Cove East (409.8 +/- 0.8 Ma for a pegmatite differentiate in a layered gabbro; Gerner, 2016). Together, these mafic intrusions may have provided the energy to disaggregate and/or prolong the lifetime of the tonalite crystal mush as well as produce resorption and reverse zoning in early forming plagioclase and pyroxene.

7.3 Injection of New Magmas into a Crystal Mush Reservoir

Intrusions of various structural styles are present in the study area and suggest pulsed injections occurred throughout the thermal evolution of the mush reservoir. Thin (5-20 cm wide) north-striking intermediate to granitic dykes cut across all units and display sharp chilled contacts suggesting they intruded after complete solidification of the reservoir. However, these dykes were not dated and the time gap between complete solidification of the host and dyke intrusion is unknown. In contrast, the presence of a broken-up tonalite dyke with sharp contacts (Figure 2.11) suggests intrusion occurred earlier when the crystal mush was crystalline enough to sustain brittle deformation but was still hot enough to flow. Enclaves also appear to be the products of earlier intrusions at a deeper level in the magma chamber based on different compositional groups of enclaves occurring together in parts of the study area. These were likely later transported to the current interpreted shallow level in the magma chamber.

Three groups of enclaves are reported at Wild Cove East based on distinct mineral chemistry, composition, and crystallinity (Table 3.1). The exact mechanisms for their formation are unknown but are inferred to be magmatic based on their ellipsoidal-rounded shapes. The lack of chilled margins of enclaves may be due to their compositional similarity to their hosts, suggesting they were at similar temperatures, or it may suggest enclaves were completely solid when they encountered the tonalite immediately surrounding it (Wiebe and Collins, 1998). The stretching direction of some enclaves is parallel to nearby flow fabric and/or schlieren in the host rocks, suggesting some enclaves

were transported in a partially molten state within a crystal mush. All enclaves display evidence of hybridization, due to the mixing of crystals and liquid, which likely occurred at levels deeper than the current level of emplacement (Wiebe and Collins, 1998).

7.3.1. Proposed formation of Group 1 enclaves

The enclaves with the most evolved chemical compositions in the study area are assigned to Group 1. Due to the commonly stretched appearance of Group 1 enclaves, along with sharing compositional similarity of plagioclase rims with the enclosing enclave-poor tonalite unit, it is interpreted that Group 1 enclaves were still partially molten when they encountered the host tonalitic mush. In combination with their low estimated emplacement crystallinity (Table 3.1; section 3.3.1), it is interpreted that these enclaves formed during the break-up of crystal-poor dykes due to rheological instability after injection in a more viscous host (Wiebe and Collins, 1998; Figure 7.2). Evidence of this process having taken place is demonstrated by a meter-wide quartz diorite dyke that shows evidence of localized break-up into rounded globules within its margins due to interaction with host material (Figure 2.12). Since these enclaves occur amongst other populations, it is assumed that these injections took place primarily at depth.

7.3.2. Proposed formation of Group 2 and Group 3 enclaves

Group 3 enclaves represent the most primitive enclave compositions in the study area and are commonly rounded and coarse-grained (Table 3.1; section 3.3.3). Unlike Group 1, these enclaves have higher estimated emplacement crystallinities and plagioclase rims do not share compositional similarity to rims in adjacent host rocks. Based on their lack of chilled margins and stretching, it is interpreted that these enclaves were likely significantly rigid by the time they encountered their host rocks at the current level. These enclaves may have formed by the disaggregation of earlier mush material by intrusions at deeper levels in the magma chamber and were later rounded during transport (Wiebe and Collins, 1998; Figure 7.3). Group 2 enclaves contain characteristics of both Group 1 and Group 3. Like Group 1, they are commonly stretched and plagioclase rims display compositional overlap with those in the surrounding enclave-rich tonalite host. However, it is estimated they had high emplacement crystallinities similar to Group 3 (Table 3.1; section 3.3.2) enclaves and, as such, may have formed by either of the two processes described above.

7.2.3. Mineral evidence for changing chemical environments

Mineral textures, such as mottled cores in plagioclase, record changes in the chemical environments experienced by crystals during their histories. Enclave plagioclase generally contain mottled less evolved (higher An content) cores (andesine) and more

evolved rims (oligoclase), suggesting melting of the earliest plagioclase was likely due to decompression during ascent of the enclave magmas (Nelson and Montana, 1992). Plagioclase in the host rocks, particularly in the enclave-poor tonalite, generally display the opposite trend, with mottled cores being more evolved than the rims. This suggests that crystals in the host mushes were affected by a combination of changing chemical environments (i.e. mafic recharge) and decompression melting (Streck, 2008; Nelson and Montana, 1992).

7.4. Mixing of Crystals in a Crystal Mush Reservoir

The juxtaposition of texturally and compositionally distinct crystal populations in host rocks, enclaves, and dykes suggest the units of Wild Cove East experienced processes such as crystal capture and displacement earlier in their histories (Bergantz *et al*, 2015). For example, plagioclase containing distinct core compositions and chemical trends are observed at the thin section scale in the enclave-poor tonalite unit and suggests the mush represents an accumulation of crystals with different histories that were captured during earlier recharge events (Bergantz *et al*, 2015). Furthermore, the proportion of crystals displaying complex zoning or resorption varies between sample taken from different parts of the enclave-poor tonalite unit. Some samples appear to be petrographically simple and other nearby show greater complexity. This could reflect the heterogeneity in temperature and/or chemical environments experienced by individual crystals during

complex mixing events in a crystal mush (Bergantz *et al*, 2015). For example, a fresh intrusion could disrupt the less crystalline components of a mush in the immediate vicinity of the intrusion to produce localized mixing and heat transfer, while mush nearby would be relatively undisturbed. Enclaves also display heterogeneities at the mineral scale, as evidenced by anomalous clinopyroxene crystals with distinct zoning and compositions (Figures 4.17, 4.19) and suggest enclave magmas similarly collected foreign crystals earlier in their histories, which then formed outer zones with discrete compositions. It is interpreted that most of these processes took place at deeper levels in the crust.

Heterogeneities in texture and composition are also observed at the hand sample scale in CL-imaged zircons from dated units. Since zircon is a strongly refractory mineral, it is possible that crystals survived recharging events that re-dissolved earlier mush material, and zircons were then free to be transported and eventually deposited at the current interpreted shallow level. Consistent with textures observed in both plagioclase and pyroxene, this suggests accessory minerals, like zircon, experienced complex histories which likely involved displacement between multiple magmas or mushes during their ascent through the crust (Storm *et al*, 2012). It is possible that textural and chemical heterogeneities exist in other accessory minerals, such as apatite, that were not analysed as part of this study.

7.5. Movement and Cooling of Enclaves in a Crystal Mush

Enclaves of Wild Cove East are commonly stretched in a direction parallel to the dominant fabric in the enclosing host rocks, suggesting some enclaves flowed within their mobile hosts. Relative motion between enclaves and host rocks is further emphasized by the appearance of curved schlieren in the enclave-rich tonalite unit, suggesting deformation of the host mush was related to movement of the enclaves within it (Wiebe *et al*, 2007). The shape of schlieren in the enclave-rich tonalite unit is generally related to the enclaves themselves, appearing parallel to the enclave stretching directions or “tails” converging behind individual enclaves (Figure 2.17). This suggests that schlieren in the enclave-rich tonalite unit formed in response to movement of the enclaves (Wiebe *et al*, 2007). The field-scale deformation indicators along with the high crystallinities in both host rock units (volume fractions $\Rightarrow 0.2$), suggests that the mushes displayed a plastic rheology with a yield strength (Fernandez and Barbarin, 1991; Wiebe *et al*, 2007). Specific gravity measurements and simple density models (using KWare MAGMA) suggest the enclave rocks are approximately 100-200 kg/m³ (Table D.1) denser than the host rocks that contain them, which is expected based on the enclaves having less silicic compositions (i.e lower wt % SiO₂) than the host rocks that contain them. The variation in size and distribution of schlieren in both the enclave-poor tonalite and enclave-rich tonalite units likely reflects a heterogenous distribution of crystals within each crystal mush. Enclaves likely sank in the mush until they reached regions with higher crystal concentrations which had a sufficient yield strength to stop sinking (Wiebe *et al*, 2007).

Simple cooling models (using KWare 3DHEAT) suggest that after being introduced into an intermediate mush reservoir of approximately 950 °C, a meter-wide crystal-free intermediate enclave at approximately 1100 °C will thermally equilibrate on the order of tens of days. Consequently, it is unlikely that enclaves that are compositionally similar to their host, such as the Group 1 and 2 enclaves of Wild Cove East, will ever be completely solid while the host is still hot. Instead, enclaves quickly reach the approximate temperature of the host and then cool together in the reservoir over a much longer time (~74 kyrs estimated by KWare 3DHEAT, ~8kyrs estimated by the simple conductive cooling timescale $\tau = D^2/4 \kappa$). This is supported by similar rim compositions of plagioclase between Group 1 and 2 enclaves and the enclave-rich tonalite unit. The discrepancy between the estimated cooling timescales and the difference in U/Pb zircon ages between the units is likely due to inherent limitations involving the accurate resolution of a series of events so close in time using the U-Pb zircon technique.

7.6 Emplacement of Wild Cove East Units

With respect to the rocks of Wild Cove East, we interpret that nearly all units including intermediate host rocks, enclaves, and dykes, experienced “unzipping” processes, as described by Burgisser and Bergantz (2011), earlier in their magmatic histories at deeper levels. This is supported by the heterogeneity in mineral textures and samples observed in most samples. Field relationships suggest the enclave-rich tonalite

unit intrudes the enclave-poor tonalite in various parts of the study area, such as inclusions of enclave-poor tonalite material occurring within parts of the enclave-rich tonalite. Our interpretation is that the enclave-rich tonalite represents a remobilized melt that intruded through areas of structural weakness in the enclave—poor tonalite mush. Refractory minerals such as pyroxene may have been sheared out and deposited along the boundaries between the mobile enclave-rich tonalite and the more crystalline enclave-rich tonalite.

It is possible that multiple “unzipping” events affected the rocks of Wild Cove East and the current configuration of the rocks represents a snapshot of the last events frozen in place. During the second stage of the unzipping process, the rapid remobilization and rise of the melt-rich layer causes vigorous mixing to take place in the mush. This may account for the wide range in mineral textures and compositions within the enclave-poor tonalite unit. The heterogeneity in the amount of resorbed plagioclase observed in samples taken from different parts of the enclave-poor tonalite unit may indicate that some regions were affected by these earlier mixing events and some were not. One composition of magma involved in these recharging events may be represented by the intrusion of the mafic layered sill at the eastern end of the study area and the related layered gabbros of the coeval Tilting Layered Suite.

The enclaves present in the enclave-rich tonalite unit may represent either the disaggregation of earlier mush material (Group 2 or 3 enclaves) or the break-up of smaller injections into the mobile melt-rich layer at depth (Group 1 or 2 enclaves). Vigorous mixing

during the unzipping processes may have resulted in the juxtaposition of enclaves of different chemical groups in the same part of the study area. The scarce enclaves present in the enclave-poor tonalite unit may have been emplaced during previous unzipping events that affected the crystal mush reservoir.

7.7 Conclusion

This study, through the integration of observations at the map scale, outcrop scale, thin section scale, and mineral scale, highlights the pervasive effects of interactions between liquid and crystals that can arise during magma mingling. Complexity is not only present at the current interpreted shallow level, but also occurred at depth based on units being composed of complex aggregations of crystals and liquid with disparate chemistries and ages. This internal petrologic complexity has important implications for the interpretation of whole-rock chemical analyses of such a suite of diorite to tonalite, especially in the interpretations of linear trends on chemical plots. The interpretations of U-Pb isotopic ages of zircon is also affected if the processes involved extended to lengths of time greater than the age resolution of the technique. The processes also explain why two zircon crystals yielding the same age from the same rock sample (within the resolution of the technique) may display very different degrees of internal complexity. Likewise, adjacent plagioclase and pyroxene crystals may have different chemical zonation and internal complexity. Therefore, it is important to stress that bulk rock

chemistry and U/Pb zircon ages taken from crystal mushes might be misleading and cautious appraisal is therefore required.

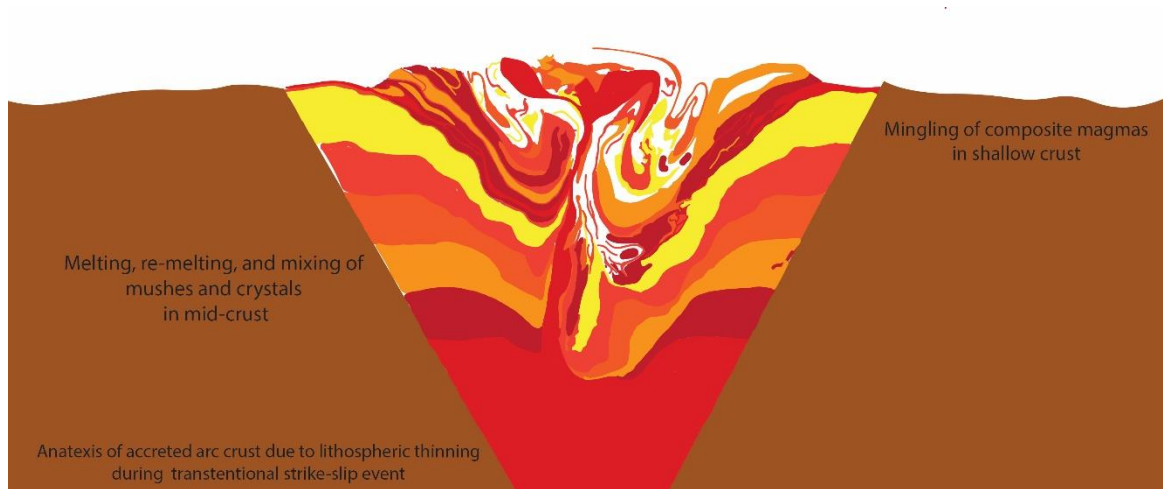


Figure 7.1. Simulation of the intrusion of new magma below an olivine crystal mush with ~40% porosity by Schliecher et al (2016). Colours represent mechanically neutral particles that act as tracers for the mixing simulation. The initial neighbor distance (IND) mixing index (Deen et al., 2010) is used to quantify the progression of mixing in the crystal mush and is obtained by recording the distances between initially neighbouring particles at the start of mixing and then summing them at every subsequent step as the particles are dispersed.

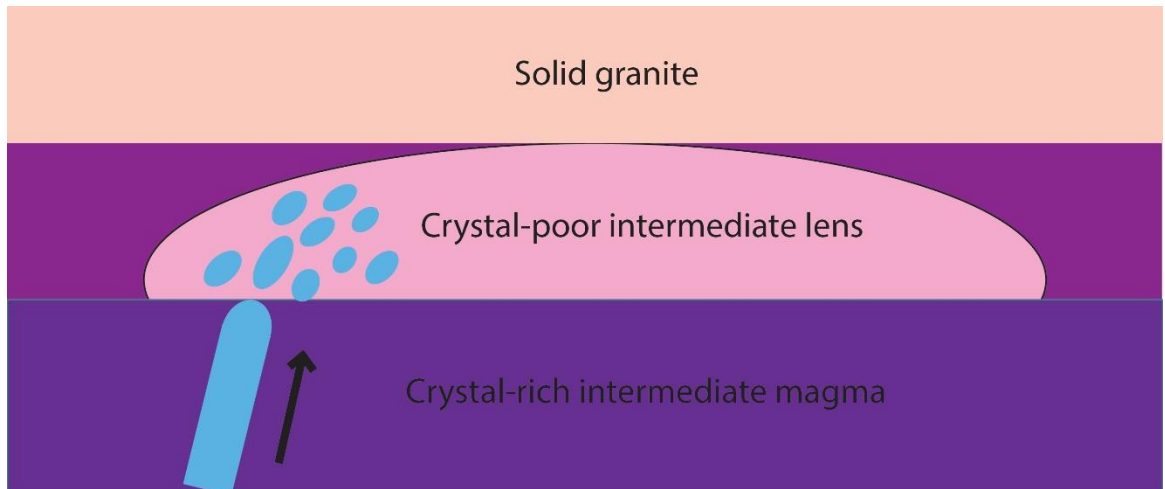


Figure 7.2. Illustration of a potential process that formed Group 1 and Group 2 enclaves at Wild Cove East. Due to rheological instability, a dyke experiences break-up into globules when intruded into a more felsic crystal-pool magma.

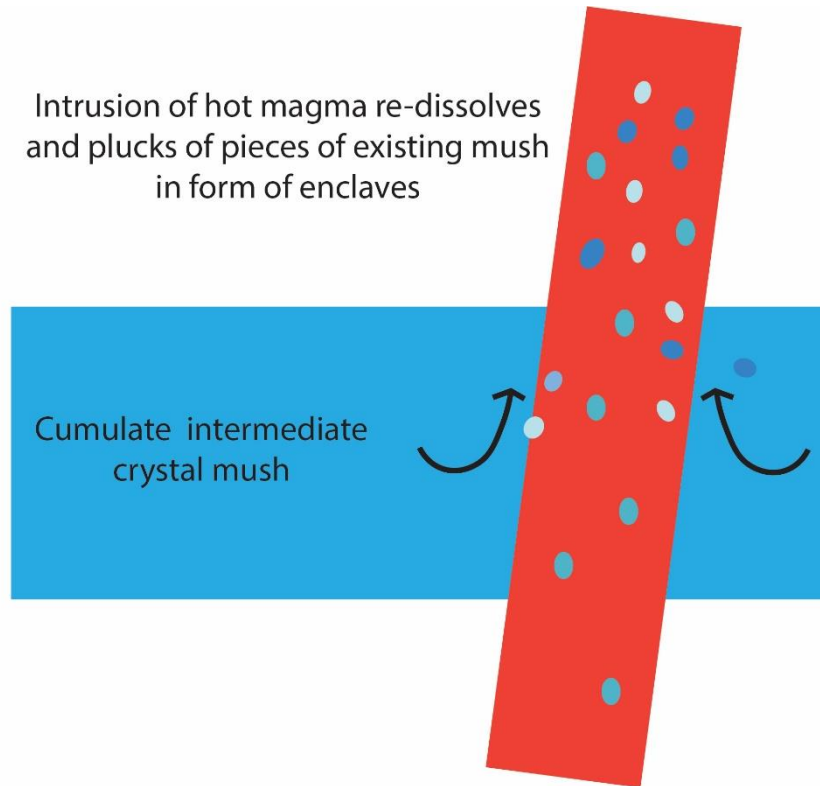


Figure 7.3. Illustration of a potential process that formed Group 2 and Group 3 enclaves at Wild Cove East. A hot magma injected through a colder crystal mush causes localized melting and mixing to take place in the mush. Pieces of the mush are plucked by the injected magma which are rounded into globules during transport to higher levels.

References

1. Andrews, B., Gardner, J. and Housh, T. (2008). Repeated recharge, assimilation, and hybridization in magmas erupted from El Chichón as recorded by plagioclase and amphibole phenocrysts. *Journal Of Volcanology And Geothermal Research*, 175(4), 415-426.
2. Astbury, L.A, Petrelli, M., Arienzo, I., D'Antonio, M., Morgavi, D. and Perugini, D. (2016). Using trace element mapping to identify discrete magma mixing events from the Astroni 6 eruption. AGU Fall Meeting 2016 abstract. V33E-3176.
3. Aydin, Ns. (1994). Physical characteristics of the Tilting Layered Suite, Fogo Island, Newfoundland. *South African Journal of Geology*, 97(4), 496-506.
4. Bachmann, O. and Huber, C. (2016). Silicic magma reservoirs in the Earth's crust. *American Mineralogist*, 101(11), 2377-2404.
5. Baird, D.M. (1958) *Fogo Island map-area, Newfoundland*. Geological Survey of Canada. Memoir 301, p. 63.
6. Barbarin, B. (1988). Field evidence for successive mixing and mingling between the Piolard Diorite and the Saint-Julien-la-Vetre Monzogranite (Nord-Forez, Massif Central, France). *Can. J. Earth Sci.*, 25, 49-59.
7. Barbarin, B. (2005). Mafic magmatic enclaves and mafic rocks associated with some granitoids of the central Sierra Nevada batholith, California: nature, origin, and relations with the hosts. *Lithos*, 80(1-4), 155-177.
8. Bergantz, G.W., Schleicher, J.M. and Burgisser, A. (2015). Open-system dynamics and mixing in magma mushes. *Nature Geoscience*. (8), 793-796.
9. Black, L.P., Kamo, S.L., Allen, C.M., Aleinkoff, J.N., Davis, D.W., Korsch, R.J. and Foudoulis, C. (2003). TEMORA 1: a new zircon standard for Phanerozoic U-Pb geochronology. *Chemical Geology*, 200, 155-170.

10. Blundy, J., Cashman, K. and Humphreys, M. (2006). Magma heating by decompression-driven crystallization beneath andesite volcanoes. *Nature*, 443, 76-80.
11. Bottinga, Y. and Weill, D. (1972). The viscosity of magmatic silicate liquids; a model calculation. *American Journal of Science*, 272(5), 438-475.
12. Bradley, D. (1983). Tectonics of the Acadian orogeny in New England and adjacent Canada, *Jour. Geology*, 91, 381-400.
13. Burgisser, A. and Bergantz, G. (2011). A rapid mechanism to remobilize and homogenize highly crystalline magma bodies. *Nature*, 471(7337), 212-215.
14. Burnham, C.W. (1980). The importance of volatile constituents. *EIR*, 439-482.
15. Burnham, C.W., and Ohmoto, H. (1980). Late-stage processes of felsic magmatism
16. Chen, B., Chen, Z.C. and Jahn, B.M. (2009). Origin of Mafic Enclaves from The Taihang Mesozoic Orogen, North China Craton. *Lithos*, 110(1-4), 343-358.
17. Clemens, J.D., and Mawer, C.K. (1992). Granitic magma transport by fracture propagation, *Tectonophysics*, 204, 339-360.
18. Clemens, J. and Petford, N. (1999). Granitic melt viscosity and silicic magma dynamics in contrasting tectonic settings. *Journal of the Geological Society*, 156(6), 1057-1060.
19. Currie, K.L. (1997). Fogo map-area, Newfoundland. Geological Survey of Canada Open File 3466.
20. Currie, K.L. (2003). Emplacement of the Fogo Island batholith, Newfoundland. *Atlantic Geology*, 39(2).
21. Deen, N.G., Willem, G., Sander, G., and Kuipers, J.A.M. (2010). Numerical analysis of solids mixing in pressurized fluidized beds, *Ind. Eng. Chem. Red.*, 49(11), 5246-5253.
22. Didier, J. (1973). Granites and their enclaves, *Elsevier, Amsterdam*, 393.

23. Didier, J. and Barbarin, B. (1991). *Enclaves and granite petrology* (1st ed., 19-23). Amsterdam: Elsevier.
24. Dorais, M., Wintsch, R., Nelson, W., and Tubrett, M. (2009). Insights into the Acadian orogeny, New England Appalachians: a provenance study of the Carrabassett and Kittery formations, Maine. *Atlantic Geology*, 45(0), 50.
25. Dube, B., Lauziere, K., and Tremblay, A. (1992). Structural geology of a crustal scale fault zone: the Cape Ray Fault coastal section, southwestern Newfoundland, *Current Research, Part D: Geol. Survey Canada Paper 92-1D*, 199-209.
26. Elliot, C., Dunning, G., and Williams, P. (1991). New U/Pb zircon age constraints on the timing of deformation in north-central Newfoundland and implications for early Paleozoic Appalachian orogenesis. *Geological Society of America Bulletin*, 103(1), 125-135.
27. Fernandez, A.N. and Barbarin, B. (1991) *Enclaves and granite petrology* (1st ed., pp. 263-275). Amsterdam: Elsevier
28. Ferrill, B., and Thomas, W. (1988). Acadian dextral transpression and synorogenic sedimentary successions in the Appalachians, *Geology*, 16, 604-608.
29. Frost, T.P., and Mahood, G.A. (1987). Field, chemical and physical constraints on mafic-felsic interaction in the Lamarck Granodiorite, Sierra Nevada, California, *Geological Society of America Bulletin*, 99, 272-291.
30. Fyffe, L.R., Pickerill, R.K., and Stringer, P. (1999). Stratigraphy, sedimentology and structure of the Oak Bay and Waweig formations, Mascarene basins: implications for the Paleotectonic evolution of southwestern New Brunswick, *Atlantic Geology*, 35, 59-84.
31. Geological Survey. (2017). *Nr.gov.nl.ca*. Retrieved 1 May 2017, from <http://www.nr.gov.nl.ca/mines&en/geosurvey/maps/>
32. Getson, J.M., and Whittington, A.G. (2007). Liquid and magma viscosity in the anorthite-forsterite-diopside-quartz system and implications for the viscosity-

temperature paths of cooling magmas, *J. Geophys. Res.*, *112*, B10203, doi: 10.1029/2006JB004812.

- 33.** Glazner, A.F., Bartley, J.M., Law, B., and Coleman, D.S. (2012) Ladder dikes, crazy geochemistry and liquid immiscibility in otherwise sane granites. *Geological Society of America Abstracts with Programs*, *44* (3), 21.
- 34.** Gorner, E. (2016). A mapping, petrographic, and mineral chemistry study of intrusions in the Tilting Igneous Suite, Fogo Island, Newfoundland, *Memorial University of Newfoundland B.Sc Hons thesis*, 1-69.
- 35.** Hamilton, M.A. and Kerr, A. (2016). New U-Pb dates from Silurian rocks on Fogo Island: Preliminary stratigraphic and tectonic implications. *Current Research. Newfoundland and Labrador Department of Natural Resources Geological Survey*, *16*(1), 123-132.
- 36.** Hibbard, J. (1994). Kinematics of Acadian Deformation in the Northern and Newfoundland Appalachians, *The Journal of Geology*, *102*, 215-228.
- 37.** Hodge, K., Carzzo, G., and Jellinek, A. (2012) Experimental constraints on the deformation and breakup of injected magma. *Earth and Planetary Science Letters*, *325-326*, 52-62.
- 38.** Holdsworth, R., (1991). The geology and structure of the Gander-Avalon boundary zone in northeastern Newfoundland, *Current Research: Newfoundland Dept. Mines and Energy, Geol. Survey Branch, Rept.*, *91*(1), 109-126.
- 39.** Huber, C., Bachmann, O., and Manga, M. (2009). Homogenization processes in silicic magma chambers by stirring and mushification. *Earth and Planetary Science Letters*, *283*, 38-47.
- 40.** Huppert, H.E., Sparks, R.S.J., and Turner, J.S. (1984). Some effects of viscosity on the dynamics of replenished magma chamber, *J. Geophys. Res.*, *89*, 6857-6877.

41. Irvine, T., Andersen, J., and Brooks, C. (1998). Included blocks (and blocks within blocks) in the Skaergaard intrusion: Geologic relations and the origins of rhythmic modally graded layers. *Geological Society of America Bulletin*, 110(11), 1398-1447.
42. Jaffey, A. H., Flynn, K. F., Glendenin, L. E., Bentley, W. C. and Essling, A. M. (1971) Precision measurement of half-lives and specific activities of ²³⁵U and ²³⁸U. *Phys. Rev*, 4, 1889.
43. Johnson, K., and Barnes, C.G. (2006). Magma mixing and mingling in the Greyback pluton, Klamath Mountains, Oregon. *Geol. Soc. Amer. Spec. Pap*, 410, 247-267.
44. Kerr, A. (2013). The Fogo Process from a Geologist's Perspective: A Discussion of Models and Research Problems. *Current Research, Newfoundland and Labrador Department of Natural Resources*, 13(1), 233-265
45. Kretz, R. (1983). Symbols for rock-forming minerals. *American Mineralogist*, 68, 277-279.
46. Lacroix, A. (1890). Sur les enclaves acides des roches volcaniques d'Auvergne. *Bull. Serv. Carte Geol. Fr*, 2, 25-56.
47. Lebas, M.J., Lemaitre, R.W., Streckeisen, A. and Zanettin, B. (1986). A Chemical Classification of Volcanic-Rocks Based on the Total Alkali Silica Diagram. *Journal of Petrology* 27(3), 745-750.
48. MacLachlan, K., O'Brien, B., and Dunning, G. (2001). Redefinition of the Wild Bight Group, Newfoundland: implications for models of island-arc evolution in the Exploits Subzone. *Canadian Journal of Earth Sciences*, 38(6), 889-907.
49. Mahon, K.I., Harrison, T.M. and Drew, D.A. (1988). Ascent of granitoid diapir in a temperature varying medium. *J. Geophys. Res.*, 93, 1174-1188.
50. Marsh, B.D. (1981). On the crystallinity, probability of occurrence, and rheology of lava and magma. *Contrib. Mineral. Petrol.* 78, 85-98.

51. Marsh, B. D. (2002). On bimodal differentiation by solidification front instability in basaltic magmas, part 1: basic mechanics. *Geochimica et Cosmochimica Acta*, 66(12), 2211-2229.
52. McBirney, A., and Murase, R. Rheological properties of magmas. *Ann. Rev. Earth Planet. Sci*, 12, 337-357.
53. McBirney, A. (2007). *Igneous petrology* (1st ed.). Boston: Jones and Bartlett Publishers, 193-204.
54. McNicoll, V.C., Squires, G.C., Wardle, R.J., Dunning, G.R., and O'Brien, B.H. (2006). U-Pb Geochronological evidence for Devonian deformation and gold mineralization in the eastern Dunnage Zone, Newfoundland. *Current Research. Newfoundland and Labrador Department of Natural Resources Geological Survey*, 06(1), 45-60.
55. Miller, J.S., Matzel, J.P., Miller, C.F., Burgess, S.D., Miller, R.B. (2007). Zircon growth and recycling during the assembly of large, composite arc plutons. *Journal of Volcanology and Geothermal Research*, 167, 282-299.
56. Murphy, J., Keppie, J., Nance, R., and Dostal, J. (2010). Comparative evolution of the Iapetus and Rheic Oceans: A North America perspective. *Gondwana Research*, 17(2-3), 482-499.
57. Nabelek, P., Hofmeister, A., and Whittington, A. (2012). The influence of temperature-dependent thermal diffusivity on the conductive cooling rates of plutons and temperature-time paths in contact aureoles. *Earth and Planetary Science Letters*, 317-318, 157-164.
58. Nelson S.T., and Montana, A. (1992) Sieve-textured plagioclase in volcanic rocks produced by rapid decompression. *Am Mineral*, 77, 1242-1249.
59. O'Brien, B., O'Brien, S., and Dunning, G. (1991). Silurian cover, Late Precambrian-Early Ordovician basement, and the chronology of Silurian orogenesis in the Hermitage Flexure (Newfoundland Appalachians), *Am. Jour. Sci.*, 291, 760-799.

60. Pabst, A. (1928). Observations on inclusions in the granitic rocks of the Sierra Nevada, *Univ. California Publ., Dep. Geol. Sci. Bull*, 67, 325-386.
61. Paterson, S. (2009). Magmatic tubes, pipes, troughs, diapirs, and plumes: Late-stage convective instabilities resulting in compositional diversity and permeable networks in crystal-rich magmas of the Tuolumne batholith, Sierra Nevada, California. *Geosphere*, 5(6), 496-527.
62. Paterson, S.R., Okaya, D., Memeti, V., Economos, R., and Miller, R.B. (2011). Magma addition and flux calculations of incrementally constructed magma chambers in continental margin arcs: Combined field, geochronologic, and thermal modelling studies. *Geosphere*, 7(6), 1439-1468.
63. Pearce, J.A. (1982). Trace element characteristics of lavas from destructive plate boundaries. *Andesites*, 525-548
64. Peretyazhko, I.S. (2010). Genesis of mineralized cavities (miaroles) in granitic pegmatites and granites, *Petrologiya*, 18(2), 195-222.
65. Petford, N., Cruden, A.R., McCaffrey, K.J.W., and Vigneresse, J.L. (2000). Granite magma formation, transport and emplacement in the Earth's crust, *Nature*, 408, 669-673.
66. Philpotts, A., and Carroll, M. (1996). Physical properties of partly melted tholeiitic basalt. *Geology*, 24(11), 1029-1032.
67. Pollock, J.C., Wilton, D.H.C., van Staal, C.R., and Morrissey, K.D. (2007). U-Pb detrital zircon geochronological constraints on the early Silurian collision of Ganderia and Laurentia along the Dog Bay Line: The terminal Iapetan suture in the Newfoundland Appalachians, *American Journal of Science*, 307, 399-433.
68. Ruprecht, R., Bergantz, G.R., Cooper, K.M., Hildreth, W., and Hildreth, W. (2012). The crustal magma storage system of Volcan Quizapu, Chile, and the effects of magma mixing on magma diversity, *Journal of Petrology*, 53(4), 801-840.

69. Sandeman, H.A., and Malpas, J. (1995). Epizonal I and A-type granites and associated ash-flow tuffs, Fogo Island, northeast Newfoundland. *Canadian Journal of Earth Sciences*, 32, 1832–1844.
70. Schleicher, J.M., Bergantz, G.W., Breidenthal, R.E., and Burgisser, A. (2016). Time scales of mixing in magma mushes. *Geophys. Res. Lett.*, 43, 1543-1550.
71. Shaw, H. (1965). Comments on viscosity, crystal settling, and convection in granitic magmas. *American Journal of Science*, 263(2), 120-152.
72. Smith, R.L., (1979). Ash-flow magmatism, *Geol. Soc. America Spec. Paper 180*, 5-28.
73. Sparks, G.W. and Dunning, G.R. (2014) Late Neoproterozoic epithermal alteration and mineralization in the western Avalon zone: a summary of mineralogical investigations and new U/Pb geochronological results. *Current Research, Newfoundland and Labrador Department of Natural Resources Geological Survey, 14-1*, 99-128.
74. Stacey, J. S. and Kramers, J. D. (1975). Approximation of terrestrial lead isotope evolution by a two-stage model. *Earth and Planetary Science Letters*, 26(2), 207-221.
75. Stern, C., Huang, W., and Wyllie, P. (1975). Basalt-andesite-rhyolite-H₂O: Crystallization intervals with excess H₂O and H₂O-undersaturated liquidus surfaces to 35 kilobars, with implications for magma genesis. *Earth and Planetary Science Letters*, 28(2), 189-196.
76. Storm, S., Shane, P., and Schmitt A.K. (2012) Decoupled crystallization and eruption histories of the rhyolite magmatic system at Tarawera volcano revealed by zircon ages and growth rates. *Contrib Mineral Petrol.* 163, 505-519.
77. Streck, M.J. (2008). Mineral textures and zoning as evidence for open system processes, *Putirka KD, Tepley III FJ (eds) Minerals, inclusions and volcanic processes. Miner Soc Am and Geochem Soc, Rev Mineral*, 595-622.

- 78.** Taylor, S.R. and McLennan, S.M. (1985). The Continental Crust; Its composition and evolution; an examination of the geochemical record preserved in sedimentary rocks. *Blackwell, Oxford*. 312.
- 79.** Tindle, A.G. (1991). *Enclaves and granite petrology* (1st ed., 313-331). Amsterdam: Elsevier.
- 80.** Tobisch, O., McNulty, B., and Vernon, R. (1997). Microgranitoid enclave swarms in granitic plutons, central Sierra Nevada, California. *Lithos*, 40(2-4), 321-339.
- 81.** Valverde-Vaquero, P., van Staal, C.R., McNicoll, V., and Dunning, G. (2006). Middle Ordovician magmatism and metamorphism along the Gander margin in Central Newfoundland, *Journal of the Geological Society London*, 163, 347-362.
- 82.** van der Pluijm, B. and van Staal, C. (1988). Characteristics and evolutions of the Central Mobile Belt, Canadian Appalachians, *Jour. Geology*, 96, 535-547.
- 83.** van Staal, C.R. (1994). The Brunswick subduction complex in the Canadian Appalachians: record of the Late Ordovician to Late Silurian collision between Laurentia and the Gander margin of Avalon, *Tectonics*, 13, 946-962.
- 84.** van Staal, C.R. (2005). The Canadian Appalachians: record of the Late Ordovician to Late Silurian collision between Laurentia and the Gander margin of Avalon, *Tectonics*, 13, 946-962.
- 85.** van Staal, C.R. and Barr, S.M., (2012). Lithospheric architecture and tectonic evolution of the Canadian Appalachians and associated Atlantic margin, in Percival, J.A., Cook, F.A., and Clowes, R.M., eds., *Tectonic Styles in Canada: The LITHOPROBE perspective: Geological Association of Canada Special Paper 49*, 41-95.
- 86.** Van Staal, C., Zagorevski, A., McNicoll, V., and Rogers, N. (2014). Time-Transgressive Salinic and Acadian Orogenesis, Magmatism and Old Red Sandstone Sedimentation in Newfoundland. *Geoscience Canada*, 41(2), 138.
- 87.** Vernon, R.H. (1984). Microgranitoid enclaves in granite – globules of hybrid magma quenched in a plutonic environment. *Nature*, 309, 438-439.

- 88.** Ver Straeten, C.A., (2010). Lessons from the foreland basin: Northern Appalachian basin perspectives on the Acadian orogeny. *Geological Society of America Memoir 206*, 251-282.
- 89.** Vogel, T.A. (1982). Magma mixing in the acidic-basic complex of Ardnamurchan: implications on the evolution of shallow magma chambers, *Contrib. Mineral. Petrol*, 79, 411-423.
- 90.** Waldron, J., and Milne, J. (1991). Tectonic history of the central Humber Zone, western Newfoundland Appalachians: post-Taconian deformation in the Old Man's Pond area. *Canadian Journal of Earth Sciences*, 28(3), 398-410.
- 91.** Wiebe, R. (1968). Plagioclase stratigraphy; a record of magmatic conditions and events in a granite stock. *American Journal of Science*, 266(8), 690-703.
- 92.** Wiebe, R. (1994). Silicic Magma Chambers as Traps for Basaltic Magmas: The Cadillac Mountain Intrusive Complex, Mount Desert Island, Maine. *The Journal of Geology*, 102(4), 423-437
- 93.** Wiebe, R., Smith, D., Sturm, M., King, E.M., Seckler, M.S. (1997). Enclaves in the Cadillac Mountain Granite (Coastal Maine): Samples of Hybrid Magma from the Base of the Chamber. *Journal of Petrology*, 38(3), 393-423.
- 94.** Wiebe, R., and Collins, W. (1998). Depositional features and stratigraphic sections in granitic plutons: implications for the emplacement and crystallization of granitic magma. *Journal of Structural Geology*, 20(9-10), 1273-1289.
- 95.** Wiebe, R., Jellinek, M., Markley, M., Hawkins, D., and Snyder, D. (2007). Steep schlieren and associated enclaves in the Vinalhaven granite, Maine: possible indicators for granite rheology. *Contributions To Mineralogy And Petrology*, 153(2), 121-138.
- 96.** Wiebe, R., Jellinek, A., and Hodge, K. (2017). New insights into the origin of ladder dikes: Implications for punctuated growth and crystal accumulation in the Cathedral Peak granodiorite. *Lithos*, 277, 241-258.

97. Williams, H. (1979). Appalachian Orogen in Canada. *Canadian Journal of Earth Sciences*, 16(3), 792-807.
98. Williams, H. and Hatcher, R. (1982). Suspect terranes and accretionary history of the Appalachian orogen, *Geology*, 10, 530-536.
99. Williams, H., and Hiscott, R.N. (1987). Definition of the Iapetus rift-drift transition in western Newfoundland, *Geology*, 15, 1044-1047.
100. Williams, H., Colman-Sadd, S.P., and Swinden, H.S. (1988). Tectonostratigraphic subdivisions of central Newfoundland, *Current Research, Part B. Geological Survey of Canada, Paper 88-1B*, 91-98.
101. Williams, H., Currie, K.L. and Piasecki, M.A.J. (1993). The Dog Bay Line, a Silurian terrane boundary in northeast Newfoundland. *Canadian Journal of Earth Sciences*, 29, 2481-2494.
102. Williams, H. (1993). Acadian orogeny in Newfoundland. *Geological Society of America Special Paper 275*, 123-133
103. Williams, H. (2004). *Geological Survey of Newfoundland. Nr.gov.nl.ca*. Retrieved 10 May 2017, from <http://www.nr.gov.nl.ca/mines&en/geosurvey/maps/>
104. Winter, J. (2010). *An introduction to igneous and metamorphic petrology*. Upper Saddle River, NJ: Prentice Hall
105. Yücel, C., Arslan, M., Temizel, İ. and Abdioğlu, E. (2013). Volcanic facies and mineral chemistry of Tertiary volcanics in the northern part of the Eastern Pontides, northeast Turkey: implications for pre-eruptive crystallization conditions and magma chamber processes. *Mineralogy and Petrology*, 108(3), 439-467.
106. Zavala, K., Leitch, A.M. and Fisher, G. (2011). Silicic segregations of the Ferrar Dolerite Sills, Antarctica. *Journal of Petrology*, 52, 1927-1964.

Appendix A. Sample Numbers and Locations

Sample locations were acquired using a Garmin GPSmap 62 unit and are accurate to 2-3 meters. Grid 1 samples were taken from the detailed map area of Figure 2.4. Grid 2 samples were taken from a second hand-drawn map area (not shown) near *b* in Figure 2.2. Numbering system is based on the date when the sample was taken (e.g. 072803B was the second sample taken on from a third location on July 28, 2015). Samples beginning with 16 were taken in the summer of 2016 (e.g. 16070906 was the sixth sample taken on July 9, 2016).

Table A.1. Sample Locations, UTM zone 21 U

Sample #	Sample Description	Easting	Northing
<i>Eastern Map Area</i>			
071001	Enclave-poor tonalite w/o enclaves	Grid 2	Grid 2
071002	Enclave contained in enclave-poor tonalite	Grid 2	Grid 2
071003	Diorite on Turpins trail near shore	709677	5511350
071004	Granite on Turpins trail near forest	709690	5511388
071005	Massive Diorite	Grid 2	Grid 2
071302	Biotite granite	Grid 2	Grid 2
071303	Rhyolite dyke near metasedimentary xenoliths	709701	5511588

071414	Pyroxene-rich rock at base of mafic layered intrusion	710176	5511484
071415A	Pyroxene-rich rock near middle of mafic layered intrusion	710226	5511476
071415B	Pegmatite differentiate in mafic layered intrusion	710226	5511476
071416	Feldspar rich rock near top of mafic layered intrusion	710257	5511497
071417	Potential top of mafic layered intrusion	710406	5511640
072606	Sample of enclave-poor tonalite	709980	5511555
072607	Contact across schlieren	709980	5511555
072804A	Small fine grained mafic enclave without phenocrysts	709701	5511623
072804B	Fine-grained enclave taken close to metasedimentary unit	709807	5511578
072804C	Large fine-grained mafic enclave, no phenocrysts	709807	5511578
072805A	Large medium-grained enclave; cuts across schlieren	710028	5511561
072805B	Fine-grained mafic enclave w feldspar phenocrysts	710028	5511561
072806A	Fine-grained mafic enclave, w plagioclase phenocrysts	710121	5511539
072806B	Fine-grained mafic enclave, w plagioclase phenocrysts	710121	5511539
072806C	Fine-grained mafic enclave; no plagioclase phenocrysts	710121	5511539
080301	Metasedimentary xenolith	709654	5511741
080302	Biotite granite	709651	5511736
16070901	Host Rock several meters east of northern intermediate dykes	709760	5511595
16070902	Host Rock 100 m SE of 16070901	709651	5511820
16070903	Enclave-poor tonalite unit	709653	5511860
16070904	Enclave-poor tonalite host a few hundred m east of 16070903	709834	5511558
16070905	Enclave-rich tonalite on other side of gulley from 16070904	709916	5511523
16070906	Large Felsic Dyke	709956	5511565
16070907	Schlieren sample swirling around enclave	709956	5511565

16070908	Host rock sample taken close to mafic layered intrusion	709956	5511565
16070909	Piece of mafic layered intrusion further up from olivine-rich sample	709956	5511565
16070910	"pre-pegmatite" (rock taken immediately adjacent to pegmatite)	709956	5511565
16070911	Sample taken near top of mafic layered intrusion	709956	5511565
<i>Northern Map Area</i>			
071601	med-grained brecciated mafic dyke w feldspar phenocrysts	710005	5511587
071601B	Med-grained brecciated mafic dyke w feldspar phenocrysts	710005	5511587
071601C	nearby enclave of similar composition to above dyke	710005	5511587
071602	diorite host containing previous samples	710021	5511565
071603A	Dark mafic enclave further east down shore	710044	5511567
071603B	diorite host which contains above sample	710044	5511567
071604	mafic enclave that looks similar to 071603A	710024	5511577
072001A	Gabbro base of sill W of Grid 1	707689	5511688
072001B	Taken from center part of sill	707689	5511688
072001C	Dioritic top of sill	707689	5511688
072001D	Diorite unit in contact with top of sill	707689	5511688
072601	Sample of thinner S dyke	709653	5511864
072602	Sample of larger N dyke	709653	5511864
072603	Sample of host diorite	709653	5511864
072604	Sample of diorite "block"	709660	5511697
072605	Sample of diorite	709660	5511697
072608	Contact between granite dyke and diorite host	709953	5511553
072609A	Enclave; med grained w plag phenocrysts	710001	5511568
072609B	Enclave; fine grained w plag phenocrysts	710001	5511568

072609C	Enclave; med grained w fldpr phenocrysts	710001	5511568
072801A	fine-grained mafic enclave, cusplate margins, no phenocrysts	709657	5511845
072801B	fine-grained mafic, rounded margin, border granite unit	709657	5511845
072802A	diorite type enclave contained in leucodiorite host	709667	5511782
072802B	fine-grained mafic enclave with cusplate margins, sparse fldspr phenocrysts	709667	5511782
072802C	med-grained mafic enclave w plag phenocrysts. Large, contains smaller enclave within it	709667	5511782
072802D	Sample of host diorite	709667	5511782
072803A	Medium-grained enclave w cusplate margins	709669	5511718
072803B	fine-grained mafic enclave w cusplate margins and plag phenocrysts	709669	5511718
072804D	med-grained enclave contained in diorite host rock	709908	5511560
16070803	Sample of chilled diorite dyke	709956	5511565
<i>Detailed Map Area</i>			
071301	Rhyolite/aplite	Grid 1	Grid 1
071401	Piece of broken-up tonalite dyke	709691	5511642
071402	contact between granite and enclave-poor tonalite	709689	5511641
071404	Sample of enclave-poor tonalite w/o xenoliths	709693	5511638
071405A	Sample of biotite granite	709685	5511645
071405B	Sample of contact between biotite granite and enclave-poor tonalite	709685	5511645
071406	Enclave-rich tonalite w enclaves	709688	5511636
071407	Enclave-rich tonalite w enclaves	709687	5511645
071408	Enclave-poor tonalite far from enclave rich zone	709694	5511633
071409	Sample of biotite granite	709686	5511651
071410	enclave within enclave-rich tonalite	709689	5511635
071411	Contact between enclave-rich tonalite and enclave	709688	5511635

071412	Dark enclave with cusped margin and contact w host diorite	709705	5511624
071413	Intermediate dyke w chilled margins	709947	5511518
BG-0620	Quartz Diorite	Grid 1	Grid 1
BG-0621	Biotite granite	Grid 1	Grid 1

Appendix B. Petrographic Characteristics of Units

Table B.1. Mineralogy and petrographic characteristics of samples

Sample #	Field Name	Mineralogy	IUGS Classification
<i>Eastern Map Area</i>			
071004	Granite on Turpin's Trail	Qtz (35%), Plag (30%), Kspar (25%), Bt (<5%)	Biotite Monzogranite
071302	Granite Unit Contained in Grid 2	Kspar (55%), Qtz (30%), Plag (10%), Bt (5%)	Biotite Syenogranite
071413	Mafic dyke along shore near metasedimentary xenoliths	Plag (45%), Opx (25%), Hbl (15%), Cpx (15%)	Gabbroic rock *
071414	Pyroxene-rich rock at base of sill	Olv (40%), Plag (25%), Opx (20%), Bt (15%)	Troctolite
071415A	Pyroxene-rich rock further up sill from 071414	Plag (35%), Opx (20%), Cpx (15%), Olv (15%), Hbl (10%), Bt (10%)	Olivine Gabbro
071417	Potential top of mafic sill	Plag (35%), Qtz (20%), Cpx (15%), Bt (15%), Hbl (5%), Opx (5%)	Hornblende Augite Biotite Tonalite
071602	Host rock of Grid 2 area mafic dyke	Plag (65%), Hbl (20%), Qtz (5%), Opx (5%), Bt (5%), <Cpx (5%)	Opx-bearing Biotite Hornblende Quartz Diorite
072606	Massive diorite north of Grid 2	Plag (55%), Qtz (15%), Hbl (10%), Bt (10%), Cpx (5%), Opx (<5%)	Biotite Hornblende Tonalite
072804A	Small fine-grained mafic enclave without phenocrysts	Plag (50%), Bt (30%), Hbl (15%), Qtz (5%)	Hornblende Biotite Quartz Diorite

072804B	Fine-grained metasedimentary xenolith	Qtz (50%), Cpx (35%), Plag (20%), Opx (<5%)	Granulite Facies Metasedimentary Rock
072804C	Large fine-grained dark enclave without phenocrysts	Qtz (50%), Plag (35%), Hbl (10%), Cpx (10%), Bt (5%)	Metasedimentary Rocks
072804D	Medium-grained enclave contained in diorite host rock	Plag (55%), Hbl (20%), Bt (15%), Qtz (10%), Cpx (<5%)	Biotite Hornblende Quartz Diorite
072803A	Medium-grained enclave with cusped margins	Plag (50%), Bt (25%), Hbl (10%), Qtz (10%), Opx (5%), Cpx (<5%)	Biotite Hornblende Quartz Diorite
<i>Northern Map Area</i>			
071601	Brecciated mafic dyke near Grid 2	Plag (55%), Qtz (15%), Bt (10%), Hbl (5%), Opx (5%), Cpx (<5%)	Opx-bearing Hornblende Biotite Quartz Diorite
071601A	Brecciated mafic dyke near Grid 2	Plag (45%), Opx (20%), Bt (15%), Hbl (10%), Qtz (10%), Cpx (<5%)	Opx-bearing Hornblende Biotite Quartz Diorite*
071601C	Nearby large (1m) long enclave of similar composition to nearby dyke	Plag (75%), Cpx (15%), Bt (5%), Opx (5%)	Pyroxene-bearing Biotite Diorite *
071603A	Mafic enclave further east down shore	Plag (40%), Qtz (15%), Hbl (15%), Opx (15%), Cpx (10%), Bt (5%)	Pyroxene-bearing Biotite Hornblende Quartz Diorite *
071603B	Diorite host w fine-grained mafic enclave contact	Plag (80%), Qtz (10%), Bt (10%), Hbl (5%), Opx (5%), Cpx (<5%)	Opx-bearing Hornblende Biotite Quartz Diorite
071604	Mafic enclave that looks similar to 071603A	Plag (50%), Hbl (25%), Bt (10%), Qtz (10%)	Biotite Hornblende Quartz Diorite
072802A	Diorite-type enclave contained in leucodiorite host	Plag (40%), Qtz (35%), Hbl (10%), Bt (10%), Cpx (5%)	Biotite Hornblende Tonalite
072802A	Diorite-type enclave contained in leucodiorite host	Plag (35%), Qtz (20%), Hbl (20%), Bt (15%), Cpx (<5%)	Biotite Hornblende Tonalite

072802B	Fine-grained mafic enclave with cusped margins and sparse feldspar phenocrysts	Plag (40%), Qtz (25%), Hbl (20%), Bt (10%), Cpx (5%)	Biotite Hornblende Tonalite
072802C	Medium-grained mafic enclave with feldspar phenocrysts	Plag (50%), Hbl (30%), Bt (15%), Qtz (5%), Cpx (<5%)	Biotite Hornblende Quartz Diorite
072803B	Fine-grained mafic enclave with cusped margins and sparse feldspar phenocrysts	Plag (40%), Qtz (20%), Hbl (20%), Bt (15%), Cpx (5%)	Biotite Hornblende Tonalite
<i>Detailed Map Area</i>			
071002A	Enclave contained in enclave-poor tonalite	Plag (50%), Qtz (25%), Hbl (15%), Bt (10%), Cpx (5%)	Biotite Hornblende Tonalite
071301	Aplite unit	Plag (60%), Qtz (40%)	Aplite
071401	Broken-up tonalite dyke	Plag (40%), Qtz (35%), Cpx (10%), Bt (5%), Hbl (<5%), Opx (<5%), Kspar (<5%)	Augite-Bearing Hornblende Biotite Tonalite *
071402	Granite Unit (including contact with Grid 1)	Plag (50%), Qtz (35%), Bt (10%), Kspar (5%)	Biotite Tonalite (?)
071403	Intrusion displaying chilled margin on one side	Plag (70%), Qtz (10%), Hbl (10%), Cpx (5%), Bt (5%), Opx (<5%)	Augite Biotite Hornblende Quartz Diorite
071404	Sample of contact enclave-poor tonalite host and enclave (Enclave Side)	Hbl (35%), Plag (30%), Qtz (25%), Bt (5%), Cpx (5%), Opx (<5%)	Biotite Hornblende Tonalite
071404	Sample of enclave-poor tonalite host and enclave (Host Side)	Plag (60%), Qtz (15%), Bt (15%), Hbl (10%), Cpx (<5%)	Hornblende Biotite Quartz Diorite
071405	Granite Unit (Grid 1)	Qtz (40%), Kspar (35%), Plag (25%), Bt (<5%)	Biotite Monzogranite
071405A	Granite Unit (Grid 1)	Kspar (40%), Qtz (40%), Plag (20%), Bt (<5%)	Biotite Monzogranite

071405B	Granite unit including contact with enclave-poor tonalite unit (not seen in thin section)	Qtz (35%), Kspar (30%), Plag (30%), Bt (5%)	Biotite Monzogranite
071406	Enclave-rich tonalite unit	Plag (75%), Qtz (20%), Bt (5%), Hbl (<5%), Cpx (<5%)	Biotite Tonalite
071408	Host rock far from enclave-rich zone	Plag (75%), Qtz (10%), Cpx (10%), Bt (5%), Opx (<5%)	Biotite Augite Quartz Diorite *
071410	Whole enclave contained in enclave-rich tonalite	Plag (30%), Qtz (35%), Hbl (15%) Bt (10%), Opx (10 %)	Biotite Hornblende Tonalite
071412	Dark cusped enclave w contact with host rock (Host Side)	Plag (45%), Qtz (20%), Bt (10%), Hbl (10%), Cpx (5%), Opx (<5%)	Augite-bearing Hornblende Biotite Tonalite
071412	Dark cusped enclave w contact with host rock (Enclave Side)	Plag (30%), Qtz (25%), Bt (20%), Hbl (15%), Cpx (5%), Opx (5%)	Pyroxene-bearing Hornblende Biotite Tonalite

Appendix C. Results of geochemical analyses

Table C.1. ICP-MS analyses for host rocks

	071404	071406	071602	071603B	16070901	16070902	16070904	16070905	16070908
<i>Major Elements (Wt %)</i>									
SiO ₂	59.98	67.99	56.73	58.29	62.59	61.08	60.5	58.76	60.01
Al ₂ O ₃	16.74	15.51	16.32	17.54	16.29	16.47	16.98	15.89	16.7
Fe ₂ O ₃ (T)	6.02	3.77	6.57	6.1	5.15	6.26	5.81	8.73	6.32
MnO	0.102	0.068	0.123	0.119	0.098	0.106	0.119	0.153	0.104
MgO	3.32	1.46	4.35	3.23	2.59	3.17	2.99	2.53	3.26
CaO	5.75	3.5	6.9	5.82	4.47	5.57	4.63	4.41	6.02
Na ₂ O	4.39	4.84	4.28	4.45	4.4	4.82	4.17	4.81	4.59
K ₂ O	1.42	1.31	1.11	1.28	1.87	1.3	2.3	1.93	1.43
TiO ₂	1.002	0.592	1.038	1.002	0.829	1.017	0.973	1.209	1.03
P ₂ O ₅	0.21	0.13	0.17	0.22	0.19	0.24	0.22	0.64	0.27
LOI	1.01	0.93	1.49	1.71	1.2	0.51	1.83	0.9	0.58
Total	99.94	100.1	99.08	99.77	99.68	100.5	100.5	99.97	100.3
<i>Trace Elements (ppm)</i>									
Sc	14	9	19	14	11	15	14	13	15
Be	2	2	2	2	2	2	2	2	2
V	123	63	97	130	91	124	116	80	124
Ba	329	400	265	629	563	343	1002	479	325
Sr	456	303	508	537	384	412	503	435	437
Y	17	17	18	16	17	19	17	33	19
Zr	202	191	91	193	190	248	176	381	176
Cr	70	N.d	90	60	50	50	60	30	50
Co	17	8	22	16	13	17	17	16	18
Ni	30	N.d	40	30	20	N.d	30	N.d	30
Cu	N.d	N.d	20	10	N.d	20	10	20	20
Zn	70	50	70	70	50	70	70	110	70
Ga	20	19	19	20	20	21	20	20	21
Ge	1	1	1	1	1	1	1	1	1
As	N.d	N.d	6	8	N.d	N.d	8	7	N.d
Rb	41	24	28	32	55	28	71	38	34
Nb	7	5	8	7	6	8	7	13	7
	N.d	N.d	N.d	N.d	N.d	N.d	N.d	N.d	N.d
Ag	N.d	0.5	N.d	N.d	N.d	N.d	N.d	1.3	N.c
In	N.d	N.d	N.d	N.d	N.d	N.d	N.d	N.d	N.c
Sn	N.d	1	N.d	N.d	N.d	1	1	1	1
Sb	N.d	1.4	N.d	1.5	N.d	N.d	N.d	1.6	N.d
Cs	1.6	1	0.9	1.5	1.5	1.3	2.6	1.3	1.2
La	22.4	24.8	20.5	20.6	24.6	25.9	23.9	35.6	24.9
Ce	46.2	48.7	41.5	42	50.5	53.3	48.8	80.6	52
Pr	5.07	5.05	4.57	4.56	5.36	5.69	5.34	9.29	5.69
Nd	19.5	19.8	19	18.2	20.3	22.1	20.9	38.1	22.4
Sm	4.1	3.9	4.1	3.9	4	4.8	4.2	8.3	5
Eu	1.37	1.08	1.58	1.48	1.27	1.52	1.31	2.64	1.45
Gd	3.7	3.8	3.8	3.6	3.5	4.5	3.9	7.6	4.2
Tb	0.6	0.6	0.6	0.5	0.6	0.7	0.6	1.2	0.7
Dy	3.3	3.4	3.7	3	3.3	3.8	3.4	6.7	3.7
Ho	0.6	0.6	0.7	0.6	0.6	0.7	0.7	1.2	0.7
Er	1.9	1.8	2	1.7	1.8	2.1	1.8	3.3	2.1
Tm	0.27	0.25	0.31	0.24	0.25	0.28	0.27	0.44	0.3
Yb	1.7	1.6	1.9	1.6	1.7	1.9	1.8	2.8	2
Lu	0.25	0.23	0.28	0.24	0.25	0.27	0.26	0.41	0.29
Hf	4.6	4.2	2.1	3.9	4.3	5.5	4	7.5	3.9
Ta	0.5	0.3	0.6	0.5	0.6	0.5	0.5	0.7	0.5
W	N.d	N.d	N.d	N.d	N.d	N.d	N.d	N.d	N.d
Tl	0.2	N.d	N.d	0.1	0.3	N.d	0.3	0.1	0.1
Pb	12	11	10	12	11	10	12	10	11
Bi	N.d	N.d	N.d	N.d	N.d	N.d	N.d	N.d	N.d
Th	5	3.5	3.5	3.1	6	4.8	5.5	4.9	3.9
U	1.4	1.1	1.1	1.1	1.3	1.3	1.5	1.6	1.1

Table C.2. ICP-MS analyses for mafic magmatic enclaves

	071410	071412	072802B	072802C	072803B	072804A	072804D
<i>Major Elements (Wt %)</i>							
SiO ₂	59.22	57.64	57.27	55.66	56.87	55.68	54.08
Al ₂ O ₃	16.19	15.6	16.1	16.56	15.79	15.96	16.16
Fe ₂ O ₃ (T)	6.12	7.33	7.88	8.69	7.7	7.99	10.19
MnO	0.149	0.115	0.123	0.135	0.15	0.148	0.143
MgO	3.9	4.65	3.56	4.39	4.24	4.32	4.17
CaO	5.42	6.5	5.9	6.81	6.22	6.2	5.86
Na ₂ O	4.93	4.08	4.43	4.05	3.87	3.94	4.02
K ₂ O	1.79	1.23	1.76	1.4	1.29	2.06	1.51
TiO ₂	0.895	1.2	1.649	1.785	1.323	1.521	2.499
P ₂ O ₅	0.17	0.23	0.38	0.4	0.26	0.32	0.48
LOI	1.23	0.67	0.89	0.71	2.39	0.93	0.83
Total	100	99.25	99.95	100.6	100.1	99.07	99.94
<i>Trace Elements (ppm)</i>							
Sc	21	19	16	18	20	17	15
Be	2	2	2	2	2	2	1
V	125	141	151	165	165	147	153
Ba	487	241	280	285	431	621	248
Sr	352	385	446	547	430	408	496
Y	35	21	22	26	20	18	20
Zr	160	140	172	184	143	100	218
Cr	60	90	60	60	70	100	30
Co	19	25	24	27	24	25	30
Ni	30	50	40	50	40	60	30
Cu	20	40	30	30	80	30	40
Zn	90	90	90	90	80	100	90
Ga	20	19	20	19	17	19	19
Ge	2	2	2	2	1	2	2
As	6	5	7	5	7	36	6
Rb	46	30	55	42	41	64	39
Nb	9	8	12	10	8	9	17
Mo	N.d	N.d	N.d	N.d	N.d	N.d	N.c
Ag	N.d	N.d	0.6	0.5	0.5	N.d	0.6
In	N.d	N.d	N.d	N.d	N.d	N.d	N.d
Sn	2	1	2	2	2	12	2
Sb	1.4	0.8	1	0.9	1.4	0.9	0.8
Cs	1.8	1.4	2.1	1.8	1.7	1.8	1.6
La	28.6	19.9	27.9	30.8	20	22.7	24.4
Ce	61.2	42.8	60.7	68	43.8	47.7	54.2
Pr	7.52	5.08	7.15	7.73	5.17	5.68	6.52
Nd	29.1	19.5	27.3	28.2	20	22.1	26.5
Sm	6.6	4.4	5.9	5.6	4.5	4.6	5.4
Eu	1.39	1.28	1.59	1.77	1.3	1.31	1.61
Gd	5.9	4	5.1	5.2	4.2	4.3	5.1
Tb	1	0.6	0.8	0.8	0.6	0.6	0.8
Dy	6.4	3.8	4.5	5.1	3.9	3.6	4.3
Ho	1.3	0.7	0.9	0.9	0.7	0.7	0.8
Er	3.8	2	2.3	2.7	2.1	1.9	2.3
Tm	0.58	0.31	0.36	0.41	0.34	0.28	0.32
Yb	3.8	2.1	2.4	2.7	2.2	1.9	2.2
Lu	0.57	0.3	0.33	0.4	0.33	0.28	0.32
Hf	4.2	3.4	4.2	4.4	3.1	2.7	4.6
Ta	0.7	0.8	1	0.9	0.7	0.8	1.3
W	2	6	3	2	3	2	3
Tl	0.3	0.2	0.3	0.3	0.3	0.5	0.2
Pb	24	13	18	12	15	25	16
Bi	N.d	N.d	N.d	N.d	N.d	0.7	N.d
Th	4.5	4.3	5.2	5.8	4.1	3.5	3.5
U	1.2	1.2	1.4	1.6	1.4	1.1	1.2

* N.d = Not detected

Table C.3. ICP-MS analyses for dykes and sills

	071401	160705A	072001B
<i>Major Elements (Wt %)</i>			
SiO ₂	59.51	57.34	51.15
Al ₂ O ₃	16.3	16.16	16.34
Fe ₂ O ₃ (T)	5.7	7.58	11.66
MnO	0.134	0.174	0.176
MgO	2.59	4.14	4.42
CaO	5.79	5.68	6.06
Na ₂ O	5.36	3.61	4.12
K ₂ O	1.61	1.81	2.01
TiO ₂	0.69	1.445	2.592
P ₂ O ₅	0.18	0.27	0.62
LOI	0.73	1.99	1.62
Total	98.59	100.2	100.8
<i>Trace Elements (ppm)</i>			
Sc	14	17	16
Be	2	2	3
V	116	141	163
Ba	437	1462	401
Sr	419	446	595
Y	27	22	29
Zr	96	235	267
Cr	20	70	40
Co	13	23	33
Ni	N.d	40	30
Cu	20	30	30
Zn	100	90	100
Ga	21	19	21
Ge	2	1	1
As	6	N.d	5
Rb	24	60	38
Nb	5	9	19
Mo	N.d	N.d	N.d
Ag	N.d	N.d	0.8
In	N.d	N.d	N.d
Sn	3	1	2
Sb	1.1	N.d	2
Cs	0.7	2.4	1.4
La	39.4	24.2	29.1
Ce	79.2	54.5	67.4
Pr	9.02	6.14	8.01
Nd	33.6	23.9	33.3
Sm	7	5.1	7.8
Eu	1.27	1.49	2.65
Gd	6	4.7	7.1
Tb	1	0.8	1.1
Dy	5.3	4.3	6.1
Ho	1	0.8	1.1
Er	2.8	2.4	3
Tm	0.42	0.33	0.4
Yb	2.6	2.3	2.6
Lu	0.41	0.33	0.38
Hf	2.7	5.1	5.6
Ta	0.5	0.6	1.3
W	3	N.d	N.d
Tl	0.1	0.3	0.2
Pb	16	19	7
Bi	N.d	N.d	N.d
Th	4.4	7.2	3.7
U	1.2	2.7	1.1

Table C.4. EMPA results for enclave plagioclase

	Enclave Group	TiO2 wt%	K2O wt%	CaO wt%	Na2O wt%	Al2O3 wt%	SiO2 wt%	FeO wt%	Total wt%	Ti atFrac	K atFrac	Ca atFrac	Na atFrac	Si atFrac	Al atFrac	Fe atFrac
71410 Matrix plag 3 core	1	0.0121	0.1098	4.326	9.0615	23.2399	62.7855	0.1668	99.7016	0.0003	0.0047	0.1542	0.5847	2.0893	0.9115	0.0046
71410 Matrix plag 3 rim	1	0.0154	0.2503	3.8509	9.1719	22.6869	62.9584	0.1387	99.0725	0.0004	0.0107	0.138	0.595	2.1063	0.8946	0.0039
71410 Megacrystic plag 2 Line 001	1	0.0099	0.2858	6.6356	7.5202	25.2335	60.5151	0.1843	100.3844	0.0002	0.0121	0.2365	0.485	2.0127	0.9892	0.0051
71410 Megacrystic plag 2 Line 002	1	0.0165	0.1589	6.6068	7.717	24.8709	59.6704	0.1499	99.1904	0.0004	0.0068	0.2385	0.504	2.0099	0.9875	0.0042
71410 Megacrystic plag 2 Line 003	1	-0.0088	0.6122	4.039	8.8594	22.7384	63.205	0.1728	99.618	-0.0002	0.026	0.1442	0.5725	2.1062	0.8931	0.0048
71410 Megacrystic plag 2 Line 004	1	0.0099	0.202	5.5967	8.2251	24.3435	61.4194	0.1909	99.9875	0.0002	0.0086	0.1997	0.5312	2.0456	0.9556	0.0053
71410 Megacrystic plag 2 Line 005	1	0.0187	0.1728	5.9616	7.9331	24.4138	60.5513	0.1585	99.2098	0.0005	0.0074	0.2146	0.5167	2.034	0.9666	0.0045
71410 Megacrystic plag 2 Line 006	1	0.0154	0.4204	6.5467	7.4205	24.9253	59.8198	0.1522	99.3003	0.0004	0.018	0.236	0.4841	2.0126	0.9884	0.0043
71410 Megacrystic plag 2 Line 007	1	-0.0154	0.256	6.272	7.7503	24.7281	60.1223	0.145	99.25829	-0.0004	0.011	0.2259	0.5052	2.0214	0.9799	0.0041
71410 Megacrystic plag 2 Line 008	1	0.0187	0.4409	5.5783	8.1015	23.9435	61.1347	0.1793	99.3969	0.0005	0.0189	0.2005	0.5269	2.0504	0.9466	0.005
71410 Megacrystic plag 2 Line 009	1	0.0011	0.2076	4.3388	9.0262	23.1763	62.7206	0.1195	99.5901	0	0.0088	0.1549	0.5832	2.0901	0.9103	0.0033
71410 Megacrystic plag 2 Line 010	1	0.0176	0.1445	4.1008	9.1773	23.1325	63.5917	0.1257	100.2901	0.0004	0.0061	0.1452	0.5879	2.1011	0.9009	0.0035
71410 Megacrystic plag 1 Line 001	1	0.0121	0.2272	6.9793	7.4273	25.2923	60.119	0.1647	100.2219	0.0003	0.0097	0.2494	0.4802	2.0047	0.9941	0.0046
71410 Megacrystic plag 1 Line 002	1	0.0055	0.1841	4.683	8.74	23.4087	62.9372	0.1451	100.1036	1E-04	0.0078	0.1663	0.5618	2.0863	0.9146	0.004
71410 Megacrystic plag 1 Line 003	1	-0.0099	0.4764	5.1832	8.4325	23.8457	62.1753	0.1621	100.2653	-0.0002	0.0202	0.1844	0.543	2.0649	0.9334	0.0045
71410 Megacrystic plag 1 Line 004	1	-0.0011	0.5287	5.1374	8.1648	23.9105	61.4083	0.2014	99.35	0	0.0226	0.1845	0.5306	2.0582	0.9446	0.0056
71410 Megacrystic plag 1 Line 005	1	0.0286	0.5812	4.756	8.5471	23.4767	62.6335	0.1817	100.2048	0.0007	0.0246	0.1692	0.5502	2.0794	0.9187	0.005
71410 Megacrystic plag 1 Line 006	1	0.0132	0.5331	5.2307	8.2854	23.7242	62.0348	0.1777	99.9909	0.0003	0.0227	0.1867	0.535	2.066	0.9313	0.0049
71410 Megacrystic plag 1 Line 007	1	0.0286	0.2256	6.7095	7.5735	25.1687	60.0898	0.1797	99.9754	0.0007	0.0096	0.2402	0.4907	2.008	0.9914	0.005
71410 Megacrystic plag 1 Line 008	1	0.0242	0.118	6.0728	7.9156	24.5733	60.6994	0.116	99.5193	0.0006	0.005	0.2178	0.5138	2.0319	0.9696	0.0032
71410 Megacrystic plag 1 Line 009	1	0.0132	0.2074	5.0815	8.6312	23.7339	61.9927	0.2067	99.8666	0.0003	0.0088	0.1814	0.5576	2.0654	0.9321	0.0058
71410 Megacrystic plag 1 Line 010	1	0.022	0.3731	4.5926	8.7034	23.2371	63.1172	0.1909	100.2363	0.0005	0.0158	0.163	0.5591	2.091	0.9074	0.0053
072802B mottplag A Line 001	2	0.0125	0.3261	5.8427	8.2804	24.1992	59.9992	0.1745	98.83459	0.0017	0.075	1.129	2.8955	10.8201	5.1439	0.0263
072802B mottplag A Line 002	2	0.0164	0.3235	6.691	7.6475	24.9603	58.6447	0.1451	98.4285	0.0022	0.0749	1.3009	2.6907	10.6411	5.3384	0.022
072802B mottplag A Line 003	2	0.0145	0.3043	7.3091	7.1379	25.4055	58.001	0.1537	98.326	0.002	0.0706	1.4238	2.5162	10.5446	5.4441	0.0234
072802B mottplag A Line 004	2	0.0259	0.3217	6.462	7.7314	24.6139	59.2144	0.1484	98.5177	0.0035	0.0743	1.2537	2.7144	10.7215	5.253	0.0225
072802B mottplag A Line 005	2	0.0349	0.3196	7.5381	7.057	25.8241	57.8422	0.1571	98.773	0.0048	0.0739	1.4632	2.4788	10.4781	5.514	0.0238
072802B mottplag A Line 006	2	0.0194	0.1817	6.7731	7.5913	25.3467	58.615	0.1249	98.65211	0.0026	0.0419	1.3127	2.6625	10.6024	5.404	0.0189
072802B mottplag A Line 007	2	0.0204	0.3237	6.8449	7.607	24.7817	58.926	0.1319	98.63559	0.0028	0.0748	1.3281	2.6708	10.6699	5.2892	0.02
072802B mottplag A Line 008	2	0.0438	0.3353	7.1831	7.3071	25.2465	57.9524	0.157	98.2252	0.006	0.0779	1.4015	2.58	10.5528	5.4187	0.0239
072802B mottplag A Line 009	2	0.0165	0.34	7.769	6.8462	25.8849	57.5062	0.1769	98.5397	0.0022	0.0788	1.5124	2.4118	10.448	5.5433	0.0269
072802B mottplag A Line 010	2	0.0224	0.3605	7.3369	7.3489	25.3555	57.8242	0.1715	98.4199	0.0031	0.0837	1.4304	2.5927	10.5212	5.4379	0.0261
072802B mottplag A Line 011	2	0.0194	0.4774	6.7575	7.3356	25.2308	58.6634	0.1693	98.6534	0.0026	0.1103	1.3108	2.575	10.62	5.3838	0.0256
072802B mottplag A Line 012	2	0.0055	0.4666	6.4801	7.5426	24.8469	59.5688	0.1538	99.06431	0.0007	0.1072	1.25	2.6328	10.7235	5.2722	0.0232
072802B mottplag A Line 013	2	0.0285	0.3419	8.7458	5.8612	26.703	55.1139	0.2232	97.01749	0.004	0.0807	1.734	2.1029	10.198	5.8239	0.0345
072802B mottplag A Line 014	2	0.0065	0.3493	8.6589	6.4459	26.6132	56.6661	0.1937	98.9336	0.0009	0.0809	1.684	2.2685	10.285	5.6935	0.0294
072802B mottplag A Line 015	2	0.021	0.3056	8.6285	6.3568	26.5587	56.4387	0.1875	98.4968	0.0029	0.071	1.6846	2.2458	10.2834	5.7039	0.0286
072802B mottplag A Line 016	2	0.0244	0.2557	8.3092	6.7544	26.2805	56.7542	0.1941	98.5725	0.0033	0.0594	1.6207	2.3841	10.3314	5.639	0.0296
072802B mottplag A Line 017	2	0.031	0.2459	9.5017	6.0111	27.6717	55.0093	0.2898	98.76051	0.0042	0.0572	1.8575	2.1265	10.036	5.9506	0.0442
072802B mottplag A Line 018	2	0.165	0.3076	7.6678	6.9057	26.6288	56.7831	0.5751	99.0331	0.0225	0.0711	1.4897	2.4279	10.2959	5.6911	0.0872
072802B mottplag A Line 019	2	0.0249	0.3809	7.2318	7.234	25.7239	58.5798	0.2311	99.4064	0.0034	0.0874	1.394	2.5234	10.5385	5.4547	0.0348
072802B mottplag A Line 020	2	0.005	0.3343	4.7432	8.6475	23.4496	61.5651	0.3123	99.05701	0.0007	0.0764	0.9109	3.0053	11.0345	4.954	0.0468
072802B mottplag B Line 001	2	0.0284	0.3171	4.9923	8.4347	23.6732	61.6488	0.256	99.35049	0.0038	0.0723	0.9556	2.9215	11.0125	4.9845	0.0382
072802B mottplag B Line 002	2	0.0443	6.5397	0.8964	3.7368	31.2579	54.3538	0.4239	97.2528	0.0062	1.5419	0.1775	1.3391	10.0452	6.8091	0.0655
072802B mottplag B Line 003	2	0.054	0.202	9.6624	6.1028	27.4054	55.148	0.1541	98.62869	0.0074	0.0471	1.8709	2.1607	10.0697	5.8983	0.0235
072802B mottplag B Line 004	2	0.0359	0.4522	6.0039	7.8588	24.3716	59.3173	0.1449	98.18459	0.0049	0.1048	1.1681	2.7668	10.7702	5.2159	0.022
072802B mottplag B Line 005	2	0.0355	0.2646	8.345	6.6652	26.5325	56.8385	0.1579	98.8392	0.0048	0.0613	1.6226	2.3452	10.314	5.675	0.024
072802B mottplag B Line 006	2	0.0279	0.3934	7.2072	7.1671	25.4304	57.6887	0.2039	98.11861	0.0038	0.0915	1.4083	2.5343	10.5203	5.4663	0.0311
072802B mottplag B Line 007	2	0.014	0.319	6.4461	6.0942	28.9086	55.8269	0.1729	97.78169	0.0019	0.074	1.2562	2.1491	10.1532	6.1971	0.0263
072802B mottplag B Line 008	2	0.0404	0.3372	8.0352	6.6539	26.0275	56.9656	0.1893	98.2491	0.0055	0.0785	1.5704	2.3532	10.3902	5.5956	0.0289
072802B mottplag B Line 009	2	0.0195	0.3822	7.7839	6.8104	25.9131	57.778	0.1864	98.8735	0.0026	0.0883	1.5101	2.3909	10.4609	5.53	0.0282
072802B mottplag B Line 010	2	0.0269	0.3467	8.0496	6.8463	26.2054	57.2978	0.1696	98.9423	0.0037	0.0801	1.5629	2.4055	10.3827	5.5972	0.0257
072802B mottplag B Line 011	2	0.014	0.32	8.5104	6.3549	26.4703	56.2808	0.1755	98.1259	0.0019	0.0746	1.6673	2.253	10.2905	5.7048	0.0268
072802B mottplag B Line 012	2	0.03	0.4004	7.6597	6.8774	26.126	57.7935	0.1842	99.07119	0.0041	0.0923	1.4829	2.4095	10.4421	5.564	0.0278
072802B mottplag B Line 013	2	0.007	0.5213	6.5301	7.5338	24.9197	59.3407	0.1909	99.0435	0.0009	0.1199	1.2611	2.6329	10.6954	5.294	0.0288
072802B mottplag B Line 014	2	0.028	0.3887	7.5769	7.0206	25.9273	58.1052	0.1691	99.2158	0.0038	0.0894	1.4644	2.4555	10.4808	5.5124	0.0255
072802B mottplag B Line 015	2	0.016	0.3239	7.935	6.7057	26.2723	57.3145	0.1712	98.7386	0.0022	0.0749	1.5419	2.358	10.3938	5.6158	0.026
072802B mottplag B Line 016	2	0.0454	0.4754	6.0432	7.7863	24.4938	59.865	0.2012	98.91031	0.0061	0.1093	1.1667	2.7203	10.7865	5.2019	0.0303
072802B mottplag B Line 017	2	0.017	0.5131	6.0866	7.8075	24.3864	60.4356	0.1668	99.413	0.0023	0.1173	1.1687	2.7129	10.8301	5.151	0.025
072802B mottplag B Line 018	2	0.0475	0.2466	9.9503	5.8078	27.8958	55.0246	0.1865	99.1591	0.0065	0.0572	1.938	2.047	10.0018	5.9767	0.0284

Table C.4. EPMA results for enclave plagioclase (cont)

Enclave Group		TiO2 wt%	K2O wt%	CaO wt%	Na2O wt%	Al2O3 wt%	SiO2 wt%	FeO wt%	Total wt%	Ti atFrac	K atFrac	Ca atFrac	Na atFrac	Si atFrac	Al atFrac	Fe atFrac
072802B mottplag B Line 019	2	0.0632	0.2086	4.6216	9.0173	23.6547	63.2638	0.2392	101.0684	0.0083	0.0467	0.8684	3.0662	11.0945	4.8896	0.0351
072802B mottplag B Line 020	2	0.0154	0.4409	5.5936	8.178	23.9977	60.3776	0.1392	98.7424	0.0021	0.1014	1.0804	2.8583	10.8833	5.0987	0.021
072804A Megacrystic plag 1 Line 001	2	0.0132	0.2352	4.9614	8.8076	23.8054	62.5663	0.1607	100.5498	0.0003	0.0099	0.1759	0.5649	2.0697	0.9282	0.0044
072804A Megacrystic plag 1 Line 002	2	0.0285	0.2385	5.5141	8.3441	24.3845	62.1633	0.1867	100.8597	0.0007	0.01	0.195	0.534	2.0517	0.9486	0.0052
072804A Megacrystic plag 1 Line 003	2	0.0418	0.302	7.8745	6.9675	26.384	59.0138	0.139	100.7226	0.001	0.0128	0.2809	0.4497	1.9645	1.0352	0.0039
072804A Megacrystic plag 1 Line 004	2	0.0308	0.26	8.0999	6.7881	26.5743	58.601	0.1202	100.4743	0.0008	0.0111	0.2897	0.4393	1.956	1.0455	0.0034
072804A Megacrystic plag 1 Line 005	2	0.0154	0.158	6.7452	7.618	25.4049	60.2848	0.1288	100.3551	0.0004	0.0067	0.2405	0.4915	2.0058	0.9963	0.0036
072804A Megacrystic plag 1 Line 006	2	0.0077	0.2085	8.0512	6.9496	26.5941	58.6536	0.1284	100.5931	0.0002	0.0089	0.2877	0.4493	1.9557	1.0452	0.0036
072804A Megacrystic plag 1 Line 007	2	0.032	0.2017	10.8169	5.1498	28.7526	54.97	0.128	100.051	0.0008	0.0087	0.3915	0.3373	1.8566	1.1447	0.0036
072804A Megacrystic plag 1 Line 008	2	0.0341	0.3637	7.6176	7.0417	26.0337	59.0386	0.1306	100.26	0.0009	0.0155	0.2729	0.4564	1.9736	1.0258	0.0037
072804A Megacrystic plag 1 Line 009	2	0.0154	0.3777	7.2008	7.3224	25.5896	59.1307	0.1362	99.7728	0.0004	0.0162	0.2591	0.4767	1.9854	1.0127	0.0038
072804A Megacrystic plag 1 Line 010	2	0.0198	0.1229	5.2647	8.4887	24.4082	62.2573	0.2204	100.782	0.0005	0.0052	0.1861	0.5431	2.0543	0.9493	0.0061
072804A Megacrystic plag 2 Line 001	2	0.0254	0.1487	10.1322	5.6378	28.2125	55.8848	0.1113	100.1527	0.0006	0.0064	0.3655	0.3681	1.8817	1.1197	0.0031
072804A Megacrystic plag 2 Line 002	2	0.0066	0.1163	10.6265	5.4613	28.7542	55.1463	0.1467	100.2579	0.0002	0.005	0.3838	0.3569	1.8587	1.1423	0.0041
072804A Megacrystic plag 2 Line 003	2	0.0066	0.1351	8.9768	6.392	27.3596	57.2208	0.1077	100.1986	0.0002	0.0058	0.3227	0.4159	1.92	1.0821	0.003
072804A Megacrystic plag 2 Line 004	2	0.0418	0.2092	7.7394	7.1281	26.0556	58.8976	0.129	100.2007	0.0011	0.0089	0.2774	0.4623	1.9701	1.0273	0.0036
072804A Megacrystic plag 2 Line 005	2	0.0044	0.1207	9.6601	5.9807	27.9733	56.807	0.1304	100.6766	1E-04	0.0051	0.3462	0.3878	1.8998	1.1027	0.0036
072804A Megacrystic plag 2 Line 006	2	0.0297	0.1921	9.1014	6.2863	27.497	57.074	0.1201	100.3006	0.0008	0.0082	0.3271	0.4089	1.9144	1.0871	0.0034
072804A Megacrystic plag 2 Line 007	2	-0.0066	0.1284	10.1862	5.7483	28.3346	56.0197	0.1134	100.524	-0.0002	0.0055	0.3663	0.374	1.88	1.1208	0.0032
072804A Megacrystic plag 2 Line 008	2	0.0584	0.2345	9.6323	6.0055	27.8797	56.8098	0.1634	100.7836	0.0015	0.01	0.3451	0.3894	1.8997	1.0989	0.0046
072804A Megacrystic plag 2 Line 009	2	0.0176	0.3973	6.3026	7.8066	24.9529	60.6438	0.1277	100.2485	0.0004	0.0169	0.225	0.5042	2.0202	0.9798	0.0036
072804A Megacrystic plag 2 Line 010	2	0.0099	1.2043	4.2576	8.5055	23.3217	63.2704	0.1341	100.7035	0.0002	0.0508	0.1508	0.5453	2.0918	0.9088	0.0037
072802C matrix plag 1 core	3	0.0544	0.2685	8.859	6.1992	26.6449	55.4184	0.1354	97.5798	0.0075	0.0631	1.7476	2.213	10.2027	5.782	0.0209
072802C matrix plag 1 rim a	3	-0.0015	0.3744	6.1392	7.9137	24.3899	59.0308	0.2188	98.0653	-0.0002	0.0869	1.197	2.7923	10.7418	5.2313	0.0333
072802C matrix plag 1 rim b	3	0.013	0.1311	6.8347	7.4944	25.1967	57.6629	0.2677	97.60049	0.0018	0.0306	1.3407	2.6604	10.5567	5.4372	0.041
072802C matrix plag 2 core	3	0.057	0.1773	11.1087	5.1431	28.7725	52.7684	0.1825	98.2095	0.0079	0.0417	2.1935	1.8377	9.7242	6.2497	0.0281
072802C matrix plag 2 rim a	3	0.0159	0.3292	5.0769	8.6736	23.4081	60.69	0.2646	98.4583	0.0022	0.0759	0.9831	3.0394	10.9678	4.9862	0.04
072802C matrix plag 2 rim b	3	0.0179	0.4254	5.0059	8.5595	23.3991	61.0262	0.1559	98.5899	0.0024	0.0978	0.9669	2.9919	11.001	4.9719	0.0235
072802C zoned plag Line 001	3	0.0295	0.172	11.2789	5.0752	29.4329	53.5443	0.1399	99.6727	0.004	0.0398	2.1923	1.7851	9.713	6.2933	0.0212
072802C zoned plag Line 002	3	0.1657	0.797	9.805	4.5584	28.7203	52.3194	1.0238	97.3896	0.0232	0.1892	1.9551	1.6448	9.7363	6.2997	0.1593
072802C zoned plag Line 003	3	0.0391	0.2205	11.3516	4.897	28.8242	53.4682	0.1502	98.9508	0.0054	0.0514	2.2224	1.735	9.7695	6.2078	0.0229
072802C zoned plag Line 004	3	0.0295	0.1985	11.7748	4.6873	29.6002	53.1054	0.1631	99.5588	0.004	0.046	2.2938	1.6524	9.6548	6.3431	0.0248
072802C zoned plag Line 005	3	0.078	0.3451	10.4464	4.78	29.1359	52.7864	0.3013	97.8731	0.0108	0.0812	2.0644	1.7094	9.7356	6.3339	0.0465
072802C zoned plag Line 006	3	0.0425	0.2154	11.6599	4.6812	29.5758	53.0842	0.1686	99.4276	0.0058	0.05	2.2737	1.6519	9.6608	6.3443	0.0257
072802C zoned plag Line 007	3	0.0385	0.1966	11.5944	4.8109	29.3205	53.3047	0.1581	99.42369	0.0053	0.0456	2.2607	1.6975	9.6999	6.2889	0.0241
072802C zoned plag Line 008	3	0.0471	0.1715	11.9121	4.7202	29.702	52.6909	0.1616	99.4054	0.0065	0.0399	2.3266	1.6683	9.6046	6.3817	0.0246
072802C zoned plag Line 009	3	0.0135	0.3044	7.5957	6.9494	25.7608	57.9417	0.1172	98.6827	0.0018	0.0704	1.4746	2.4414	10.498	5.5014	0.0178
072802C zoned plag Line 010	3	0.0125	0.4563	5.7619	7.9522	24.158	60.8241	0.1868	99.3518	0.0017	0.1042	1.1055	2.761	10.8912	5.0988	0.028

Table C.5. EPMA results for enclave pyroxene

Enclave Group	TiO2 wt%	MnO wt%	Cr2O3 wt%	K2O wt%	CaO wt%	Na2O wt%	Al2O3 wt%	SiO2 wt%	MgO wt%	FeO wt%	Total wt%	Ti atFrac	Mn atFrac	Cr atFrac	K atFrac	Ca atFrac	Na atFrac	Al atFrac	Si atFrac	Mg atFrac	Fe atFrac	
071410 cpx inc1	1	0.115	0.37	0.003	0.004	21.823	0.426	0.722	52.215	14.775	9.146	99.597	0.003	0.012	0	0	0.879	0.031	0.032	1.962	0.828	0.287
071410 cpx inc 3	1	0.147	0.412	-0.007	0.005	22.199	0.467	0.775	51.848	14.281	9.274	99.402	0.004	0.013	0	0	0.898	0.034	0.034	1.958	0.804	0.293
071410 cpx inc 2	1	0.166	0.412	-0.004	-0.001	21.755	0.392	0.846	51.819	14.452	9.203	99.04	0.005	0.013	0	0	0.882	0.029	0.038	1.96	0.815	0.291
071410 cpx inc 4	1	0.437	0.35	0.01	0.216	11.867	0.571	3.198	51.279	16.487	12.076	96.491	0.013	0.011	0	0.01	0.485	0.042	0.144	1.957	0.938	0.385
71410 Cpx 1 L1	1	0.167	0.26	0.014	0.005	22.076	0.443	1.079	53.529	15.724	6.77	100.067	0.005	0.008	0	0	0.873	0.032	1.975	0.047	0.865	0.209
71410 Cpx 1 L2	1	1.363	0.173	0.023	0.583	11.763	1.641	6.255	49.137	17.792	8.669	97.399	0.038	0.005	0.001	0.028	0.473	0.119	1.844	0.277	0.995	0.272
71410 Cpx 1 L3	1	1.517	0.176	0.023	0.588	11.838	1.71	6.633	48.538	17.275	9.487	97.785	0.043	0.006	0.001	0.028	0.477	0.125	1.824	0.294	0.968	0.298
71410 Cpx 1 L4	1	1.536	0.15	0.003	0.436	12.682	1.54	5.511	49.623	17.509	8.835	97.825	0.043	0.005	0	0.021	0.509	0.112	1.858	0.243	0.977	0.277
71410 Cpx 1 L5	1	0.745	0.197	0.008	0.092	18.194	0.706	2.232	51.756	16.072	7.611	97.612	0.021	0.006	0	0.004	0.734	0.052	1.949	0.099	0.902	0.24
71410 Cpx 1 L6	1	0.147	0.347	0.007	0.003	21.194	0.457	0.819	53.361	14.678	8.981	99.994	0.004	0.011	0	0	0.845	0.033	1.986	0.036	0.814	0.28
71410 Cpx 1 L7	1	0.217	0.356	-0.014	0.008	21.112	0.445	1.036	53.054	14.116	9.714	100.044	0.006	0.011	0	0	0.844	0.032	1.98	0.046	0.785	0.303
71410 Cpx 1 L8	1	0.182	0.405	-0.005	0.004	21.485	0.433	0.997	53.214	14.743	8.51	99.969	0.005	0.013	0	0	0.856	0.031	1.979	0.044	0.817	0.265
71410 Cpx 1 L9	1	0.333	0.446	0.164	0.1	20.096	0.558	1.775	52.546	14.471	9.064	99.554	0.009	0.014	0.005	0.005	0.804	0.04	1.963	0.078	0.806	0.283
71410 Cpx 1 L10	1	0.161	0.49	0.17	0.004	21.453	0.463	0.959	52.973	14.242	9.025	99.94	0.004	0.015	0.005	0	0.858	0.034	1.978	0.042	0.793	0.282
71410 Cpx 2core	1	0.129	0.494	-0.011	-0.006	21.214	0.448	0.59	53.094	14.181	9.482	99.616	0.004	0.016	0	0	0.852	0.033	1.99	0.026	0.792	0.297
71410 Cpx 2rim	1	0.097	0.591	0.008	0.005	21.39	0.397	0.59	53.317	13.881	9.676	99.954	0.003	0.019	0	0	0.857	0.029	1.994	0.026	0.774	0.303
072802B cpxcoreA	2	0.169	0.272	0.023	-0.003	21.47	0.375	1.051	51.543	14.309	10.082	99.291	0.005	0.009	0.001	0	0.87	0.027	0.047	1.95	0.807	0.319
072802B cpxcorrimA	2	0.261	0.308	0.033	0.006	21.661	0.407	1.201	51.874	14.319	10.541	100.61	0.007	0.01	0.001	0	0.869	0.03	0.053	1.941	0.799	0.33
072802B cpxcoreB	2	0.097	0.277	0.086	-0.001	23.115	0.288	0.722	51.91	14.187	8.906	99.587	0.003	0.009	0.003	0	0.933	0.021	0.032	1.956	0.797	0.281
072802B cpxcoreA	2	0.139	0.303	0.005	-0.002	21.905	0.405	0.729	51.954	14.026	10.142	99.608	0.004	0.01	0	0	0.886	0.03	0.032	1.962	0.789	0.32
072802B cpxclnArim	2	0.157	0.339	0.006	0.001	21.464	0.422	0.674	51.701	13.974	10.667	99.406	0.004	0.011	0	0	0.872	0.031	0.03	1.96	0.79	0.338
072802B cpxclnBcore	2	0.123	0.281	0.009	-0.002	21.842	0.388	0.703	51.92	14.244	9.998	99.507	0.004	0.009	0	0	0.884	0.028	0.031	1.961	0.802	0.316
072802B cpx clnBrim	2	0.142	0.435	-0.015	-0.001	21.88	0.398	0.728	51.821	13.752	10.48	99.619	0.004	0.014	-0.001	0	0.887	0.029	0.032	1.961	0.776	0.332
072802B cpxinc1	2	0.356	0.302	0.003	0.005	21.663	0.467	1.475	50.849	13.654	10.414	99.187	0.01	0.01	0	0	0.882	0.034	0.066	1.933	0.774	0.331
072802B cpxinc2	2	0.315	0.301	0.025	0.004	21.851	0.425	1.172	51.279	13.674	10.113	99.158	0.009	0.01	0.001	0	0.889	0.031	0.052	1.947	0.774	0.321
072802B cpxinc3	2	0.344	0.336	0.001	0.002	21.182	0.419	1.263	51.458	13.961	10.826	99.792	0.01	0.011	0	0	0.857	0.031	0.056	1.943	0.786	0.342
072802B cpxinc4a	2	0.214	0.707	-0.005	0.004	0.901	0.012	0.699	50.131	19.56	25.857	98.082	0.006	0.023	0	0	0.038	0.001	0.032	1.951	1.135	0.842
072802B cpxinc4b	2	0.28	0.314	-0.009	0.009	21.689	0.456	1.216	51.099	13.691	10.275	99.021	0.008	0.01	0	0.001	0.884	0.034	0.054	1.944	0.776	0.327
072802B cpxcoreA	2	0.169	0.272	0.023	-0.003	21.47	0.375	1.051	51.543	14.309	10.082	99.291	0.005	0.009	0.001	0	0.87	0.027	0.047	1.95	0.807	0.319
072802B cpxcorrimA	2	0.261	0.308	0.033	0.006	21.661	0.407	1.201	51.874	14.319	10.541	100.61	0.007	0.01	0.001	0	0.869	0.03	0.053	1.941	0.799	0.33
072802B cpxclnAcore	2	0.139	0.303	0.005	-0.002	21.905	0.405	0.729	51.954	14.026	10.142	99.608	0.004	0.01	0	0	0.886	0.03	0.032	1.962	0.789	0.32
072802B cpxclnArim	2	0.157	0.339	0.006	0.001	21.464	0.422	0.674	51.701	13.974	10.667	99.406	0.004	0.011	0	0	0.872	0.031	0.03	1.96	0.79	0.338
072802B cpxclnBcore	2	0.123	0.281	0.009	-0.002	21.842	0.388	0.703	51.92	14.244	9.998	99.507	0.004	0.009	0	0	0.884	0.028	0.031	1.961	0.802	0.316
072802B cpx clnBrim	2	0.142	0.435	-0.015	-0.001	21.88	0.398	0.728	51.821	13.752	10.48	99.619	0.004	0.014	-0.001	0	0.887	0.029	0.032	1.961	0.776	0.332
072804A cpx1core	2	0.086	0.407	0.194	0.13	11.134	0.322	54.126	1.835	17.812	10.983	97.03	0.002	0.013	0.006	0.006	0.447	0.023	2.026	0.081	0.994	0.344
072804A cpx1rim2	2	0.445	0.342	0.292	0.287	11.837	0.503	51.261	4.188	15.446	12.738	97.339	0.013	0.011	0.009	0.014	0.481	0.037	1.943	0.187	0.873	0.404
072804A cpx1rim1	2	0.248	0.458	0.113	0.097	11.592	0.265	54.395	1.72	17.457	11.391	97.736	0.007	0.014	0.003	0.005	0.463	0.019	2.027	0.075	0.97	0.355
072802C cpxcorecore	3	0.167	0.319	-0.008	-0.002	21.887	0.4	0.822	51.406	14.67	9.515	99.175	0.005	0.01	0	0	0.888	0.029	0.037	1.947	0.828	0.301
072802C cpxcorrim	3	0.165	0.316	0.024	0.002	22.491	0.408	0.848	51.907	14.279	9.351	99.79	0.005	0.01	0.001	0	0.907	0.03	0.038	1.953	0.801	0.294
072802C cpxcln1core	3	0.177	0.28	-0.004	-0.003	21.817	0.39	0.847	49.467	14.199	9.197	96.367	0.005	0.009	0	0	0.914	0.03	0.039	1.933	0.827	0.301
072802C cpxcln1rim	3	0.165	0.264	0.014	0.006	21.808	0.337	0.771	51.94	14.678	9.51	99.492	0.005	0.008	0	0	0.88	0.025	0.034	1.957	0.824	0.3
072802C cpxcln2core	3	0.08	0.939	0.016	0.008	1.041	0.031	0.327	52.977	18.471	22.317	96.208	0.002	0.031	0.001	0	0.043	0.002	0.015	2.053	1.067	0.723
072802C cpxcln2rim	3	0.305	0.353	0.001	0.287	11.233	0.718	4.687	49.757	14.825	14.503	96.669	0.009	0.012	0	0.014	0.464	0.054	0.213	1.917	0.852	0.467
072802C cpxcorecore	3	0.167	0.319	-0.008	-0.002	21.887	0.4	0.822	51.406	14.67	9.515	99.175	0.005	0.01	0	0	0.888	0.029	0.037	1.947	0.828	0.301
072802C cpxcorrim	3	0.165	0.316	0.024	0.002	22.491	0.408	0.848	51.907	14.279	9.351	99.79	0.005	0.01	0.001	0	0.907	0.03	0.038	1.953	0.801	0.294
072802C cpxcln1core	3	0.177	0.28	-0.004	-0.003	21.817	0.39	0.847	49.467	14.199	9.197	96.367	0.005	0.009	0	0	0.914	0.03	0.039	1.933	0.827	0.301
072802C cpxcln1rim	3	0.165	0.264	0.014	0.006	21.808	0.337	0.771	51.94	14.678	9.51	99.492	0.005	0.008	0	0	0.88	0.025	0.034	1.957	0.824	0.3

Table C.6. EPMA results for enclave biotite

	Enclave Group	TiO2 wt%	MnO wt%	Cl wt%	K2O wt%	SiO2 wt%	Al2O3 wt%	MgO wt%	FeO wt%	Total wt%	F atFrac	Ti atFrac	Mn atFrac	Cl atFrac	K atFrac	Si atFrac	Al atFrac	Mg atFrac	Fe atFrac
071410 bt1core	1	4.183	0.195	0.098	9.48	36.42	13.289	12.316	17.9	93.689	-0.144	0.487	0.025	0.026	1.872	5.636	2.424	2.841	2.316
071410 bt1rim	1	4.633	0.251	0.075	9.53	36.65	13.422	12.069	17.678	94.117	-0.148	0.536	0.033	0.02	1.87	5.636	2.433	2.767	2.273
071410 bt2core	1	4.11	0.241	0.094	9.804	36.658	13.793	11.834	18.847	95.172	-0.158	0.473	0.031	0.024	1.914	5.61	2.488	2.7	2.412
071410 bt2rim 2	1	4.549	0.216	0.087	9.731	36.675	13.561	11.816	18.491	94.929	-0.15	0.524	0.028	0.023	1.901	5.617	2.448	2.698	2.369
071410 bt2rim1	1	4.476	0.25	0.084	9.722	36.838	13.554	11.985	18.579	95.284	-0.156	0.514	0.032	0.022	1.892	5.621	2.438	2.726	2.371
072804A btcore	2	3.812	0.161	0.061	9.605	36.748	14.475	11.161	19.447	95.223	-0.197	0.438	0.021	0.016	1.872	5.615	2.607	2.542	2.485
072804A btrim1	2	3.287	0.208	0.051	8.275	35.563	14.725	11.892	19.904	93.617	-0.237	0.383	0.027	0.014	1.636	5.512	2.69	2.748	2.58

Table C.7. EPMA results for enclave hornblende

	Enclave Group	TiO2 wt%	MnO wt%	Cr2O3 wt%	K2O wt%	CaO wt%	Na2O wt%	Al2O3 wt%	SiO2 wt%	MgO wt%	FeO wt%	Total wt%	Ti atFrac	Mn atFrac	Cr atFrac	K atFrac	Ca atFrac	Na atFrac	Al atFrac	Si atFrac	Mg atFrac	Fe atFrac
072802B cpxcorehblrimA	2	1.357	0.352	0.011	0.51	11.273	0.93	5.538	48.433	13.168	15.284	96.857	0.152	0.044	0.001	0.097	1.796	0.268	0.97	7.2	2.918	1.9
072802B hblcln 1core	2	1.358	0.269	0.015	0.512	11.065	1.13	5.508	48.135	13.47	15.12	96.582	0.152	0.034	0.002	0.097	1.767	0.326	0.968	7.175	2.993	1.885
072802B hblcln1rim	2	1.339	0.373	0.004	0.516	11.08	1.075	5.42	48.597	13.144	15.834	97.384	0.149	0.047	0	0.098	1.76	0.309	0.947	7.202	2.904	1.963
072802B cpxcorehblrimB	2	1.213	0.382	0.009	0.496	11.111	1.026	5.332	48.53	13.136	15.805	97.04	0.136	0.048	0.001	0.094	1.77	0.296	0.935	7.217	2.912	1.966
072802B hblcln2core	2	1.177	0.349	0.004	0.511	11.557	0.846	5.349	48.541	13.096	15.617	97.047	0.132	0.044	0.001	0.097	1.841	0.244	0.937	7.216	2.902	1.941
072802B hblcln2rim	2	1.125	0.417	0	0.464	11.149	0.99	5.11	49.28	13.18	15.743	97.458	0.125	0.052	0	0.087	1.765	0.284	0.89	7.282	2.903	1.946
072802C cpxcorehblrim1	3	1.395	0.235	0.006	0.594	11.851	1.109	5.999	48.513	13.798	14.683	98.183	0.154	0.029	0.001	0.111	1.861	0.315	1.036	7.11	3.014	1.8
072802C cpxcorehblrim2	3	1.353	0.357	0.01	0.487	11.177	0.962	5.587	48.671	13.711	15.044	97.36	0.15	0.045	0.001	0.092	1.768	0.275	0.972	7.185	3.017	1.857
072802C hblcln1core	3	1.452	0.276	0.014	0.61	11.138	1.09	6.113	47.613	13.74	15.026	97.072	0.162	0.035	0.002	0.116	1.772	0.314	1.07	7.07	3.041	1.866
072802C hblcln1rim	3	1.349	0.32	-0.002	0.521	11.2	0.974	5.893	48.717	13.939	14.701	97.614	0.149	0.04	0	0.098	1.764	0.278	1.021	7.16	3.054	1.807
072802C hblcln2core	3	1.226	0.338	-0.001	0.48	11.108	1.084	5.414	49.126	14.021	14.682	97.478	0.136	0.042	0	0.09	1.75	0.309	0.938	7.225	3.074	1.806
072802C hblcln2rim	3	1.092	0.304	0.007	0.454	10.7	0.826	5.164	48.021	12.182	15.109	93.859	0.125	0.039	0.001	0.089	1.753	0.245	0.931	7.342	2.776	1.932
hornblende 2core	2	1.425	0.377	-0.021	0.467	10.909	1.059	5.469	48.851	13.512	15.245	97.293	0.041	0.012	-0.001	0.023	0.45	0.079	0.248	1.882	0.776	0.491
hornblende 2rim2	2	1.437	0.367	0.021	0.53	11.106	1.081	5.881	48.047	12.979	15.311	96.76	0.042	0.012	0.001	0.026	0.462	0.081	0.269	1.867	0.752	0.498
hornblende 2rim2	2	5.836	0.172	-0.006	0.203	6.224	0.108	12.243	33.182	14.371	17.719	90.051	0.188	0.006	0	0.011	0.286	0.009	0.618	1.421	0.918	0.635
hornblende 1core	2	1.415	0.442	0.027	0.464	11.147	1.066	5.624	48.488	13.342	15.338	97.353	0.041	0.014	0.001	0.023	0.461	0.08	0.256	1.872	0.768	0.495
hornblende 1rim	2	1.465	0.359	0.042	0.484	11.152	1.157	5.819	48.218	13.158	15.609	97.462	0.043	0.012	0.001	0.024	0.462	0.087	0.265	1.862	0.758	0.504

Table C.7. EPMA results for host rock plagioclase

Unit		TiO2 wt%	K2O wt%	CaO wt%	Na2O wt%	Al2O3 wt%	SiO2 wt%	FeO wt%	Total wt%	Ti atFrac	K atFrac	Ca atFrac	Na atFrac	Al atFrac	Si atFrac	Fe atFrac
Core 2 Qdx Plag core A	Enclave-Rich Tonalite	0.0161	0.1927	5.2452	8.43	22.5804	66.128	0.2003	102.7927	0.0021	0.0422	0.9654	2.8078	4.5719	11.3593	0.0288
Core 2 Qdx Plag rim A	Enclave-Rich Tonalite	0.0196	0.2127	5.5649	8.3112	22.9795	65.587	0.1518	102.7984	0.0025	0.0467	1.0255	2.7717	4.6585	11.2754	0.0218
Core 2 Qdx Plag core B	Enclave-Rich Tonalite	0.0196	0.1777	5.7238	8.3348	23.2981	65.6785	0.2197	103.4522	0.0025	0.0388	1.049	2.7642	4.697	11.2337	0.0314
Core 2 Qdx Plag rim B	Enclave-Rich Tonalite	0.0206	0.247	5.2682	8.2372	23.0724	66.4806	0.1587	103.4847	0.0026	0.0537	0.9623	2.7229	4.6362	11.3335	0.0226
Core 2 Qdx Plag core C	Enclave-Rich Tonalite	0.0025	0.4019	6.7206	7.351	23.8546	64.1548	0.203	102.6884	0.0003	0.0886	1.244	2.4622	4.8571	11.0825	0.0293
Core 2 Qdx Plag rim C	Enclave-Rich Tonalite	0.0161	0.24	4.7928	8.4576	22.3108	67.1726	0.371	103.3609	0.0021	0.0522	0.8759	2.7971	4.4854	11.4571	0.0529
Core 2 Plag contact qdx rim	Enclave-Rich Tonalite	-0.0015	0.1909	5.1135	8.5335	22.42	66.2123	0.1675	102.6362	-0.0002	0.0419	0.9423	2.8455	4.5446	11.3867	0.0241
Core 2 Plag contact qdx core	Enclave-Rich Tonalite	0.0051	0.2939	5.4956	8.2598	22.6126	65.0843	0.1509	101.9022	0.0007	0.0651	1.0221	2.7798	4.6262	11.2965	0.0219
071406 Plag 1 core	Enclave-Rich Tonalite	-0.0077	0.5001	5.4862	8.1836	62.0067	24.2012	0.2242	100.5943	-0.0002	0.0211	0.1947	0.5257	2.0542	0.945	0.0062
071406 Plag 1 rim 1	Enclave-Rich Tonalite	0.0362	0.3398	4.2747	9.0896	64.0465	23.4774	0.2198	101.484	0.0009	0.0142	0.1498	0.5764	2.0947	0.9051	0.006
071406 Plag 1 rim 2	Enclave-Rich Tonalite	0.0176	0.4507	4.7488	8.6187	63.1216	23.794	0.2068	100.9582	0.0004	0.0189	0.1675	0.5502	2.0782	0.9234	0.0057
071406 Plag 2 core	Enclave-Rich Tonalite	0.0428	0.453	4.9081	8.5806	62.2618	23.5695	0.1951	100.0109	0.0011	0.0192	0.175	0.5537	2.0721	0.9246	0.0054
071406 Plag 2 rim 1	Enclave-Rich Tonalite	0.0362	0.5666	4.4454	8.7303	63.475	23.4472	0.1979	100.8986	0.0009	0.0238	0.1568	0.5574	2.0901	0.91	0.0055
071406 Plag 2 rim 2	Enclave-Rich Tonalite	0.0164	0.1461	4.1234	8.3963	63.6792	23.3115	0.255	100.9279	0.0004	0.0061	0.1453	0.5992	2.0943	0.9037	0.007
Core 2 Qd Plag core A	Enclave-Poor Tonalite	0.0091	0.1643	6.5144	8.0043	23.3413	65.0378	0.2162	103.2874	0.0012	0.036	1.1984	2.6647	4.7236	11.1663	0.031
Core 2 Qd Plag rim A	Enclave-Poor Tonalite	0.0121	0.1241	5.4258	8.3081	22.4801	65.3481	0.1648	102.0631	0.0016	0.0274	1.0062	2.788	4.6266	11.3096	0.0238
Core 2 Qd Plag core B	Enclave-Poor Tonalite	-0.0035	0.121	4.2123	9.0646	21.7246	68.0695	0.1883	103.3768	-0.0005	0.0263	0.7679	2.9905	4.3567	11.5814	0.0268
Core 2 Qd Plag rim B	Enclave-Poor Tonalite	0.006	0.1613	5.2055	8.4144	22.6861	65.6051	0.1438	102.2222	0.0008	0.0355	0.9633	2.8178	4.6181	11.3303	0.0208
Core 2 Qd Plag core C	Enclave-Poor Tonalite	-0.001	0.1182	4.487	8.8776	22.2753	67.3515	0.1934	103.302	-1E-04	0.0257	0.8195	2.9341	4.4753	11.4801	0.0276
Core 2 Qd Plag rim C	Enclave-Poor Tonalite	0.0283	0.1937	5.4744	8.3848	22.7812	65.1355	0.1362	102.1341	0.0037	0.0428	1.0156	2.8149	4.6491	11.2774	0.0197
Core 2 Plag contact qd core	Enclave-Poor Tonalite	0.0147	0.0999	5.0406	8.7126	22.4557	66.302	0.1875	102.813	0.0019	0.0219	0.9272	2.9003	4.544	11.3825	0.0269
Core 2 Plag contact qd rim	Enclave-Poor Tonalite	0.004	0.0993	5.635	8.3893	23.3369	65.7696	0.1217	103.3558	0.0005	0.0217	1.0324	2.7815	4.7035	11.2461	0.0174
16071901 plag acc 1 core	Enclave-Poor Tonalite	0.061	0.27	9.3073	6.0557	26.2744	59.694	0.2305	101.8929	0.0081	0.0605	1.7521	2.0629	5.4409	10.4874	0.0339
16071901 plag acc 1 rim	Enclave-Poor Tonalite	0.016	0.1232	5.2361	8.5	23.1317	65.9868	0.1213	103.1151	0.0021	0.0269	0.9605	2.8215	4.6675	11.2963	0.0174
16071901 plag acc 2 core	Enclave-Poor Tonalite	0.0605	0.2577	8.876	6.0852	25.6851	60.1612	0.1832	101.3089	0.008	0.058	1.6763	2.0797	5.3361	10.6038	0.027
16071901 plag acc 2 rim	Enclave-Poor Tonalite	-0.0055	0.0932	5.45	8.3021	23.5585	65.0667	0.174	102.639	-0.0007	0.0205	1.0054	2.7715	4.7807	11.202	0.025
071408 matrix plag 2 core	Enclave-Poor Tonalite	0.021	0.307	8.2763	6.5869	58.1313	26.5362	0.148	100.0067	0.0005	0.0131	0.2976	0.4286	1.9509	1.0497	0.0042
071408 matrix plag 2 rim	Enclave-Poor Tonalite	-0.011	0.4265	5.502	8.0918	61.7073	24.0361	0.1628	99.9155	-0.0003	0.0181	0.1965	0.5229	2.0564	0.9441	0.0045
071408 megacrystic plag Line 001	Enclave-Poor Tonalite	-0.0077	0.4317	5.4481	8.1526	62.2491	24.035	0.1834	100.4922	-0.0002	0.0182	0.1934	0.5236	2.0618	0.9383	0.0051
071408 megacrystic plag Line 002	Enclave-Poor Tonalite	-0.0088	0.414	6.0988	7.7967	60.8021	24.6202	0.1675	99.8905	-0.0002	0.0176	0.2183	0.505	2.031	0.9694	0.0047
071408 megacrystic plag Line 003	Enclave-Poor Tonalite	0.0066	0.4537	5.7124	7.9245	61.1897	24.0324	0.1773	99.4966	0.0002	0.0194	0.205	0.5147	2.0497	0.9489	0.005
071408 megacrystic plag Line 004	Enclave-Poor Tonalite	0.0166	0.5462	0.0472	0.7306	64.8833	18.3655	0.0733	99.7637	0.0004	0.692	0.0018	0.0491	2.2494	0.7505	0.0021
071408 megacrystic plag Line 005	Enclave-Poor Tonalite	0.0243	0.3392	7.3968	7.0055	59.4991	25.6691	0.1875	100.1215	0.0006	0.0145	0.2649	0.454	1.9887	1.0113	0.0052
071408 megacrystic plag Line 006	Enclave-Poor Tonalite	0.0342	0.3492	7.6018	6.9625	59.0529	25.6835	0.1945	99.8786	0.0009	0.0149	0.2733	0.4529	1.9811	1.0156	0.0055
071408 megacrystic plag Line 007	Enclave-Poor Tonalite	0.0209	0.4183	7.2022	7.1855	59.4583	25.6738	0.2344	100.1934	0.0005	0.0178	0.258	0.4658	1.9876	1.0116	0.0066
071408 megacrystic plag Line 008	Enclave-Poor Tonalite	0.0319	0.3977	6.9924	6.8884	58.5323	24.903	0.802	98.5477	0.0008	0.0173	0.2551	0.4547	1.9927	0.9993	0.0228
071408 megacrystic plag Line 009	Enclave-Poor Tonalite	0.0265	0.3583	7.4675	7.0475	58.8548	25.8634	0.1882	99.8062	0.0007	0.0153	0.2687	0.4588	1.9761	1.0236	0.0053
071408 megacrystic plag Line 010	Enclave-Poor Tonalite	0.0242	0.3629	6.8738	7.4472	59.7984	25.2016	0.1654	99.8735	0.0006	0.0155	0.2467	0.4836	2.0028	0.9949	0.0046
071408 matrix plag 1 core	Enclave-Poor Tonalite	0.0364	0.2368	9.7945	5.754	56.1839	27.969	0.172	100.2466	0.0009	0.0102	0.3531	0.3754	1.8904	1.1092	0.0077
071408 matrix plag 1 rim	Enclave-Poor Tonalite	0.0044	0.4364	5.0879	8.3573	62.1484	23.7365	0.1398	99.91071	1E-04	0.0185	0.1815	0.5395	2.0691	0.9315	0.0039
071408 matrix plag 2 Line 001	Enclave-Poor Tonalite	0.043	0.2925	6.9041	7.3381	59.9837	25.3277	0.1385	100.0276	0.0011	0.0125	0.2471	0.4753	2.0036	0.9972	0.0039
071408 matrix plag 2 Line 002	Enclave-Poor Tonalite	0.0232	0.2986	7.8827	6.7662	58.1989	26.1697	0.1351	99.4744	0.0006	0.0128	0.2847	0.4422	1.9616	1.0397	0.0038
071408 matrix plag 2 Line 003	Enclave-Poor Tonalite	0.0176	0.3106	8.1716	6.6026	58.0297	26.3637	0.1494	99.6452	0.0004	0.0133	0.2948	0.4311	1.9541	1.0464	0.004
071408 matrix plag 2 Line 004	Enclave-Poor Tonalite	0.0198	0.3558	7.3577	6.9516	59.0431	25.7762	0.1433	99.6475	0.0005	0.0152	0.2648	0.4527	1.9829	1.0203	0.004
071408 matrix plag 2 Line 005	Enclave-Poor Tonalite	0.0397	0.3224	7.7683	6.7873	58.2393	25.9155	0.155	99.22749	0.001	0.0139	0.2812	0.4446	1.9676	1.032	0.0044
071408 matrix plag 2 Line 006	Enclave-Poor Tonalite	0.022	0.3912	7.2261	7.183	59.4952	25.7315	0.1844	100.2334	0.0006	0.0167	0.2586	0.4652	1.9873	1.0131	0.0052
071408 matrix plag 2 Line 007	Enclave-Poor Tonalite	0.0464	0.2867	7.2739	4.1087	43.4009	19.967	0.1494	75.233	0.0016	0.0163	0.3483	0.356	1.9396	1.0518	0.0056
071408 matrix plag 2 Line 008	Enclave-Poor Tonalite	0.0275	0.1909	6.5487	7.6558	60.4585	25.1406	0.0954	100.1174	0.0007	0.0081	0.2338	0.4947	2.0147	0.9875	0.0027
071408 matrix plag 2 Line 009	Enclave-Poor Tonalite	0.011	0.1861	5.8892	7.966	60.9948	24.3914	0.1691	99.6076	0.0003	0.0079	0.211	0.5165	2.0397	0.9614	0.0047
071408 matrix plag 2 Line 010	Enclave-Poor Tonalite	0.0099	0.3647	6.114	7.7831	61.1045	24.6703	0.1022	100.1487	0.0002	0.0155	0.2181	0.5023	2.0339	0.9679	0.0028
16071901 groundmass plag 1 core	Contact	0.0085	0.1566	6.7566	7.4986	23.9165	62.463	0.2244	100.9822	0.0011	0.0351	1.273	2.5431	4.9571	10.9836	0.0327
16071901 groundmass plag 1 rim	Contact	0.034	0.1584	6.7658	4.337	24.9038	64.6418	0.2495	101.0903	0.0044	0.0349	1.2531	1.4536	5.0739	11.1734	0.0361
16071901 groundmass plag 2 core	Contact	0.019	0.2565	5.7163	8.2555	23.447	64.8268	0.1931	102.7142	0.0025	0.0564	1.0561	2.76	4.7652	11.1776	0.0278
16071901 groundmass plag 2 rim	Contact	0.008	0.1249	6.0417	7.9675	23.5425	63.7332	0.16	101.5778	0.001	0.0278	1.1288	2.6939	4.8388	11.1134	0.0233

Table C.9. EPMA results for host rock pyroxene

	Unit	TiO2 wt%	MnO wt%	Cr2O3 wt%	K2O wt%	CaO wt%	Na2O wt%	Al2O3 wt%	SiO2 wt%	MgO wt%	FeO wt%	Total wt%	Ti atFrac	Mn atFrac	Cr atFrac	K atFrac	Ca atFrac	Na atFrac	Al atFrac	Si atFrac	Mg atFrac	Fe atFrac
071406 cpx1core	Enclave-Rich Tonalite	0.146	0.414	0.003	0.034	20.98	0.575	0.645	53.045	13.967	10.798	100.607	0.004	0.013	0	0.002	0.839	0.042	0.028	1.98	0.777	0.337
071406 cpx1rim1	Enclave-Rich Tonalite	0.102	0.607	0.005	0.029	21.538	0.485	0.579	53.47	14.292	8.936	100.044	0.003	0.019	0	0.001	0.86	0.035	0.025	1.993	0.794	0.278
071406 cpx1rim2	Enclave-Rich Tonalite	0.16	0.547	0.001	0.016	21.559	0.451	0.585	53.634	14.432	8.984	100.368	0.004	0.017	0	0.001	0.858	0.032	0.026	1.992	0.799	0.279
071406 cpx2core	Enclave-Rich Tonalite	0.202	0.451	0.009	0.009	21.402	0.456	0.759	53.252	14.147	9.695	100.383	0.006	0.014	0	0	0.854	0.033	0.033	1.983	0.785	0.302
071406 cpx2rim1	Enclave-Rich Tonalite	0.11	0.38	0.016	-0.004	21.281	0.443	0.673	53.499	14.664	8.983	100.044	0.003	0.012	0.001	0	0.848	0.032	0.03	1.99	0.813	0.279
071406 cpx2rim2	Enclave-Rich Tonalite	0.14	0.451	0.004	0.001	21.112	0.475	0.675	53.421	14.415	9.526	100.219	0.004	0.014	0	0	0.842	0.034	0.03	1.989	0.8	0.297
Core 2 qdxcpx1core	Enclave-Rich Tonalite	0.025	0.356	0.041	0.032	14.465	0.152	0.773	50.577	17.494	9.83	93.747	0.001	0.012	0.001	0.002	0.608	0.012	0.036	1.985	1.023	0.323
Core 2 qdxcpx1rim	Enclave-Rich Tonalite	0.08	0.45	0.009	0.055	12.62	0.135	0.854	51.274	16.458	12.131	94.065	0.002	0.015	0	0.003	0.53	0.01	0.04	2.012	0.962	0.398
Core 2 qdxcpx2core	Enclave-Rich Tonalite	0.086	0.39	0.023	0.043	12.798	0.116	0.921	52.168	16.434	12.242	95.222	0.002	0.013	0.001	0.002	0.531	0.009	0.042	2.019	0.948	0.396
Core 2 qdxcpx2rim	Enclave-Rich Tonalite	0.085	0.39	0.007	0.032	16.299	0.137	0.66	43.643	15.974	9.614	86.841	0.003	0.014	0	0.002	0.757	0.012	0.034	1.892	1.032	0.349
071408 cpx1core	Enclave-Poor Tonalite	0.261	0.276	0.006	0.003	20.493	0.357	0.813	52.87	14.452	10.511	100.042	0.007	0.009	0	0	0.821	0.026	0.036	1.977	0.806	0.329
071408 cpx1rim	Enclave-Poor Tonalite	0.28	0.372	-0.014	0.008	21.097	0.386	0.987	52.763	14.165	9.537	99.579	0.008	0.012	0	0	0.847	0.028	0.044	1.978	0.791	0.299
071408 cpx2L1	Enclave-Poor Tonalite	0.396	0.198	-0.002	0.005	21.984	0.374	1.643	53.081	15.026	7.78	100.484	0.011	0.006	0	0	0.869	0.027	0.071	1.958	0.826	0.24
071408 cpx2L2	Enclave-Poor Tonalite	0.511	0.234	0.041	0.001	21.854	0.414	1.972	52.484	14.868	7.865	100.245	0.014	0.007	0.001	0	0.867	0.03	0.086	1.944	0.821	0.244
071408 cpx2L3	Enclave-Poor Tonalite	0.5	0.212	0.018	0.008	21.58	0.38	1.862	52.402	15.216	7.753	99.931	0.014	0.007	0.001	0	0.858	0.027	0.081	1.944	0.842	0.241
071408 cpx2L4	Enclave-Poor Tonalite	0.76	0.195	0.021	0.013	21.719	0.441	2.316	52.225	15.248	7.347	100.286	0.021	0.006	0.001	0.001	0.859	0.032	0.101	1.929	0.84	0.227
071408 cpx2L5	Enclave-Poor Tonalite	0.578	0.204	0.033	-0.004	20.889	0.351	1.97	52.51	15.54	7.975	100.047	0.016	0.006	0.001	0	0.828	0.025	0.086	1.943	0.857	0.247
071408 cpx2L6	Enclave-Poor Tonalite	0.691	0.193	0.095	0.029	20.818	0.457	2.494	52.017	15.295	7.273	99.363	0.019	0.006	0.003	0.001	0.829	0.033	0.109	1.934	0.848	0.226
071408 cpx2L7	Enclave-Poor Tonalite	0.714	0.183	0.252	0.024	21.313	0.473	2.583	51.737	15	7.305	99.585	0.02	0.006	0.007	0.001	0.849	0.034	0.113	1.924	0.831	0.227
071408 cpx2L8	Enclave-Poor Tonalite	0.444	0.206	0.232	0.003	21.583	0.38	1.971	52.484	15.045	7.466	99.815	0.012	0.007	0.007	0	0.858	0.027	0.086	1.947	0.832	0.232
071408 cpx2L9	Enclave-Poor Tonalite	0.229	0.227	0.123	0.056	13.008	0.277	6.658	44.652	15.992	14.68	95.902	0.007	0.008	0.004	0.003	0.55	0.021	0.31	1.761	0.94	0.484
071408 cpx2L10	Enclave-Poor Tonalite	0.295	0.371	0.01	0.037	21.225	0.416	1.139	52.908	14.321	9.296	100.017	0.008	0.012	0	0.002	0.848	0.03	0.05	1.973	0.796	0.29
Core 2 qdcp1core	Enclave-Poor Tonalite	0.133	0.553	-0.006	0.027	11.969	0.208	1.066	51.507	17.801	10.89	94.149	0.004	0.018	0	0.001	0.499	0.016	0.049	2.003	1.032	0.354
Core 2 qdcp1rim	Enclave-Poor Tonalite	0.174	0.416	-0.001	0.118	12.578	0.247	1.859	49.456	16.418	11.786	93.051	0.005	0.014	0	0.006	0.536	0.019	0.087	1.966	0.973	0.392
Core 2 qdcp2core	Enclave-Poor Tonalite	0.057	0.555	0.017	0.03	12.145	0.167	0.378	52.499	18.676	10.132	94.655	0.002	0.018	0.001	0.002	0.501	0.013	0.017	2.022	1.072	0.326
16071901 gmcp2corea	Enclave-Poor Tonalite	0.052	0.443	0.023	0.028	11.885	0.131	0.787	53.66	18.817	9.478	95.304	0.002	0.014	0.001	0.001	0.483	0.01	0.035	2.037	1.065	0.301
16071901 gmcp2rima	Enclave-Poor Tonalite	0.042	0.461	0.002	0.021	11.941	0.181	0.683	53.175	18.238	10.152	94.895	0.001	0.015	0	0.001	0.49	0.013	0.031	2.036	1.041	0.325
16071901 gmcp2coreb	Enclave-Poor Tonalite	0.05	0.322	-0.009	0.021	12.32	0.143	0.467	53.925	19.418	8.537	95.195	0.001	0.01	0	0.001	0.5	0.01	0.021	2.042	1.096	0.27
16071901 gmcp2rimb	Enclave-Poor Tonalite	0.131	0.253	0.013	0.235	11.949	0.518	4.436	49.231	15.156	12.373	94.295	0.004	0.008	0	0.012	0.502	0.039	0.205	1.929	0.885	0.405
16071901 cpxacc1core	Contact	0.079	0.224	0.012	0.014	12.745	0.084	0.681	54.449	19.587	7.987	95.863	0.002	0.007	0	0.001	0.512	0.006	0.03	2.041	1.095	0.25
16071901 cpxacc2corea	Contact	0.107	0.328	0.019	0.011	22.47	0.401	0.605	51.312	14.194	8.365	97.812	0.003	0.011	0.001	0.001	0.921	0.03	0.027	1.964	0.81	0.268
16071901 cpxacc2rima	Contact	0.086	0.308	0.023	0.002	22.72	0.327	0.533	51.201	14.165	8.522	97.886	0.002	0.01	0.001	0	0.932	0.024	0.024	1.961	0.809	0.273
16071901 cpxacc2corec	Contact	0.077	0.262	0.022	0.003	23.428	0.302	0.394	51.03	13.955	8.106	97.578	0.002	0.009	0.001	0	0.965	0.023	0.018	1.962	0.8	0.261
16071901 cpxacc2cored	Contact	0.077	0.274	0.014	0.012	22.905	0.354	0.512	51.783	13.901	8.445	98.276	0.002	0.009	0	0.001	0.935	0.026	0.023	1.972	0.789	0.269
16071901 cpxacc2coree	Contact	0.047	0.292	0.011	-0.004	23.611	0.283	0.426	51.524	13.897	8.197	98.285	0.001	0.009	0	0	0.965	0.021	0.019	1.966	0.79	0.262
16071901 cpxacc2coref	Contact	0.117	0.276	0.032	0.009	22.66	0.378	0.739	51.35	14	8.624	98.184	0.003	0.009	0.001	0.001	0.927	0.028	0.033	1.96	0.797	0.275
16071901 cpxacc2coreg	Contact	0.096	0.316	0.025	0.011	23.406	0.281	0.376	51.506	14.075	8.117	98.209	0.003	0.01	0.001	0.001	0.957	0.021	0.017	1.965	0.801	0.259
16071901 cpxacc2coreh	Contact	0.078	0.281	0.022	-0.002	22.444	0.321	0.583	51.21	13.903	9.111	97.951	0.002	0.009	0.001	0	0.922	0.024	0.026	1.963	0.794	0.292

Table C.10. EPMA results for host rock biotite

	Unit	TiO2 wt%	MnO wt%	Cl wt%	K2O wt%	Al2O3 wt%	SiO2 wt%	MgO wt%	FeO wt%	Total wt%	Ti atFrac	Mn atFrac	Cl atFrac	K atFrac	Al atFrac	Si atFrac	Mg atFrac	Fe atFrac
071406 bt2core	Enclave-Rich Tonalite	4.62	0.137	0.044	9.621	13.424	36.815	10.235	20.268	95.012	0.535	0.018	0.012	1.891	2.438	5.673	2.351	2.612
071406 bt2rim1	Enclave-Rich Tonalite	4.041	0.177	0.058	9.817	14.25	36.738	9.856	20.791	95.549	0.467	0.023	0.015	1.924	2.58	5.643	2.257	2.671
071406 bt2rim2	Enclave-Rich Tonalite	4.517	0.139	0.061	9.73	13.611	36.678	10.355	20.058	94.983	0.524	0.018	0.016	1.913	2.473	5.653	2.379	2.585
071406 bt1core	Enclave-Rich Tonalite	4.552	0.187	0.071	9.745	13.491	37.075	11.606	18.678	95.175	0.522	0.024	0.018	1.897	2.427	5.658	2.641	2.384
071406 bt1rim1	Enclave-Rich Tonalite	1.955	0.204	0.096	9.859	15.526	37.018	12.757	17.441	94.644	0.224	0.026	0.025	1.915	2.786	5.636	2.895	2.221
071406 bt1rim2	Enclave-Rich Tonalite	3.521	0.17	0.065	9.741	14.543	37.097	12.182	17.933	95.017	0.403	0.022	0.017	1.889	2.606	5.64	2.761	2.28
071408 bt1core	Enclave-Poor Tonalite	4.887	0.142	0.064	8.814	13.431	36.025	13.052	18.023	94.181	0.564	0.019	0.017	1.725	2.428	5.526	2.984	2.312
071408 bt1rim1	Enclave-Poor Tonalite	4.907	0.127	0.078	9.329	13.467	36.509	13.035	17.377	94.577	0.563	0.016	0.02	1.815	2.421	5.569	2.964	2.217
071408 bt1rim2	Enclave-Poor Tonalite	4.929	0.111	0.073	9.26	13.443	36.57	13.15	17.349	94.626	0.565	0.014	0.019	1.8	2.413	5.57	2.986	2.21
071408 bt2core	Enclave-Poor Tonalite	5.001	0.18	0.075	9.627	13.312	36.591	13.09	17.218	94.782	0.573	0.023	0.02	1.871	2.39	5.573	2.972	2.193
071408 bt2rim1	Enclave-Poor Tonalite	4.852	0.183	0.066	8.953	13.443	36.138	13.221	17.304	93.888	0.56	0.024	0.017	1.753	2.431	5.545	3.024	2.22
071408 bt2rim2	Enclave-Poor Tonalite	4.873	0.194	0.072	9.548	13.635	37.236	12.692	17.174	95.18	0.554	0.025	0.019	1.843	2.431	5.632	2.862	2.172

Table C.11. EPMA results for host rock amphibole

		TiO2 wt%	MnO wt%	Cr2O3 wt%	K2O wt%	CaO wt%	Na2O wt%	Al2O3 wt%	SiO2 wt%	MgO wt%	FeO wt%	Total wt%	Ti atFrac	Mn atFrac	Cr atFrac	K atFrac	Ca atFrac	Na atFrac	Al atFrac	Si atFrac	Mg atFrac	Fe atFrac
core2qdcpxcorr1hblrim	Enclave-Rich Tonalite	1.087	0.558	0.015	0.517	11.225	0.948	5.399	48.98	13.853	14.496	97.107	0.121	0.07	0.002	0.097	1.781	0.271	0.94	7.235	3.05	1.791
core2qdcpxcorr2hblrim	Enclave-Poor Tonalite	1.049	0.5	0.013	0.482	11.549	1.058	5.366	48.324	13.804	14.106	96.249	0.118	0.063	0.002	0.092	1.845	0.306	0.943	7.206	3.069	1.759
16070901cpxacc2hblA	Contact	0.998	0.215	0.034	0.395	11.634	1.039	4.823	49.625	15.809	12.288	96.859	0.12	0.028	0.004	0.074	1.825	0.295	0.833	7.267	3.451	1.505
16071901cpxacc2hblB	Contact	0.625	0.197	0.046	0.009	12.123	0.717	3.65	51.145	16.235	11.217	95.963	0.069	0.024	0.005	0.002	1.901	0.204	0.63	7.484	3.541	1.373

Table C.12. EPMA results for dyke/sill plagioclase

	SiO ₂ wt%	TiO ₂ wt%	Al ₂ O ₃ wt%	CaO wt%	Na ₂ O wt%	Al ₂ O ₃ wt%	SiO ₂ wt%	FeO wt%	Total wt%	Ti atFrac	K atFrac	Ca atFrac	Na atFrac	Al atFrac	Si atFrac	Fe atFrac
072601 plag2L1	QD dyke	0.007	0.179	10.941	5.252	28.87	57.656	0.122	103.027	0.001	0.04	2.046	1.777	5.938	10.06	0.018
072601 plag2L2	QD dyke	0.013	0.417	6.138	7.684	24.473	64.195	0.113	103.033	0.002	0.091	1.131	2.562	4.961	11.04	0.016
072601 plag2L3	QD dyke	-0.002	0.204	9.262	6.056	27.316	59.882	0.139	102.857	0	0.045	1.725	2.041	5.596	10.409	0.02
072601 plag2L4	QD dyke	0.014	0.16	5.585	8.567	24.092	65.483	0.255	104.155	0.002	0.035	1.018	2.825	4.829	11.135	0.036
072601 plag2L5	QD dyke	0.007	11.135	0.587	0.107	32.373	53.526	0.193	97.929	0.001	2.638	0.117	0.038	7.087	9.941	0.03
072601 plag2L6	QD dyke	0.001	1.974	12.263	6.406	24.381	57.144	1.07	103.239	0	0.45	2.35	2.222	5.14	10.221	0.16
072601 plag2L7	QD dyke	0.025	2.544	4.247	2.351	27.619	53.944	0.797	91.527	0.004	0.626	0.878	0.879	6.28	10.407	0.129
072601 plag2L8	QD dyke	0.002	0.309	5.539	8.351	24	65.055	0.142	103.398	0	0.067	1.016	2.773	4.844	11.139	0.02
072601 plag2L9	QD dyke	0.018	0.182	10.094	4.796	26.297	51.424	0.193	93.004	0.003	0.045	2.096	1.802	6.007	9.966	0.031
072601 plag2L10	QD dyke	0.015	0.202	10.116	5.658	27.744	57.758	0.116	101.609	0.002	0.045	1.915	1.938	5.777	10.203	0.017
072601 plag2L11	QD dyke	0.031	0.491	10.605	5.516	27.635	58.25	0.373	102.901	0.004	0.11	1.99	1.873	5.704	10.2	0.055
072601 plag2L12	QD dyke	0.044	0.16	10.534	5.459	28.341	57.959	0.226	102.724	0.006	0.036	1.974	1.851	5.843	10.137	0.033
072601 plag2L13	QD dyke	0.007	0.164	10.798	5.361	28.514	57.82	0.102	102.766	0.001	0.037	2.023	1.817	5.876	10.109	0.015
072601 plag2L14	QD dyke	0.009	0.222	9.843	5.939	27.415	58.869	0.099	102.398	0.001	0.05	1.847	2.016	5.658	10.308	0.015
072601 plag2L15	QD dyke	0.032	0.192	10.546	5.361	28.298	57.912	0.118	102.46	0.004	0.043	1.98	1.821	5.845	10.148	0.017
072601 plag2L16	QD dyke	2.359	0.169	9.951	4.701	24.062	49.435	13.046	103.722	0.332	0.04	1.993	1.704	5.301	9.24	2.039
072601 plag2L17	QD dyke	0.045	0.204	9.967	5.775	27.844	58.768	0.122	102.725	0.006	0.045	1.864	1.955	5.728	10.257	0.018
072601 plag2L18	QD dyke	-0.005	0.506	5.359	8.291	23.719	65.016	0.11	102.995	-0.001	0.111	0.987	2.763	4.806	11.176	0.016
072601 plag2L19	QD dyke	0.02	0.389	6.134	7.982	24.265	63.993	0.208	102.99	0.002	0.086	1.133	2.668	4.93	11.03	0.03
072601 plag2L20	QD dyke	0.016	0.32	6.146	8.122	24.367	63.871	0.133	102.975	0.002	0.07	1.135	2.715	4.951	11.011	0.019
072601 plag1L1	QD dyke	0.069	0.182	10.587	5.576	28.065	57.62	0.116	102.216	0.009	0.041	1.995	1.902	5.819	10.135	0.017
072601 plag1L2	QD dyke	0.025	0.242	10.513	5.302	27.635	56.791	0.168	100.676	0.003	0.055	2.012	1.836	5.817	10.142	0.025
072601 plag1L3	QD dyke	0.325	0.538	9.309	5.371	26.891	55.794	2.602	100.83	0.044	0.124	1.8	1.879	5.72	10.069	0.393
072601 plag1L4	QD dyke	0.069	12.972	0.465	1.61	18.922	66.455	0.13	100.623	0.009	2.993	0.09	0.565	4.034	12.021	0.02
072601 plag1L5	QD dyke	0.018	0.367	7.004	7.465	24.912	62.943	0.118	102.827	0.002	0.081	1.298	2.503	5.078	10.885	0.017
072601 plag1L6	QD dyke	0.022	0.187	11.231	5.031	28.611	56.046	0.118	101.245	0.003	0.043	2.141	1.736	6.001	9.973	0.018
072601 plag1L7	QD dyke	0.016	0.236	9.39	6.05	26.509	58.941	0.107	101.249	0.002	0.053	1.779	2.075	5.526	10.424	0.016
072601 plag1L8	QD dyke	0.005	0.544	5.571	8.042	23.298	64.707	0.11	102.278	0.001	0.12	1.034	2.7	4.755	11.203	0.016
072601 plag1L9	QD dyke	0.014	0.169	9.298	6.121	26.684	59.518	0.1	101.904	0.002	0.038	1.749	2.083	5.52	10.446	0.015
072601 plag1L10	QD dyke	0.013	0.186	9.094	6.33	26.44	59.736	0.114	101.912	0.002	0.042	1.71	2.154	5.47	10.484	0.017
072601 plag1L11	QD dyke	-0.001	0.149	9.805	6.034	26.965	58.363	0.123	101.439	0	0.034	1.858	2.069	5.621	10.321	0.018
072601 plag1L12	QD dyke	0.013	0.198	6.627	7.564	24.362	62.85	0.2	101.814	0.002	0.044	1.238	2.557	5.007	10.959	0.029
072601 plag1L13	QD dyke	0.014	0.299	5.187	3.939	15.929	39.656	0.189	65.214	0.003	0.104	1.517	2.085	5.126	10.825	0.043
072601 plag1L14	QD dyke	0.001	0.26	7.877	6.938	25.682	62.101	0.106	102.966	0	0.057	1.46	2.326	5.235	10.74	0.015
072601 plag1L15	QD dyke	0.237	3.79	3.141	10.414	11.231	24.657	0.096	53.567	0.067	1.81	1.26	7.559	4.955	9.23	0.03
072601 plag1L16	QD dyke	0.024	0.312	8.816	6.232	25.954	59.666	0.097	101.101	0.003	0.071	1.67	2.136	5.408	10.547	0.014
072601 plag1L17	QD dyke	0.015	0.311	7.3	7.185	24.725	61.864	0.11	101.511	0.002	0.07	1.371	2.442	5.109	10.845	0.016
072601 plag1L18	QD dyke	0.004	0.176	9.95	5.81	27.242	58.25	0.142	101.574	0.001	0.04	1.883	1.99	5.671	10.287	0.021
072601 plag1L19	QD dyke	0.023	0.29	9.283	6.03	26.696	58.402	0.176	100.9	0.003	0.066	1.767	2.077	5.589	10.373	0.026
072601 plag1L20	QD dyke	0.03	0.198	11.512	5.077	28.308	56.179	0.15	101.454	0.004	0.045	2.193	1.75	5.933	9.99	0.022
072601 plag1L21	QD dyke	0.018	0.436	6.345	7.791	23.841	63.335	0.129	101.896	0.002	0.097	1.185	2.633	4.898	11.04	0.019
072601 plag1L22	QD dyke	-0.01	0.503	6.76	7.087	24.363	62.705	0.13	101.537	-0.001	0.112	1.266	2.403	5.021	10.964	0.019
072601 plag1L23	QD dyke	0.041	0.211	10.608	5.582	27.923	58.147	0.131	102.642	0.005	0.047	1.99	1.895	5.763	10.182	0.019
072601 plag1L24	QD dyke	0.021	0.186	10.316	5.633	27.189	57.326	0.118	100.789	0.003	0.042	1.971	1.947	5.714	10.22	0.018
072601 plag1L25	QD dyke	0.035	0.334	6.168	7.722	23.672	64.275	0.136	102.343	0.004	0.074	1.144	2.592	4.83	11.125	0.02
072601 gmplag1co	QD dyke	0.064	0.196	10.189	5.526	27.126	56.978	0.129	100.209	0.009	0.045	1.957	1.921	5.731	10.213	0.019
072601 gmplag1rir	QD dyke	0.001	0.368	5.19	8.213	22.88	64.21	0.196	101.059	0	0.082	0.974	2.788	4.721	11.24	0.029
072001A plag1core Chilled Diorite Sill		0.068	0.536	10.556	5.224	27.847	56.629	0.134	100.993	0.009	0.122	2.017	1.806	5.854	10.1	0.02
072001A plag1rim Chilled Diorite Sill		0.014	0.338	5.731	8.11	23.351	65.473	0.161	103.178	0.002	0.074	1.053	2.697	4.72	11.228	0.023
072001A plag2core Chilled Diorite Sill		0.045	0.253	8.974	6.308	25.977	60.44	0.135	102.132	0.006	0.056	1.683	2.14	5.358	10.576	0.02

Table C.12. EPMA results for dyke/sill plagioclase (cont)

	Unit	TiO2 wt%	K2O wt%	CaO wt%	Na2O wt%	Al2O3 wt%	SiO2 wt%	FeO wt%	Total wt%	Ti atFrac	K atFrac	Ca atFrac	Na atFrac	Al atFrac	Si atFrac	Fe atFrac	
072001A	plag2rim	Chilled Diorite Sill	0.004	0.465	4.476	8.882	22.479	67.34	0.184	103.83	0.001	0.101	0.815	2.927	4.503	11.445	0.026
071414	plag2core	layer intrusion (bottom)	0.024	0.051	14.052	3.44	30.056	53.725	0.221	101.569	0.003	0.012	2.688	1.191	6.325	9.592	0.033
071414	plag2rim	layer intrusion (bottom)	0.005	0.029	11.313	5.015	27.787	55.341	0.405	99.894	0.001	0.007	2.19	1.756	5.916	9.996	0.061
071414	plag1core	layer intrusion (bottom)	0.006	0.05	13.454	3.7	29.488	54.01	0.185	100.894	0.001	0.012	2.587	1.287	6.236	9.69	0.028
071414	plag1rim	layer intrusion (bottom)	-0.011	0.102	13.955	3.566	30.283	53.273	0.232	101.4	-0.002	0.023	2.677	1.238	6.39	9.538	0.035
071415	plag1rim	layer intrusion (middle)	0.018	0.242	11.32	4.912	27.819	56.413	0.262	100.986	0.002	0.055	2.165	1.7	5.852	10.068	0.039
071415	plag2core	layer intrusion (middle)	0.041	0.141	10.293	5.378	26.661	59.043	0.299	101.856	0.005	0.032	1.941	1.835	5.529	10.389	0.044
071415	plag2rim	layer intrusion (middle)	0.018	0.247	11.768	4.624	29.117	57.704	0.347	103.824	0.002	0.055	2.188	1.556	5.954	10.011	0.05
071415	plag1core	layer intrusion (middle)	0.02	0.285	11.919	4.583	29.024	57.2	0.286	103.317	0.003	0.064	2.228	1.551	5.97	9.981	0.042
071415	plag3core	layer intrusion (middle)	0.026	0.485	8.947	5.889	26.481	60.798	0.295	102.921	0.004	0.107	1.664	1.982	5.419	10.556	0.043
071415	plag3rim	layer intrusion (middle)	0.043	0.299	11.23	4.906	28.022	57.753	0.347	102.6	0.006	0.067	2.111	1.669	5.795	10.133	0.051

Table C.13. EPMA results for dyke/sill pyroxene

	Unit	TiO2 wt%	MnO wt%	Cr2O3 wt%	K2O wt%	CaO wt%	Na2O wt%	Al2O3 wt%	SiO2 wt%	MgO wt%	FeO wt%	Total wt%	Ti atFrac	Mn atFrac	Cr atFrac	K atFrac	Ca atFrac	Na atFrac	Al atFrac	Si atFrac	Mg atFrac	Fe atFrac	
072601	cpx2hblrim	Qd dykes	1.136	0.287	0.001	0.475	11.687	0.803	5.893	47.774	13.401	14.564	96.022	0.128	0.036	0	0.091	1.874	0.233	1.039	7.15	2.99	1.823
072601	cpx1hblrim	Qd dykes	1.121	0.3	0.076	0.46	11.028	1.015	5.121	49.093	14.476	14.49	97.18	0.124	0.038	0.009	0.086	1.742	0.29	0.89	7.235	3.18	1.786
072001A	hbl1core	Chilled tonalite sill	1.46	0.209	-0.001	0.667	10.37	1.222	6.33	46.531	12.155	17.92	96.863	0.166	0.027	0	0.128	1.676	0.358	1.126	7.02	2.734	2.261
072001A	cpx1hblrim	Chilled tonalite sill	1.099	0.268	0.002	0.483	11.171	0.916	5.551	47.703	11.991	17.517	96.7	0.124	0.034	0	0.093	1.802	0.267	0.985	7.181	2.691	2.205
072001A	cpx2hblrim	Chilled tonalite sill	1.194	0.244	-0.017	0.499	11.042	0.764	5.538	47.66	12.711	16.553	96.189	0.135	0.031	-0.002	0.096	1.781	0.223	0.983	7.175	2.852	2.084
071414	opx2core	Maf Lay Int (Bottom)	0.019	0.277	0.014	0.001	0.498	0.003	1.163	53.074	31.797	10.986	97.832	0.001	0.009	0	0	0.019	0	0.05	1.923	1.717	0.333
071414	opx2rim	Maf Lay Int (Bottom)	0.105	0.245	0.04	0	0.882	0.02	0.865	52.597	31.641	10.879	97.273	0.003	0.008	0.001	0	0.034	0.001	0.037	1.92	1.722	0.332
071414	opx1core	Maf Lay Int (Bottom)	0.198	0.253	0.117	0.004	1.02	0.03	1.283	51.942	31.334	11.083	97.264	0.005	0.008	0.003	0	0.04	0.002	0.055	1.901	1.71	0.339
071414	opx1rim	Maf Lay Int (Bottom)	0.065	0.248	0.029	0.002	0.574	0.01	0.711	52.881	31.324	11.001	96.846	0.002	0.008	0.001	0	0.023	0.001	0.031	1.936	1.71	0.337
071415	cpx3core	Maf Lay Int (Middle)	0.155	0.384	0.047	-0.001	0.976	0.023	1.254	51.53	27.354	15.587	97.31	0.004	0.012	0.001	0	0.039	0.002	0.055	1.923	1.522	0.486
071415	cpx3rim	Maf Lay Int (Middle)	0.171	0.352	0.027	0.002	1.203	0	1.156	51.22	27.986	15.018	97.136	0.005	0.011	0.001	0	0.048	0	0.051	1.913	1.558	0.469
071415	cpx1corea	Maf Lay Int (Middle)	0.34	0.197	0.186	-0.001	22.628	0.337	1.893	48.709	15.32	6.859	96.469	0.01	0.007	0.006	0	0.94	0.025	0.086	1.888	0.885	0.222
071415	cpx1rima	Maf Lay Int (Middle)	0.345	0.207	0.125	0.002	22.8	0.328	1.758	49.457	15.384	6.679	97.084	0.01	0.007	0.004	0	0.939	0.024	0.08	1.901	0.881	0.215
071415	cpx1coreb	Maf Lay Int (Middle)	0.365	0.208	0.121	0.003	22.633	0.378	1.835	50.463	15.457	6.902	98.365	0.01	0.007	0.004	0	0.918	0.028	0.082	1.911	0.872	0.219
071415	cpx1rimb	Maf Lay Int (Middle)	0.398	0.201	0.102	0	22.838	0.359	1.974	49.637	14.884	6.823	97.215	0.012	0.007	0.003	0	0.939	0.027	0.089	1.905	0.851	0.219
071415	cpx1corec	Maf Lay Int (Middle)	0.336	0.202	0.095	0.001	22.631	0.386	1.9	48.223	15.401	6.96	96.134	0.01	0.007	0.003	0	0.945	0.029	0.087	1.879	0.895	0.227
071415	cpx1rimc	Maf Lay Int (Middle)	0.317	0.188	0.086	-0.004	22.581	0.331	1.618	49.877	15.798	6.852	97.645	0.009	0.006	0.003	0	0.924	0.024	0.073	1.904	0.899	0.219
071415	cpx2core	Maf Lay Int (Middle)	1.46	0.168	0.291	0.371	19.222	0.992	5.601	46.613	15.352	8.424	98.494	0.042	0.005	0.009	0.018	0.784	0.073	0.251	1.775	0.872	0.268
071415	cpx2rim	Maf Lay Int (Middle)	0.361	0.196	0.05	0.007	22.665	0.279	1.82	49.016	15.487	6.747	96.628	0.01	0.006	0.002	0	0.938	0.021	0.083	1.894	0.892	0.218

Table C.14. EPMA results for dyke/sill hornblende

		TiO2 wt%	MnO wt%	Cr2O3 wt%	K2O wt%	CaO wt%	Na2O wt%	Al2O3 wt%	SiO2 wt%	MgO wt%	FeO wt%	Total wt%	Ti atFrac	Mn atFrac	Cr atFrac	K atFrac	Ca atFrac	Na atFrac	Al atFrac	Si atFrac	Mg atFrac	Fe atFrac
core2qdcpxcorr1hblrim	Enclave-Rich Tonalite	1.087	0.558	0.015	0.517	11.225	0.948	5.399	48.98	13.853	14.496	97.107	0.121	0.07	0.002	0.097	1.781	0.271	0.94	7.235	3.05	1.791
core2qdcpxcorr2hblrim	Enclave-Poor Tonalite	1.049	0.5	0.013	0.482	11.549	1.058	5.366	48.324	13.804	14.106	96.249	0.118	0.063	0.002	0.092	1.845	0.306	0.943	7.206	3.069	1.759
16070901cpxacc2hb1A	Contact	0.998	0.215	0.034	0.395	11.634	1.039	4.823	49.625	15.809	12.288	96.859	0.12	0.028	0.004	0.074	1.825	0.295	0.833	7.267	3.451	1.505
16071901cpxacc2hb1B	Contact	0.625	0.197	0.046	0.009	12.123	0.717	3.65	51.145	16.235	11.217	95.963	0.069	0.024	0.005	0.002	1.901	0.204	0.63	7.484	3.541	1.373

Table C.15. EPMA results for dyke/sill olivine

	Unit	TiO2 wt%	MnO wt%	Cr2O3 wt%	CaO wt%	Al2O3 wt%	SiO2 wt%	MgO wt%	FeO wt%	Total wt%	Ti atFrac	Mn atFrac	Cr atFrac	Ca atFrac	Al atFrac	Si atFrac	Mg atFrac	Fe atFrac
071414olv3core	Mafic Layered Intrusion (bot)	0.003	0.276	-0.009	0.023	0.008	37.88	44.661	17.199	100.041	0	0.006	0	0.001	0	0.965	1.696	0.366
071414olv3rim	Mafic Layered Intrusion (bot)	0.032	0.251	0.009	0.036	-0.005	38.245	44.999	16.559	100.126	0.001	0.005	0	0.001	0	0.97	1.701	0.351
071414olv2core	Mafic Layered Intrusion (bot)	0.002	0.251	0.006	0.025	0.004	37.971	44.488	16.847	99.594	0	0.005	0	0.001	0	0.97	1.694	0.36
071414olv2rim	Mafic Layered Intrusion (bot)	0.013	0.255	0.012	0.019	-0.031	37.906	44.434	16.688	99.297	0	0.005	0	0.001	-0.001	0.971	1.696	0.357
071414olv1rim	Mafic Layered Intrusion (bot)	-0.013	0.243	-0.003	0.022	-0.006	38.333	44.722	17.07	100.368	0	0.005	0	0.001	0	0.972	1.69	0.362
071414olv1core	Mafic Layered Intrusion (bot)	0.014	0.242	0.02	0.026	0.013	37.921	44.602	17.218	100.055	0	0.005	0	0.001	0	0.966	1.694	0.367

Table C.16 Extended EPMA results for enclave plagioclase

Enclave Group	Acc V.	Beam Curr(A)	Beam Dia(um)	Ti SD(%)	K SD(%)	Ca SD(%)	Na SD(%)	Al SD(%)	Si SD(%)	Fe SD(%)	Ti DL(ppm-1s)	K DL(ppm-1s)	Ca DL(ppm-1s)	Na DL(ppm-1s)	Al DL(ppm-1s)	Si DL(ppm-1s)	Fe DL(ppm-1s)	
071410 mtrx3core	1	15	1.991E-08	3	128.89	4.99	0.45	0.79	0.29	0.27	8.29	1.264	25.723	20.579	59.752	109.326	41.895	55.675
071410 mtrx3rim	1	15	1.991E-08	3	104	2.76	0.48	0.78	0.29	0.28	10.03	1.29	25.723	20.559	63.105	110.701	42.145	58.257
071410 meg2 L1	1	15	1.991E-08	3	165.18	2.52	0.36	0.87	0.3	0.26	7.58	1.335	25.75	20.566	59.56	108.212	42.225	55.201
071410 meg2 L2	1	15	1.991E-08	3	92.13	3.8	0.36	0.86	0.3	0.26	9.2	1.216	26.186	20.693	60.937	107.634	43.076	56.714
071410 meg2 L3	1	15	1.991E-08	3	100	1.57	0.47	0.8	0.29	0.28	8.13	1.297	25.236	20.909	59.223	108.213	42.513	56.517
071410 meg2 L4	1	15	1.991E-08	3	165.18	3.22	0.4	0.83	0.3	0.27	7.45	1.335	26.335	20.315	64.273	108.649	42.762	56.126
071410 meg2 L5	1	15	1.99E-08	3	85.45	3.52	0.38	0.85	0.3	0.27	8.75	1.277	25.111	20.274	62.237	110.721	43.29	56.45
071410 meg2 L6	1	15	1.99E-08	3	104	1.98	0.37	0.88	0.3	0.26	9.22	1.29	26.027	20.461	56.806	109.888	42.691	57.882
071410 meg2 L7	1	15	1.99E-08	3	100	2.67	0.37	0.86	0.3	0.26	9.79	1.372	24.678	20.589	56.3	109.583	41.869	59.35
071410 meg2 L8	1	15	1.991E-08	3	88.63	1.91	0.4	0.84	0.3	0.27	8.11	1.329	25.621	20.555	59.029	107.221	41.824	58.916
071410 meg2 L9	1	15	1.991E-08	3	1452.58	3.12	0.45	0.79	0.29	0.27	11.1	1.329	25.503	20.663	59.223	110.606	42.338	56.019
071410 meg2 L10	1	15	1.991E-08	3	86.15	4.04	0.47	0.78	0.29	0.27	10.84	1.21	25.413	20.192	63.421	109.496	42.245	57.577
071410 meg1 L1	1	15	1.99E-08	3	126.29	2.93	0.35	0.88	0.3	0.26	8.63	1.237	25.618	20.23	59.319	107.692	42.293	58.051
071410 meg1 L2	1	15	1.99E-08	3	290.52	3.4	0.44	0.8	0.29	0.27	9.52	1.316	25.72	20.522	61.451	112.36	42.047	57.171
071410 meg1 L3	1	15	1.99E-08	3	100	1.83	0.41	0.82	0.3	0.27	8.65	1.341	25.798	20.663	61.077	108.478	41.071	57.108
071410 meg1 L4	1	15	1.989E-08	3	100	1.73	0.42	0.83	0.3	0.27	7.24	1.379	26.385	20.579	59.512	108.023	41.066	57.438
071410 meg1 L5	1	15	1.989E-08	3	54.12	1.63	0.43	0.81	0.29	0.27	7.95	1.203	26.277	20.444	62.513	108.737	42.191	58.06
071410 meg1 L6	1	15	1.989E-08	3	119.02	1.69	0.41	0.83	0.3	0.27	7.92	1.271	24.506	20.312	60.749	108.178	42.485	56.236
071410 meg1 L7	1	15	1.989E-08	3	57.56	2.94	0.36	0.87	0.3	0.26	8.06	1.29	25.507	21.175	59.223	107.479	42.983	58.464
071410 meg1 L8	1	15	1.989E-08	3	64.6	4.66	0.38	0.85	0.3	0.26	11.73	1.23	25.215	20.919	57.507	107.521	43.291	58.122
071410 meg1 L9	1	15	1.989E-08	3	119.02	3.1	0.42	0.81	0.3	0.27	7.04	1.271	24.967	20.952	60.749	109.144	41.112	56.818
071410 meg1 L10	1	15	1.988E-08	3	70.71	2.13	0.44	0.81	0.29	0.27	7.61	1.23	25.726	21.103	61.451	111.841	42.724	57.884
072802B mottA L1	2	15	2.002E-08	3	83.04	1.38	0.28	1.18	0.47	0.3	5.92	46.645	12.282	15.682	82.289	65.452	111.146	39.091
072802B mottA L2	2	15	2.003E-08	3	64.92	1.38	0.26	1.23	0.46	0.3	6.96	47.782	12.16	15.888	87.557	67.113	108.467	39.332
072802B mottA L3	2	15	2.004E-08	3	76.72	1.43	0.25	1.28	0.46	0.31	6.57	49.973	12.06	15.991	89.169	66.485	111.078	38.922
072802B mottA L4	2	15	2.003E-08	3	41.6	1.39	0.27	1.22	0.46	0.3	6.94	47.221	12.334	16.063	82.707	67.45	113.069	40.23
072802B mottA L5	2	15	2.003E-08	3	31.88	1.39	0.25	1.29	0.45	0.31	6.41	47.897	12.313	16.303	90.204	70.043	112.617	38.596
072802B mottA L6	2	15	2.004E-08	3	56	2.06	0.26	1.24	0.46	0.3	8.04	48.451	12.277	16.168	86.936	67.061	109.481	40.023
072802B mottA L7	2	15	2.004E-08	3	50.87	1.39	0.26	1.23	0.46	0.3	7.53	45.95	12.456	15.837	82.578	67.709	113.179	39.15
072802B mottA L8	2	15	2.004E-08	3	23.56	1.36	0.25	1.26	0.46	0.31	6.33	42.813	12.443	15.803	86.437	67.683	114.283	37.859
072802B mottA L9	2	15	2.004E-08	3	66.87	1.33	0.24	1.31	0.45	0.31	5.81	49.326	12.044	16.252	84.132	67.217	113.623	38.807
072802B mottA L10	2	15	2.004E-08	3	46.35	1.29	0.25	1.26	0.46	0.31	5.99	45.719	12.401	15.94	80.162	68.759	109.485	38.973
072802B mottA L11	2	15	2.003E-08	3	57.85	1.08	0.26	1.26	0.46	0.3	6.08	50.192	12.198	16.226	80.779	66.616	109.565	39.228
072802B mottA L12	2	15	2.003E-08	3	194.76	1.09	0.26	1.24	0.46	0.3	6.57	48.999	12.215	15.896	79.24	61.204	110.852	38.988
072802B mottA L13	2	15	2.003E-08	3	40.04	1.33	0.23	1.42	0.44	0.31	4.9	49.87	12.414	16.46	81.868	66.353	107.614	40.191
072802B mottA L14	2	15	2.003E-08	3	164.44	1.3	0.23	1.35	0.44	0.31	5.38	48.781	12.043	16.262	81.813	67.139	110.416	38.763
072802B mottA L15	2	15	2.004E-08	3	51.29	1.43	0.23	1.36	0.45	0.31	5.51	47.56	12.258	16.445	82.366	69.618	111.497	38.544
072802B mottA L16	2	15	2.003E-08	3	44.2	1.62	0.23	1.32	0.45	0.31	5.48	47.445	12.422	16.355	87.11	67.786	110.403	39.888
072802B mottA L17	2	15	2.002E-08	3	36.42	1.66	0.22	1.39	0.44	0.32	3.9	48.999	12.345	16.556	70.062	68.912	110.526	39.026
072802B mottA L18	2	15	2.002E-08	3	8.21	1.42	0.24	1.31	0.45	0.31	2.32	46.762	12.13	16.309	91.42	66.327	114.457	38.502
072802B mottA L19	2	15	2.002E-08	3	43.08	1.24	0.25	1.27	0.45	0.3	4.62	47.105	12.309	16.112	87.677	66.195	109.956	38.318
072802B mottA L20	2	15	2.002E-08	3	205.43	1.35	0.31	1.15	0.48	0.3	3.59	46.988	12.011	15.785	85.607	64.158	115.417	37.352
072802B mottB L1	2	15	2.002E-08	3	38.87	1.39	0.3	1.17	0.47	0.3	4.29	48.231	11.923	15.714	94.325	68.25	112.912	38.786
072802B mottB L2	2	15	2.002E-08	3	25.74	0.26	0.78	1.78	0.41	0.32	2.9	48.338	11.914	14.758	77.725	67.269	111.376	38.767
072802B mottB L3	2	15	2.002E-08	3	21.03	0.91	0.22	1.39	0.44	0.32	6.57	46.762	12.354	15.956	81.628	70.541	110.058	38.989
072802B mottB L4	2	15	2.001E-08	3	30.73	1.11	0.28	1.21	0.47	0.3	6.95	47.329	11.958	15.92	84.748	65.957	113.351	39.148
072802B mottB L5	2	15	2.001E-08	3	32.09	1.57	0.23	1.33	0.45	0.31	6.42	48.999	12.074	16.445	81.894	67.812	108.339	38.823
072802B mottB L6	2	15	2.002E-08	3	39.29	1.22	0.25	1.28	0.46	0.31	5.09	47.897	12.362	16.197	88.221	67.321	109.338	37.966
072802B mottB L7	2	15	2.002E-08	3	76.76	1.4	0.27	1.38	0.43	0.31	5.84	48.231	12.295	15.855	81.152	66.432	107.575	37.998
072802B mottB L8	2	15	2.003E-08	3	27.24	1.34	0.24	1.33	0.45	0.31	5.43	46.645	12.259	16.549	87.557	67.76	109.016	38.174
072802B mottB L9	2	15	2.003E-08	3	56.12	1.24	0.24	1.31	0.45	0.31	5.58	48.563	12.215	15.922	80.726	66.826	108.784	38.991
072802B mottB L10	2	15	2.002E-08	3	38.04	1.32	0.24	1.31	0.45	0.31	5.99	44.413	12.431	16.142	81.868	65.238	112.911	38.43
072802B mottB L11	2	15	2.001E-08	3	78.25	1.39	0.23	1.36	0.45	0.31	5.89	49.221	12.34	16.462	84.157	70.018	111.562	39.057
072802B mottB L12	2	15	2.001E-08	3	36.21	1.2	0.24	1.3	0.45	0.31	5.64	46.988	12.112	16.209	81.787	65.639	112.509	38.969
072802B mottB L13	2	15	2.001E-08	3	148.46	1.03	0.26	1.24	0.46	0.3	5.43	47.329	12.531	16.043	82.079	67.321	112.479	38.524
072802B mottB L14	2	15	2.001E-08	3	40.64	1.23	0.24	1.29	0.45	0.31	6.05	49.76	12.497	16.221	83.876	65.692	109.035	38.847
072802B mottB L15	2	15	2.002E-08	3	66.88	1.37	0.24	1.32	0.45	0.31	5.9	47.782	12.049	16.318	80.162	64.646	110.07	38.042
072802B mottB L16	2	15	2.001E-08	3	24.5	1.08	0.27	1.22	0.46	0.3	5.18	46.645	12.033	16.039	91.655	66.773	110.116	38.311
072802B mottB L17	2	15	2.001E-08	3	59.99	1.03	0.27	1.22	0.47	0.3	6.14	45.245	12.197	15.845	87.529	67.631	112.226	39.038
072802B mottB L18	2	15	2.001E-08	3	23.98	1.66	0.21	1.43	0.43	0.32	5.5	47.668	12.292	16.622	86.538	66.485	111.443	38.078
072802B mottB L19	2	15	2.002E-08	3	18.48	1.86	0.32	1.13	0.47	0.29	4.52	47.668	12.04	15.698	85.483	64.943	113.933	38.686
072802B mottB L20	2	15	2.002E-08	3	72.63	1.13	0.29	1.19	0.47	0.3	7.2	50.511	12.119	15.578	88.659	67.631	113.164	39.208
0728																		

Table C.17. Extended EPMA results for enclave plagioclase (cont)

072804A meg1 L2	2	15	1.993E-08	3	54.66	2.81	0.4	0.82	0.3	0.27	7.66	1.216	24.88	20.448	62.053	110.155	42.774	57.059
072804A meg1 L3	2	15	1.993E-08	3	36.65	2.4	0.33	0.91	0.3	0.25	10.12	1.145	24.902	20.932	57.058	107.712	43.238	59.138
072804A meg1 L4	2	15	1.993E-08	3	55.56	2.67	0.33	0.92	0.31	0.25	11.49	1.341	25.777	21.505	57.058	107.636	43.142	59.107
072804A meg1 L5	2	15	1.993E-08	3	103.02	3.76	0.36	0.86	0.3	0.26	10.65	1.277	25.27	20.823	58.052	106.714	41.953	58
072804A meg1 L6	2	15	1.993E-08	3	197.43	3.09	0.33	0.91	0.31	0.25	10.56	1.244	25.437	21.298	58.932	109.546	42.931	57.15
072804A meg1 L7	2	15	1.994E-08	3	53.31	3.2	0.28	1.07	0.32	0.24	10.96	1.329	26.516	21.35	56.046	108.449	43.496	59.735
072804A meg1 L8	2	15	1.993E-08	3	49.87	2.15	0.34	0.9	0.3	0.26	10.6	1.322	25.443	21.109	56.857	110.139	42.421	58.527
072804A meg1 L9	2	15	1.993E-08	3	106.9	2.08	0.35	0.88	0.3	0.26	10.21	1.329	24.709	20.869	61.822	109.107	43.697	58.502
072804A meg1 L10	2	15	1.993E-08	3	78.57	4.52	0.41	0.82	0.3	0.27	6.81	1.237	25.224	20.626	63.736	107.132	43.266	58.722
072804A meg2 L1	2	15	1.993E-08	3	64.63	3.91	0.29	1.02	0.31	0.25	12.51	1.29	25.434	21.528	56.655	107.536	44.661	60.371
072804A meg2 L2	2	15	1.993E-08	3	251.66	4.84	0.28	1.03	0.32	0.24	9.47	1.366	26.908	21.334	55.739	105.262	43.661	57.601
072804A meg2 L3	2	15	1.993E-08	3	247.21	4.3	0.31	0.95	0.31	0.25	12.44	1.341	26.528	21.145	58.981	106.333	43.163	57.766
072804A meg2 L4	2	15	1.993E-08	3	40.26	3.09	0.34	0.9	0.3	0.26	10.74	1.284	25.522	21.145	58.835	105.526	43.481	58.716
072804A meg2 L5	2	15	1.993E-08	3	353.55	4.63	0.3	0.99	0.31	0.25	10.28	1.284	26.041	21.027	60.702	107.374	42.57	56.045
072804A meg2 L6	2	15	1.993E-08	3	57.73	3.29	0.31	0.96	0.31	0.25	11.15	1.348	25.956	21.412	54.703	105.529	42.355	56.73
072804A meg2 L7	2	15	1.993E-08	3	100	4.47	0.29	1.01	0.31	0.24	11.73	1.421	26.675	21.1	57.656	105.329	43.228	56.763
072804A meg2 L8	2	15	1.993E-08	3	30.01	2.9	0.3	0.98	0.31	0.25	8.58	1.297	26.748	21.624	55.636	107.84	44.857	57.092
072804A meg2 L9	2	15	1.993E-08	3	91.43	2.05	0.37	0.85	0.3	0.26	10.73	1.29	26.039	20.007	54.859	108.085	43.428	57.905
072804A meg2 L10	2	15	1.993E-08	3	155.95	1.07	0.46	0.81	0.29	0.27	10.23	1.257	26.177	20.407	58.199	109.151	42.024	57.54
072804A mtrx1core	2	15	1.993E-08	3	146.97	2.68	0.36	0.86	0.3	0.26	9.1	1.316	24.855	20.532	61.358	107.365	42.594	58.152
072804A mtrx1rim1	2	15	1.993E-08	3	36.11	2.62	0.35	0.89	0.3	0.26	6.21	1.257	26.05	21.116	60.133	106.577	42.704	57.532
072804A mtrx1rim2	2	15	1.993E-08	3	100	1.97	0.45	0.8	0.29	0.27	4.95	1.379	25.425	20.789	64.849	109.851	42.61	57.601
072804A mtrx2core	2	15	1.993E-08	3	106.86	4.38	0.35	0.86	0.3	0.26	14.69	1.23	25.015	20.686	57.058	108.037	42.353	60.976
072804A mtrx2rim	2	15	1.993E-08	3	92.28	3.32	0.44	0.79	0.29	0.27	14.79	1.303	25.621	20.213	63.781	111.185	42.305	57.288
072802C zoned L1	3	15	2.002E-08	3	37.09	2.16	0.2	1.53	0.42	0.32	7.19	47.445	12.421	16.88	80.805	67.554	111.264	39.359
072802C zoned L2	3	15	2.002E-08	3	8.17	0.79	0.21	1.62	0.43	0.32	1.61	46.535	12.468	16.683	71.469	66.116	107.889	40.77
072802C zoned L3	3	15	2.001E-08	3	28.72	1.81	0.2	1.57	0.43	0.32	6.9	47.668	12.604	16.917	81.946	67.605	108.016	40.391
072802C zoned L4	3	15	2.001E-08	3	38.16	1.94	0.19	1.59	0.42	0.32	6.34	48.999	12.496	17.054	73.348	68.53	107.662	39.726
072802C zoned L5	3	15	2.001E-08	3	14.92	1.32	0.21	1.58	0.42	0.32	3.77	45.486	12.418	17.108	75.41	69.165	106.725	38.806
072802C zoned L6	3	15	2.002E-08	3	27.82	1.83	0.2	1.6	0.42	0.32	6.12	50.403	12.459	16.77	78.8	68.069	109.336	39.364
072802C zoned L7	3	15	2.002E-08	3	29.7	1.94	0.2	1.58	0.42	0.32	6.61	48.893	12.361	16.97	84.619	66.063	109.685	40.529
072802C zoned L8	3	15	2.001E-08	3	24.68	2.15	0.19	1.59	0.42	0.32	6.34	48.781	12.343	17.145	73.702	66.747	111.171	39.281
072802C zoned L9	3	15	2.001E-08	3	78.83	1.43	0.24	1.29	0.45	0.31	8.23	47.782	11.966	16.163	77.28	65.904	109.917	38.301
072802C zoned L10	3	15	2.001E-08	3	88.45	1.11	0.28	1.21	0.47	0.3	5.55	49.87	12.308	15.729	83.797	64.267	112.689	38.675
072802C mtrx1 core	3	15	2.002E-08	3	21.1	1.55	0.23	1.37	0.44	0.31	7.32	47.445	12.053	16.377	77.503	66.222	110.508	38.765
072802C mtrx1rima	3	15	2.002E-08	3	100	1.26	0.27	1.21	0.47	0.3	4.85	49.326	12.393	16.003	82.314	65.452	110.445	38.501
072802C mtrx1rimb	3	15	2.003E-08	3	82.13	2.63	0.26	1.25	0.46	0.31	4.18	48.004	12.224	15.967	85.911	69.543	113.749	39.402
072802C mtrx2core	3	15	2.002E-08	3	20.08	2.11	0.2	1.52	0.43	0.32	5.69	46.879	12.56	16.88	78.719	68.3	110.071	39.005
072802C mtrx2rima	3	15	2.002E-08	3	66	1.37	0.3	1.15	0.48	0.3	4.17	47.105	12.166	15.354	75.611	66.8	113.05	38.702
072802C mtrx2rimb	3	15	2.002E-08	3	55.83	1.16	0.3	1.16	0.48	0.3	6.42	44.413	12.104	15.562	80.831	67.087	109.896	38.298

Table C.18. Extended EPMA results for enclave pyroxene

	Enclave Group	TiO2 wt%	MnO wt%	Cr2O3 wt%	K2O wt%	CaO wt%	Na2O wt%	Al2O3 wt%	SiO2 wt%	MgO wt%	FeO wt%	Total wt%	Ti atFrac	Mn atFrac	Cr atFrac	K atFrac	Ca atFrac	Na atFrac	Al atFrac	Si atFrac	Mg atFrac	Fe atFrac
071410 cpx inc1	1	0.115	0.37	0.003	0.004	21.823	0.426	0.722	52.215	14.775	9.146	99.597	0.003	0.012	0	0	0.879	0.031	0.032	1.962	0.828	0.287
071410 cpx inc 3	1	0.147	0.412	-0.007	0.005	22.199	0.467	0.775	51.848	14.281	9.274	99.402	0.004	0.013	0	0	0.898	0.034	0.034	1.958	0.804	0.293
071410 cpx inc 2	1	0.166	0.412	-0.004	-0.001	21.755	0.392	0.846	51.819	14.452	9.203	99.04	0.005	0.013	0	0	0.882	0.029	0.038	1.96	0.815	0.291
071410 cpx inc 4	1	0.437	0.35	0.01	0.216	11.867	0.571	3.198	51.279	16.487	12.076	96.491	0.013	0.011	0	0.01	0.485	0.042	0.144	1.957	0.938	0.385
71410 Cpx 1 L1	1	0.167	0.26	0.014	0.005	22.076	0.443	1.079	53.529	15.724	6.77	100.067	0.005	0.008	0	0	0.873	0.032	1.975	0.047	0.865	0.209
71410 Cpx 1 L2	1	1.363	0.173	0.023	0.583	11.763	1.641	6.255	49.137	17.792	8.669	97.399	0.038	0.005	0.001	0.028	0.473	0.119	1.844	0.277	0.995	0.272
71410 Cpx 1 L3	1	1.517	0.176	0.023	0.588	11.838	1.71	6.633	48.538	17.275	9.487	97.785	0.043	0.006	0.001	0.028	0.477	0.125	1.824	0.294	0.968	0.298
71410 Cpx 1 L4	1	1.536	0.15	0.003	0.436	12.682	1.54	5.511	49.623	17.509	8.835	97.825	0.043	0.005	0	0.021	0.509	0.112	1.858	0.243	0.977	0.277
71410 Cpx 1 L5	1	0.745	0.197	0.008	0.092	18.194	0.706	2.232	51.756	16.072	7.611	97.612	0.021	0.006	0	0.004	0.734	0.052	1.949	0.099	0.902	0.24
71410 Cpx 1 L6	1	0.147	0.347	0.007	0.003	21.194	0.457	0.819	53.361	14.678	8.981	99.994	0.004	0.011	0	0	0.845	0.033	1.986	0.036	0.814	0.28
71410 Cpx 1 L7	1	0.217	0.356	-0.014	0.008	21.112	0.445	1.036	53.054	14.116	9.714	100.044	0.006	0.011	0	0	0.844	0.032	1.98	0.046	0.785	0.303
71410 Cpx 1 L8	1	0.182	0.405	-0.005	0.004	21.485	0.433	0.997	53.214	14.743	8.51	99.969	0.005	0.013	0	0	0.856	0.031	1.979	0.044	0.817	0.265
71410 Cpx 1 L9	1	0.333	0.446	0.164	0.1	20.096	0.558	1.775	52.546	14.471	9.064	99.554	0.009	0.014	0.005	0.005	0.804	0.04	1.963	0.078	0.806	0.283
71410 Cpx 1 L10	1	0.161	0.49	0.17	0.004	21.453	0.463	0.959	52.973	14.242	9.025	99.94	0.004	0.015	0.005	0	0.858	0.034	1.978	0.042	0.793	0.282
71410 Cpx 2core	1	0.129	0.494	-0.011	-0.006	21.214	0.448	0.59	53.094	14.181	9.482	99.616	0.004	0.016	0	0	0.852	0.033	1.99	0.026	0.792	0.297
71410 Cpx 2rim	1	0.097	0.591	0.008	0.005	21.39	0.397	0.59	53.317	13.881	9.676	99.954	0.003	0.019	0	0	0.857	0.029	1.994	0.026	0.774	0.303
072802B cpxccoreA	2	0.169	0.272	0.023	-0.003	21.47	0.375	1.051	51.543	14.309	10.082	99.291	0.005	0.009	0.001	0	0.87	0.027	0.047	1.95	0.807	0.319
072802B cpxccoreB	2	0.261	0.308	0.033	0.006	21.661	0.407	1.201	51.874	14.319	10.541	100.61	0.007	0.01	0.001	0	0.869	0.03	0.053	1.941	0.799	0.33
072802B cpxccoreC	2	0.097	0.277	0.086	-0.001	23.115	0.288	0.722	51.91	14.187	8.906	99.587	0.003	0.009	0.003	0	0.933	0.021	0.032	1.956	0.797	0.281
072802B cpxccoreD	2	0.139	0.303	0.005	-0.002	21.905	0.405	0.729	51.954	14.026	10.142	99.608	0.004	0.01	0	0	0.886	0.03	0.032	1.962	0.789	0.32
072802B cpxclnArim	2	0.157	0.339	0.006	0.001	21.464	0.422	0.674	51.701	13.974	10.667	99.406	0.004	0.011	0	0	0.872	0.031	0.03	1.96	0.79	0.338
072802B cpxclnBcore	2	0.123	0.281	0.009	-0.002	21.842	0.388	0.703	51.92	14.244	9.998	99.507	0.004	0.009	0	0	0.884	0.028	0.031	1.961	0.802	0.316
072802B cpx clnBrim	2	0.142	0.435	-0.015	-0.001	21.88	0.398	0.728	51.821	13.752	10.48	99.619	0.004	0.014	-0.001	0	0.887	0.029	0.032	1.961	0.776	0.332
072802B cpxinc1	2	0.356	0.302	0.003	0.005	21.663	0.467	1.475	50.849	13.654	10.414	99.187	0.01	0.01	0	0	0.882	0.034	0.066	1.933	0.774	0.331
072802B cpxinc2	2	0.315	0.301	0.025	0.004	21.851	0.425	1.172	51.279	13.674	10.113	99.158	0.009	0.01	0.001	0	0.889	0.031	0.052	1.947	0.774	0.321
072802B cpxinc3	2	0.344	0.336	0.001	0.002	21.182	0.419	1.263	51.458	13.961	10.826	99.792	0.01	0.011	0	0	0.857	0.031	0.056	1.943	0.786	0.342
072802B cpxinc4a	2	0.214	0.707	-0.005	0.004	0.901	0.012	0.699	50.131	19.56	25.857	98.082	0.006	0.023	0	0	0.038	0.001	0.032	1.951	1.135	0.842
072802B cpxinc4b	2	0.28	0.314	-0.009	0.009	21.689	0.456	1.216	51.099	13.691	10.275	99.021	0.008	0.01	0	0.001	0.884	0.034	0.054	1.944	0.776	0.327
072802B cpxccoreA	2	0.169	0.272	0.023	-0.003	21.47	0.375	1.051	51.543	14.309	10.082	99.291	0.005	0.009	0.001	0	0.87	0.027	0.047	1.95	0.807	0.319
072802B cpxccoreB	2	0.261	0.308	0.033	0.006	21.661	0.407	1.201	51.874	14.319	10.541	100.61	0.007	0.01	0.001	0	0.869	0.03	0.053	1.941	0.799	0.33
072802B cpxclnAcore	2	0.139	0.303	0.005	-0.002	21.905	0.405	0.729	51.954	14.026	10.142	99.608	0.004	0.01	0	0	0.886	0.03	0.032	1.962	0.789	0.32
072802B cpxclnArim	2	0.157	0.339	0.006	0.001	21.464	0.422	0.674	51.701	13.974	10.667	99.406	0.004	0.011	0	0	0.872	0.031	0.03	1.96	0.79	0.338
072802B cpxclnBcore	2	0.123	0.281	0.009	-0.002	21.842	0.388	0.703	51.92	14.244	9.998	99.507	0.004	0.009	0	0	0.884	0.028	0.031	1.961	0.802	0.316
072802B cpx clnBrim	2	0.142	0.435	-0.015	-0.001	21.88	0.398	0.728	51.821	13.752	10.48	99.619	0.004	0.014	-0.001	0	0.887	0.029	0.032	1.961	0.776	0.332
072804A cpx1core	2	0.086	0.407	0.194	0.13	11.134	0.322	54.126	1.835	17.812	10.983	97.03	0.002	0.013	0.006	0.006	0.447	0.023	2.026	0.081	0.994	0.344
072804A cpx1rim2	2	0.445	0.342	0.292	0.287	11.837	0.503	51.261	4.188	15.446	12.738	97.339	0.013	0.011	0.009	0.014	0.481	0.037	1.943	0.187	0.873	0.404
072804A cpx1rim1	2	0.248	0.458	0.113	0.097	11.592	0.265	54.395	1.72	17.457	11.391	97.736	0.007	0.014	0.003	0.005	0.463	0.019	2.027	0.075	0.97	0.355
072802C cpxccore	3	0.167	0.319	-0.008	-0.002	21.887	0.4	0.822	51.406	14.67	9.515	99.175	0.005	0.01	0	0	0.888	0.029	0.037	1.947	0.828	0.301
072802C cpxccore	3	0.165	0.316	0.024	0.002	22.491	0.408	0.848	51.907	14.279	9.351	99.79	0.005	0.01	0.001	0	0.907	0.03	0.038	1.953	0.801	0.294
072802C cpxcln1core	3	0.177	0.28	-0.004	-0.003	21.817	0.39	0.847	49.467	14.199	9.197	96.367	0.005	0.009	0	0	0.914	0.03	0.039	1.933	0.827	0.301
072802C cpxcln1rim	3	0.165	0.264	0.014	0.006	21.808	0.337	0.771	51.94	14.678	9.51	99.492	0.005	0.008	0	0	0.88	0.025	0.034	1.957	0.824	0.3

Table C.19. Extended EPMA results for enclave biotite

Enclave Group	Acc. V.	Beam Curr(A)	Beam Dia(um)	F SD(%)	Ti SD(%)	Mn SD(%)	Cl SD(%)	K SD(%)	Si SD(%)	Al SD(%)	Mg SD(%)	Fe SD(%)	F DL(ppm-1s)	Ti DL(ppm-1s)	Mn DL(ppm-1s)	Cl DL(ppm-1s)	K DL(ppm-1s)	Si DL(ppm-1s)	Al DL(ppm-1s)	Mg DL(ppm-1s)	Fe DL(ppm-1s)
071410 bt 1 core	1	15	1.992E-08	10	100	1.65	6.93	7.66	0.36	0.39	0.38	0.45	179.466	1.464	46.492	25.603	28.499	102.315	38.451	34.907	65.446
071410 bt 1 rim	1	15	1.992E-08	10	100	1.56	5.53	9.64	0.36	0.39	0.38	0.45	176.343	1.432	44.111	27.328	28.178	103.976	37.48	36.086	65.598
071410 bt 2 core	1	15	1.993E-08	10	100	1.65	5.67	8.05	0.35	0.39	0.38	0.46	176.472	1.36	43.702	26.631	29.811	104.99	38.511	33.872	65.157
071410 bt 2rim 2	1	15	1.992E-08	10	100	1.57	6.54	8.73	0.36	0.39	0.38	0.46	176.863	1.409	48.507	28.008	28.571	108.431	38.673	34.833	66.798
071410 bt 2rim1	1	15	1.992E-08	10	100	1.59	5.52	8.97	0.36	0.39	0.38	0.46	178.003	1.495	43.702	27.912	28.973	103.475	38.707	35.332	65.345
072804A bcore	2	15	1.994E-08	10	100	1.73	7.93	11.04	0.36	0.39	0.37	0.47	176.067	1.534	45.316	26.122	28.839	104.551	39.011	36.594	65.917
072804A btrim1	2	15	1.994E-08	10	100	1.87	6.44	13.34	0.39	0.4	0.36	0.46	179.882	1.461	45.052	27.719	28.781	103.924	37.611	36.299	66.967

Table C.20. Extended EPMA results for enclave hornblende

Enclave Group	Acc. V.	Beam Curr(A)	Beam Dia(um)	Ti SD(%)	Mn SD(%)	Cr SD(%)	K SD(%)	Ca SD(%)	Na SD(%)	Al SD(%)	Si SD(%)	Mg SD(%)	Fe SD(%)	Ti DL(ppm-1s)	Mn DL(ppm-1s)	Cr DL(ppm-1s)	K DL(ppm-1s)	Ca DL(ppm-1s)	Na DL(ppm-1s)	Al DL(ppm-1s)	Si DL(ppm-1s)	Mg DL(ppm-1s)	Fe DL(ppm-1s)
072802HbblrimA	2	15	2.015E-08	1	2.05	3.09	75.96	1.03	0.2	4.15	1.06	0.34	0.32	50.511	32.163	39.356	13.294	17.398	71.498	61.602	108.706	27.916	41.973
072802B hbbllean1core	2	15	2.016E-08	1	2.05	3.82	55.24	1.03	0.2	3.67	1.06	0.34	0.31	51.457	33.429	38.313	13.189	17.819	68.57	60.051	109.884	27.646	43.273
072802B hbbllean1rim	2	15	2.016E-08	1	2.06	2.97	213.69	1.02	0.2	3.86	1.08	0.34	0.32	49.87	32.309	38.969	13.15	17.92	77.112	67.087	108.951	27.833	42.933
072802B cpcorehbblrim3	2	15	2.017E-08	1	2.18	2.91	92.67	1.05	0.2	3.91	1.08	0.34	0.32	50.721	32.138	40.424	13.22	17.534	70.677	62.837	110.903	28.499	42.803
072802B hbbllean2core	2	15	2.017E-08	1	2.22	3.13	189.07	1.02	0.19	4.35	1.08	0.34	0.32	50.511	32.79	39.554	12.948	18.011	68.313	62.587	105.526	27.359	43.958
072802B hbbllean2rim	2	15	2.017E-08	1	2.29	2.75	100	1.09	0.2	4.02	1.11	0.34	0.32	51.457	32.526	40.305	12.945	17.878	72.993	63.336	104.871	27.419	42.632
072802C cpcorehbblrim1	3	15	2.019E-08	1	2.02	4.11	155.86	0.94	0.19	3.58	1.01	0.34	0.31	51.769	31.721	42.052	13.367	18.023	66.163	59.876	110.403	27.482	42.737
072802C cpcorehbblrim2	3	15	2.017E-08	1	2.05	3.02	79.85	1.06	0.2	4.05	1.05	0.34	0.31	50.511	31.172	39.194	13.183	17.88	71.104	61.913	108.209	27.605	43.405
072802C hbbllean1core	3	15	2.017E-08	1	1.96	3.7	58.61	0.92	0.2	3.78	1.01	0.34	0.31	49.221	32.598	37.868	13.327	17.965	73.171	61.97	106.406	28.023	42.273
072802C hbbllean1rim	3	15	2.017E-08	1	2.06	3.24	100	1.03	0.2	4.02	1.02	0.34	0.31	52.282	30.895	40.266	13.751	17.852	71.469	59.613	109.402	27.112	42.672
072802C hbbllean2core	3	15	2.018E-08	1	2.18	3.17	100	1.07	0.2	3.76	1.07	0.34	0.31	52.588	31.991	39.031	13.281	17.886	70.097	59.876	106.932	27.995	41.362
072802C hbbllean2rim	3	15	2.017E-08	1	2.29	3.41	123.4	1.1	0.2	4.47	1.09	0.34	0.33	46.645	31.894	38.06	13.025	17.614	72.964	58.638	109.309	26.891	42.895

Table C.21. Extended EPMA results for host rock plagioclase

	Unit	Acc V.	Beam Curr	Beam Dia(um)	Ti SD(%)	K SD(%)	Ca SD(%)	Na SD(%)	Al SD(%)	Si SD(%)	Fe SD(%)	Ti DL(ppm-1s)	K DL(ppm-1s)	Ca DL(ppm-1s)	Na DL(ppm-1s)	Al DL(ppm-1s)	Si DL(ppm-1s)	Fe DL(ppm-1s)
071406 Plag1core	Endave-Rich Tonalite	15	1.99E-08	3	100	1.77	0.4	0.83	0.27	0.3	6.63	1.36	25.41	20.739	60.038	1.36	20.739	1.36
071406 Plag1rim1	Endave-Rich Tonalite	15	1.99E-08	3	42.32	2.24	0.46	0.79	0.27	0.29	6.58	1.167	25.098	20.549	63.646	1.167	20.549	1.167
071406 Plag1rim2	Endave-Rich Tonalite	15	1.99E-08	3	92.28	1.88	0.43	0.81	0.27	0.29	7.13	1.303	25.184	20.471	61.077	1.303	20.471	1.303
071406 Plag2core	Endave-Rich Tonalite	15	1.99E-08	3	39.47	1.87	0.42	0.81	0.27	0.29	7.48	1.29	25.111	20.062	62.421	1.29	20.062	1.29
071406 Plag2rim1	Endave-Rich Tonalite	15	1.99E-08	3	43.39	1.64	0.45	0.81	0.27	0.29	7.16	1.203	25.117	20.609	63.871	1.203	20.609	1.203
071406 Plag2rim2	Endave-Rich Tonalite	15	1.99E-08	3	101.32	3.97	0.47	0.77	0.27	0.29	5.8	1.348	24.991	21.211	62.878	1.348	21.211	1.348
Core 2 QdxPlagcoreA	Endave-Rich Tonalite	15	1.99E-08	3	68.32	1.97	0.3	1.17	0.49	0.3	5.18	48.893	11.987	15.525	85.051	48.893	15.525	48.893
Core 2 QdxPlagrimA	Endave-Rich Tonalite	15	1.99E-08	3	55.29	1.86	0.29	1.19	0.48	0.3	6.61	47.782	12.252	15.831	89.508	47.782	15.831	47.782
Core 2 QdxPlagcoreB	Endave-Rich Tonalite	15	1.99E-08	3	55.65	2.1	0.28	1.18	0.48	0.3	4.86	48.118	12.106	15.465	86.936	48.118	15.465	48.118
Core 2 QdxPlagrimB	Endave-Rich Tonalite	15	1.99E-08	3	50.64	1.66	0.3	1.19	0.48	0.3	6.41	45.719	11.99	15.558	89.966	45.719	15.558	45.719
Core 2 QdxPlagcoreC	Endave-Rich Tonalite	15	1.99E-08	3	421.9	1.21	0.26	1.27	0.47	0.31	5.13	48.563	12.355	16.013	90.492	48.563	16.013	48.563
Core 2 QdxPlagrimC	Endave-Rich Tonalite	15	1.98E-08	3	64.95	1.7	0.31	1.18	0.49	0.3	3.18	46.299	11.962	15.451	86.563	46.299	15.451	46.299
Core 2 Plagcotactqdxrim	Endave-Rich Tonalite	15	1.97E-08	3	100	1.99	0.3	1.17	0.49	0.3	6.04	46.645	11.886	15.609	83.54	46.645	15.609	46.645
Core 2 Plagcotactqdxcore	Endave-Rich Tonalite	15	1.97E-08	3	211.66	1.49	0.29	1.19	0.49	0.31	6.65	48.451	12.032	15.66	85.66	48.451	15.66	48.451
Core 2 QdPlagcoreA	Endave-Poor Tonalite	15	1.98E-08	3	116	2.25	0.27	1.21	0.48	0.31	4.91	47.329	12.24	15.841	86.086	47.329	15.841	47.329
Core 2 QdPlagrimA	Endave-Poor Tonalite	15	1.98E-08	3	86.2	2.76	0.29	1.19	0.49	0.31	6.19	46.535	12.081	15.383	84.261	46.535	15.383	46.535
Core 2 QdPlagcoreB	Endave-Poor Tonalite	15	1.98E-08	3	100	2.82	0.33	1.13	0.5	0.3	5.51	48.338	12.017	15.229	81.55	48.338	15.229	48.338
Core 2 QdPlagrimB	Endave-Poor Tonalite	15	1.98E-08	3	184.46	2.23	0.3	1.18	0.49	0.3	6.92	50.613	11.718	15.615	84.081	50.613	15.615	50.613
Core 2 QdPlagcoreC	Endave-Poor Tonalite	15	1.97E-08	3	100	2.9	0.32	1.15	0.49	0.3	5.31	46.988	12.182	15.422	82.655	46.988	15.422	46.988
Core 2 QdPlagrimC	Endave-Poor Tonalite	15	1.97E-08	3	39.37	1.99	0.29	1.18	0.49	0.31	7.34	48.004	12.173	15.595	88.365	48.004	15.595	48.004
Core 2 Plagntctqdxcore	Endave-Poor Tonalite	15	1.97E-08	3	76.56	3.3	0.3	1.16	0.49	0.3	5.48	49.87	12.144	15.258	89.605	49.87	15.258	49.87
Core 2 Plagntctqdxrim	Endave-Poor Tonalite	15	1.97E-08	3	251.6	3.32	0.29	1.18	0.48	0.3	8.09	48.004	12.107	15.698	85.508	48.004	15.698	48.004
16071901 gmplag1core	Endave-Poor Tonalite	15	2E-08	3	124.92	2.35	0.26	1.25	0.47	0.31	4.85	48.231	12.598	15.595	87.505	48.231	15.595	48.231
16071901 gmplag1rim	Endave-Poor Tonalite	15	2E-08	3	31.54	2.27	0.26	1.66	0.46	0.31	4.38	45.838	12.01	15.954	73.612	45.838	15.954	45.838
16071901 gmplag2core	Endave-Poor Tonalite	15	2E-08	3	52.89	1.62	0.28	1.18	0.48	0.31	5.42	44.29	12.255	15.745	86.013	44.29	15.745	44.29
16071901 gmplag2rim	Endave-Poor Tonalite	15	2E-08	3	131.99	2.72	0.27	1.2	0.47	0.31	6.4	48.004	12.082	16.021	81.813	48.004	16.021	48.004
071408 matrixplag2core	Endave-Poor Tonalite	15	1.99E-08	3	78.6	2.38	0.32	0.94	0.25	0.31	9.37	1.31	25.126	20.965	58.737	1.31	20.965	1.31
071408 matrixplag2rim	Endave-Poor Tonalite	15	1.99E-08	3	100	1.95	0.4	0.84	0.27	0.3	8.73	1.322	25.031	20.803	62.787	1.322	20.803	1.322
071408 mgplag1	Endave-Poor Tonalite	15	1.99E-08	3	100	1.94	0.4	0.84	0.27	0.3	7.65	1.31	25.443	20.233	60.276	1.31	20.233	1.31
071408 mgplag2	Endave-Poor Tonalite	15	1.99E-08	3	100	1.99	0.38	0.86	0.26	0.3	8.51	1.354	25.437	20.905	60.937	1.354	20.905	1.354
071408 mgplag3	Endave-Poor Tonalite	15	1.99E-08	3	246.08	1.88	0.39	0.85	0.27	0.3	8.02	1.335	25.54	20.404	57.755	1.335	20.404	1.335
071408 mgplag4	Endave-Poor Tonalite	15	1.99E-08	3	99.55	0.28	10.63	3.14	0.3	0.28	17.72	1.322	27.934	21.531	49.831	1.322	21.531	1.322
071408 mgplag5	Endave-Poor Tonalite	15	1.99E-08	3	68.63	2.27	0.34	0.9	0.26	0.3	7.61	1.316	26.365	21.047	56.554	1.316	21.047	1.316
071408 mgplag6	Endave-Poor Tonalite	15	1.99E-08	3	48.17	2.2	0.34	0.91	0.26	0.3	7.56	1.271	25.297	21.207	55.275	1.271	21.207	1.271
071408 mgplag7	Endave-Poor Tonalite	15	1.99E-08	3	79.3	1.98	0.35	0.89	0.26	0.3	6.39	1.322	25.857	20.609	54.65	1.322	20.609	1.322
071408 mgplag8	Endave-Poor Tonalite	15	1.99E-08	3	51.72	2.03	0.35	0.92	0.26	0.31	2.58	1.284	25.316	21.142	58.101	1.284	21.142	1.284
071408 mgplag9	Endave-Poor Tonalite	15	1.99E-08	3	66.41	2.17	0.34	0.9	0.26	0.3	7.76	1.391	25.654	21.305	59.271	1.391	21.305	1.391
071408 mgplag10	Endave-Poor Tonalite	15	1.99E-08	3	71.29	2.15	0.36	0.88	0.26	0.3	8.83	1.372	25.126	20.932	59.174	1.372	20.932	1.372
071408 mtrxplag1core	Endave-Poor Tonalite	15	1.99E-08	3	46.65	2.86	0.3	1	0.25	0.31	5.79	1.31	26.192	21.165	54.493	1.31	21.165	1.31
071408 mtrxplag1rim	Endave-Poor Tonalite	15	1.99E-08	3	357.07	1.92	0.42	0.82	0.27	0.3	10.02	1.297	24.88	21.093	59.943	1.297	21.093	1.297
071408 mtrxplag2L1	Endave-Poor Tonalite	15	1.99E-08	3	38.97	2.48	0.36	0.88	0.26	0.3	9.87	1.271	25.845	21.106	58.64	1.271	21.106	1.271
071408 mtrxplag2L2	Endave-Poor Tonalite	15	1.99E-08	3	67.85	2.44	0.33	0.92	0.26	0.31	10.55	1.237	25.531	21.014	58.15	1.237	21.014	1.237
071408 mtrxplag2L3	Endave-Poor Tonalite	15	1.99E-08	3	88.83	2.39	0.33	0.93	0.25	0.31	9.31	1.251	26.221	21.308	57.904	1.251	21.308	1.251
071408 mtrxplag2L4	Endave-Poor Tonalite	15	1.99E-08	3	78.96	2.18	0.34	0.91	0.26	0.3	9.63	1.244	25.212	21.243	59.512	1.244	21.243	1.244
071408 mtrxplag2L5	Endave-Poor Tonalite	15	1.99E-08	3	40.82	2.34	0.34	0.92	0.26	0.31	8.93	1.23	26.221	20.972	57.507	1.23	20.972	1.23
071408 mtrxplag2L6	Endave-Poor Tonalite	15	1.99E-08	3	70.36	2.07	0.35	0.89	0.26	0.3	7.66	1.223	25.944	20.753	57.358	1.223	20.753	1.223
071408 mtrxplag2L7	Endave-Poor Tonalite	15	1.99E-08	3	34.83	2.44	0.35	1.19	0.29	0.36	9.26	1.203	23.587	20.636	43.846	1.203	20.636	1.203
071408 mtrxplag2L8	Endave-Poor Tonalite	15	1.99E-08	3	56.14	3.26	0.37	0.86	0.26	0.3	14.01	1.203	24.641	20.437	57.606	1.203	20.437	1.203
071408 mtrxplag2L9	Endave-Poor Tonalite	15	1.99E-08	3	143.53	3.39	0.39	0.84	0.27	0.3	8.32	1.284	26.012	20.915	56.3	1.284	20.915	1.284
071408 mtrxplag2L10	Endave-Poor Tonalite	15	1.99E-08	3	154.36	2.17	0.38	0.85	0.26	0.3	13.06	1.244	26.359	20.424	57.656	1.244	20.424	1.244
16071901 plagacc1core	Contact	15	2E-08	3	18.55	1.57	0.22	1.4	0.45	0.32	4.64	45.719	12.457	16.723	83.097	45.719	16.723	45.719
16071901 plagacc1rim	Contact	15	2E-08	3	68.61	2.79	0.3	1.16	0.48	0.3	8.05	49.11	12.28	15.562	81.257	49.11	15.562	49.11
16071901 plagacc2core	Contact	15	2E-08	3	19.78	1.62	0.23	1.39	0.45	0.32	5.69	49.221	12.369	16.316	84.157	49.221	16.316	49.221
16071901 plagacc2rim	Contact	15	2E-08	3	100	3.47	0.29	1.18	0.47	0.3	5.84	47.782	12.256	15.809	81.761	47.782	15.809	47.782

Table C.22. Extended EPMA results for host rock pyroxene

Unit	Acc V.	Beam Cu	Beam Dia(um)	Ti SD(%)	Mn SD(%)	Cr SD(%)	K SD(%)	Ca SD(%)	Na SD(%)	Al SD(%)	Si SD(%)	Mg SD(%)	Fe SD(%)	Ti DL(ppm)	Mn DL(ppm)	Cr DL(ppm)	K DL(ppm)	Ca DL(ppm)	Na DL(ppm)	Al DL(ppm)	Si DL(ppm)	Mg DL(ppm)	Fe DL(ppm)		
071406 cpx 1 core	Enclave-Rich	Tonalite	15	1.99E-08	3	15.09	3.85	345.74	14.05	0.2	3.85	2.07	0.32	0.42	0.59	1.50669	42.38099	53.80201	78.3791	23.60416	48.01858	33.49203	112.623	38.24176	62.34993362
071406 cpx 1 rim 1	Enclave-Rich	Tonalite	15	1.99E-08	3	19.56	3.07	223.68	15.62	0.2	4.25	2.21	0.31	0.41	0.65	1.414649	46.03754	53.63035	27.90584	23.7209	47.47937	32.98055	109.2888	35.53067	62.85949707
071406 cpx 1 rim 2	Enclave-Rich	Tonalite	15	1.99E-08	3	13.07	3.28	999.49	27.62	0.2	4.41	2.23	0.31	0.41	0.65	1.341434	45.77736	54.16108	27.79978	24.12538	45.82367	34.43113	112.6111	36.84303	62.44151739
071406 cpx 2 core	Enclave-Rich	Tonalite	15	1.99E-08	3	11.03	3.72	128.73	47.63	0.2	4.32	1.87	0.31	0.41	0.62	1.384553	45.18497	53.718	27.24308	24.12817	43.4524	34.2673	107.0155	35.65845	64.88999994
071406 cpx 2 rim 1	Enclave-Rich	Tonalite	15	1.99E-08	3	18.44	4.12	71.47	100	0.2	4.43	2	0.31	0.41	0.65	1.420521	43.15167	51.46003	28.16419	23.84012	44.94114	32.66101	107.2809	35.14804	64.57508313
071406 cpx 2 rim 2	Enclave-Rich	Tonalite	15	1.99E-08	3	14.24	3.71	286.11	785.92	0.2	4.38	2.01	0.31	0.41	0.63	1.296687	44.78571	55.34681	28.07916	23.64497	49.54336	33.52218	111.9679	35.66494	60.24719238
Core 2 qdx cpx corroded 1 core	Enclave-Rich	Tonalite	15	1.99E-08	3	46.28	3.06	20.73	8.84	0.18	13.85	3.25	0.33	0.27	0.44	52.0782	31.17249	36.89701	12.82777	17.95749	68.44175	57.28138	103.9428	28.12892	41.70980453
Core 2 qdx cpx corroded 1 rim	Enclave-Rich	Tonalite	15	1.99E-08	3	15.43	2.61	98.44	5.53	0.19	14.46	3.05	0.32	0.28	0.4	49.4363	31.34848	39.13264	12.87576	17.86701	61.42137	56.60641	105.2786	27.13774	42.3760376
Core 2 qdx cpx corroded 2 core	Enclave-Rich	Tonalite	15	1.99E-08	3	14.95	2.87	35.63	6.52	0.19	17.06	2.97	0.32	0.28	0.4	51.5569	31.04704	37.42258	13.16447	17.71493	66.81365	61.71527	110.5491	28.72813	41.2088876
Core 2 qdx cpx corroded 2 rim	Enclave-Rich	Tonalite	15	1.99E-08	3	14.57	2.86	114.51	8.67	0.16	14.89	3.67	0.35	0.29	0.45	49.10999	30.79309	37.24948	12.72771	17.84376	66.61869	59.75928	103.5393	28.24741	41.6447258
071408 cpx 1 core	Enclave-Poor	Tonalite	15	1.99E-08	3	9.04	5.37	212.46	139.72	0.2	5.18	1.8	0.32	0.41	0.6	1.366213	46.55548	53.80201	28.58189	23.24707	46.32041	34.16796	112.2919	34.34123	61.88833618
071408 cpx 1 rim	Enclave-Poor	Tonalite	15	1.99E-08	3	8.64	4.25	100	52.19	0.2	5.06	1.58	0.32	0.41	0.83	1.384553	45.05162	56.3476	26.90522	23.19059	50.62888	33.74073	110.4703	36.21409	64.38828613
071408 cpx 2 Line 001	Enclave-Poor	Tonalite	15	1.99E-08	3	6.7	6.92	100	87.58	0.2	4.99	1.16	0.32	0.4	0.7	1.353787	46.16805	53.69698	27.0794	24.06235	46.93396	33.24665	108.5544	37.61135	63.64807129
071408 cpx 2 Line 002	Enclave-Poor	Tonalite	15	1.99E-08	3	5.78	6.03	30.26	417.75	0.2	4.6	1.05	0.32	0.4	0.7	1.461308	45.58076	52.20922	28.46607	24.13977	44.81385	33.66931	106.8258	34.96307	63.40715027
071408 cpx 2 Line 003	Enclave-Poor	Tonalite	15	1.99E-08	3	5.88	6.47	67.05	56.33	0.2	4.98	1.08	0.32	0.4	0.7	1.467165	44.98579	53.03403	27.85074	23.4897	47.89928	33.61885	107.7604	35.10216	64.56278992
071408 cpx 2 Line 004	Enclave-Poor	Tonalite	15	1.99E-08	3	4.31	6.87	60.68	33.9	0.2	4.56	0.96	0.32	0.4	0.72	1.270553	44.65115	55.45211	28.10917	23.55426	49.65871	35.66186	105.9419	35.45573	63.68282318
071408 cpx 2 Line 005	Enclave-Poor	Tonalite	15	1.99E-08	3	5.23	6.75	38.16	100	0.2	5.18	1.05	0.32	0.39	0.69	1.384553	45.97313	53.92779	28.53619	23.32141	46.0727	34.24273	112.8556	35.50245	65.5745163
071408 cpx 2 Line 006	Enclave-Poor	Tonalite	15	1.99E-08	3	4.64	6.81	14.59	15.89	0.2	4.39	0.92	0.32	0.4	0.73	1.347625	43.49378	53.99404	27.76184	23.33607	48.07812	34.38803	108.5003	37.728	64.34250641
071408 cpx 2 Line 007	Enclave-Poor	Tonalite	15	1.99E-08	3	4.72	7.17	5.88	18.38	0.2	4.23	0.91	0.32	0.4	0.72	1.545204	43.97628	57.86523	27.23253	23.5014	45.06627	35.29477	107.6711	36.45386	63.58818939
071408 cpx 2 Line 008	Enclave-Poor	Tonalite	15	1.99E-08	3	6.37	6.77	7.21	126.8	0.2	5	1.05	0.32	0.4	0.72	1.461308	46.74798	56.06636	28.22973	22.80886	48.61069	34.54018	107.8734	35.23543	64.76393081
071408 cpx 2 Line 009	Enclave-Poor	Tonalite	15	1.99E-08	3	9.89	6.12	11.67	8.77	0.26	6.1	0.55	0.35	0.39	0.5	1.384553	45.51371	54.99549	27.76766	23.55592	52.89458	35.65524	104.1234	36.75294	63.75662613
071408 cpx 2 Line 010	Enclave-Poor	Tonalite	15	1.99E-08	3	8.43	4.26	130.03	12.16	0.2	4.67	1.45	0.32	0.41	0.64	1.426369	44.98579	57.01162	26.66675	23.53952	46.68951	33.65548	109.9724	33.89381	61.89724408
16071901 groundmass cpx 2 core a	Enclave-Poor	Tonalite	15	2.03E-08	3	22.29	2.62	35.68	10.19	0.19	15.43	3.21	0.31	0.26	0.45	49.76017	31.77012	37.50834	13.01563	17.63929	70.24763	59.81771	107.0892	28.48711	40.52824482
16071901 groundmass cpx 2 rim a	Enclave-Poor	Tonalite	15	2.03E-08	3	27.71	2.52	397.07	13.46	0.19	11.84	3.53	0.31	0.26	0.43	51.45702	30.56608	38.78185	12.93729	17.57425	68.15831	60.3122	108.378	28.4108	41.24243393
16071901 groundmass cpx 2 core b	Enclave-Poor	Tonalite	15	2.03E-08	3	23.68	3.2	100	13.08	0.19	13.67	4.59	0.31	0.25	0.47	51.35066	30.12465	38.89998	12.62958	17.98059	65.33961	60.80265	109.9312	27.25869	41.5173378
16071901 groundmass cpx 2 rim b	Enclave-Poor	Tonalite	15	2.03E-08	3	10.23	3.95	64.76	1.72	0.19	5.89	1.19	0.33	0.29	0.39	51.14359	32.71799	38.73552	13.17592	18.0248	73.73092	60.03208	104.9134	27.81161	42.1795845
Core 2 qd cpx corroded 1 core	Enclave-Poor	Tonalite	15	1.99E-08	3	10.01	2.29	100	10.61	0.19	11.1	2.71	0.32	0.27	0.42	49.22117	31.99136	38.96148	12.90246	17.69164	70.9844	61.57357	101.9966	28.82679	42.57457352
Core 2 qd cpx corroded 1 rim	Enclave-Poor	Tonalite	15	1.99E-08	3	8.32	2.79	100	2.92	0.19	10.09	1.95	0.33	0.28	0.4	51.66283	32.62301	39.27004	13.06435	18.04417	74.54691	62.6425	107.6536	28.60602	42.07194901
Core 2 qd cpx corroded 2 core	Enclave-Poor	Tonalite	15	1.99E-08	3	21.16	2.25	48.53	9.35	0.19	12.13	5.41	0.32	0.26	0.44	50.0235	30.30672	36.40165	12.58548	17.27608	61.5911	60.3701	105.7684	28.33848	40.6227684
16071901 cpx acc 1 core	Contact		15	2.03E-08	3	15.33	4.21	67.03	19.06	0.19	21.19	3.51	0.31	0.25	0.45	48.99854	30.58932	37.97876	12.89569	17.77415	67.10277	59.08304	102.9252	28.18569	41.93576335
16071901 cpx acc 1 core a	Contact		15	2.03E-08	3	12.3	3.24	45.1	24.07	0.14	6.73	3.8	0.32	0.3	0.48	51.2441	31.77012	39.07141	13.47666	19.70942	66.32291	62.55878	107.2121	27.48195	42.975287
16071901 cpx acc 2 rim a	Contact		15	2.03E-08	3	14.38	3.4	38.68	154.76	0.14	7.87	4.12	0.32	0.3	0.48	49.54675	32.08968	39.45503	13.50276	19.27032	69.62915	61.14648	109.0103	27.71392	43.63241577
16071901 cpx acc 2 core b	Contact		15	2.03E-08	3	15.71	3.81	39.61	93.17	0.14	8.03	5.16	0.32	0.3	0.49	48.45076	31.72124	38.63496	13.23286	19.53593	63.76515	62.78179	108.2054	28.02728	42.01651382
16071901 cpx acc 2 core c	Contact		15	2.03E-08	3	16.98	3.67	95.46	23.2	0.14	7.26	4.28	0.32	0.3	0.48	54.09534	31.49811	38.02863	13.15642	19.72235	64.54312	62.58669	110.1371	28.07288	42.55665588
16071901 cpx acc 2 core d	Contact		15	2.03E-08	3	25.34	3.54	79.8	100	0.13	8.92	4.89	0.32	0.3	0.48	51.5569	32.16286	39.47778	13.44185	19.79321	73.0833	62.97628	111.21	27.52879	42.06488994
16071901 cpx acc 2 core e	Contact		15	2.03E-08	3	11.03	3.76	28.14	29.67	0.14	7.18	3.32	0.32	0.3	0.47	48.89342	33.38239	40.32772	13.579	19.59286	71.10361	61.0607	106.3752	28.09752	42.06768594
16071901 cpx acc 2 core f	Contact		15	2.03E-08	3	13	3.33	35.27	24.3	0.14	8.59	5.32	0.32	0.3	0.49	48.66929	31.91778	39.8675	12.816	19.4478	66.81385	62.78179	103.9288	27.9229	42.49985054
16071901 cpx acc 2 core g	Contact		15	2.03E-08	3	16.6	3.6	40.16	100	0.14	7.92	3.86	0.32	0.3	0.46	53.29885	31.37397	40.7289	13.93114	19.65283	68.09171	60.21523	112.6204	27.55738	42.73154881

Table C.23. Extended EPMA results for host rock biotite

	Enclave Group	Acc V.	Beam Curr(A)	Beam Dia(um)	F SD(%)	Ti SD(%)	Mn SD(%)	Cl SD(%)	K SD(%)	Si SD(%)	Al SD(%)	Mg SD(%)	Fe SD(%)	F DL(ppm-1s)	Ti DL(ppm-1s)	Mn DL(ppm-1s)	Cl DL(ppm-1s)	K DL(ppm-1s)	Si DL(ppm-1s)	Al DL(ppm-1s)	Mg DL(ppm-1s)	Fe DL(ppm-1s)
071410 bt 1 core	1	15	1.992E-08	10	100	1.65	6.93	7.66	0.36	0.39	0.38	0.45	0.45	179.466	1.484	46.492	25.603	28.499	102.315	38.451	34.907	65.446
071410 bt 1 rim	1	15	1.992E-08	10	100	1.56	5.53	9.64	0.36	0.39	0.38	0.45	0.45	176.343	1.432	44.111	27.328	28.178	103.976	37.48	36.086	65.598
071410 bt2core	1	15	1.993E-08	10	100	1.65	5.67	8.05	0.35	0.39	0.38	0.46	0.44	176.472	1.36	43.702	26.631	29.811	104.99	38.511	33.872	65.157
071410 bt2rim 2	1	15	1.992E-08	10	100	1.57	6.54	8.73	0.36	0.39	0.38	0.46	0.44	176.863	1.409	48.507	28.008	28.571	108.431	38.673	34.833	66.796
071410 bt2rim1	1	15	1.992E-08	10	100	1.59	5.52	8.97	0.36	0.39	0.38	0.46	0.44	178.003	1.495	43.702	27.912	28.973	103.475	38.707	35.332	65.345
072804A btcore	2	15	1.994E-08	10	100	1.73	7.93	11.04	0.36	0.39	0.37	0.47	0.43	176.067	1.534	45.316	26.122	28.839	104.551	39.011	36.594	65.917
072804A btrim1	2	15	1.994E-08	10	100	1.87	6.44	13.34	0.39	0.4	0.36	0.46	0.43	179.882	1.461	45.052	27.719	28.781	103.924	37.611	36.299	66.967

Table C.24. Extended EPMA results for host rock amphibole

	Unit	Acc V.	Beam Curr(A)	Beam Dia(um)	Ti SD(%)	Mn SD(%)	Cr SD(%)	K SD(%)	Ca SD(%)	Na SD(%)	Al SD(%)	Si SD(%)	Mg SD(%)	Fe SD(%)	Ti DL(ppm-1s)	Mn DL(ppm-1s)	Cr DL(ppm-1s)	K DL(ppm-1s)	Ca DL(ppm-1s)	Na DL(ppm-1s)	Al DL(ppm-1s)	Si DL(ppm-1s)	Mg DL(ppm-1s)	Fe DL(ppm-1s)
Core 2 qd4pcorr1hblrim	Enclave-Rich Tonalite	15	2.044E-08	1	2.31	2.24	57.89	1.02	0.2	4.09	1.07	0.34	0.31	0.36	50.613	32.598	40.528	13.437	17.993	75.209	67.643	109.789	27.398	43.423
Core 2 qd4pcorr2hblrim	Enclave-Poor Tonalite	15	2.044E-08	1	2.37	2.42	62.35	1.06	0.19	3.74	1.07	0.34	0.31	0.36	51.457	32.91	39.023	13.11	17.808	85.672	59.789	109.989	27.929	43.665
16071901 cpnac2hblg	Contact	15	2.035E-08	1	2.43	4.32	26.31	1.21	0.19	3.76	1.13	0.34	0.29	0.39	49.76	30.769	40.002	13.205	17.85	86.227	58.219	109.514	27.902	41.411
16071901 cpnac2hbla	Contact	15	2.035E-08	1	3.23	4.71	19.75	29.73	0.19	4.72	1.32	0.33	0.28	0.41	48.999	31.795	39.815	13.191	17.769	71.044	61.003	107.296	28.313	41.464

Table C.25 Extended EPMA results for dyke/sill plagioclase

	Unit	Acc V.	Beam Curr(A)	Beam Dia(um)	Ti SD(%)	K SD(%)	Ca SD(%)	Na SD(%)	Al SD(%)	Si SD(%)	Fe SD(%)	Ti DL(ppm-1s)	K DL(ppm-1s)	Ca DL(ppm-1s)	Na DL(ppm-1s)	Al DL(ppm-1s)	Si DL(ppm-1s)	Fe DL(ppm-1s)
072601 plag2L1	QD Dyke	15	2E-08	3	145.6	2.12	0.2	1.51	0.43	0.33	8.11	49.76	12.757	16.854	84.031	69.794	113.685	39.147
072601 plag2L2	QD Dyke	15	2E-08	3	82.49	1.18	0.27	1.23	0.46	0.31	8.58	48.231	12.259	15.972	90.087	63.885	118.943	38.779
072601 plag2L3	QD Dyke	15	2E-08	3	100	1.89	0.22	1.39	0.44	0.32	7.17	49.547	12.296	16.431	77.974	68.988	122.393	38.763
072601 plag2L4	QD Dyke	15	2E-08	3	76.71	2.27	0.29	1.16	0.47	0.3	4.32	46.417	12.23	15.688	84.773	66.721	118.693	39.043
072601 plag2L5	QD Dyke	15	2E-08	3	136.46	0.19	1.03	15.34	0.4	0.34	5.45	46.535	12.292	15.223	58.686	66.956	114.362	39.273
072601 plag2L6	QD Dyke	15	2E-08	3	1053.56	0.47	0.19	1.37	0.47	0.33	1.53	48.669	12.206	16.287	78.911	69.743	120.846	38.205
072601 plag2L7	QD Dyke	15	2.001E-08	3	44.09	0.42	0.33	2.3	0.43	0.34	1.85	48.338	12.318	15.042	76.037	69.291	119.96	38.1
072601 plag2L8	QD Dyke	15	2.001E-08	3	726.48	1.42	0.29	1.17	0.47	0.31	6.98	50.294	11.966	15.765	77.78	63.748	125.836	38.381
072601 plag2L9	QD Dyke	15	2E-08	3	58.27	2.05	0.21	1.57	0.45	0.35	5.31	46.535	12.184	16.564	67.583	67.424	112.613	37.786
072601 plag2L10	QD Dyke	15	2E-08	3	72.72	1.92	0.21	1.45	0.43	0.33	8.33	48.893	12.409	16.576	80.591	65.585	119.758	38.394
072601 plag2L11	QD Dyke	15	2E-08	3	36.28	1.06	0.21	1.47	0.44	0.32	3.22	48.781	12.418	16.829	82.472	66.01	116.021	39.31
072601 plag2L12	QD Dyke	15	2E-08	3	24.95	2.26	0.21	1.47	0.43	0.33	4.73	45.95	12.299	16.861	72.64	66.59	119.174	38.558
072601 plag2L13	QD Dyke	15	2E-08	3	158.44	2.23	0.2	1.49	0.43	0.33	9.5	50.613	12.351	16.981	79.701	66.406	117.509	39.173
072601 plag2L14	QD Dyke	15	2E-08	3	132.45	1.78	0.21	1.41	0.44	0.32	9.79	51.244	12.308	16.456	77.445	69.089	118.217	39.546
072601 plag2L15	QD Dyke	15	2E-08	3	34.45	1.96	0.21	1.49	0.43	0.33	8.23	47.56	12.111	16.814	84.694	63.858	117.34	38.686
072601 plag2L16	QD Dyke	15	2E-08	3	1.52	2.22	0.21	1.69	0.48	0.35	0.38	53.6	13.168	16.974	79.564	68.172	113.131	40.814
072601 plag2L17	QD Dyke	15	2E-08	3	23.86	1.9	0.21	1.43	0.43	0.32	8.15	44.05	12.331	16.669	72.46	66.511	116.339	39.446
072601 plag2L18	QD Dyke	15	2.001E-08	3	100	1.04	0.29	1.18	0.47	0.3	8.82	49.973	12.264	15.641	88.097	66.616	120.834	38.927
072601 plag2L19	QD Dyke	15	2E-08	3	53.97	1.22	0.27	1.2	0.47	0.31	5.04	46.535	11.895	16.007	82.079	67.838	118.868	38.201
072601 plag2L20	QD Dyke	15	2E-08	3	64.21	1.41	0.27	1.2	0.47	0.31	7.29	47.221	12.514	15.928	86.514	66.695	120.297	37.628
072601 plag1L1	QD Dyke	15	2.001E-08	3	16.64	2.05	0.21	1.46	0.43	0.33	8.51	46.069	12.152	16.901	78.334	67.966	117.131	39.68
072601 plag1L2	QD Dyke	15	2E-08	3	42.8	1.68	0.21	1.5	0.44	0.33	6	46.762	12.176	16.637	83.126	70.292	117.603	38.034
072601 plag1L3	QD Dyke	15	2E-08	3	4.92	1	0.22	1.5	0.44	0.33	0.91	45.131	12.578	16.931	78.965	63.721	114.813	39.162
072601 plag1L4	QD Dyke	15	2E-08	3	16.96	0.18	1.21	2.84	0.52	0.3	7.72	46.879	12.848	15.519	73.817	69.342	128.933	39.795
072601 plag1L5	QD Dyke	15	2E-08	3	63.18	1.27	0.25	1.25	0.46	0.31	8.23	49.326	12.186	16.124	85.026	65.452	120.227	38.646
072601 plag1L6	QD Dyke	15	2E-08	3	52.26	2.02	0.2	1.53	0.43	0.33	8.42	49.76	12.35	16.88	71.409	67.45	114.628	39.595
072601 plag1L7	QD Dyke	15	2.001E-08	3	67.31	1.69	0.22	1.39	0.45	0.32	9.03	48.118	11.966	16.51	71.498	64.727	116.634	38.726
072601 plag1L8	QD Dyke	15	2.001E-08	3	208.33	0.99	0.29	1.2	0.48	0.31	8.84	47.668	12.107	15.942	93.083	66.037	120.894	39.192
072601 plag1L9	QD Dyke	15	2E-08	3	75.25	2.17	0.22	1.39	0.44	0.32	9.47	47.221	12.221	16.612	82.549	64.43	119.682	38.171
072601 plag1L10	QD Dyke	15	2E-08	3	83.23	2.02	0.22	1.37	0.45	0.32	8.52	46.762	12.103	16.332	84.976	67.398	113.838	38.742
072601 plag1L11	QD Dyke	15	2E-08	3	100	2.38	0.21	1.4	0.44	0.32	7.96	47.897	12.248	16.524	79.564	65.825	116.112	38.796
072601 plag1L12	QD Dyke	15	2E-08	3	80.68	1.95	0.26	1.24	0.47	0.31	5.26	47.105	12.27	15.716	82.498	63.419	123.421	38.793
072601 plag1L13	QD Dyke	15	2E-08	3	72.32	1.41	0.3	1.73	0.57	0.39	5.39	45.245	11.104	14.407	65.242	52.64	99.731	37.507
072601 plag1L14	QD Dyke	15	2.001E-08	3	1090.86	1.62	0.24	1.3	0.45	0.31	9	50.403	12.549	16.246	80.456	65.692	115.658	38.46
072601 plag1L15	QD Dyke	15	2.001E-08	3	6.06	0.34	0.39	1.04	0.71	0.5	8.87	43.683	11.34	13.758	94.716	63.363	104.315	33.93
072601 plag1L16	QD Dyke	15	2E-08	3	45.55	1.42	0.23	1.38	0.45	0.32	9.96	48.004	12.389	16.497	84.236	66.38	120.11	39.523
072601 plag1L17	QD Dyke	15	2E-08	3	67.74	1.44	0.25	1.28	0.46	0.31	8.77	46.879	12.719	15.965	85.179	65.904	118.962	38.754
072601 plag1L18	QD Dyke	15	2E-08	3	262.2	2.13	0.21	1.43	0.44	0.32	6.92	48.118	12.553	16.618	80.539	70.118	117.025	37.789
072601 plag1L19	QD Dyke	15	2E-08	3	48.53	1.49	0.22	1.4	0.44	0.32	5.91	48.118	12.419	16.183	78.773	68.3	114.686	39.427
072601 plag1L20	QD Dyke	15	2.001E-08	3	36.47	1.95	0.2	1.53	0.43	0.33	6.58	46.535	12.571	17.164	78.28	66.616	116.126	37.998
072601 plag1L21	QD Dyke	15	2.001E-08	3	56.11	1.14	0.27	1.22	0.47	0.31	7.68	44.651	12.249	15.868	85.784	66.222	118.7	39.176
072601 plag1L22	QD Dyke	15	2E-08	3	100	1.03	0.26	1.28	0.46	0.31	7.57	50.828	11.74	15.643	81.204	63.913	121.948	38.513
072601 plag1L23	QD Dyke	15	1.999E-08	3	26.39	1.85	0.21	1.46	0.43	0.32	7.46	44.888	12.206	16.675	76.577	66.826	117.678	38.136
072601 plag1L24	QD Dyke	15	2E-08	3	53.35	2.02	0.21	1.45	0.44	0.33	8.39	49.65	12.232	16.541	82.289	66.721	117.249	39.441
072601 plag1L25	QD Dyke	15	2E-08	3	31.17	1.35	0.27	1.23	0.47	0.31	7.38	46.645	12.109	15.93	85.381	67.735	121.825	39.269
072601 gmplag1core	QD Dyke	15	2.001E-08	3	18.13	1.94	0.21	1.47	0.44	0.33	7.61	47.329	12.153	16.56	80.913	68.043	123.24	38.715
072601 gmplag1rim	QD Dyke	15	2.001E-08	3	1053.56	1.27	0.3	1.19	0.48	0.31	5.27	48.669	12.146	15.521	90.302	63.032	121.254	38.021
072001A plag1core	Chilled Diorite Sill	15	2.001E-08	3	17.26	1	0.21	1.51	0.43	0.33	7.39	46.762	12.316	16.808	83.46	69.266	118.57	38.759
072001A plag1rim	Chilled Diorite Sill	15	2E-08	3	78.08	1.34	0.28	1.2	0.48	0.3	6.33	49.11	12.037	15.855	84.694	67.528	117.355	38.921
072001A plag 2 core	Chilled Diorite Sill	15	1.999E-08	3	25.09	1.63	0.22	1.37	0.45	0.32	7.48	47.445	12.332	16.583	85.179	64.185	122.065	39.524
072001A plag 2 rim	Chilled Diorite Sill	15	2E-08	3	266.34	1.1	0.32	1.14	0.49	0.3	5.66	48.893	12.149	15.339	95.915	64.889	124.401	39.029
071414 plag 2 core	Mafic Layered Intrusion (Bot)	15	1.969E-08	3	45.45	5.89	0.18	1.9	0.42	0.34	4.91	47.897	12.525	16.77	74.519	66.669	117.184	39.017
071414 plag 2 rim	Mafic Layered Intrusion (Bot)	15	1.969E-08	3	211.66	9.48	0.2	1.56	0.44	0.34	3.04	48.451	12.146	16.641	80.696	66.826	122.777	38.621
071414 plag 1 core	Mafic Layered Intrusion (Bot)	15	1.968E-08	3	174.8	6.02	0.18	1.83	0.42	0.34	5.68	47.897	12.641	16.904	73.554	65.505	119.116	38.842
071414 plag 1 rim	Mafic Layered Intrusion (Bot)	15	1.968E-08	3	100	3.22	0.18	1.86	0.42	0.34	4.76	49.65	12.199	17.227	73.229	70.043	115.644	39.397
071415 plag 1 core	Mafic Layered Intrusion (Mid)	15	1.969E-08	3	53.48	1.52	0.2	1.63	0.43	0.33	3.98	46.069	12.35	16.983	76.065	65.158	113.42	38.823
071415 plag 1 rim	Mafic Layered Intrusion (Mid)	15	1.969E-08	3	58.76	1.68	0.2	1.57	0.44	0.33	4.25	45.599	12.068	16.751	78.307	67.605	121.853	38.471
071415 plag 2 core	Mafic Layered Intrusion (Mid)	15	1.97E-08	3	27.21	2.55	0.21	1.51	0.45	0.32	3.79	45.95	12.529	16.502	89.169	65.452	119.826	37.888
071415 plag 2 rim	Mafic Layered Intrusion (Mid)	15	1.969E-08	3	59.18	1.67	0.2	1.62	0.43	0.33	3.51	45.95	12.245	16.744	76.856	64.943	119.637	40.533
071415 plag 3 core	Mafic Layered Intrusion (Mid)	15	1.968E-08	3	40.88	1.07	0.23	1.43	0.45	0.32	3.82	46.299	12.005	16.326	82.447	64.808	124.813	37.637
071415 plag 3 rim	Mafic Layered Intrusion (Mid)	15	1.969E-08	3	26.85	1.46	0.2	1.58	0.44	0.33	3.41	48.338	12.248	16.717	85.96	69.467	121.003	38.422

Table C.26 Extended EPMA results for dyke/sill pyroxene

	Unit	Acc V.	Beam Curr(A)	Beam Dia(um)	Ti SD(%)	K SD(%)	Ca SD(%)	Na SD(%)	Al SD(%)	Si SD(%)	Fe SD(%)	Ti DL(ppm-1s)	K DL(ppm-1s)	Ca DL(ppm-1s)	Na DL(ppm-1s)	Al DL(ppm-1s)	Si DL(ppm-1s)	Fe DL(ppm-1s)
072601 cpxcorrcore2L21	QD Dyke	15	2.027E-08	3	28.48	27.83	0.53	39.22	4.87	0.32	0.3	53.797	13.336	16.475	66.323	59.201	102.806	43.744
072601 plag2cpxinc1	QD Dyke	15	2.028E-08	3	13.33	100	0.14	7.14	3.44	0.32	0.43	54.196	13.45	19.8	71.891	61.772	106.891	43.065
072601 plag2cpxinc2	QD Dyke	15	2.028E-08	3	8.71	11.26	0.14	8.13	3.51	0.32	0.45	49.11	13.259	19.513	71.227	63.94	110.542	42.96
072601 plag2cpxinc3a	QD Dyke	15	2.028E-08	3	7.33	5.07	0.35	18.66	2.38	0.32	0.3	49.87	13.393	16.764	68.061	61.432	103.827	42.813
072601 plag2cpxinc3b	QD Dyke	15	2.028E-08	3	8.83	2.76	0.19	7.15	1.84	0.32	0.4	50.828	13.042	17.904	64.875	63.858	101.829	41.785
072601 cpxcorrcore1	QD Dyke	15	2.028E-08	3	32.69	18.76	0.82	50.65	7.13	0.32	0.32	53.093	12.763	16.228	70.342	62.976	105.35	42.038
072601 plag1cpxinc1	QD Dyke	15	2.028E-08	3	9.73	32.5	0.14	6.48	3.37	0.32	0.44	49.547	13.538	19.596	67.328	60.457	102.635	42.581
072601 plag1cpxinc2	QD Dyke	15	2.03E-08	3	10.13	17.21	0.14	7.03	3.24	0.32	0.42	53.994	13.694	19.136	66.619	57.403	105.809	42.017
072601 plag1cpxinc3	QD Dyke	15	2.029E-08	3	9.56	26.45	0.14	7.93	3.34	0.32	0.44	52.692	13.243	19.795	70.984	61.998	109.279	42.08
072601 zonedcpx2L1	QD Dyke	15	2.029E-08	3	5.44	107.12	0.14	7.16	2.78	0.32	0.44	52.588	13.149	19.216	69.507	65.719	109.001	43.115
072601 zonedcpx2L2	QD Dyke	15	2.029E-08	3	5.35	79.77	0.14	6.13	2.46	0.32	0.46	51.868	12.989	19.371	67.422	61.089	107.066	41.428
072601 zonedcpx2L3	QD Dyke	15	2.03E-08	3	6.46	73.7	0.14	4.88	2.37	0.32	0.44	53.6	13.462	19.554	71.861	64.213	109.845	41.899
072601 zonedcpx2L4	QD Dyke	15	2.03E-08	3	3.97	4.76	0.16	6.36	1.9	0.32	0.45	49.326	13.375	18.507	67.233	60.051	106.405	42.253
072601 zonedcpx2L5	QD Dyke	15	2.029E-08	3	5.21	19.66	0.14	5.87	2.43	0.32	0.47	50.721	13.594	19.028	62.083	65.639	108.243	43.311
072601 zonedcpx2L6	QD Dyke	15	2.03E-08	3	4.91	24.71	0.14	6.97	2.48	0.32	0.44	49.11	13.381	18.972	73.936	61.772	107.662	42.457
072601 zonedcpx2L7	QD Dyke	15	2.03E-08	3	5.61	677.07	0.14	7.04	2.52	0.32	0.45	53.196	13.315	19.612	69.32	59.554	107.818	42.797
072601 zonedcpx2L8	QD Dyke	15	2.03E-08	3	6.33	74.28	0.14	7.72	2.75	0.32	0.44	52.588	13.538	19.622	75.036	58.757	107.78	42.208
072601 zonedcpx2L9	QD Dyke	15	2.03E-08	3	4.75	23.61	0.15	6.91	2.39	0.32	0.42	50.721	13.19	19.038	70.617	63.059	102.939	41.693
072601 zonedcpx2L10	QD Dyke	15	2.03E-08	3	4.59	27.37	0.14	6.85	2.36	0.32	0.46	50.403	13.289	19.413	67.296	63.198	106.615	43.174
072601 zonedcpx2L11	QD Dyke	15	2.031E-08	3	6.64	8.76	0.14	5.88	2.41	0.32	0.48	50.403	13.515	19.508	68.693	60.688	107.317	41.39
072601 zonedcpx2L12	QD Dyke	15	2.03E-08	3	3.99	15.52	0.15	5.97	1.93	0.32	0.49	50.294	13.092	18.812	67.807	62.279	102.653	41.384
072601 zonedcpx2L13	QD Dyke	15	2.03E-08	3	2.8	7.65	0.15	5.11	1.45	0.33	0.46	50.828	13.153	19.026	73.291	59.525	105.589	42.311
072601 zonedcpx2L14	QD Dyke	15	2.031E-08	3	4.11	8.32	0.14	5.47	1.88	0.32	0.46	50.403	13.322	19.344	67.197	59.672	105.975	41.782
072601 zonedcpx2L15	QD Dyke	15	2.03E-08	3	8.48	38	0.14	6.63	3.45	0.32	0.44	52.282	13.378	19.214	70.062	62.67	106.235	43.085
072601 zonedcpx1L1	QD Dyke	15	2.02E-08	3	6.03	18.74	0.14	6.25	2.8	0.32	0.46	51.457	13.117	18.648	59.307	63.446	107.277	43.124
072601 zonedcpx1L2	QD Dyke	15	2.021E-08	3	5.85	4.22	0.14	4.4	2.15	0.32	0.46	51.663	13.483	19.453	63.222	59.818	106.956	41.164
072601 zonedcpx1L3	QD Dyke	15	2.021E-08	3	5.46	1.48	0.14	3.97	1.52	0.33	0.46	53.994	13.225	19.402	78.8	68.504	109.287	41.216
072601 zonedcpx1L4	QD Dyke	15	2.022E-08	3	4.83	11.71	0.15	7.62	1.7	0.38	0.48	51.244	12.876	18.464	50.407	54.178	102.864	42.234
072601 zonedcpx1L5	QD Dyke	15	2.021E-08	3	5.69	2.62	0.22	7.61	1.88	0.75	0.79	40.362	10.579	15.496	41.734	33.957	61.116	35.713
072601 zonedcpx1L6	QD Dyke	15	2.021E-08	3	4.88	1.32	0.15	4.89	1.02	0.33	0.48	52.893	13.358	17.71	67.936	60.889	105.498	41.116
072601 zonedcpx1L7	QD Dyke	15	2.022E-08	3	2.43	1.94	0.15	4.11	1.26	0.33	0.42	52.692	12.87	18.791	73.142	57.281	106.077	41.865
072601 zonedcpx1L8	QD Dyke	15	2.021E-08	3	2.63	2.83	0.17	4.52	1.33	0.33	0.44	49.11	13.39	18.246	68.913	58.099	104.753	41.623
072601 zonedcpx1L9	QD Dyke	15	2.021E-08	3	3.35	9.5	0.14	5.28	1.65	0.32	0.47	52.386	13.213	19.305	64.238	65.211	106.45	43.221
072601 zonedcpx1L10	QD Dyke	15	2.021E-08	3	3.17	6.19	0.14	4.6	1.49	0.32	0.46	50.929	13.381	19.405	70.617	60.63	108.454	41.892
072601 zonedcpx1L11	QD Dyke	15	2.001E-08	3	2.5	7.89	0.14	4.63	1.35	0.33	0.47	50.192	13.258	19.134	69.538	58.219	108.715	42.209
072601 zonedcpx1L12	QD Dyke	15	2.001E-08	3	2.38	5.51	0.15	4.9	1.28	0.34	0.45	53.395	13.399	18.806	75.41	60.659	101.782	42.223
072601 zonedcpx1L13	QD Dyke	15	2.001E-08	3	3.36	3.83	0.15	4.28	1.29	0.33	0.44	49.221	12.869	18.851	64.308	63.94	107.264	42.426
072601 zonedcpx1L14	QD Dyke	15	2.001E-08	3	5.29	10.28	0.14	6.76	2.15	0.32	0.5	49.547	13.368	18.883	68.411	64.43	106.981	43.99
072601 zonedcpx1L15	QD Dyke	15	2.002E-08	3	2.12	2.61	0.14	4.87	1.55	0.33	0.46	52.177	12.807	18.998	67.552	61.375	109.593	42.87
072601 zonedcpx1L16	QD Dyke	15	2.001E-08	3	3	1.94	0.19	5.08	1.12	0.33	0.39	51.037	12.9	17.711	65.538	61.998	105.048	42.311
072601 zonedcpx1L17	QD Dyke	15	2.001E-08	3	16.62	2.72	0.55	9.19	2.05	0.24	1.12	49.87	12.099	15.023	65.672	65.665	128.516	37.154
072601 zonedcpx1L18	QD Dyke	15	2.001E-08	3	1.87	0.8	0.19	3.2	0.99	0.35	0.36	48.563	13.295	17.894	75.926	61.46	101.249	42.701
072601 zonedcpx1L19	QD Dyke	15	2E-08	3	1.91	0.81	0.19	3.42	0.95	0.35	0.35	52.484	13.282	17.936	67.265	63.556	103.244	43.782
072601 zonedcpx1L20	QD Dyke	15	1.987E-08	3	10.57	20.3	0.14	6.89	3.44	0.32	0.44	51.037	13.269	19.544	67.296	62.949	109.178	42.681
072001A cpxcorrcore1	Chilled Diorite Sill	15	2.03E-08	3	14.12	159	0.14	7.11	4.22	0.32	0.38	50.613	13.575	19.556	57.573	56.576	106.941	43.119
072001A cpxcorrcore1	Chilled Diorite Sill	15	2.02E-08	3	7.98	28.59	0.14	9.04	3.97	0.31	0.39	48.999	13.262	19.335	65.372	64.376	108.593	44.137
072001A cpx 1 core	Chilled Diorite Sill	15	2.021E-08	3	26.9	13.54	0.2	13.5	4.18	0.3	0.39	50.929	13.177	17.447	68.442	58.787	110.017	41.102
072001A cpx 1 rim	Chilled Diorite Sill	15	2.021E-08	3	9.92	2.05	0.2	9.22	2.8	0.31	0.37	49.65	12.963	17.663	63.566	62.921	107.693	42.683
072001A cpx 2 core	Chilled Diorite Sill	15	2.021E-08	3	6.27	10.34	0.19	22.06	3.52	0.31	0.38	49.436	13.222	17.706	70.402	62.363	108.794	42.476
072001A cpx 2 rim	Chilled Diorite Sill	15	2.021E-08	3	20.1	6.35	0.19	16.98	3.03	0.32	0.35	51.144	13.187	18.206	72.042	60.022	108.01	42.869
072001A cpx corrcore2	Chilled Diorite Sill	15	2.02E-08	3	7.38	4.74	0.19	12.09	3.37	0.31	0.36	48.118	13.281	18.13	62.224	62.223	109.327	42.403
071414 opx 2 core	Mafic Layered Sill (Bot)	15	1.981E-08	3	56.93	219.96	1.14	558.3	2.63	0.33	0.42	49.326	12.66	15.428	69.881	58.219	102.365	39.663
071414 opx 2 rim	Mafic Layered Sill (Bot)	15	1.98E-08	3	12.04	805.4	0.8	69.48	3.18	0.33	0.42	48.563	12.569	15.706	59.89	58.578	101.739	40.846
071414 opx 1 core	Mafic Layered Sill (Bot)	15	1.981E-08	3	7.27	65.5	0.73	50.2	2.48	0.33	0.42	49.11	12.626	15.329	62.742	57.888	104.39	40.399
071414 opx 1 rim	Mafic Layered Sill (Bot)	15	1.98E-08	3	18.15	172.04	1.04	143.78	3.58	0.33	0.42	48.669	12.565	15.584	65.307	57.037	104.154	40.57
071415 cpx 3 core	Mafic Layered Sill (Mid)	15	1.98E-08	3	8.88	100	0.75	73.16	2.52	0.33	0.35	50.511	12.684	15.872	67.869	58.876	103.067	40.362
071415 cpx 3 rim	Mafic Layered Sill (Mid)	15	1.981E-08	3	8.32	118.2	0.66	6012.4	2.64	0.33	0.36	51.457	12.567	15.877	70.771	58.638	101.481	41.176
071415 cpx 1 core a	Mafic Layered Sill (Mid)	15	1.981E-08	3	5.06	100	0.14	7.95	1.91	0.33	0.54	50.929	13.253	19.397	73.936	60.515	103.416	42.58
071415 cpx 1 rim a	Mafic Layered Sill (Mid)	15	1.98E-08	3	5.08	125.09	0.14	7.96	1.99	0.33	0.55	52.484	13.105	19.331	71.197	61.744	104.213	41.407
071415 cpx 1 core b	Mafic Layered Sill (Mid)	15	1.98E-08	3	4.76	85.38	0.14	7.18	1.96	0.33	0.54	49.11	13.14	19.479	69.785	63.639	103.931	41.491
071415 cpx 1 rim b	Mafic Layered Sill (Mid)	15	1.981E-08	3	4.53	2218.29												

Table C.27. Extended EPMA results for dyke/sill hornblende

	Unit	Acc V.	Beam Curr(A)	Beam Dia(um)	Ti SD(%)	Mn SD(%)	Cr SD(%)	K SD(%)	Ca SD(%)	Na SD(%)	Al SD(%)	Si SD(%)	Mg SD(%)	Fe SD(%)	Ti DL(ppm-1s)	Mn DL(ppm-1s)	Cr DL(ppm-1s)	K DL(ppm-1s)	Ca DL(ppm-1s)	Na DL(ppm-1s)	Al DL(ppm-1s)	Si DL(ppm-1s)	Mg DL(ppm-1s)	Fe DL(ppm-1s)
071414 Hbl 1 core	Mafic Layered Intrusion (Bottom)	15	2.044E-08	1	1.33	10.52	2.72	0.77	0.19	2.24	0.73	0.36	0.28	0.5	50.511	31.198	39.14	13.177	17.805	79.864	65.051	109.463	27.752	42.16
071414 Hbl 1 rim	Mafic Layered Intrusion (Bottom)	15	2.044E-08	1	1.44	10.15	3.13	0.79	0.19	2.36	0.71	0.36	0.28	0.48	47.221	32.357	38.908	13.011	17.781	64.707	60.109	108.075	28.618	42.243
071414 Hbl 2 core	Mafic Layered Intrusion (Bottom)	15	2.045E-08	1	2.18	8.77	4.71	0.87	0.19	2.31	0.73	0.36	0.27	0.49	49.221	30.563	38.977	12.826	17.515	74.98	66.327	106.837	28.264	41.761
071414 Hbl 2 rim	Mafic Layered Intrusion (Bottom)	15	2.044E-08	1	2.12	9.93	3.43	0.84	0.19	2.4	0.74	0.36	0.27	0.5	49.221	31.374	39.14	12.809	17.596	71.621	62.223	104.034	28.711	41.593
071415 Hbl core	Mafic Layered Intrusion (Middle)	15	2.044E-08	1	1.24	6.31	9.21	0.65	0.19	2.59	0.72	0.36	0.3	0.42	52.79	30.692	39.217	13.158	17.892	76.065	64.484	108.804	27.626	43.211
071415 Hbl rim	Mafic Layered Intrusion (Middle)	15	2.045E-08	1	1.23	6.91	9.75	0.62	0.19	2.76	0.72	0.37	0.3	0.41	53.797	31.864	40.072	13.376	17.822	74.923	67.087	109.233	28.24	42.666

Table C. 28. Extended EPMA results for dyke/sill olivine

	Unit	Acc V.	Beam Curr(A)	Beam Dia(um)	Ti SD(%)	Mn SD(%)	Cr SD(%)	Ca SD(%)	Al SD(%)	Si SD(%)	Mg SD(%)	Fe SD(%)	Ti DL(ppm-1s)	Mn DL(ppm-1s)	Cr DL(ppm-1s)	Ca DL(ppm-1s)	Al DL(ppm-1s)	Si DL(ppm-1s)	Mg DL(ppm-1s)	Fe DL(ppm-1s)
071414 olivine 3 core	Mafic Layered Intrusion (Bottom)	15	1.971E-08	3	312.66	3.67	100	14.43	188.28	0.4	0.17	0.33	50.294	31.073	40.394	15.845	55.042	93.955	30.802	41.165
071414 olivine 3 rim	Mafic Layered Intrusion (Bottom)	15	1.971E-08	3	33.17	3.94	87.88	9.62	100	0.4	0.17	0.34	46.299	30.997	36.429	15.599	56.235	96.837	31.089	41.497
071414 olivine 2 core	Mafic Layered Intrusion (Bottom)	15	1.971E-08	3	435.89	4.03	139.82	13.38	366.9	0.4	0.17	0.34	50.192	32.406	38.225	15.656	55.358	91.712	30.231	41.804
071414 olivine 2 rim	Mafic Layered Intrusion (Bottom)	15	1.971E-08	3	82.73	3.89	70.2	17.75	100	0.4	0.17	0.34	50.294	30.971	38.565	15.623	58.339	96.559	30.5	42.273
071414 olivine 1 rim	Mafic Layered Intrusion (Bottom)	15	1.972E-08	3	100	4.06	100	15.33	100	0.39	0.17	0.33	50.613	31.473	38.869	15.696	54.595	96.227	30.486	42.259
071414 olivine 1 core	Mafic Layered Intrusion (Bottom)	15	1.97E-08	3	74.52	4.09	40.18	13.02	116.47	0.4	0.17	0.33	48.451	31.672	36.726	15.908	54.563	94.801	29.795	41.654

Appendix D. Rheological Properties of Units

Table D.1. Comparison of estimated density using specific gravity versus KWare MAGMA

Type	Specific Gravity (Kg/m ³)	MAGMA Value (Kg/m ³)
Enclave-Poor Tonalite	2787	2876
Enclave-Rich Tonalite	2713	2769
Biotite Granite	2658	2662
Group 1 Enclave	2792	2905
Group 2 Enclave	2856	2942
Group 3 Enclave	2919	2980